

Cyclopentadienylmagnesium Complexes in Homogeneous Catalysis

Dissertation

zur Erlangung des Grades
des Doktors der Naturwissenschaften
der Naturwissenschaftlich-Technischen Fakultät
der Universität des Saarlandes

von

M. Sc. Lisa Wirtz

Saarbrücken

2022

Tag des Kolloquiums: 22.02.2023
Dekan: Prof. Dr. Ludger Santen
Berichterstatter: Priv.-Doz. Dr. André Schäfer
Prof. Dr. Uli Kazmaier
Vorsitz: Prof. Dr. Johann Jauch
Akademischer Mitarbeiter: Dr. Andreas Rammo

The present dissertation was prepared in the time between April 2019 and August 2022 under the supervision of Dr. André Schäfer at the Department of Chemistry of the Faculty of Natural Sciences and Technology at Saarland University.

Die vorliegende Dissertation wurde im Zeitraum zwischen April 2019 und August 2022 unter der Anleitung von Dr. André Schäfer im Fachbereich Chemie der Naturwissenschaftlich-Technischen Fakultät der Universität des Saarlandes angefertigt.

Abstract

The present dissertation deals with the synthesis and characterization of two different types of complexes: magnesocenophanes and *ansa*-half-sandwich magnesium complexes. The synthesized compounds were structurally and spectroscopically characterized and their electronic properties, such as Lewis acidities, were investigated by DFT calculations. Following the successful synthesis and characterization of these magnesium complexes, their catalytic activity in dehydrocoupling and hydroelementation reactions was explored. In dehydrocoupling catalysis, magnesocenophanes and *ansa*-half-sandwich magnesium complexes are the first cyclopentadienyl-based magnesium complexes which show high catalytic activity at ambient conditions. In hydroelementation reactions, the catalytic activity of the *ansa*-half-sandwich magnesium complexes was tested in different hydroboration reactions, as well as in intramolecular hydroamination and hydroacetylenation reactions. The compounds succeeded in catalyzing the ring closing hydroamination as well as in the addition of phenylacetylene to different carbodiimides. Possible mechanisms of the catalytic reactions were investigated by DFT calculations, assisted by kinetic studies.

Zusammenfassung

Die vorliegende Arbeit beschäftigt sich mit der Synthese und Charakterisierung zweier unterschiedlicher Komplex-Typen: Magnesocenophanen und *ansa*-Halbsandwich-Magnesium-Komplexen. Die synthetisierten Verbindungen wurden strukturell und spektroskopisch charakterisiert und ihre elektronischen Eigenschaften, wie beispielsweise die Lewis Acidität, wurden mittels DFT Rechnungen untersucht. Nach der erfolgreichen Synthese der Magnesocenophane und *ansa*-Halbsandwich-Komplexe, wurde ihre katalytische Aktivität in Dehydrokupplungs- und Hydroelementierungsreaktionen getestet. Im Bereich der Dehydrokupplungskatalyse sind die Magnesocenophane und *ansa*-Halbsandwich-Komplexe die ersten Cyclopentadienyl-basierten Magnesium Katalysatoren, die eine hohe katalytische Aktivität unter Standard-Bedingungen zeigen. Im Bereich der Hydroelementierungsreaktionen wurde die katalytische Aktivität der *ansa*-Halbsandwich Magnesium Komplexe in Hydroborierungsreaktionen getestet, sowie in intramolekularen Hydroaminierungen und Hydroacetylierungen. Die Verbindungen konnten sowohl die Ringschluss-Hydroaminierung als auch die Addition von Phenylacetylen an Carbodiimide erfolgreich katalysieren. Die Mechanismen, die der Katalyse zugrunde liegen, wurden mithilfe von DFT-Rechnungen und kinetischen Studien untersucht.

List of Publications

As part of the cumulative dissertation:

- Lisa Wirtz, Wasim Haider, Volker Huch, Michael Zimmer, André Schäfer
Magnesocenophane-Catalyzed Amine Borane Dehydrocoupling.
Chem. Eur. J. **2020**, *26*, 6176-6184.

DOI: 10.1002/chem.202000106

- Lisa Wirtz, Jessica Lambert, Bernd Morgenstern, André Schäfer
Cross-Dehydrocoupling of Amines and Silanes Catalyzed by Magnesocenophanes.
Organometallics **2021**, *40*, 2108-2117.

DOI: 10.1021/acs.organomet.1c00245

- Lisa Wirtz, Kinza Yasmin Ghulam, Bernd Morgenstern, André Schäfer
Constrained Geometry *ansa*-Half-Sandwich Complexes of Magnesium – Versatile *s*-Block Catalysts.
ChemCatChem **2022**, *14*, e202201007

DOI: 10.1002/cctc.202201007

Other Publications:

- Carsten Müller, Angelika Stahlich, Lisa Wirtz, Claude Gretschi, Volker Huch, André Schäfer
Carbene Complexes of Stannocenes.
Inorg. Chem. **2018**, *57*, 8050-8053.

DOI: 10.1021/acs.inorgchem.8b01432

- Lisa Wirtz, Matthias Jourdain, Volker Huch, Michael Zimmer, André Schäfer
Synthesis, Structure, and Reactivity of Disiloxa[3]tetrelocenophanes.
ACS Omega **2019**, *4*, 18355-18360.

DOI: 10.1021/acsomega.9b02605

- Sergi Danés, Carsten Müller, Lisa Wirtz, Volker Huch, Theresa Block, Rainer Pöttgen, André Schäfer, Diego M. Andrada
Bonding Situation in Stannocene and Plumbocene N-Heterocyclic Carbene Complexes.
Organometallics **2020**, *39*, 516-527.

DOI: 10.1021/acs.organomet.9b00667

- Lisa Wirtz, André Schäfer
Main-Group Metallocenophanes. (Review)
Chem. Eur. J. **2021**, *27*, 1219-1230.

DOI: 10.1002/chem.202003161

- Nico Bachmann, [Lisa Wirtz](#), Bernd Morgenstern, Carsten Müller, André Schäfer
Crystal structure of 1,1',2,2',4,4'-hexaisopropylmagnesiumocene.
Acta Cryst. E **2022**, 78, 287-290.

DOI: 10.1107/S2056989022001189

Acknowledgment

Ein großer Dank gilt **Dr. André Schäfer**, der mir die Möglichkeit gegeben hat, meine Dissertation in seiner Arbeitsgruppe anzufertigen. Ich danke ihm für die interessante Themenstellung, sowie das in mich gesetzte Vertrauen und die Freiheit, die er mir bei der Bearbeitung der Themen und der Entwicklung neuer Methoden gegeben hat. Außerdem möchte ich mich dafür bedanken, dass ich die Magnesium-Katalyse auch auf internationalen Tagungen vorstellen und mit anderen Forschern diskutieren konnte.

Bei **Prof. Dr. Uli Kazmaier** bedanke ich mich für die wissenschaftliche Begleitung während meiner Promotion und die Übernahme des Zweitgutachtens.

Bei **Dr. Volker Huch** und **Dr. Bernd Morgenstern** bedanke ich mich für die Durchführung der Kristallstrukturanalysen und bei **Dr. Michael Zimmer** für die Unterstützung bei NMR-Experimenten. **Susanne Harling** danke ich für die Durchführung der Elementaranalysen. Ein großes Dankeschön gilt **Susanne Limbach** für die Unterstützung und Hilfsbereitschaft bei administrativen und organisatorischen Aufgaben. Bei **Sylvia Beetz** bedanke ich mich für die gute Zusammenarbeit und die Anfertigung von vielen hilfreichen Gadgets für die Arbeit im Labor.

Ganz besonders möchte ich mich bei den Mitarbeitern des Arbeitskreises Schäfer bedanken, hier vor allem bei **Dr. Wasim Haider**, **Dr. Carsten Müller** und **Inga Bischoff**, für die freundliche Aufnahme im Labor und die angenehme Arbeitsatmosphäre, sowie die vielen lustigen Momente, die wir gemeinsam innerhalb und außerhalb des Labors erlebt haben. Bei meinen ehemaligen Bachelorstudenten **Jessica Lambert**, **Kinza Ghulam**, **Nico Bachmann** und **Media Mohamad** bedanke ich mich für die gute Zusammenarbeit und die schöne Zeit im Labor. Allen aktuellen und ehemaligen Mitarbeitern der Arbeitskreise Schäfer und Kickelbick danke ich für die gute Arbeitsatmosphäre und das freundliche Miteinander im vierten Stock.

Dr. Carsten Müller, **Inga Bischoff** und **Julia Dräger** danke ich für das Korrekturlesen dieser Arbeit. Außerdem möchte ich mich bei **Julia Dräger** und **Verena Dittlinger** für die gegenseitige Unterstützung während des Studiums bedanken und die vielen lustigen und schönen Momente, die wir zusammen in dieser Zeit erlebt haben.

Meinen Eltern und meiner Schwester danke ich für die Unterstützung während meines Studiums und meiner Promotion, sowie für den Rückhalt, den sie mir immer gegeben haben. Danke für alles!

Content

List of Abbreviations	1
1. Introduction	3
1.1 Alkaline Earth Metallocenes	3
1.2 Alkaline Earth Metallocenophanes	11
1.3 <i>ansa</i> -Half-sandwich complexes of alkaline earth metals	17
1.4 Magnesium catalysis.....	21
1.4.1 Preface – Magnesium in catalysis	21
1.4.2 Dehydrocoupling catalysis	22
1.4.3 Hydroboration catalysis	32
1.4.4 Intramolecular Hydroamination	37
1.4.5 Hydroacetylenation.....	43
1.4.6 Summary – Magnesium in catalysis.....	45
2. Motivation and Aims	46
3. Results and Discussion	48
3.1 Magnesocenophane-Catalyzed Amine Borane Dehydrocoupling.....	48
3.2 Cross-Dehydrocoupling of Amines and Silanes Catalyzed by Magnesocenophanes ..	59
3.3 Constrained Geometry <i>ansa</i> -Half-Sandwich Complexes of Magnesium – Versatile <i>s</i> -Block Catalysts	70
4. Conclusion	80
5. References.....	83
6. Supporting Information	94
6.1 Magnesocenophane-Catalyzed Amine Borane Dehydrocoupling.....	94
6.2 Cross-Dehydrocoupling of Amines and Silanes Catalyzed by Magnesocenophanes	130
6.3 Constrained Geometry <i>ansa</i> -Half-Sandwich Complexes of Magnesium – Versatile <i>s</i> -Block Catalysts	157

List of Abbreviations

Ae	Alkaline earth metal
Ar	Aryl
BDE	Bond dissociation energy
Bn	Benzyl
Bu	Butyl
ⁿ Bu	<i>n</i> -Butyl
^t Bu	<i>tert</i> -Butyl
cat.	Catalytic
Cp	Cyclopentadienyl
Cp [#]	1,2,3,4-Tetramethylcyclopentadienyl
Cp [*]	Pentamethylcyclopentadienyl
Cy	Cyclohexyl
DFT	Density functional theory
Dip	2,6-Diisopropylphenyl
dme	Dimethoxyethane
dmf	Dimethylformamide
dmso	Dimethylsulfoxide
e. g.	<i>exempli gratia</i>
eq.	Equivalents
Et	Ethyl
<i>et al.</i>	<i>et alii</i>
FIA	Fluoride ion affinity
GEI	Global electrophilicity index
<i>J</i>	Coupling constant
K	Kelvin

List of Abbreviations

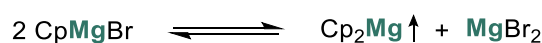
Me	Methyl
Mes	Mesityl
NMR	Nuclear magnetic resonance
Ph	Phenyl
pin	Pinacol
ppm	Parts per million
<i>i</i> Pr	<i>iso</i> -Propyl
r. t.	Room temperature
Tf	Triflyl
thf	Tetrahydrofuran
XRD	X-ray diffraction

1. Introduction

1.1 Alkaline Earth Metallocenes

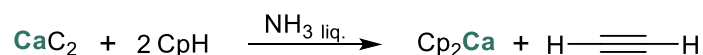
Metallocenes have been known for over 70 years, following the groundbreaking discovery of ferrocene. In 1951, the groups of Pauson and Miller independently reported the synthesis of ferrocene (bis(cyclopentadienyl)iron(II)).^[1-6] The structural elucidation of ferrocene by Fischer and coworkers in 1952 was a pioneering milestone in the research field of metallocenes and acted as a booster for further research into such sandwich complexes, with a metal bound to two cyclopentadienyl rings.^[7]

The η^5 π -type complexation of an element to a cyclopentadienide moiety is not limited to transition metals. Just a few years after the discovery of ferrocene, the first main group metallocenes were reported. In 1954, Fischer and coworkers were able to obtain magnesocene, the first main group metallocene, as a byproduct in the synthesis of vanadocene. The authors heated a mixture of the Grignard reagent cyclopentadienylmagnesiumbromide and could obtain magnesocene via sublimation (Scheme 1).^[8] Cyclopentadienylmagnesiumbromide exists in solution in an equilibrium (Schlenk equilibrium) with magnesocene and magnesium dibromide. Since cyclopentadienylmagnesiumbromide and magnesium dibromide cannot be sublimated but magnesocene can, heating the reaction mixture can remove magnesocene from the equilibrium by sublimation, which is how Fischer and coworkers were able to isolate the compound almost 70 years ago.^[8,9] Independently from Fischer *et al.*, Wilkinson and Cotton also reported magnesocene in the same year.^[10]



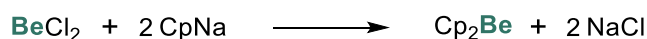
Scheme 1: First synthesis of magnesocene as conducted by Fischer and coworkers.^[8]

Two years later, in 1956, calcocene was synthesized by Ziegler and coworkers starting from cyclopentadiene and calcium carbide (Scheme 2), with acetylene as a byproduct, an important crude material in technological and industrial processes.^[11]



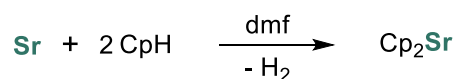
Scheme 2: First synthesis of calcocene as carried out by Ziegler and coworkers.^[11]

A few years later, Fischer and Hofmann attempted to synthesize beryllocene. After the unsuccessful attempt to react beryllium metal with gaseous cyclopentadiene, the authors succeeded by reacting cyclopentadienylsodium with berylliumchloride and were able to obtain beryllocene (Scheme 3).^[12] Beryllocene possesses a dipole moment, thus the authors assumed an unsymmetrical structure of the metallocene. Therefore, they postulated that the beryllocene exhibits two Cp-rings with different coordination modes, one coordinated η^1 and the other coordinated η^5 to the beryllium atom.^[12] This slipped sandwich structure of the beryllocene was later elucidated by single crystal X-ray diffraction (*vide infra*).^[13]



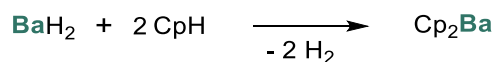
Scheme 3: First synthesis of beryllocene as conducted by Fischer and coworkers.^[12]

Completing the series of alkaline earth metallocenes, Fischer and Stölzle reported strontocene and barocene in the early 1960s. Strontocene was obtained from the reaction of cyclopentadiene and finely dispersed strontium metal in dmf (Scheme 4).^[14]



Scheme 4: First synthesis of strontocene as reported by Fischer and coworkers.^[14]

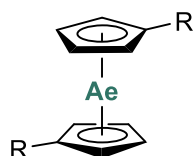
The synthesis of barocene presented great challenges for Fischer and Stölzle. As it was not successful starting from barium metal and cyclopentadiene because of the lack of an adequate solvent, but barocene was obtained in small yield by the reaction of barium hydride with cyclopentadiene (Scheme 5).^[14] From today's point of view, the synthesis of barocene could be viewed as a type of dehydrocoupling reaction, since hydrogen is released upon formation of the barium Cp bonds.



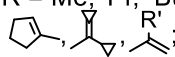
Scheme 5: First synthesis of barocene as conducted by Fischer and Stözlze.^[14]

In addition to the first reported alkaline earth metallocenes, a great number of group 2 metallocenes with various substitution patterns is known today.

1,1'- substituted metallocenes:



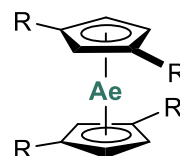
Ae = **Mg**: R = Me, ^tBu, SiMe₃, PⁱPr₂,
CHMePh, CH(cyclo-C₃H₅)₂

Ae = **Ca**: R = Me, ⁱPr, ^tBu, PPh₂,
 R' = Me, Ph, CH₂CHMe

Ae = **Sr**: R = ^tBu, PPh₂, C=(CH₂)Ph

Ae = **Ba**: R = ^tBu, PPh₂, C=(CH₂)Ph

1,1',3,3'- substituted metallocenes:



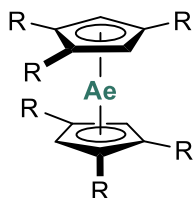
Ae = **Mg**: R = R' = ^tBu, SiMe₃;
R = SiMe₃; R' = ^tBu

Ae = **Ca**: R = R' = SiMe₃

Ae = **Sr**: R = R' = SiMe₃

Ae = **Ba**: R = R' = SiMe₃

1,1',2,2',4,4'- substituted metallocenes:



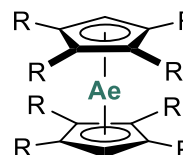
Ae = **Mg**: R = ⁱPr, ^tBu, SiMe₃

Ae = **Ca**: R = ⁱPr, ^tBu, SiMe₃

Ae = **Sr**: R = ⁱPr, ^tBu, SiMe₃

Ae = **Ba**: R = ⁱPr, ^tBu, SiMe₃

1,1',2,2',3,3',4,4'- substituted metallocenes:



Ae = **Be**: R = Me

Ae = **Mg**: R = Me, Ph

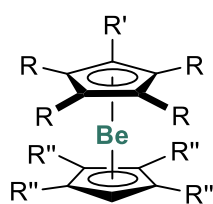
Ae = **Ca**: R = Me, ⁱPr, Ph

Ae = **Sr**: R = ⁱPr

Ae = **Ba**: R = ⁱPr, Ph

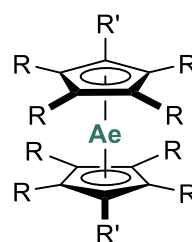
Figure 1: Selected examples of differently substituted alkaline earth metallocenes described in literature.^[15–38]

1,1',2,2',3,3',4,4',5- substituted beryllocenes:



R = R' = R'' = Me
 R = R' = Me; R'' = H

1,1',2,2',3,3',4,4',5,5'- substituted metallocenes:



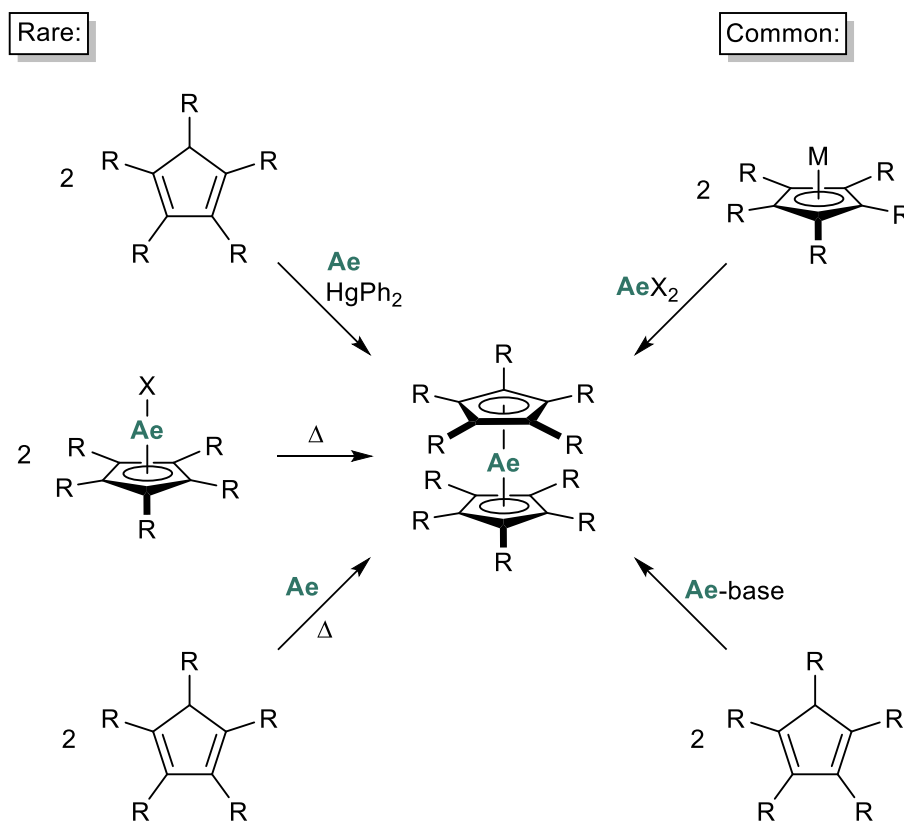
Ae = **Be**: R = R' = H, Me
 Ae = **Mg**: R = R' = H, Me, C₆H₄-4-^tBu;
 R = Me; R' = ^tBu, PPh₂, PⁱPr₂,
 (CH₂)₂CH=CH₂
 Ae = **Ca**: R = R' = H, Me, ⁱPr, Ph, C₆H₄-4-ⁿBu,
 C₆H₄-4-^tBu, C₆H₃-3,5-ⁱPr₂
 R = Me; R' = Et, ⁱPr, (CH₂)₂CH=CH₂
 Ae = **Sr**: R = R' = H, Me, ⁱPr, C₆H₄-4-ⁿBu,
 C₆H₄-4-^tBu, C₆H₃-3,5-ⁱPr₂
 R = Me; R' = (CH₂)₂CH=CH₂
 Ae = **Ba**: R = R' = H, Me, ⁱPr, Ph, C₆H₄-4-ⁿBu,
 C₆H₄-4-^tBu, C₆H₃-3,5-ⁱPr₂
 R = Me; R' = ^tBu, (CH₂)₂CH=CH₂

Figure 2: Selected examples of heteroleptic beryllocenes and selected examples of per-substituted alkaline earth metallocenes.^[8,10–12,14,15,24,25,35,38–52]

Generally, most alkaline earth metallocenes are homoleptic complexes with identical substitution patterns on both Cp rings. However, beryllocenes are an exception here, as two heteroleptic beryllocenes are known to the literature (Figure 2).^[25,52] These two heteroleptic beryllocenes exhibit one permethylated Cp ring (Cp^{*}), in combination with an unsubstituted Cp ring^[52] or with a tetramethyl Cp ring (Cp[#]), respectively.^[25] This is unique for beryllium as no heteroleptic metallocenes are known for the heavier alkaline earth metals, which may be related to the homoleptic ones being more stable and ligand exchange reactions occurring in the Schlenk-type equilibrium.

Some of the here mentioned alkaline earth metallocenes exist as donor-solvent complexes or are coordinated by other donor ligands such as amines or carbenes, due to the metal centers exhibiting Lewis acidic character. Coordinating ligands are omitted for clarity in Figure 1 and Figure 2, and not all metallocenes depicted there, are structurally authenticated by single crystal X-ray diffraction. In addition to these bis(cyclopentadienyl) complexes, a series of metallocenes containing indenyl or fluorenyl ligands exist, but are not discussed in this chapter, due to their low relevance for this thesis.

Different synthetic methods for alkaline earth metallocenes are reported in the literature that can be separated in five groups: ligand redistribution, protonolysis, salt metathesis, metal oxidation by CpH or Cp-radical and concerted redox-transmetalation ligand-exchange (Scheme 6).^[53]



Scheme 6: Rare and common used synthetic methods for the synthesis of alkaline earth metallocenes.^[53]

Protonolysis and salt metathesis are the most commonly used synthetic methods in the synthesis of metallocenes. Nowadays, metallocenes are often prepared via protonolysis by reacting substituted or unsubstituted cyclopentadienes with alkaline earth metal bases. Since Duff and coworkers established the usage of dibutylmagnesium in the synthesis of magnesocenes,^[15] it has become the most important synthetic route today.^[15,17,19–23] Fischer and Hofmann introduced the salt metathesis in 1959 with the synthesis of beryllocene (Scheme 3).^[12] Since then, this pathway has become the most important alternative to protonolysis and a number of group 2 metallocenes has been synthesized via this route.^[12,16,18,23,24,26,28,39–41] In addition, in the early days of group 2 metallocene chemistry, ligand redistribution and metal oxidation routes have been utilized in the synthesis of metallocenes. Here, Grignard-type

reagents were heated to sublime and isolate homoleptic metallocenes.^[8] Alternatively, fine dispersed alkaline earth metals were reacted with cyclopentadiene.^[14] However, nowadays, these synthetic methods are rarely used in metallocene synthesis. Finally, another possibility for the synthesis of metallocenes of alkaline earth metals is the concerted redox-transmetalation ligand-exchange. This synthesis is only used for cyclopentadienyl derivatives with a great steric demand and find application when other synthetic routes reach their limits.^[20,45]

Following the synthesis of the metallocenes, structural properties of group 2 metallocenes will now be discussed. In metallocenes of transition metals the bonding situation between the central atom and the Cp ring is most often η^5 . In main group metallocenes ring-slipping effects are quite common, with the cyclopentadienyl ring adopting lower hapticities of η^1 to η^4 (Figure 3). In addition, σ -bonded Cp rings are commonly found in *p*-block compounds.^[54,55]

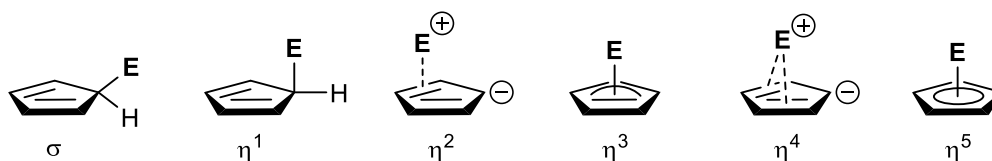


Figure 3: Possible hapticities in cyclopentadienyl compounds.^[54,55]

Group 2 metallocenes mainly exhibit one of three different structures: slipped sandwich structures, coplanar structures (ferrocene-like) and bent structures (Figure 4). The structure of the various alkaline earth metallocenes depends on the ionicity of the metal Cp bond, size of the central atom, and the steric demand of the Cp rings. The metal-ligand bonding in group 2 metallocenes has a relatively high ionic character that increases for the heavier alkaline earth metals. This ionic bonding character is, for instance, evident from the reactivity of magnesocene with dmso, which leads to a magnesium dication that is coordinated by six dmso molecules and solvent-separated cyclopentadienide anions, thus magnesocene undergoes a salt-like cation anion dissociation.^[56] Descending group two, the distance between the central atom and the cyclopentadienyl ring increases, due to the increase in size of the alkaline earth metal. Also, the metal Cp bond becomes more ionic, due to the rising electro-positive character of the metal.^[53,57]

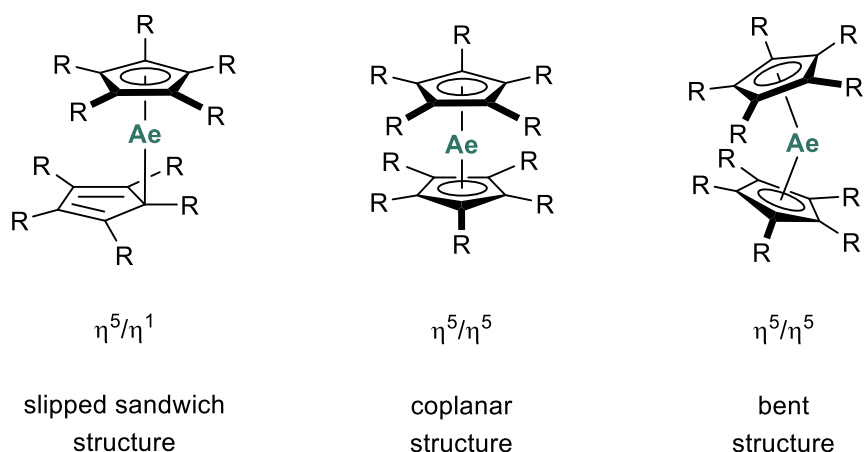


Figure 4: Slipped sandwich, coplanar and bent structure of group 2 metallocenes.

With the exception of decamethylberyllocene (Cp^*_2Be), beryllocenes possess a slipped sandwich structure, with the cyclopentadienyl rings bound in an η^1/η^5 fashion to the beryllium atom. This is due to the less ionic bonding character between beryllium and the Cp ligands and the smaller coordination sphere of beryllium, resulting in beryllocenes to adopt slipped sandwich structures, which also follow the octet rule.^[12,13,24,25,58] Decamethylberyllocene exhibits a coplanar ferrocene-like structure, presumably due to the higher steric demand of the Cp^* ligands.^[24,25] Magnesocenes are in general almost coplanar.^[42,59,60] This is however only true for compounds of the type Cp_2Mg . When additional donor ligands, such as thf, are coordinated to the magnesium atom, these magnesocene donor complexes often exhibit slipped sandwich structures as well.^[56,61–63] The heavier homologues of group two metallocenes possess bent sandwich structures, even when additional solvent molecules are coordinated to the central atom. Until now, no crystal structures of Cp_2Sr and Cp^*_2Sr exist. Calcocene, Cp_2Ca and barocene, Cp_2Ba , have polymeric structures in the solid state but are not isostructural. In Cp_2Ca , the terminal cyclopentadienyl rings are bonded η^5 to the central atom and the bridging rings retain η^1 , η^3 and η^5 bonding modes (Figure 5 left).^[44] In barocene, one barium atom is tetrahedrally surrounded by four η^5 coordinated cyclopentadienyl rings and, conversely, every cyclopentadienyl ring is coordinated by two barium atoms (Figure 5 right).^[64]

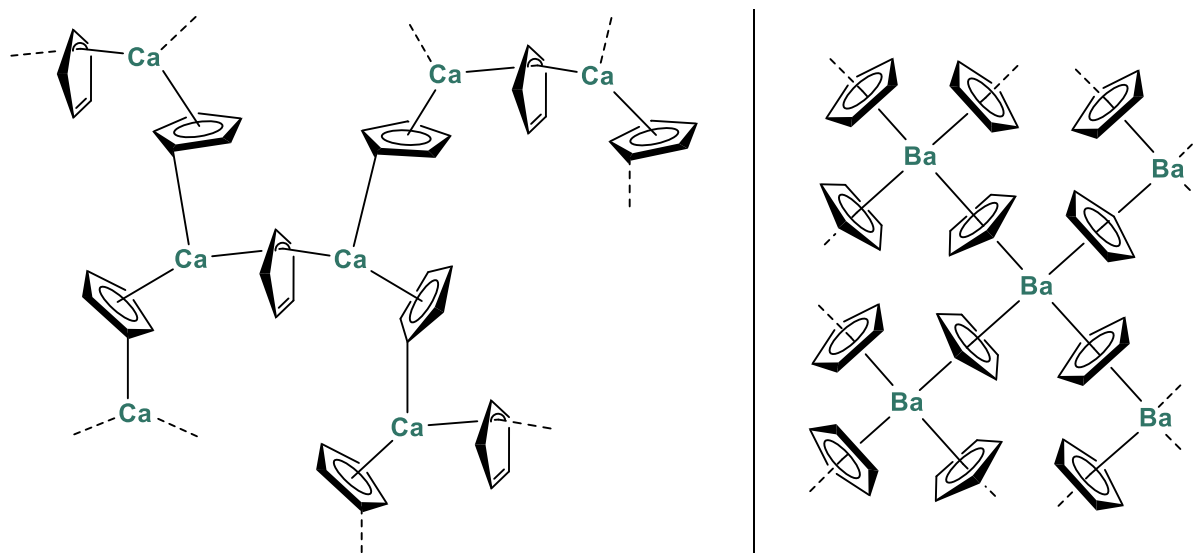


Figure 5: Left: polymeric molecular structure of calcocene; right: polymeric molecular structure of barocene.^[44,64]

In general, metallocenes of alkaline earth metals are well established and investigated, nowadays and a broad number of group 2 metallocenes with different substitution patterns is known. In terms of utility, alkaline earth metallocenes have found different applications in material science and can be used as Cp-transfer reagents. They are starting materials for the synthesis of many different cyclopentadienyl transition metal complexes^[30,57,65–67] as well as for *p*-block based cyclopentadienyl compounds.^[30,57,68] Furthermore, group 2 metallocenes are useful in chemical vapor deposition, where they are starting compounds for alkaline earth metal containing materials. Beryllocene has been used in the beam epitaxy to dope an InP semiconductor^[69] and as a starting material for the coating of capsules.^[70] Magnesiumocene is a commonly used starting compound in the deposition of MgO^[71] or found application as a *p*-type doping agent of semiconductors, for example GaAs.^[72] To obtain polycrystalline films of CaF₂ on glass or silicon surfaces, decamethylcalcocene and SiF₄ are used in a chemical vapor deposition.^[73] On rare occasions, strontocene and barocene have also been applied in chemical vapor deposition. These compounds are used in the deposition of SrTiO₃ and BaTiO₃ films.^[74,75] Usage of group 2 metallocenes in homogeneous catalysis is limited to calcocene catalysts in the polymerization of methyl methacrylate,^[76,77] and the related CpMgCl as a procatalyst for olefin polymerization.^[78]

1.2 Alkaline Earth Metallocenophanes

There are different possibilities to functionalize the cyclopentadienyl ring in sandwich complexes, of which various examples are mentioned in chapter 1.1 (*vide supra*). The substitution of both cyclopentadienyl moieties with an *ansa*-linker, thus interlinkage of the Cp rings, leads to so called *ansa*-metallocenes, also known as metallocenophanes (Figure 6). The common nomenclature for *ansa*-metallocenes specifies the bridging motif, by giving the elements of the *ansa*-bridge, followed by a number in square bracket that indicates the number of bridging atoms. For instance, a Si[2]magnesocenophane is a magnesocenophane, with the two cyclopentadienyl ligands bridged by two silicon atoms.

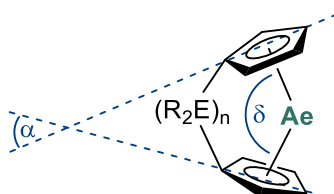


Figure 6: Schematic representation of a metallocenophane and the most relevant angles.^[79]

When the *ansa*-bridging motif is relatively short (e. g. one or two atoms), it usually results in a bent – non-coplanar – structure. In case of iron and some other transition metal metallocenophanes, these molecules can exhibit significant ring-strain, due to the strong covalent bond between the central atom and the two Cp moieties and their tendencies for a coplanar sandwich-type arrangement. In these cases, the ring strain can be estimated by the dihedral angle α between the Cp planes or the angle δ between Cp^{centroid}-metal-Cp^{centroid} (Figure 6). Furthermore, due to their ring strain, strained metallocenophanes, such as [1]ferrocenophanes, can be employed as monomers in ring-opening polymerizations.^[80] On the other hand, the ring strain in group 2 metallocenophanes is most likely not as large as in transition metal metallocenophanes, due to the relatively ionic bonding between the alkaline earth metal and the Cp rings.

Similar to the unbridged metallocenes, the first metallocenophanes were iron complexes, thus ferrocenophanes, but for over 50 years, *ansa*-metallocenes containing various transition metals as central atoms have been studied.^[81–85] Different transition metal metallocenophanes have been used in industrial olefin polymerization,^[86–89] and as mentioned before, depending on the bent geometry and the induced ring strain, some transition metal metallo-

nophanes are potent monomers for ring opening polymerization. Many examples of such ring opening polymerization reactions of ferrocenophanes,^[80,90–94] cobaltocenophanes,^[95] nickelocenophanes,^[96–99] ruthenocenophanes^[100–102] and further transition metal metallocenophanes^[103,104] are described in literature. Unlike main group metallocenes, main group metallocenophanes are much younger than their transition metal analogues. In the mid-1980s, some *p*-block metallocenophanes have been described followed by reports of *s*-block-based metallocenophanes in the early 1990s of the last century.^[79] In addition to different substituents at the cyclopentadienyl moiety, the length of the *ansa*-bridge as well as the bridging atoms can vary. While many different bridging motifs are known in transition metal metallocenophanes,^[84] *s*-block metallocenophanes exhibit exclusively one- and two-atomic *ansa*-bridging motifs.^[53,79] More than twenty metallocenophanes containing cyclopentadienyl ligands and alkaline earth metals, are described in literature (Figure 7 and Figure 8).^[53,79] Most of these compounds are magnesocenophanes or calcocenophanes, and until now, no beryllocenophane exists. Furthermore, metallocenophanes of the heavier alkaline earth metals strontium and barium are rare.^[53,79] In addition, a number of [1]- and [2]-metallocenophanes of group 2 metals containing indenyl or fluorenyl moieties are known, but only metallocenophanes with Cp rings are discussed in this chapter.

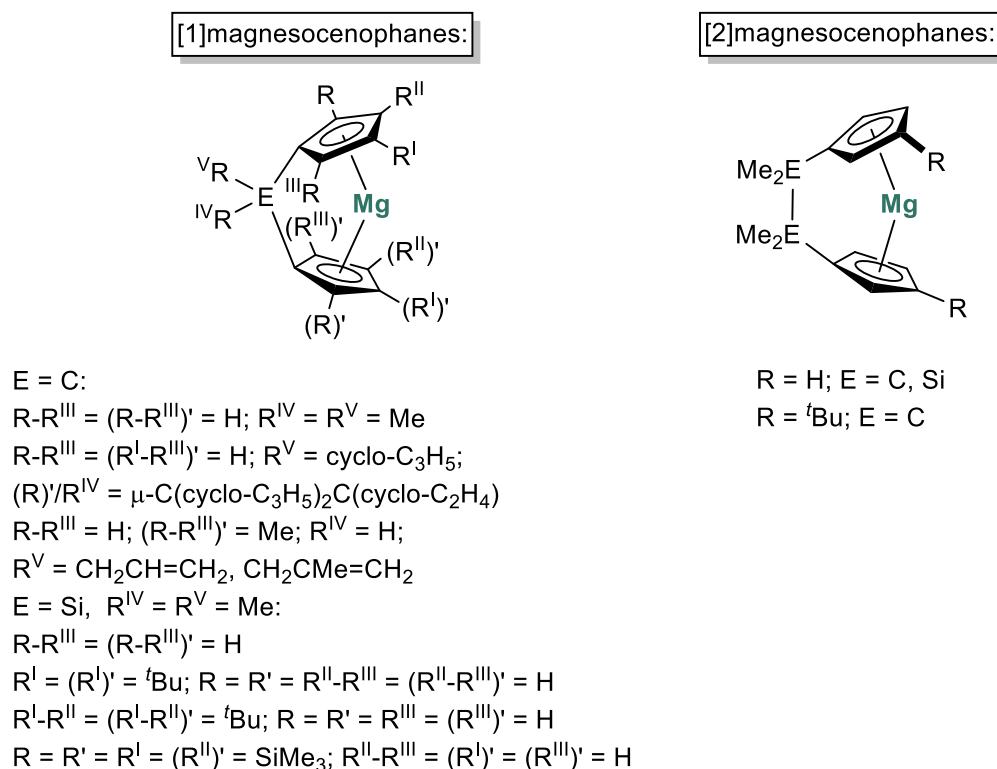


Figure 7: Selected examples of [1]- and [2]magnesocenophanes.^[53,79,105–114]

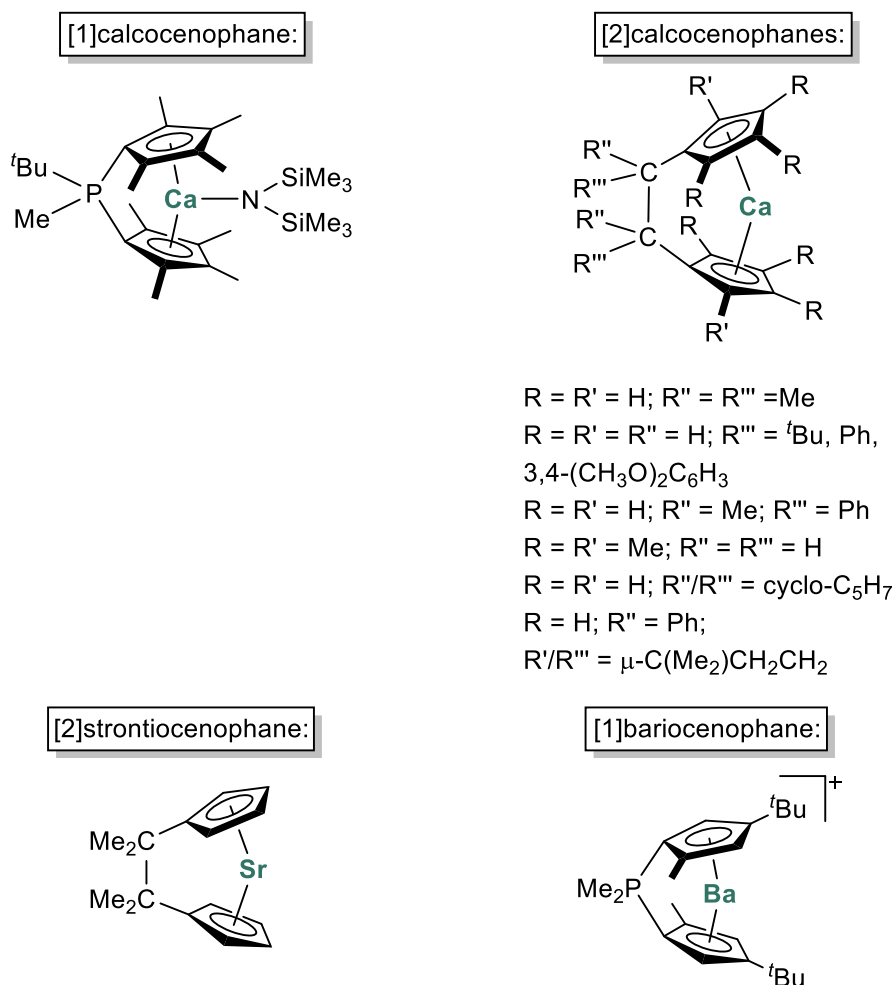
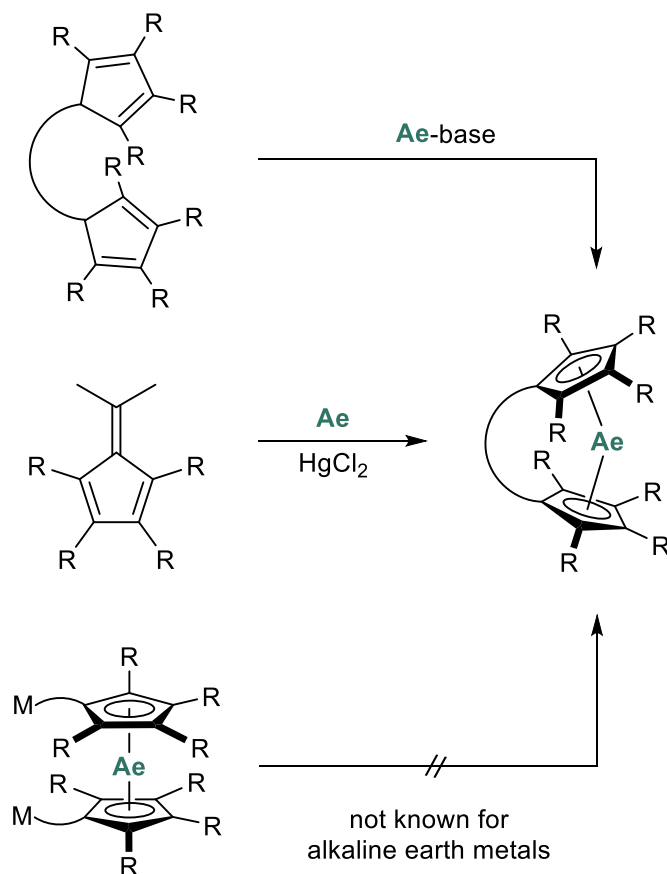


Figure 8: Selected examples of [1]- and [2]metallocenophanes of alkaline earth metals.^[34,53,79,115–124]

Noteworthy, a review, summarizing main group metallocenophanes, has been published in the course of this doctoral thesis.^[79]

Different synthetic routes for metallocenophanes are known to the literature (Scheme 7). The most common method is starting with a neutral *ansa*-ligand system and introducing the metal center by deprotonation with a suitable alkaline earth metal base. In the synthesis of magnesocenophanes, in most cases, dibutylmagnesium is used as base, as Burger and coworkers first described it in 1997. Starting with 2,2-dicyclopentadienylpropane they obtained the first magnesocenophane after treatment of the protonated ligand with dibutylmagnesium.^[105–107] Many [1]- and [2]magnesocenophanes have been prepared via the same route since then.^[108–112] In addition to dibutylmagnesium, Grignard reagents^[114] and other magnesium bases^[113] also found application in the magnesocenophane synthesis. To synthesize the heavier analogues, especially [1]metallocenophanes, the corresponding bis(trimethylsilyl)amides have been used as bases for the deprotonation of the ligand.^[118,123]

For instance, Hanusa and coworkers reported the reaction of cyclopentadienylphosphafulvene with calcium bis(trimethylsilyl)amide to obtain a phospho[1]-bridged calcoce-nophane.^[123]



Scheme 7: Common synthetic routes for the synthesis of group 2 metallocenophanes.^[85]

Another common synthesis of C[2]metallocenophanes of calcium and strontium, is the oxidative fulvene coupling. Edlmann and coworkers reported the first synthesis of C[2]calcoce-nophane and C[2]strontiocenophane via this route.^[115] Activated calcium and fulvene were reacted in a donor solvent like thf.^[115] This synthetic method often suffers from low yields, due to the fact that cyclopentadienyl radicals are formed in the initial step which can cause the formation of undesired byproducts. For instance, Shapiro *et al.* described the formation of C[2]calcoce-nophane and diisopropylcalcocene after the reaction of 6,6-dimethylfulvene with activated calcium.^[34] This synthetic route is well established and exclusively employed for the formation of C[2]calcoce-nophanes^[34,115–117,119–122,124] and the only known strontiocenophane.^[115] Since the oxidative coupling of fulvenes is restricted to the

formation of carba[2]-bridged metallocenophanes, [2]-bridged calcocenophanes with other elements than carbon in the *ansa*-bridge are less explored. Due to the lack of commercially available and easy applicable starting materials for the heavier alkaline earth metals, metallocenophanes of strontium and barium are rare.^[115,118] Moreover, introducing the *ansa*-bridge into an existing metallocene displays another synthetic method for metallocenophane synthesis. However, until now, this route is not known for the synthesis of group 2 metallocenophanes, but has only been used in transition metal metallocenophane chemistry.^[53,79]

In general, many metallocenophanes of alkaline earth metals possess a poor solubility in apolar solvents but are well soluble in donor solvents like thf or dme. Due to their Lewis acidic central atom, donor-solvent molecules and other donors can coordinate at the alkaline earth metal center. Consequently, all structurally characterized alkaline earth metallocenophanes contain donor-solvent molecules except for two calcocenophanes, of which one is coordinated by an aldimine^[115] and the other possesses an amide at the central atom.^[123] Depending on the size of the central atom and the steric demand of the cyclopentadienyl rings, it is possible that one or two solvent molecules coordinate to the central atom, and on rare occasions, complexes with three donor molecules have been observed (Figure 9). Furthermore, this phenomenon is of course also influenced by the structure and size of the coordinating donor molecule.

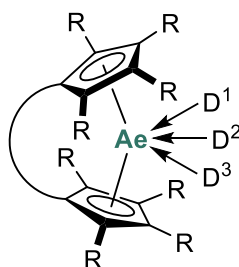


Figure 9: Schematic representation of a metallocenophane with coordinating donors D.

Due to the small coordination sphere at the magnesium atom, the coordination of more than two donors at the central atom is not known. The larger coordination sphere of calcium and barium allows for the coordination of up to three donor moieties to the central atom. For instance, Shapiro and coworkers isolated a C[2]calcocenophane bearing two dme molecules^[121] and Brintzinger *et al.* reported of a P[1]bariocenophane with three thf molecules coordinated to the central atom (Figure 10).^[118]

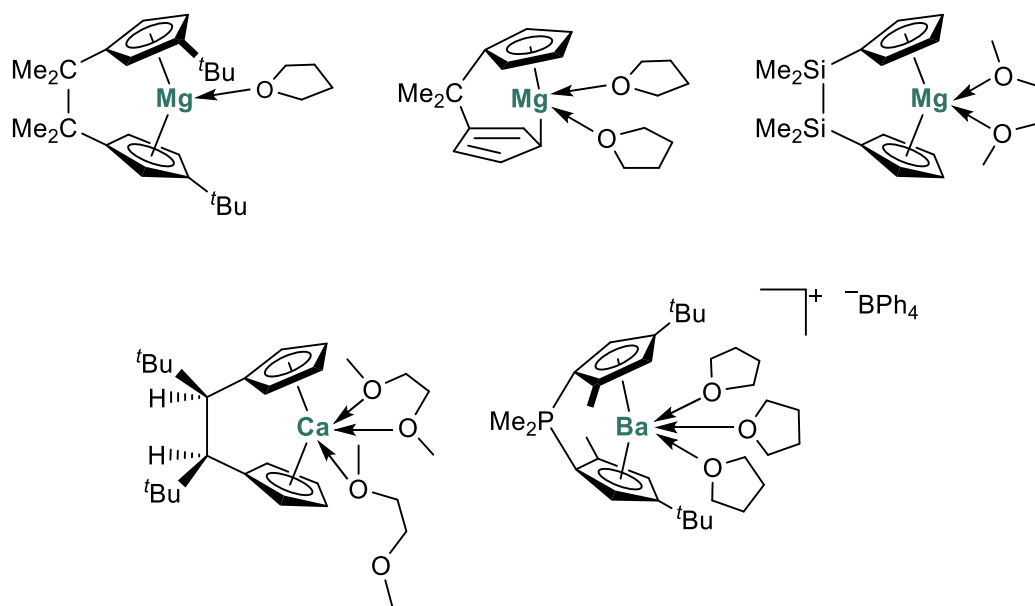


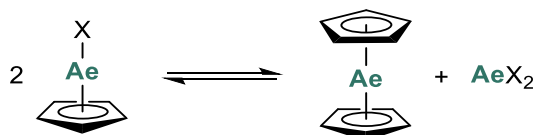
Figure 10: Selected examples of [1]- and [2]metallocenophanes with different donor-solvent molecules.^[105–107,110,111,118,121]

Structurally, group 2 metallocenophanes possess similar properties as their metallocene parent compounds discussed before (*vide supra*). Although, a number of structurally characterized group 2 metallocenophanes exists, these structures are without exception of solvent complexes, and there is no experimentally determined solid-state structure of a group 2 metallocenophane without any additional ligands coordinated to the central atom. However, these ligands can have a big influence on the structure. For instance, the coordination of thf to the central magnesium atom in [1]magnesocenophanes results in ring slipped structures in the solid-state, with one Cp ring bonded in an η^1 or η^2 fashion and the other in an η^5 fashion to the magnesium atom.^[105–108,111,113] The strontiocenophane described in literature, is the only known *ansa*-metallocene of strontium and is not structurally characterized until now.^[53,79,115]

With regard to the application of group 2 metallocenophanes, the compounds have been known to the literature for several decades, and have mainly been used as Cp transfer reagents in transmetalation reactions to synthesize *p*-block and transition metal metallocenophanes.^[57,107,109,110,119]

1.3 *ansa*-Half-sandwich complexes of alkaline earth metals

There are many known alkaline earth metal complexes of the type CpAeX/CpAeR that contain only one cyclopentadienyl moiety. In addition to the cyclopentadienyl ring, these half-sandwich complexes can possess a variety of ligands, such as, halogens (Grignard-type compounds),^[125–127] alkyl groups,^[25,113,128] amide groups,^[129] or β -diketiminato groups.^[130] As mentioned in chapter 1.1, the half-sandwich complexes CpAeX/CpAeR exist in the Schlenk equilibrium with the homoleptic Cp₂Ae and the AeX₂/AeR₂ species (Scheme 8), and homoleptic metallocenes can be isolated by sublimation and removed from the equilibrium. In particular, the isolation of the heteroleptic species CpAeX from the equilibrium is more difficult.^[126,131] For instance, Westerhausen *et al.* investigated the Schlenk equilibrium for CpMgBr and the corresponding homoleptic species. The reaction of cyclopentadiene with an *in situ* generated Grignard led to the formation of CpMgBr, which is dimeric in the solid-state. In solution, at high temperatures above 353 K, the authors observed the homoleptic magnesocene as the dominating species.^[9] Noteworthy, in this particular case, the authors were able to structurally characterize all components present in the Schlenk equilibrium (Scheme 8).^[27,53,127,132–135]



Scheme 8: Schlenk-type equilibrium of CpAeX species in solution.^[9,126,131]

In addition to the earlier described half-sandwich complexes, *ansa*-half-sandwich complexes are also known. In these complexes, the cyclopentadienyl ligand is linked via a silyl- or alkyl-bridge to the second substituent. Generally, this group is often a nitrogen-based substituent, such as an amino, amido, pyrazole or oxazole group. The *ansa*-half-sandwich ligands may be separated into two groups: monoanionic and dianionic ligands. In monoanionic *ansa*-half-sandwich ligands, only the Cp moiety of the neutral ligand can be deprotonated. In dianionic ligands, the donor group, for example an amine group, can also be deprotonated in addition to the Cp moiety (Figure 11). In this chapter, only *ansa*-half-sandwich complexes containing cyclopentadienyl ligands are mentioned. Compounds with indenyl or fluorenyl ligands are not considered.

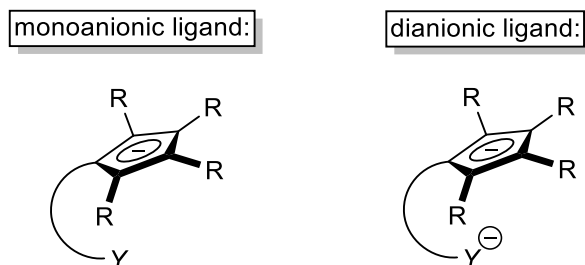
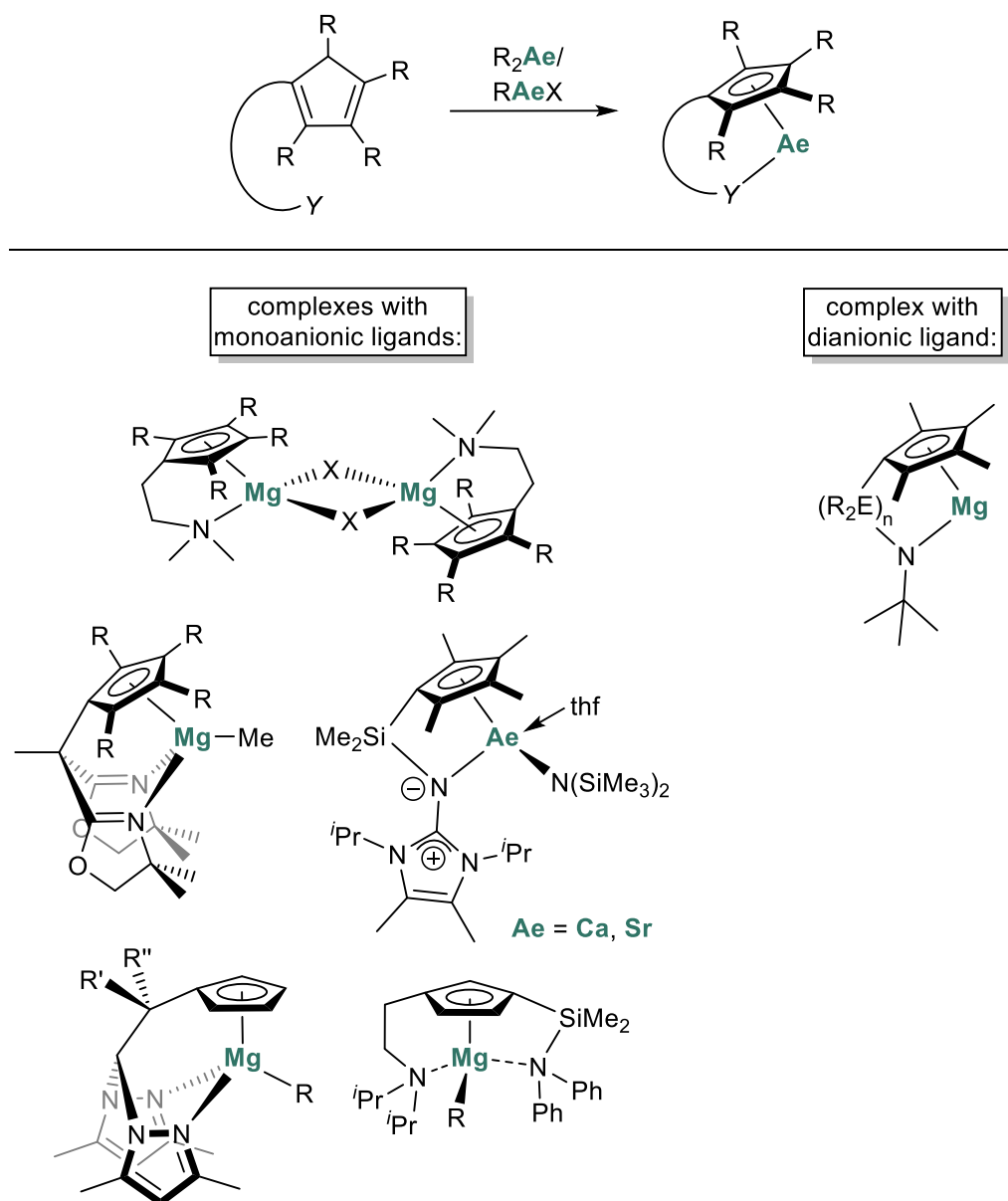


Figure 11: General structure of monoanionic and dianionic *ansa*-half-sandwich ligands.

In transition metal chemistry, such *ansa*-half-sandwich ligands are quite common,^[136–139] and the corresponding complexes, also referred to as constrained geometry complexes, are used in homogeneous catalysis such as olefin polymerization.^[139–141] Furthermore, these *ansa*-half-sandwich transition metal complexes even play an important role in industrial processes.^[142] However, such *ansa*-half-sandwich complexes of alkaline earth metals are nearly unexplored and only a few examples were known prior to this thesis. These complexes are generally synthesized via two different synthetic methods. For one, the neutral or metalated ligand may be reacted with different Grignard reagents.^[143–145] In 1995, Jutzi and coworkers received a bromide bridged dimer via this route that could be obtained as a donor stabilized monomer upon addition of thf.^[143] Furthermore, Otero and coworkers synthesized different scorpionate cyclopentadienyl complexes with this method.^[144,145] The other possible reaction route is the deprotonation of the neutral ligand with a corresponding alkaline earth metal base, for example, dialkylmagnesium,^[146,147] dibenzylmagnesium^[148] or alkaline earth metal amides.^[149,150] In addition to different reported mono- and di-bridged magnesium *ansa*-half-sandwich complexes,^[146–148] Tamm and coworkers reported calcium- and strontium-based complexes (Scheme 9).^[149,150]



Scheme 9: Synthesis of alkaline earth metal *ansa*-half-sandwich complexes and selected examples thereof.^[143–150]

These group 2 *ansa*-half-sandwich complexes generally exhibit similar structural features as the afore discussed metallocenophanes, with the cyclopentadienyl rings are usually bonded in an η^5 fashion to the alkaline earth metal.^[143–146,149,150]

With regards to their applicability, these complexes are mostly used as transmetalation reagents,^[144,147] and in some rare examples as catalysts in different reactions. For instance, the magnesium based scorpionate cyclopentadienyl complexes reported by Otero and coworkers were found to be versatile catalysts in (ring opening) polymerizations,^[144,145] and Sadow and coworkers used their scorpionate cyclopentadienyl magnesium compound as catalyst in

intramolecular hydroamination reactions.^[146] Similarly, the doubly linked magnesium complex reported by Cano and coworkers was applied in intramolecular hydroamination as well.^[148] However, application of these group 2 constrained geometry complexes in catalysis was very limited prior to the work of this thesis, which is surprising given the fact that their transition metal analogues are quite popular in catalytic transformations.

1.4 Magnesium catalysis

1.4.1 Preface – Magnesium in catalysis

Approximately 90% of the products of the chemical industry pass through at least one catalytic step in their production. Regarding sustainability, efficient catalysts and reactions with high atom economy play a tremendously important role. Catalytic reactions with high selectivity cause fewer byproducts and are economically advantageous as well as environmentally friendly.^[151] Generally, transition metals are used in catalysts for industrial processes, but due to their high abundance in the earth's crust and low carbon footprint, s-block metals have attracted much attention in the recent past as promising alternatives to transition metals. Magnesium, for example, is playing an increasingly important role, not only because of its use in Grignard reagents. In contrast to many transition metals, magnesium is one of the most abundant metals in the earth's crust (Figure 12).^[152,153]

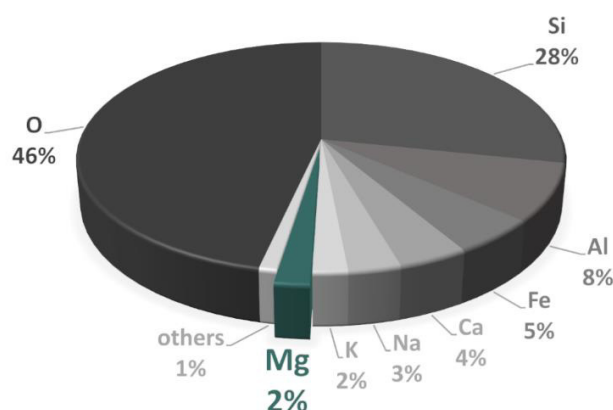


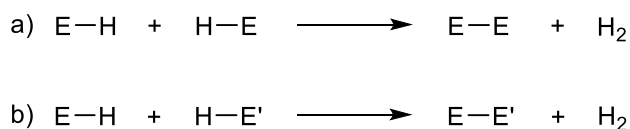
Figure 12: Distribution of the most common elements of the earth's crust.^[153]

In addition to its high abundance, the production of magnesium is environmentally friendlier than the production of many transition metals. For instance, the global warming potential of magnesium is significantly lower than that of rhodium, iridium, palladium and several other transition metals.^[154] This is because the cumulative energy demand of magnesium is not as high as for transition metals commonly used in catalysis. Another important advantage of magnesium is the low human toxicity, high biocompatibility respectively. Transition metals on the other hand can possess high toxicities.^[154] Considering these aspects, magnesium is a highly interesting metal for catalytic applications with regards to sustainability and environmental aspects.

In the following chapters, magnesium catalysis relevant to this thesis will be discussed.

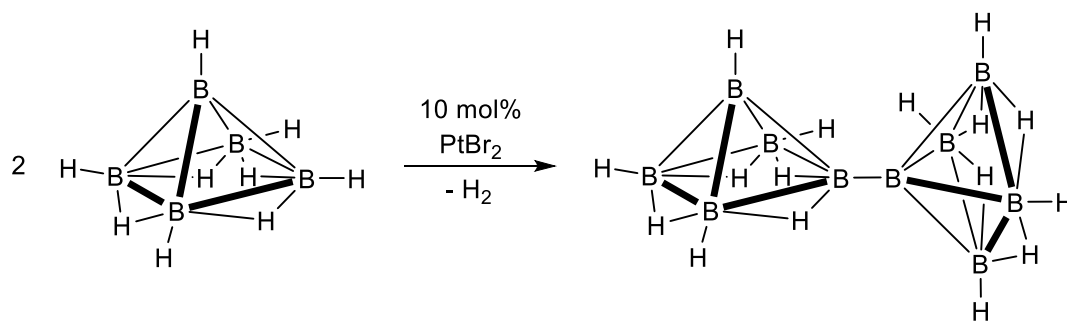
1.4.2 Dehydrocoupling catalysis

Dehydrocoupling reactions are condensation-type reactions in which element-element bonds are formed under elimination of hydrogen. This reaction type is useful for a large variety of *p*-block element hydrides and since hydrogen is the only byproduct, dehydrocoupling reactions usually exhibit high atom economies. Dehydrocoupling reactions are commonly distinguished between homo- and hetero-dehydrocoupling (Scheme 10). If the reaction takes place between two identical elements, the dehydrocoupling is referred to as homo-dehydrocoupling, while if the bond formation occurs between two different elements, it is referred to as hetero-dehydrocoupling, also known as cross-dehydrocoupling.



Scheme 10: a) Homo-dehydrocoupling; b) hetero-dehydrocoupling.

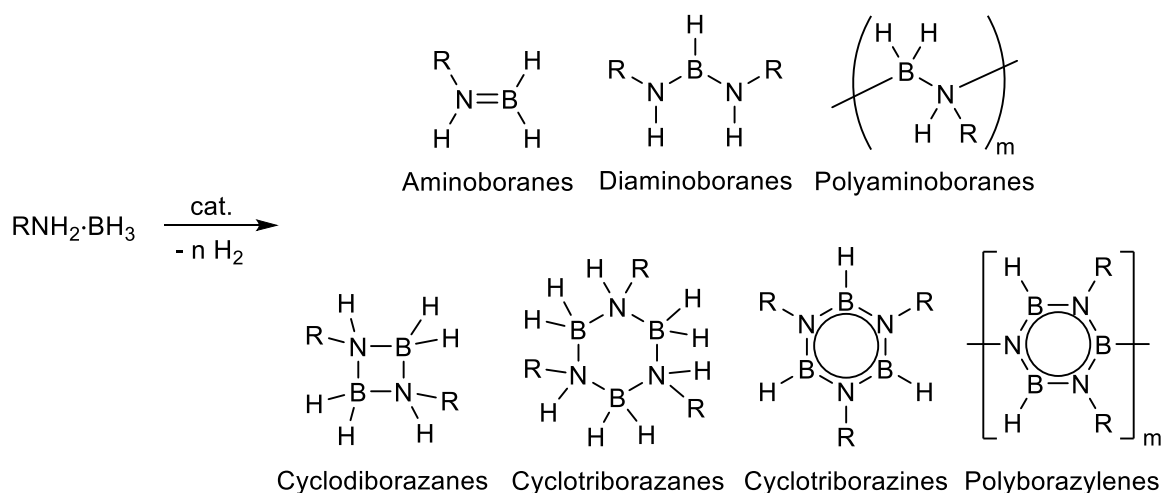
An important supportive effect for cross-dehydrocoupling is the difference in electronegativity between the element hydride substrates. Relatively electronegative elements result in the hydrogen atom to have a protic character and *vice versa*. Amines, for example, have such a polarization, with the hydrogen atom having a protic character, while in boranes or silanes the hydrogen atom has a hydridic character. Dehydrocoupling reactions can proceed under catalytic conditions, or in some cases without a catalyst. For instance, sometimes heating the reaction is sufficient to form the element-element bond and facilitate the release of hydrogen, especially if there is a difference in electronegativity of the substrates.^[155] In principle, dehydrocoupling reactions have been known for a long time. For example, the thermal decomposition of monosilane SiH_4 into elemental silicon and hydrogen was reported in 1880 by Ogier.^[156] Although the dehydrogenation of main group hydrides is known since then, the term “dehydrocoupling” was not established until 100 years later. In 1984, Sneddon and coworkers reported a dehydrodimerization of a pentaborane cluster catalyzed by a platinum(II)-catalyst. The liquid pentaborane was stirred over PtBr_2 powder resulting in hydrogen evolution and B-B coupling (Scheme 11).^[157]



Scheme 11: Dehydrodimerization of a pentaborane cluster.^[157]

One year later, the authors described additional dehydrogenative reactions of diboranes with carboranes and boranes. This was the first time, Sneddon *et al.* made use of the term “dehydrocoupling”.^[158] The traditionally used reactions for E-E or E-E' bond formation in *p*-block chemistry (with the exception of carbon) are salt metathesis, reductive couplings and high temperature condensation reactions. In contrast to these traditionally conducted reactions, the catalytic dehydrocoupling displays significant advantages as it often offers better control of the reaction process and higher selectivity.^[159,160] The importance of dehydrocoupling reactions increased because of the relevance of element-element bond formations between different main group elements for inorganic chemistry. Today, the catalytic dehydrocoupling is used for the formation of a large number of main group element-element bonds, such as B-N, B-P, B-O, Al-N, C-Si, Si-N, Si-P, Si-O, Si-S, Ge-P, Sn-Te, N-P, P-O, P-S.^[159–164] The focus in this chapter is placed on the B-N and Si-N bond formation, since these are most relevant for this thesis. Other examples are not discussed in detail.

B-N materials have gained significant importance in inorganic and materials chemistry in the recent past.^[165–169] Therefore, easy access and simple preparation methods are required. As a precursor for these materials, amine boranes have attracted great attention for B-N based polymers as well as ceramics and other materials.^[166–173] Furthermore, some amine boranes also possess potential as solid hydrogen storage materials.^[171–174] Although amine boranes can release hydrogen by thermal induction, these reactions often require high temperatures and can give undesired byproducts and/or ill-defined product mixtures.^[172] Catalytic dehydrocoupling reactions can prevent the formation of undesired byproducts, as they are generally more selective. Depending on the catalyst and the substrates, a number of coupling products can be generated via dehydrocoupling (Scheme 12).^[164]



Scheme 12: Overview of common coupling products of amine borane dehydrocoupling.^[164]

As the catalytic dehydrocoupling of amine boranes generally offers selective conversion without undesired byproducts, many catalysts for this reaction type have been developed over the course of the last decade, most of which are transition metal-based.^[159,160,162,175–177] The first metallocene-based catalyst was a titanocene compound, reported by Manners and coworkers for the dehydrocoupling of dialkylamine boranes.^[178] In contrast to transition metal-based catalysts, there are only few *s*- and *p*-block-based catalysts.^[176,177,179–181] Moreover, only a few magnesium-based catalysts for amine borane dehydrocoupling reactions had been reported prior to this thesis (Figure 13).^[182–186]

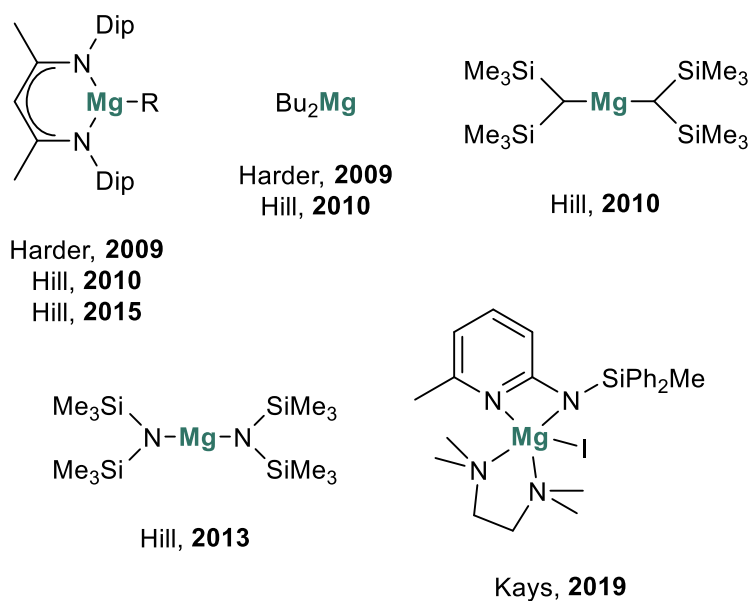
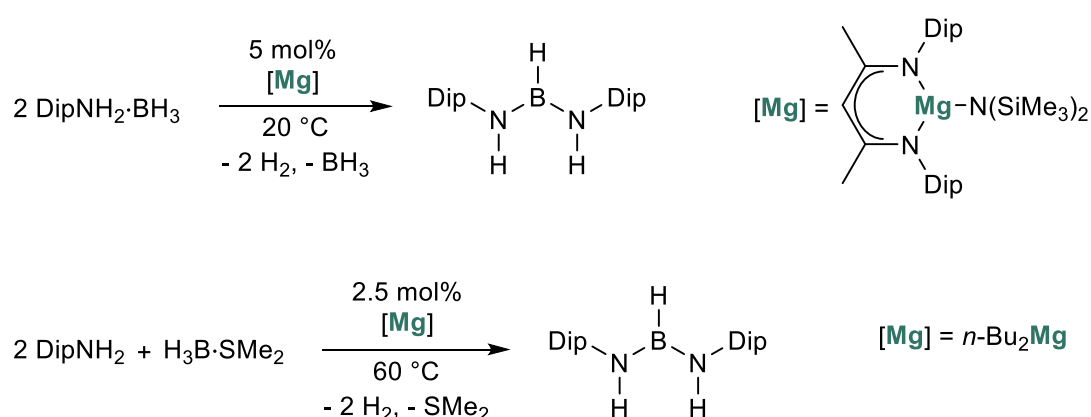


Figure 13: Selected examples of magnesium-based (pre)catalysts for amine borane dehydrocoupling.^[182–186]

Harder and coworkers described the application of a 1,3-diketimine magnesium compound as a catalyst for the dehydrocoupling of 2,6-di*i*sopropylphenylamine borane. With a catalyst loading of 5 mol%, the authors were able to obtain the corresponding bis(amino)borane. The same product, but without BH₃ as a byproduct, could be obtained by using two equivalents of 2,6-di*i*sopropylamine and one equivalent of borane dimethylsulfide under catalytic conditions. Using dibutylmagnesium as precatalyst with a catalyst loading of 2.5 mol% was also found to be possible, but only at higher temperatures, to prevent the precipitation of Mg-BH₄ (Scheme 13).^[182]

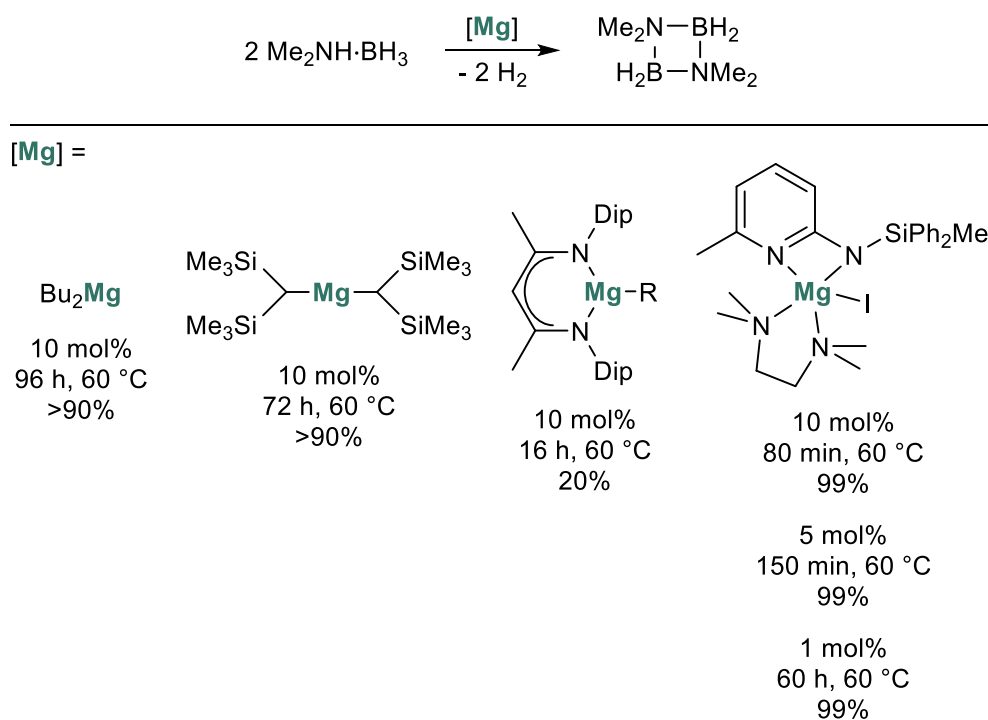


Scheme 13: Formation of a bis(amino)borane via magnesium-catalyzed dehydrocoupling reactions.^[182]

The dehydrocoupling of dimethylamine borane catalyzed by magnesium-based catalysts was first described by the working group of Hill. Dialkylmagnesium complexes were used as precatalysts. The authors achieved more than 90% conversion after 72 to 96 h, at reaction temperatures above 60 °C and with a catalyst loading of 10 mol%. Attempts to catalyze this reaction with a 1,3-diketimine magnesium complex as catalyst gave only 20% conversion after 16 hours at 60 °C (Scheme 14),^[183] and any attempt to facilitate the reactions at ambient condition seemingly failed. Although this catalytic performance was rather poor, Hill and coworkers conducted stoichiometric reactions between the magnesium compounds and the amine boranes and were able to isolate magnesium complexes with the coordinated amido boranes, which gave some insights into the mechanism.^[187,188] Furthermore, the Hill group tried to prepare an asymmetrical bis(amino)borane, by reacting a dialkylamine borane with a dialkylamine in a dehydrocoupling reaction, catalyzed by magnesium bis(trimethylsilyl)amide. With less or no heating and a catalyst loading of 2.5 mol%, Hill *et al.* obtained several asymmetric bis(amino)boranes.^[184] A few years later, Kays and coworkers reported a much more

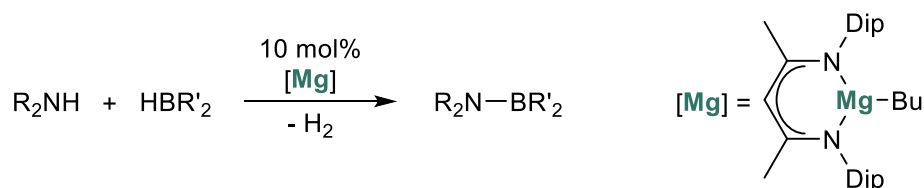
1.4 Magnesium catalysis

efficient magnesium catalyst for the dehydrogenation of dimethylamine borane. With lower catalyst loadings and shorter reaction times than in the previous work of Hill *et al.*, the authors were able to isolate the products with full conversions, although elevated temperatures of 60 °C were still required (Scheme 14).^[186]



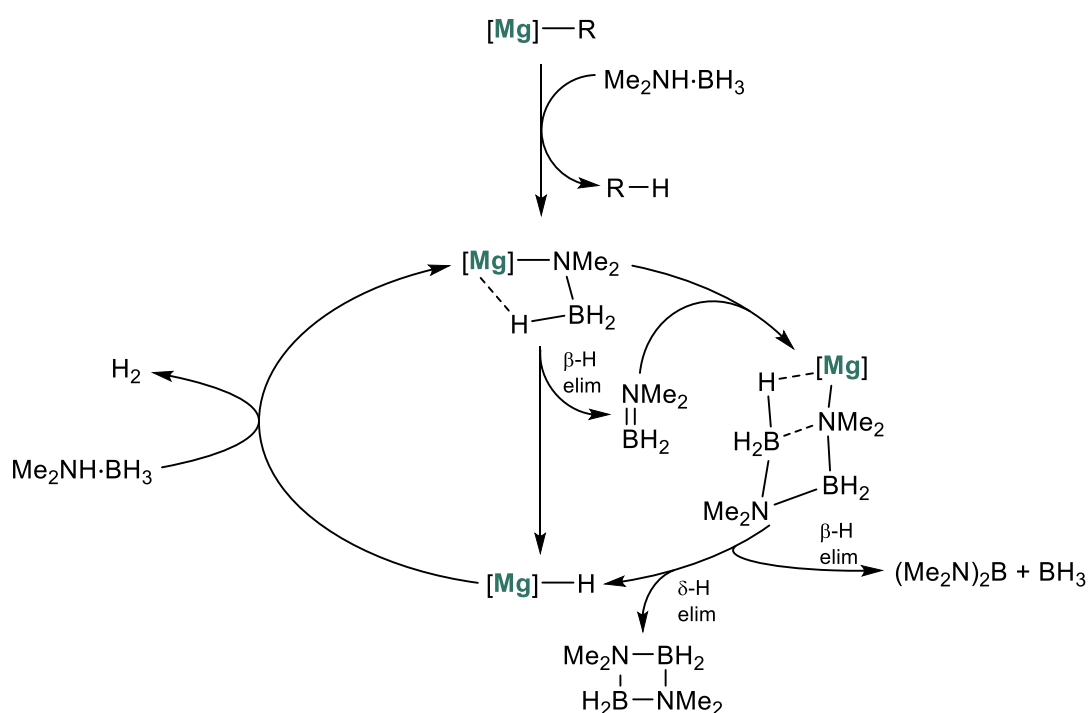
Scheme 14: Dehydrocoupling of dimethylamine borane catalyzed by different selected magnesium complexes.^[183,186]

In addition to using preformed amine borane adducts as starting materials, it is also possible to use amines and stable boranes separately. Hill and coworkers reported the dehydrocoupling of several amines and pinacolborane or 9-BBN, catalyzed by a β -diketiminato magnesium-alkyl compound. Under ambient conditions, the catalytic reactions take place in less than one hour and several amines could be coupled to pinacolborane (Scheme 15).



Scheme 15: Intermolecular amine borane dehydrocoupling catalyzed by a magnesium 1,3-diketimine.^[185]

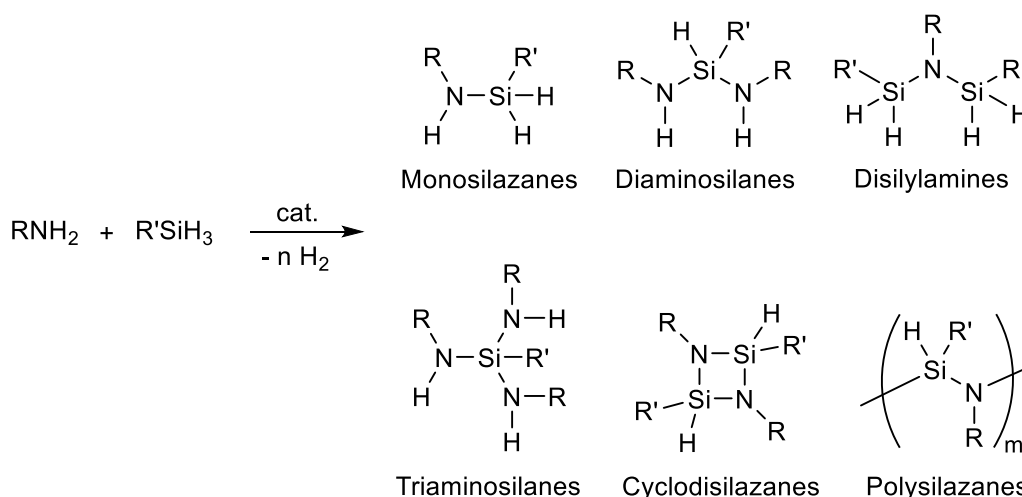
In some cases, the reactions between amines and 9-BBN required temperatures of 60 °C and a reaction time of six days to get at least 70% conversion.^[185] Although relatively little is known about the exact mechanisms of these magnesium-catalyzed amine borane dehydrocoupling reactions, there are some mechanistic proposals by the working groups of Hill and Kays.^[183,186] The authors postulate a mechanism starting with the formation of an amidoborane coordinated to the catalyst. After a β -hydride elimination, the generated aminoborane is able to insert into the Mg-N bond of the catalyst amidoborane complex. As a consequence, the catalyst is coordinated by an anionic linear diborazane moiety. This complex undergoes a δ -hydride elimination. The observed diborazane is formed and the magnesium hydride catalyst is regenerated (Scheme 16).^[164,183,189]



Scheme 16: Proposed mechanism for the dehydrocoupling of amine boranes postulated by Hill *et al.*^[164,183,189]

Kays and coworkers proposed a similar mechanism for the dehydrocoupling of dimethylamine borane, with the difference that no magnesium hydride species is formed. Furthermore, the authors assumed that their used magnesium compound acts as a catalyst and not as a precatalyst.^[186] Prior to the work within the scope of this thesis, no further magnesium-based catalysts for amine borane dehydrocoupling had been reported.^[189]

In material science and organic chemistry, the formation of Si-N bonds is of great interest. In organometallic chemistry, polysilazanes have found application as ligands and silylation agents.^[190–192] Furthermore, Si-N compounds are used as precursors for ceramics and Si-N-based polymers.^[193,194] Similar to the traditional reaction routes of B-N compounds, the formation of Si-N bonds is difficult and often causes undesired byproducts. Usually, halosilanes and metal amides or amines are reacted to obtain monosilazanes, disilylamines and diaminosilanes. During these reactions, coupling products, such as metal halide salts or hydrogen halides, are formed, which have to be separated from the products.^[195–197] Dehydrocoupling reactions are more efficient in the formation of Si-N bonds, as only hydrogen as by-product is formed.^[159,162,164,198–200] In addition, dehydrocoupling reactions can produce a number of coupling products such as monosilazanes, disilylamines, diaminosilanes, triaminosilanes, cyclic disilazanes and polysilazanes (Scheme 17). The selectivity of the reaction is thereby influenced by the catalyst as well as the reaction conditions.



Scheme 17: Possible coupling products of the amine silane cross-dehydrocoupling.^[164]

Similar to the catalytic dehydrocoupling of amine boranes, catalysts for amine silane dehydrocoupling are generally transition metal-based,^[199–205] but the interest in alkaline earth metal-based catalysts has increased in the last years. Several groups reported the application of alkaline earth metal complexes in the dehydrocoupling of amines and silanes in the recent past, including some magnesium (pre)catalysts (Figure 14).^[199,200,206–216]

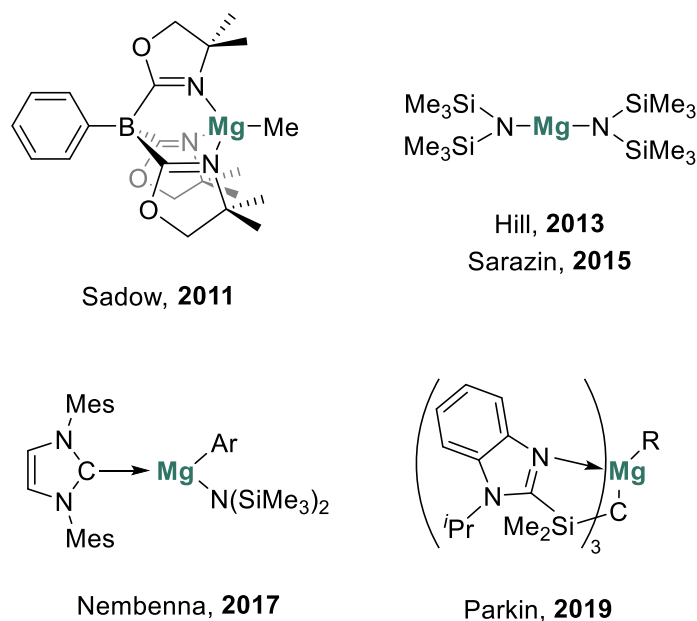
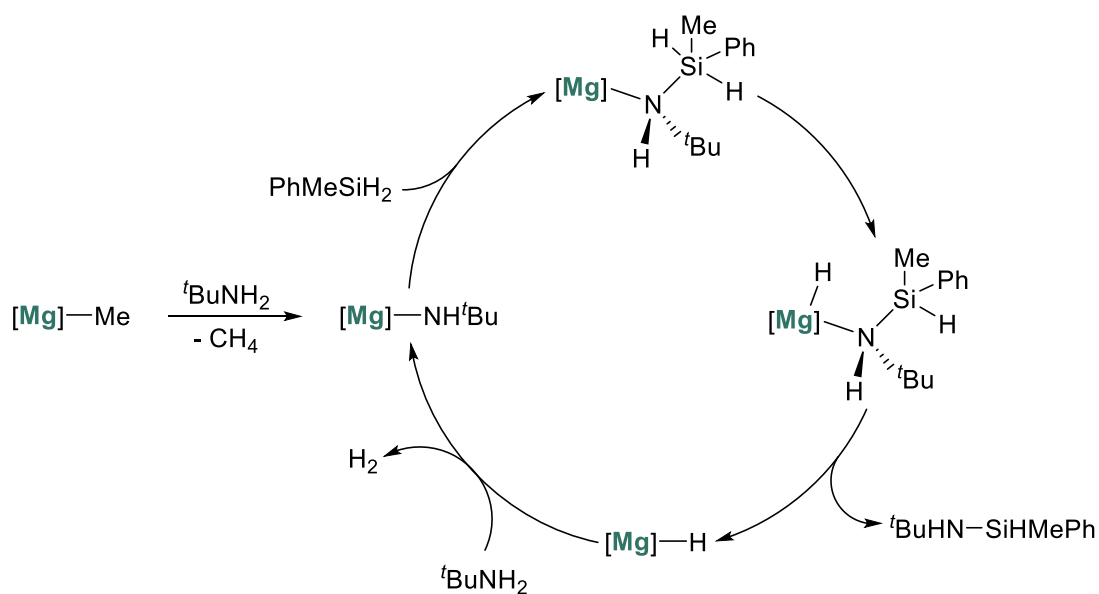


Figure 14: Selected examples of magnesium-based (pre)catalysts for the amine silane cross-dehydrocoupling.^[206–210]

The first report of a magnesium-based catalyst for Si-N bond formation was published in 2011 by Sadow and coworkers, who introduced a tris(oxazolonyl)boratomagnesium complex that could catalyze the dehydrocoupling between several amines and silanes.^[206] At room temperature, the authors were able to couple primary aliphatic amines with primary or secondary silanes and obtained high conversions. Higher temperatures were required for the dehydrocoupling of aromatic amines with silanes. The good selectivity of the catalyst and the high conversions were dependent on the employed equivalents of the substrates. Furthermore, secondary amines gave only little to no conversion even at higher temperatures.^[206] A few years later, Hill *et al.* reported the use of magnesium bis(hexamethyldisilazide) as a (pre)catalyst in the dehydrocoupling of amines and silanes. The authors obtained conversions of $\geq 95\%$ at ambient conditions for the reaction between primary/secondary amines and primary/secondary silanes. The selectivity of the catalyst was however not as high as the selectivity of the afore mentioned tris(oxazolonyl)boratomagnesium complex, as Hill *et al.* obtained mixtures of monosilazanes and diaminosilanes. The dehydrocoupling of benzylamine and phenylsilane leads to an intractable mixture of higher oligomers. Moreover, the coupling of tertiary silanes and primary amines gave only low conversions, even at higher temperatures.^[207] This observation was later confirmed by Sarazin and coworkers, with the reaction of pyrrolidine and triphenylsilane in the presence of magnesium bis(hexamethyldisilazide), giving only 2% conversion after 15 hours.^[208] Nembenna *et al.* employed a magnesium(II) carbene complex in the dehydrocoupling between amines and silanes, with a relatively broad

substrate spectrum giving high conversions at a temperature range from room temperature to 100 °C.^[209] The magnesium(II) compound, used in the dehydrocoupling between amines and silanes by Parkin and coworkers, needed reaction temperatures above 100 °C and longer reaction times.^[210]

The mechanisms of these Si-N dehydrocoupling reactions are almost unexplored. Hill and coworkers proposed a stepwise mechanism for their system with a metal centered amine deprotonation followed by a metathesis step between the silane and the magnesium amide complex.^[189,207] Sadow and coworkers performed further investigations on the mechanism for the dehydrocoupling and proposed an analogous catalytic cycle for their magnesium precatalyst. The authors postulated the formation of a magnesium amide complex resulting from the reaction of the precatalyst with the amine. The nucleophilic attack of the magnesium amide at the silicon center results in the formation of an intermediate with a penta-coordinated silicon atom. This step is followed by rapid hydride transfer to the magnesium center and yields the silazane product coordinated to the magnesium center. Separation of the product leads to a magnesium hydride species that releases hydrogen after the reaction with another equivalent of amine to reform the magnesium amide complex (Scheme 18).^[189,200,206] Although, the mechanisms of the afore discussed systems are generally not well investigated, the mechanism proposed by Sadow *et al.* most likely also applies to other magnesium-based systems.

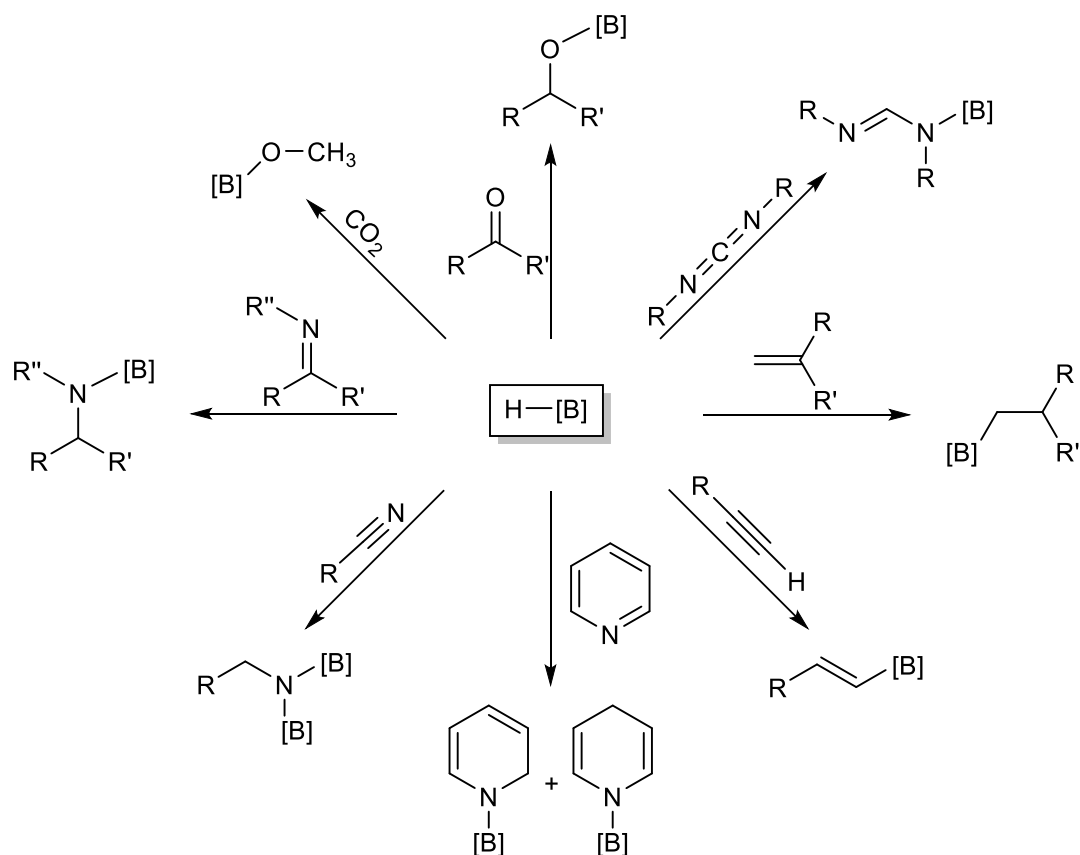


Scheme 18: Postulated catalytic cycle for the dehydrocoupling of *t*BuNH₂ and PhMeSiH₂ by Sadow *et al.*^[206]

Although dehydrocoupling is a powerful reaction class with a high atom economy, few magnesium catalysts are known for amine borane and amine silane dehydrocoupling. Generally, the catalysts that are known, often operate at elevated temperatures and need long reaction times. The reported magnesium complexes possess fundamentally different structures and no clear correlation between the nature of the ligands and the catalytic performance is evident. Furthermore, little effort into the investigation of the mechanisms have been conducted and in many cases it remains unclear if the magnesium compounds are catalysts or precatalysts. With this in mind, a large interest for the development of magnesium-based catalysts that operate at or near ambient conditions, and a more thorough mechanistic understanding, exists.

1.4.3 Hydroboration catalysis

The term hydroboration refers to the addition reaction of unsaturated organic moieties and boron-hydrogen bonds. More specifically, the boron-hydrogen group can be added to carbonyls to form boron-oxygen bonds, to imines, nitriles, pyridines and carbodiimides to form boron-nitrogen bonds and to alkenes or alkynes to form boron-carbon bonds (Scheme 19).



Scheme 19: Selected examples of hydroborations of unsaturated element-carbon bonds.

The addition of hydridoborane compounds to unsaturated organic molecules is known since the 1950s.^[217–223] In principle, the atom economy of hydroborations is 100%, assuming that only the addition product is formed quantitatively and no byproducts occur. Furthermore, the addition of boranes to alkenes or alkynes usually leads to a *cis* or a *syn* selectivity and the formation of the *anti*-Markovnikov product.^[224] The addition of a boron-hydrogen bond to an organic molecule often needs elevated reaction temperatures or long reaction times.^[223] To avoid such harsh conditions and the formation of undesired byproducts, new kinds of catalytic hydroborations are of high interest and have been investigated for decades. In addition to

many transition metal-based catalysts,^[225–243] compounds containing rare earth elements^[244–249] also serve as suitable catalysts for hydroborations. More recently, main group compounds have gained further interest as possible catalysts in hydroboration reactions. Examples are known for *p*-block elements^[243,250–261] as well as for *s*-block element-based compounds.^[242,261–275] More specifically, in the case of alkaline earth metal compounds, especially the catalytic activity of magnesium complexes has been investigated (Figure 15).

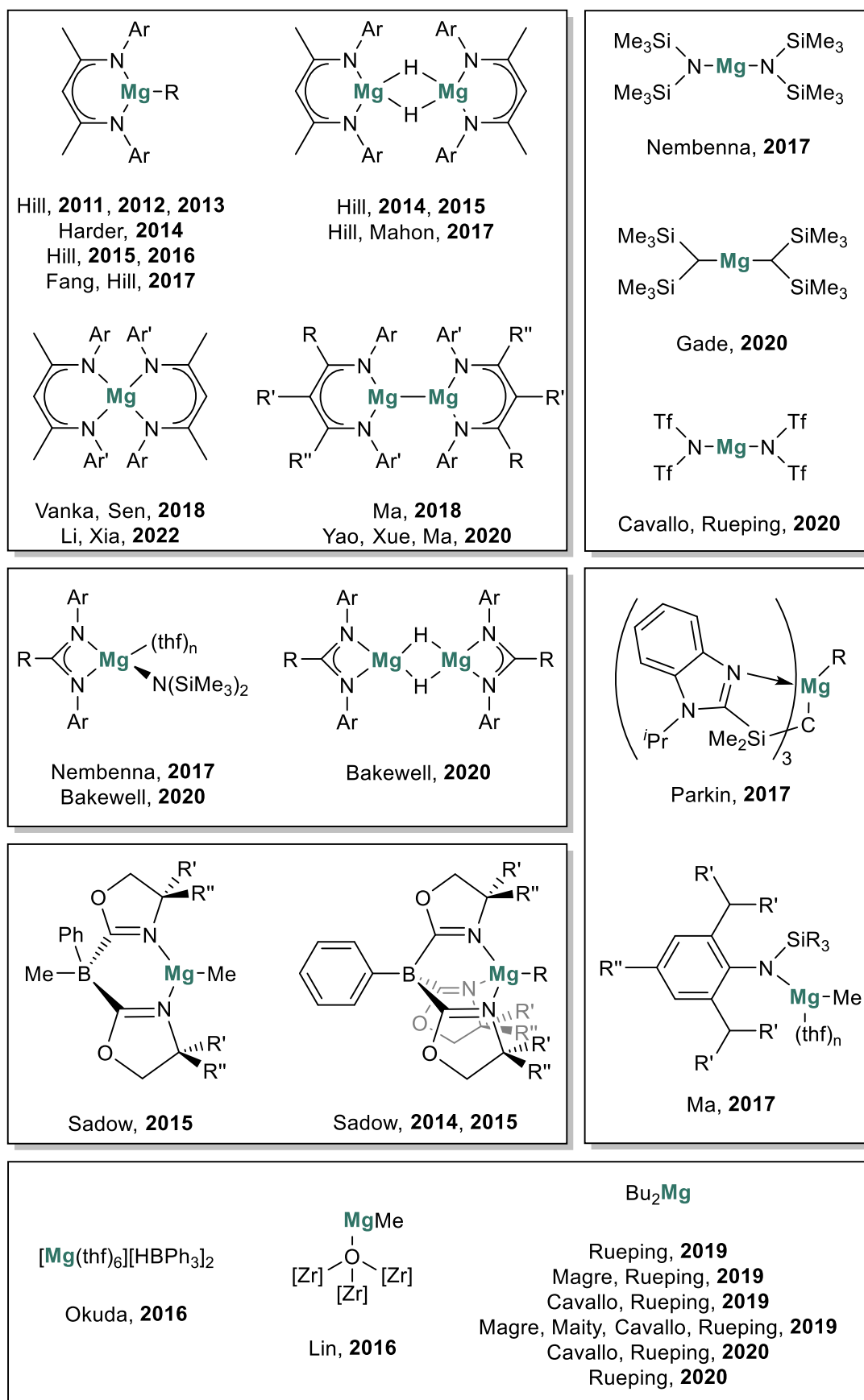


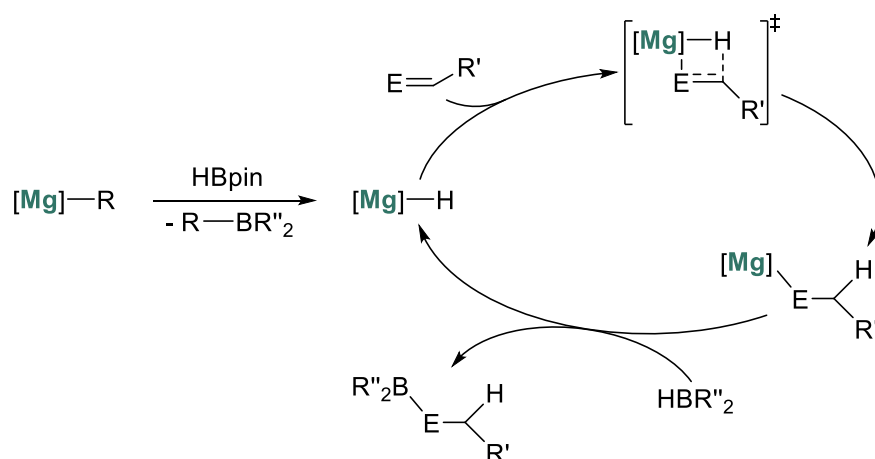
Figure 15: Selected examples of magnesium-based (pre)catalysts for hydroboration catalysis.^[276–308]

The hydroboration of carbonyls and the thereof resulting reduction of carbonyl compounds is catalyzed by different magnesium complexes and well investigated. Magnesium 1,3-diketimine complexes have been used as catalysts in hydroboration reactions. The first use of a β -diketiminato magnesium complex in such a reduction of carbonyl compounds with boranes was reported by Hill and coworkers in 2012. The butylmagnesium 1,3-diketiminato complex acts as a precatalyst and forms a dimeric β -diketiminato magnesium hydride upon reaction with pinacolborane. Hill and coworkers have shown that several aldehydes or ketones could be reduced with pinacolborane in the presence of 0.05 mol% to 0.5 mol% of the catalyst. The reactions were carried out at room temperature and the products could be obtained with yields of about 90%.^[276] Further applications of 1,3-diketimine and amidinate magnesium complexes as well as other magnesium compounds in the hydroboration of carbonyl compounds are reported by different research groups, all showing similar performance to the Hill system.^[277–290] In addition to the application of a tris(oxazoliny)boratomagnesium complex in the hydroboration of esters and the deoxygenation of amides, Sadow and coworkers reported the successful use of this magnesium compound in dehydropolymerization of poly(lactic acid) and the ring-opening of lactide by ester cleavage.^[291,292] The Rueping group investigated the application of dibutylmagnesium as precatalyst for hydroboration reactions. The authors were able to hydroborate and reduce several carbonyl compounds with the addition of dibutylmagnesium.^[293–297] An advantage of this system is the fact that dibutylmagnesium is cheap and commercially available, unlike the previously discussed complexes that required multi-step synthesis. In addition to the formation of B-O bonds, the B-N bond formation is also of broad interest. Several nitrogen containing compounds, like pyridine, could be hydroborated with pinacolborane.^[298–300,306] The hydroboration of pyridine is carried out with the addition of several magnesium 1,3-diketimine complexes, that act as (pre)catalysts.^[298–300] β -Diketiminato magnesium complexes have also been used in the hydroboration of other unsaturated carbon-element bonds. The Hill group applied the magnesium 1,3-diketimine in the generation of B-N bonds, in the hydroboration of nitriles, isonitriles, carbodiimides, isocyanates and imines.^[301–305] In contrast to the hydroboration of aldehydes and ketones, the hydroboration for these substrates usually needed elevated temperatures, from 60 °C to 100 °C. Only some imines could be hydroborated by the addition of pinacolborane and the catalyst at room temperature.^[301] The catalyst loading of 5 mol% to 10 mol% is typical for magnesium-based catalysts in these reactions. Depending on the amount of pinacolborane added to the substrates, the catalysts were able to hydroborate triple bonds twice.^[302,303] The magnesium 1,3-diketimine reported by Ma and coworkers could also facilitate the hydroboration of nitriles.^[277] For the hydroboration of carbodiimides, to generate B-N bonds, only a few magnesium catalysts are reported.^[306,308] Furthermore, 1,3-diketiminato

1.4 Magnesium catalysis

magnesium complexes,^[277] dibutylmagnesium^[307] and other magnesium compounds^[278,306] are reported to hydroborate carbon-carbon multiple bonds under harsh conditions, with reaction temperatures of up to 100 °C.^[277,278,306,307]

Several suggestions were made for the mechanism of the hydroboration of unsaturated carbon-element bonds. Generally, the authors assume a σ -bond metathesis in the initial step by the reaction of the catalyst and a borane. The formed magnesium hydride inserts into the unsaturated carbon-element bond and generates the product, coordinated to the magnesium center. The product is separated and the magnesium hydride is recovered by the addition of another equivalent of borane (Scheme 20).^[270,303] In case of element-carbon triple bonds, the mechanism is most likely analogous.



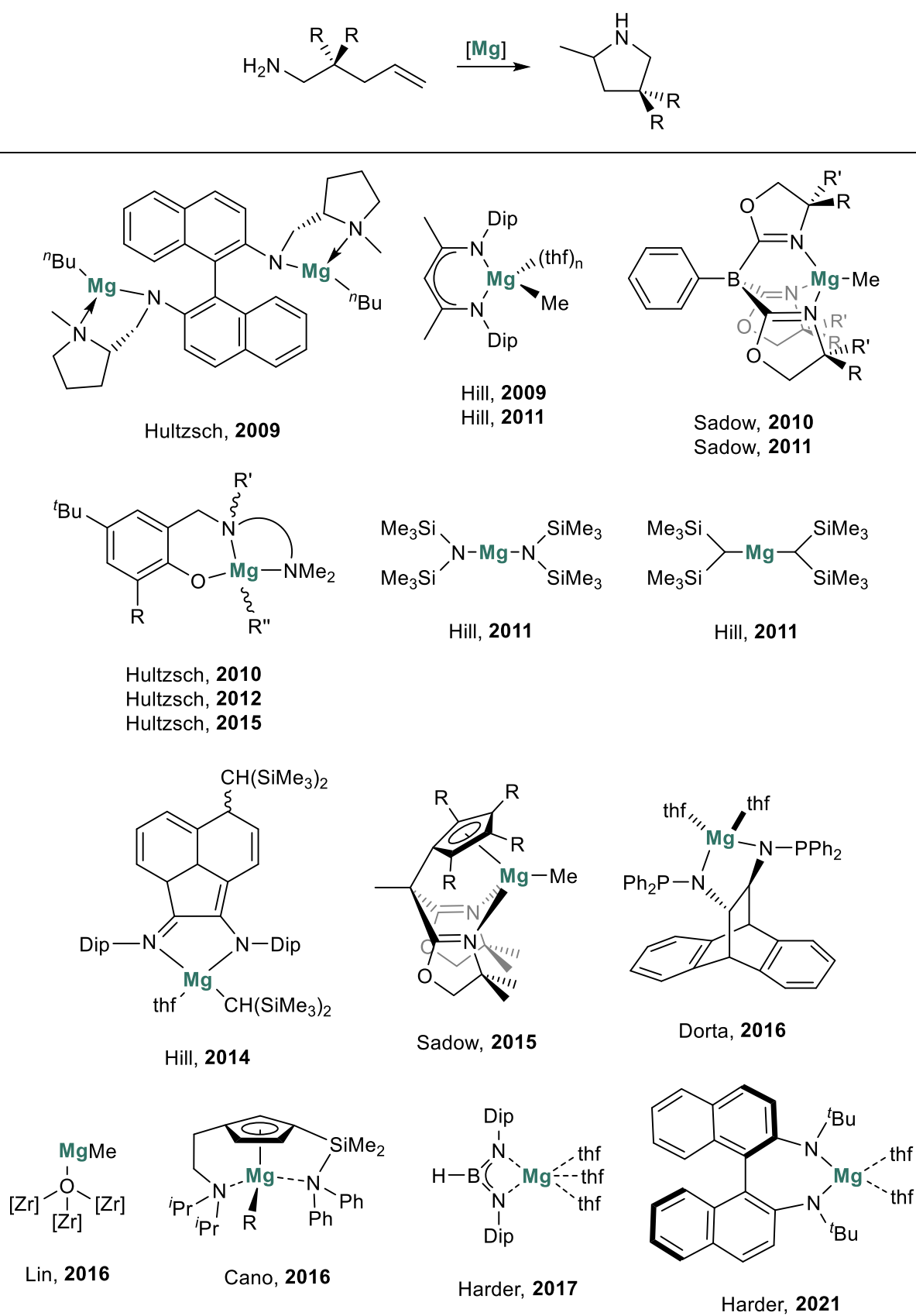
Scheme 20: Proposed mechanism for the hydroboration of unsaturated carbon-element bonds catalyzed by magnesium 1,3-diketimine.^[270,303]

Overall, hydroboration reactions catalyzed by magnesium-based complexes are far better investigated than magnesium-catalyzed amine borane or amine silane dehydrocouplings. A broad spectrum of structurally different magnesium compounds has been used in various hydroboration reactions with relatively high catalyst loadings not uncommon in hydroboration reactions. The ligand systems of the magnesium complexes are almost exclusively nitrogen-based and no clear structure-performance relationship could be identified. Furthermore, the mechanisms are often poorly investigated, so that it is unclear whether the systems act as catalysts or as precatalysts.

Therefore, the development of cheap and versatile catalysts is of great importance, and the interest in s-block-based systems has attracted increasing attention in the last decade.

1.4.4 Intramolecular Hydroamination

The demand on nitrogen-containing organic molecules is increasing as such compounds are important as fine chemicals and pharmaceuticals with a broad application spectrum. The catalytic hydroamination represents an atom-efficient and waste-free method to obtain organo-nitrogen molecules,^[309–314] with one of the main advantages being that the starting materials for hydroamination reactions are relatively abundant and cheap.^[315] The hydroamination of alkenes or alkynes is the formal addition of a N-H bond across a C-C multiple bond and can proceed intermolecularly or intramolecularly.^[311,316,317] As in the past, the research was focused on transition and rare-earth metal-based catalysts, a huge number of systems containing these metals are established and well investigated, both for inter- and intramolecular hydroamination reactions.^[310,311,316–342] In the last twenty years, the interest and research focus on main group element-based catalysts for the hydroamination has risen tremendously.^[316,332,343] For instance, simple Brønsted acids can facilitate the intramolecular hydroamination of alkenylamines in some cases.^[344] Alkali metal-based compounds, like alkali-bases, are also used as catalysts in the intramolecular hydroamination. There is an easy access to bases like butyllithium or potassium *tert*-butoxide that are able to catalyze intramolecular hydroaminations.^[345–354] Furthermore, diamidodinaphthyl dilithium salts are suitable catalysts in the intramolecular hydroamination.^[355] In the case of alkaline earth metals, catalysts for hydroamination reactions, based on the heavier elements calcium, strontium and barium, are well investigated.^[356–372] Due to the relevance of the work conducted within the scope of this thesis, this chapter will focus on intramolecular hydroamination reactions catalyzed by magnesium complexes. In the last years the focus on such systems has increased tremendously and several magnesium-based catalysts have been reported relatively recently (Scheme 21).^[146,148,268,282,313,314,373–382] Moreover, most investigated substrates in ring-closing hydroaminations were 1,4- and 1,5-aminoalkenes.^[373–375]

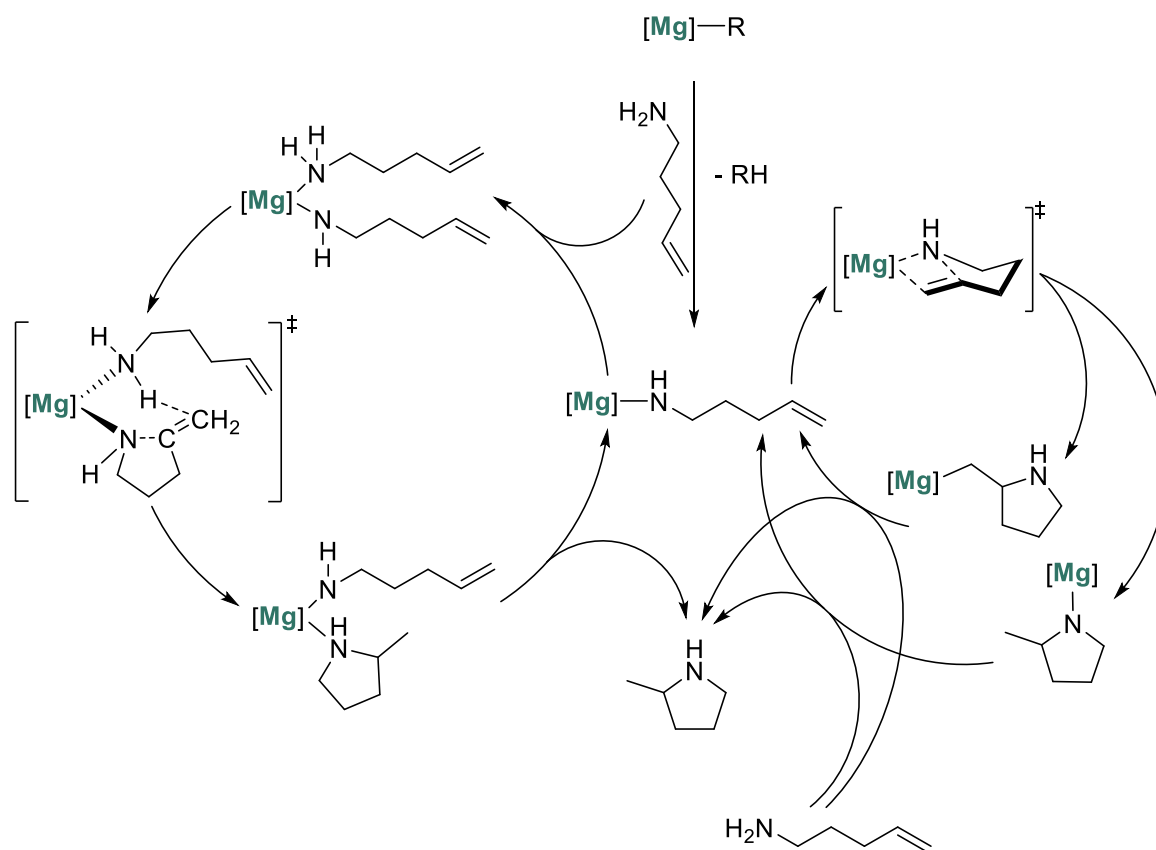


Scheme 21: Intramolecular hydroamination and selected examples of magnesium-based (pre)catalysts for this reaction.^[146,148,282,313,314,373–382]

The product formation in intramolecular hydroaminations of aminoalkenes follows the general rules for ring closures. In case of the ring closure of a pent-4-en-1-amine, the five-membered exo-product is generated.^[383] Furthermore, the Thorpe-Ingold effect plays a crucial role.^[384] The increasing steric demand of groups at the geminal position accelerates the product generation, as bulky groups at the geminal position of the substrate restrict the number of possible conformations and favors the ring closure.^[384] This phenomenon could be observed in several intramolecular hydroamination reactions catalyzed by magnesium compounds. In 2009, Hill and coworkers reported the application of a β -diketiminato magnesium complex in the intramolecular hydroamination of aminoalkenes.^[373] The authors carried out the reactions with catalyst loadings in a range between 2 mol% and 20 mol%. Generally, the reactions were conducted at room temperature in two to 48 hours, giving yields of 72% to 99%. Noteworthy, the authors used only substrates with bulky substituents in geminal position for the afore discussed reason.^[384] Generally, the magnesium 1,3-diketiminate complexes required longer reaction times to catalyze the intramolecular hydroamination, compared to calcium analogues.^[373] A few years later, the Hill group used magnesium amides and magnesium alkyl systems as precatalysts in the intramolecular hydroamination. The advantage of these compounds compared to the magnesium 1,3-diketiminate complexes is the fact that they are commercially available. With these compounds it was possible to carry out the reactions at room temperature, with yields from 40% to 99% achieved after several hours.^[374] Furthermore, the Hill group carried out some intramolecular hydroaminations catalyzed by a sterically encumbered bis(imino)acenaphthene magnesium complex. Interestingly, in case of the ring closure of 2,2-diphenylhept-6-en-1-amine, the magnesium complex was a more efficient catalyst than its calcium analog.^[375] Following this, Hultzsich and coworkers succeed in the intramolecular hydroamination with a diamidobinaphthyl magnesium complex as catalyst. Depending on the substrates and the reaction conditions, the authors obtained yields in the range of 80% to 99%.^[313] A few years later, the Hultzsich group reported the usage of phenoxyamine magnesium complexes as catalysts in the intramolecular hydroamination.^[314,376,377] The authors were able to obtain the ring closed products in yields of 80% to 99%, with the catalysts needing higher temperatures^[314,376,377] and reaction times of up to four days, however.^[314] The tris(oxazolonyl)borato magnesium complexes, synthesized by the Sadow group, are also applicable catalysts in the intramolecular hydroamination,^[378,379] as are cyclopentadienyl bis(oxazolonyl)borato magnesium complexes.^[146] The complexes catalyze ring-closing hydroaminations between room temperature and 60 °C and timeframes of 45 minutes to 24 hours, depending on the substrates, are needed. In particular, the catalytic ring closure of 2,2-dimethylpent-4-en-1-amine was challenging for this system and needed higher temperatures and/or longer reaction times while only giving yields of 12% to 50%, depending on the catalyst.^[146,378] Although, the tris(oxazolonyl)borato magnesium complexes

are suitable catalysts in the intramolecular hydroamination, they produce mostly racemic mixtures of products.^[379] Another cyclopentadienyl-based magnesium complex was applied by Cano and coworkers in the intramolecular hydroamination. The double bridged, *ansa*-half-sandwich magnesium complex catalyzes the intramolecular hydroamination of aminoalkenes with yields in a range of 70% to 99%.^[148] Harder and coworkers reported a bora amidinate magnesium complex that was able to catalyze the ring closure of 2,2-diphenylpent-4-en-1-amine at room temperature. For substrates with less bulky substituents in geminal position, higher temperatures were required.^[380] The groups of Harder and Dorta also reported these observations for the application of a chiral bis(amide) magnesium complex^[381] and a chiral amido-phosphine magnesium complex^[382] in the intramolecular hydroamination. In most cases, the magnesium complexes are suitable catalysts and provide products in good yields. Only one catalyst is able to catalyze the intramolecular hydroamination enantioselective with high ee values.^[376]

Furthermore, different working groups have made suggestions for the mechanism of the intramolecular hydroamination, with similar pathways predicted. In the initial step, a magnesium amine complex is most likely formed by the reaction of the catalyst and the substrate (Scheme 22 right side). In some cases, the authors assume that a second substrate coordinates to the magnesium center (Scheme 22 left side). After the ring closure of the aminoalkene, the product is coordinated to the magnesium center and separated by the addition of another equivalent of aminoalkene.^[373,377,378,380,381] DFT calculations support these suggestions as well as ¹H NMR spectroscopy, by verifying magnesium substrate and magnesium product complexes.^[385]



Scheme 22: Postulated mechanism of the intramolecular hydroamination of pent-4-en-1-amine catalyzed by magnesium complexes (substituents in the geminal position are omitted for clarity).^[373,377,378,380,381,385]

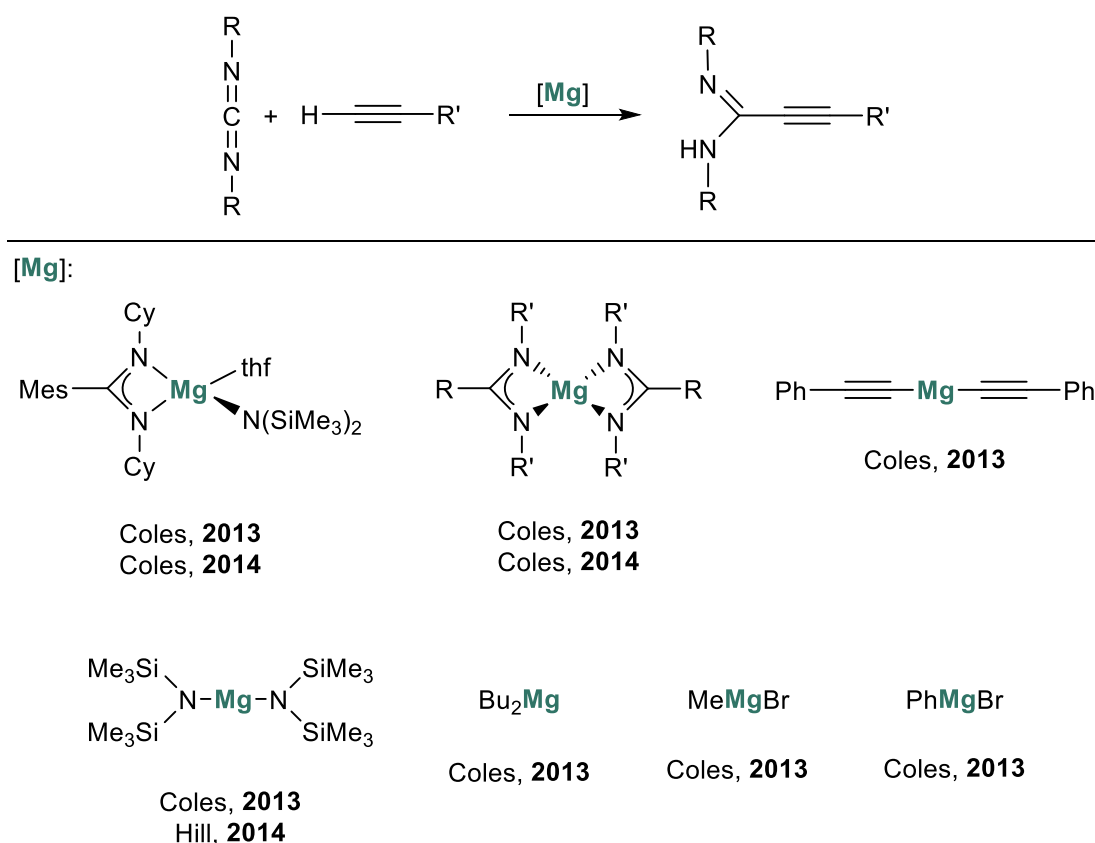
In addition to the afore presented examples of homogeneous catalysis, there is also an example for a heterogeneous magnesium-based catalyst for intramolecular hydroamination. A magnesium-based MOF displayed catalytic activity in the intramolecular hydroamination. After two days at 80 °C, with catalyst loadings of 1 mol%, the products were obtained in yields of 96% to 100%.^[282]

In summary, a number of magnesium complexes succeed in the catalytic intramolecular hydroamination. The catalysts reach high yields, but are not able to catalyze the formation of nitrogen containing heterocycles enantioselectively. Furthermore, it is noticeable that the reaction conditions have to be aggravated if the steric demand of the substituents in geminal position at the aminoalkenes decreases, due to the afore mentioned Thorpe-Ingold effect. Beyond that, it is often unclear whether the magnesium compounds acted as catalysts or precatalysts since the mechanisms are often only poorly investigated. Nevertheless, magnesium-based catalysts are a good alternative to transition metal catalysts and there is a great interest in new and suitable magnesium complexes for the intramolecular hydroamination.

Noteworthy, cyclopentadienyl-based magnesium complexes are rarely used as catalysts for the intramolecular hydroamination. In this thesis, new examples of cyclopentadienyl magnesium complexes in intramolecular hydroamination are described.

1.4.5 Hydroacetylenation

One of the most important research areas to synthetic chemistry is the development of atom-efficient catalytic carbon-carbon bond formation processes.^[386–389] For several C-H activation processes, transition or rare earth metal-based complexes are well established.^[390–396] In particular, hydroacetylenation reactions, the addition of terminal alkynes to carbodiimides, are generally catalyzed by transition or rare earth metal complexes.^[397–404] Only few examples of main group element-based catalysts are described.^[405,406] For the hydroacetylenation, catalyzed by magnesium complexes, even fewer examples are reported in literature, until now (Scheme 23).^[386,389,407]

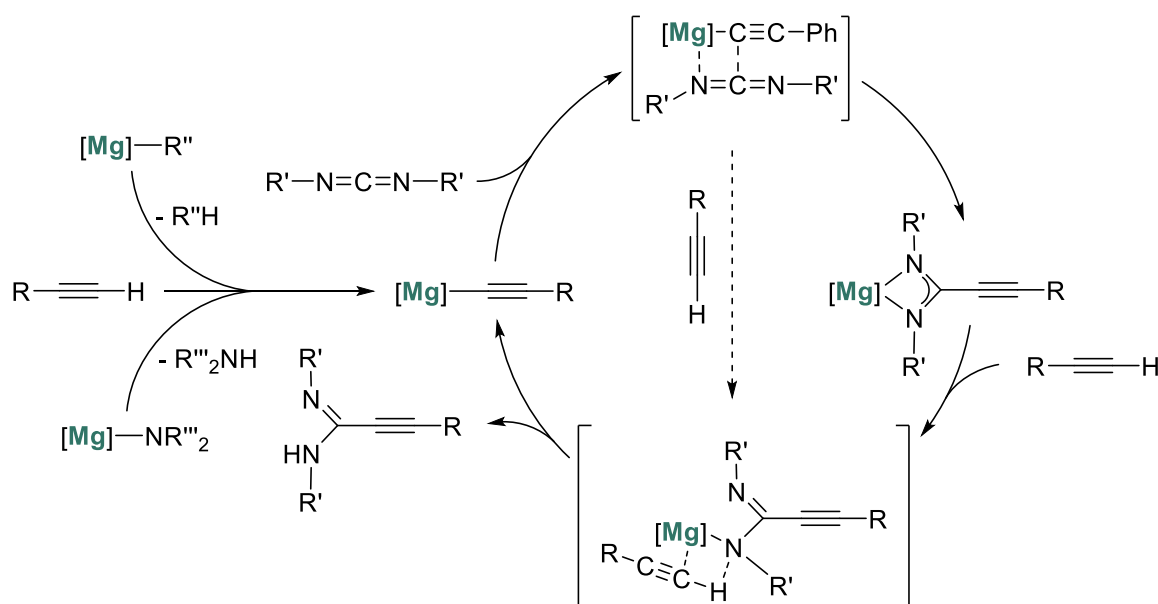


Scheme 23: Addition of terminal alkynes to carbodiimides catalyzed by magnesium complexes and selected examples of magnesium-based (pre)catalysts.^[386,389,407]

The first report stems from Coles and Schwamm, who tested the catalytic activity of a magnesium amidinate complex towards the addition of alkynes to carbodiimides. With catalyst loadings of 1 mol% to 10 mol%, conversions of up to 77% were achieved at reaction temper-

atures from 50 °C to 80 °C.^[407] Furthermore, the authors applied magnesium amidinate complexes, Grignard reagents and magnesium amides. At 80 °C, conversions of about 70% were observed for the addition of phenylacetylene to *N,N'*-diisopropylcarbodiimide after 24 hours.^[389,407] In particular, Hill and coworkers reported of magnesium bis(hexamethyldisilazide) as a precatalyst that catalyzed the hydroacetylenation at room temperature, with conversions of up to 61%.^[386]

Furthermore, the working groups of Hill and Coles proposed a possible reaction mechanism. The authors assume that the catalytically active species is formed by the reaction of the catalyst with the alkyne. After the insertion of the carbodiimide into the metal-alkyne bond, the product, coordinated to the metal center, could be formed. By adding another alkyne molecule, the product could be released and the catalytically active species could be formed to regenerate the catalytic cycle (Scheme 24).^[386,389,407]



Scheme 24: Proposed mechanism for the hydroacetylenation shown for the addition of an alkyne to a carbodiimide.^[386,389,407]

Overall, only few examples of magnesium-based catalysts for the catalytic hydroacetylenation are described in literature, with no obvious correlation between the structure of the magnesium complexes and the obtained conversions and only limited mechanistic understanding.

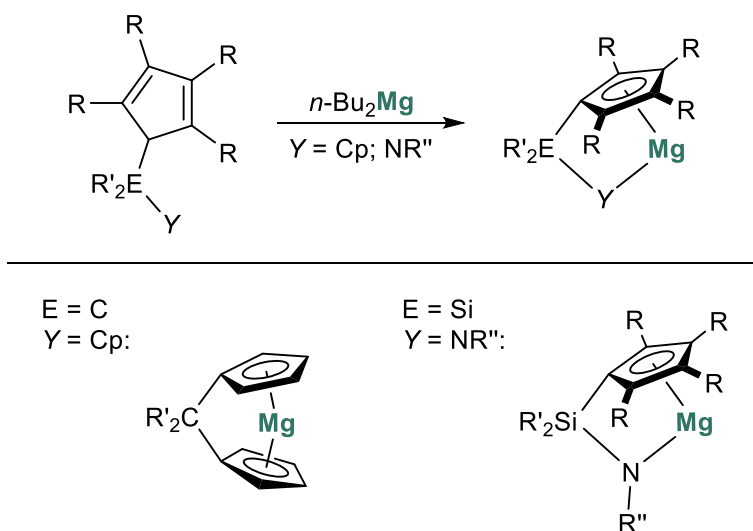
1.4.6 Summary – Magnesium in catalysis

Magnesium complexes find application as catalysts in many important reaction types in organic and inorganic chemistry. Among other examples not discussed in detail in this chapter, various magnesium compounds are known to catalyze dehydrocoupling reactions and many hydroelementation reactions.^[159,164,189,200,224,268–271,274,275,408] In general, it is difficult to see any kind of correlation between the structure of the used magnesium compounds and their catalytic activity, which could be due to the fact that many magnesium complexes are only precatalysts. Interestingly, despite a high structural diversity of the magnesium compounds used in catalysis, cyclopentadienyl-based magnesium complexes are rarely used as catalysts. In sharp contrast, transition metal-based cyclopentadienyl complexes have been used as catalysts in a broad spectrum of homogeneous catalytic transformations.^[80,89,139–141,409] Nowadays, these complexes even play an important role in industrial processes, for instance in olefin polymerization.^[142] This lack of application of cyclopentadienyl-based s-block compounds in homogeneous catalysis was one of the main motivational ideas of this doctoral thesis.

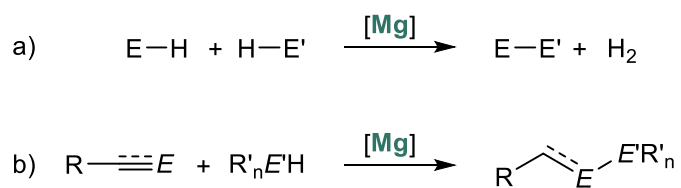
2. Motivation and Aims

As mentioned in the introduction, the high abundance of magnesium in the earth's crust and its low human toxicity are advantages for any kind of application of magnesium complexes. Concerning sustainability and environmental protection, magnesium displays a good alternative to other main group elements or transition metals, with its low global warming potential and the small CO₂ release in its production.^[152–154] Furthermore, due to the low abundance of many transition metals in the earth's crust, the preparation of corresponding transition metal catalysts is often expensive. In order to use cheaper and “greener” catalysts, a number of magnesium complexes have been applied in homogeneous catalysis in the last decades. However, at the moment, magnesium-based catalysts often require long reaction times and high reaction temperatures to generate good conversions. Moreover, many magnesium-based catalysts are used specifically for one type of catalysis and are rarely applicable to different reaction types. As outlined before, many magnesium-based catalysts are β -diketiminato magnesium systems, alkyl magnesium compounds or magnesium amide complexes.^[159,164,189,200,224,268–271,274,275,408] In sharp contrast, while cyclopentadienyl transition metal complexes are commonly used in catalysis,^[80,89,139–141,409] cyclopentadienyl-based magnesium complexes rarely found application in catalytic reactions, although they are easy to prepare and well known to the literature. For example, magnesocenophanes, which have been known for 25 years, can be obtained in a two-step synthesis.^[105–107]

Recently, there has been increasing interest in dehydrocoupling reactions due to their broad applicability for the synthesis of inorganic *p*-block molecules and their high atom economy. As a result, the interest in suitable catalysts based on magnesium has also increased tremendously. This led to the aim of this doctoral thesis, in which cyclopentadienyl-magnesium complexes should be applied in dehydrocoupling and hydroelementation catalysis. Initially, the focus was on the synthesis of two different complex types of cyclopentadienyl magnesium complexes: new magnesocenophanes and *ansa*-half-sandwich magnesium complexes (Scheme 25). Following the synthesis, the new cyclopentadienyl magnesium complexes are to be used as catalysts in homogeneous catalysis (Scheme 26).



Scheme 25: Synthesis of the new cyclopentadienyl magnesium complexes.



Scheme 26: a) Dehydrocoupling reactions and b) hydroelementation reactions catalyzed by the new magnesium compounds.

3. Results and Discussion

3.1 Magnesocenophane-Catalyzed Amine Borane Dehydrocoupling

Lisa Wirtz, Wasim Haider, Volker Huch, Michael Zimmer, André Schäfer

Chem. Eur. J. **2020**, *26*, 6176-6184.

DOI: 10.1002/chem.202000106

The above cited article was published as an “Open Access” article under the terms of Creative Commons Attribution-NonCommercial-NoDerivs License.

Copyright © (2020) The Authors. Published by Wiley-VCH Verlag GmbH & Co. KGaA.

Author contribution:

Lisa Wirtz:

Lead: Synthesis and characterization of [1]magnesocenophanes and deuterated amine borane substrates, methodology and investigation of catalytic reactions, mechanistic investigations, determination of kinetic isotope effects, writing, reviewing and editing of the supporting information;

Equal (A.S.): Synthesis of borylamido magnesium complex **5**, DFT-calculations;

Supporting: Writing, reviewing and editing of the manuscript.

Wasim Haider:

Lead: Synthesis of [2]magnesocenophanes.

Volker Huch:

Lead: X-ray analysis.

Michael Zimmer:

Lead: VT-NMR studies.

André Schäfer:

Lead: Project administration and supervision, funding acquisition, writing, reviewing and editing of the manuscript;

Equal (L.W.): Synthesis of borylamido magnesium complex **5**, DFT-calculations;

Supporting: Writing, reviewing and editing of the supporting information.

Chemistry A European Journal

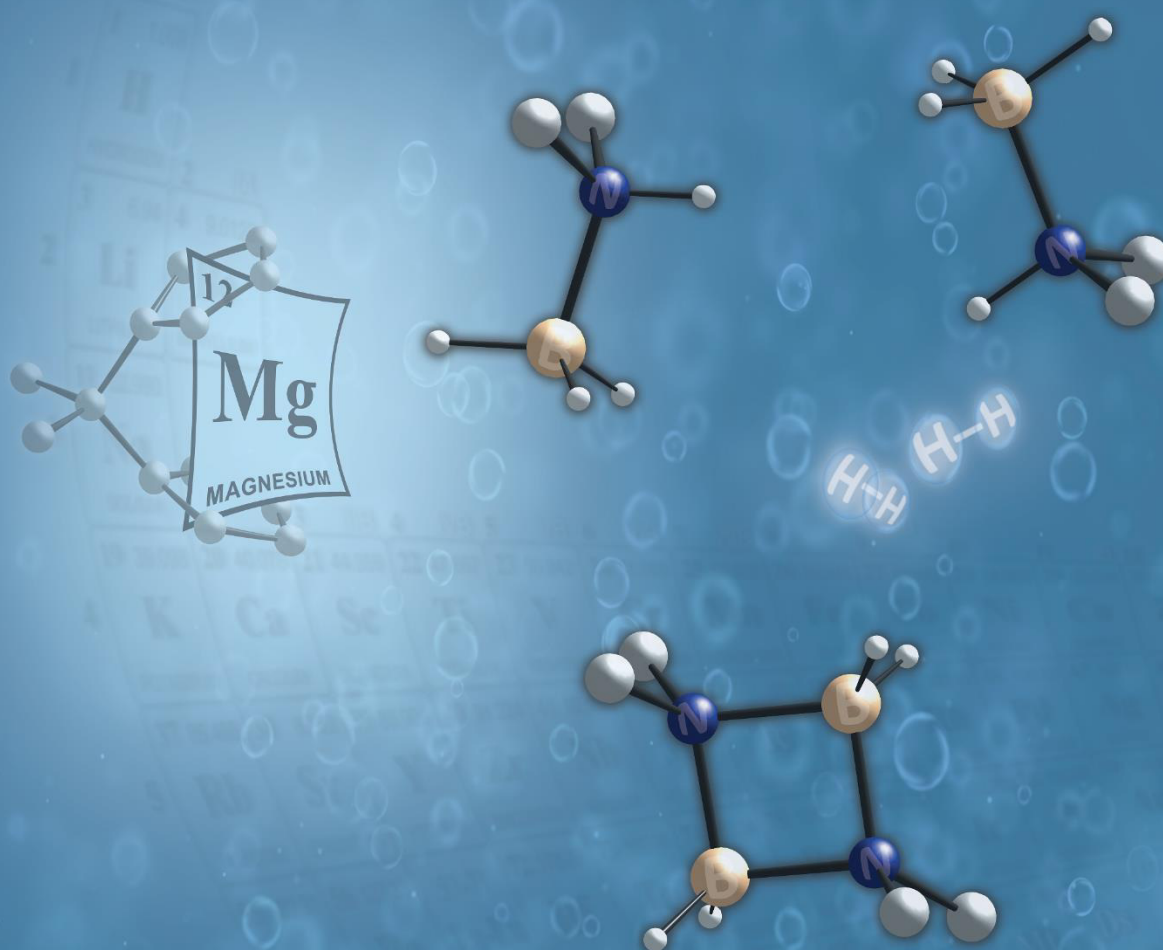
 **Chemistry
Europe**

European Chemical
Societies Publishing

Cover Feature:

A. Schäfer et al.

Magnescenophane Catalyzed Amine Borane Dehydrocoupling



28/2020

WILEY-VCH

Magnesocenophane Catalysts | Hot Paper |

Magnesocenophane-Catalyzed Amine Borane Dehydrocoupling

Lisa Wirtz, Wasim Haider, Volker Huch, Michael Zimmer, and André Schäfer*^[a]



Abstract: The Lewis acidities of a series of $[n]$ magnesocenophanes (**1 a–d**) have been investigated computationally and found to be a function of the tilt of the cyclopentadienyl moieties. Their catalytic abilities in amine borane dehydrogenation/dehydrocoupling reactions have been probed, and C[1]magnesocenophane (**1 a**) has been shown to effectively catalyze the dehydrogenation/dehydrocoupling of dimethyl-

amine borane (**2 a**) and diisopropylamine borane (**2 b**) under ambient conditions. Furthermore, the mechanism of the reaction with **2 a** has been investigated experimentally and computationally, and the results imply a ligand-assisted mechanism involving stepwise proton and hydride transfer, with dimethylaminoborane as the key intermediate.

Introduction

Amine boranes have attracted much attention over the last decades, primarily for their possible applications as solid hydrogen storage materials^[1] or as precursors in the preparation of B–N materials.^[2] Although hydrogen is eliminated from many amine boranes at high temperatures, these reactions often afford ill-defined product mixtures or suffer from mediocre yields with respect to the released hydrogen equivalents.^[1c] Since catalytic routes can overcome these shortcomings, various homogeneous and heterogeneous catalysts for dehydrogenation/dehydrocoupling of amine boranes have been reported, most of which are based on d-block elements, many on precious metals, such as rhodium or iridium.^[3] Although these operate at room temperature and with low catalyst loadings, main group element and in particular s-block metal-based catalysts have been investigated in view of lower element costs and ready availability.^[3e–g] With respect to magnesium, for example, Hill and co-workers reported the use of dialkyl- and 1,3-diketimine magnesium compounds in the dehydrocoupling of dimethylamine borane (Figure 1; I–III).^[4] In this pioneering work,^[4a] a relatively high catalyst loading of 10 mol% and an elevated temperature of 333 K were necessary to facilitate the reaction. Recently, Kays and co-workers suc-

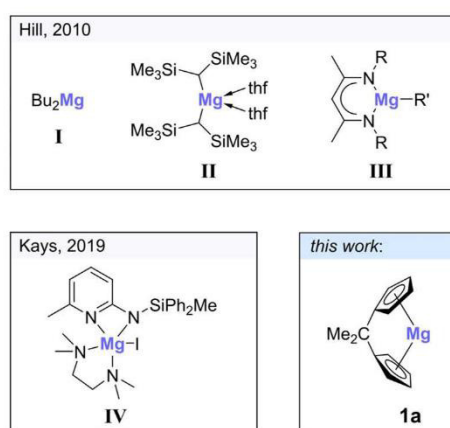


Figure 1. Examples of magnesium (pre)catalysts for dimethylamine borane dehydrogenation/dehydrocoupling.

ceeded in devising a catalytically much more active magnesium complex for the dehydrocoupling of dimethylamine borane (Figure 1; IV), allowing for shorter reaction times at lower catalyst loadings, although an elevated temperature of 333 K was still required (Figure 1).^[5] In addition, room temperature dehydrocoupling reactions of cyclic monohydro-boranes with amines and of arylamine boranes, catalyzed by magnesium compounds, have been reported.^[6] Although these systems are less powerful than many transition-metal-based catalysts, magnesium-based catalysts have notable advantages, namely the high abundance of magnesium in the Earth's crust, its non-toxic nature, and its ready availability at low cost.^[7]

Inspired by these aspects and in continuation of our group's interest in metallocenophanes of main group elements,^[8] we were intrigued to investigate the reactivity of $[n]$ magnesocenophanes towards amine boranes. Various silicon- and carbon-bridged [1]- and [2]magnesocenophanes (**1 a–d**) have been reported in the literature over the last decade (Figure 2).^[8b,9]

[a] L. Wirtz, W. Haider, Dr. V. Huch, Dr. M. Zimmer, Dr. A. Schäfer
Faculty of Natural Science and Technology
Department of Chemistry
Saarland University
Campus Saarbrücken, 66123 Saarbrücken (Germany)
E-mail: andre.schaefer@uni-saarland.de

Supporting information and the ORCID identification number for the author of this article can be found under:
<https://doi.org/10.1002/chem.202000106>.

© 2020 The Authors. Published by Wiley-VCH Verlag GmbH & Co. KGaA. This is an open access article under the terms of Creative Commons Attribution NonCommercial License, which permits use, distribution and reproduction in any medium, provided the original work is properly cited and is not used for commercial purposes.

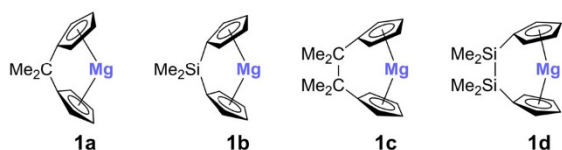


Figure 2. Silicon- and carbon-bridged [1]- and [2]magnesocenophanes **1 a–d**.

Results and Discussion

Structural and electronic properties of [*n*]magnesocenophanes

To better understand the different geometric features and electronic properties of magnesocenophanes **1 a–d**, a computational study was carried out prior to any experimental investigations. In this context, it is important to note that the reported crystal structures of magnesocenophanes **1 a–d**^[8b,9] are of solvated complexes, in which the dihedral angle α of the cyclopentadienide planes is strongly influenced by the coordination of the donor solvent molecule(s) to the magnesium atom.^[10] Therefore, dihedral angles α of the Cp planes in **1 a–d** differ significantly between the geometries obtained from DFT calculations^[11] (B3LYP-D3/def2-TZVP) under quasi-gas-phase conditions, without donor solvent coordination to the magnesium atom, and the experimental solid-state structures of the solvated complexes. This is also evident from the crystal structure of **1 a**-dme (dme = dimethoxyethane) (Figure 3), which features a dihedral angle of $\alpha = 80^\circ$, whereas a dihedral angle of $\alpha = 56^\circ$ is calculated when no solvent molecule is coordinated to the magnesium atom, illustrating the high flexibility of the Mg–Cp bonds due to their high ionic character.

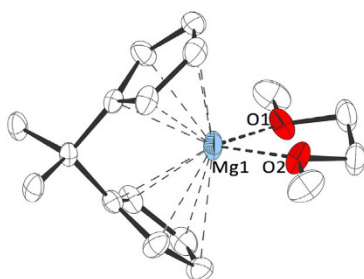


Figure 3. Molecular structure of **1 a**-dme in the crystal (thermal ellipsoids at 30% probability level; hydrogen atoms omitted for clarity; selected bond lengths and angle: Mg1–O1/O2: 205.3, Mg1–Cp^{centroid}: 230.4 pm; $\alpha = 80.1^\circ$).

Moreover, the solvent coordination in **1 a**-dme was found to be reversible in vacuo at room temperature,^[12a] unlike in the case of **1 a**-(thf)₂. The calculated binding energies of the solvent molecules to the magnesium atom are 139.6 kJ mol⁻¹ for dme in **1 a**-dme and 197.0 kJ mol⁻¹ for thf in **1 a**-(thf)₂ (100.5 kJ mol⁻¹ for binding of the first thf molecule and 96.5 kJ mol⁻¹ for binding of the second thf molecule).

Regarding electronic properties, DFT calculations predict an increase in fluoride ion affinity (FIA)^[13] and global electrophilicity

index ω (GEI)^[14] as a function of tilt of the cyclopentadienyl moieties, quantified by the dihedral angle α , in solvent-free magnesocenophanes **1 a–d** (Figure 4). This is primarily a result of a lowering in energy of the LUMO in these systems, which has a large coefficient of high *s* character at the magnesium atom.

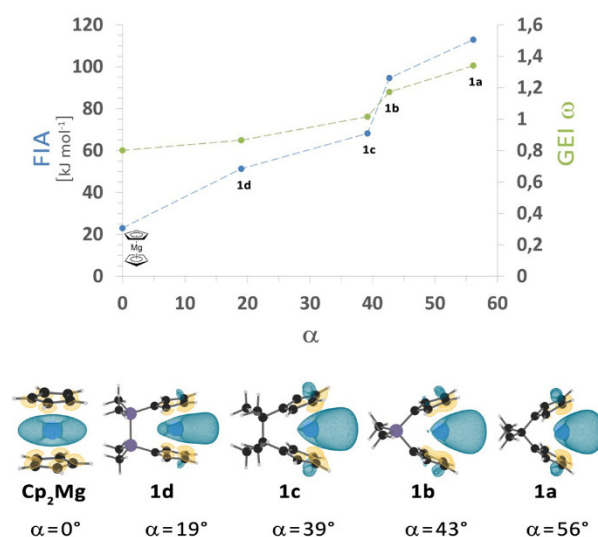


Figure 4. Calculated fluoride ion affinities (FIA) and global electrophilicity indices ω (GEI) as a function of the dihedral angle between the Cp planes (α), and isosurface plots of LUMOs (isovalue = 0.035) of magnesocene (Cp₂Mg) and magnesocenophanes **1 a–d** (calculated at the B3LYP-D3/def2-TZVP level of theory^[11]).

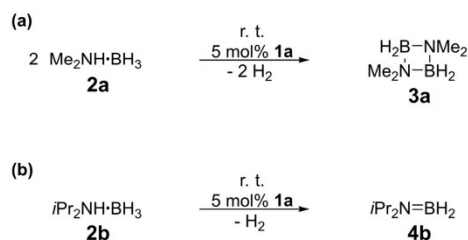
Therefore, according to these results, C[1]magnesocenophane **1 a** should be the most Lewis acidic compound in this series. This might result in a higher catalytic reactivity, as Lewis acidity can be important for substrate binding, although it has to be taken into consideration that magnesocenophanes **1 a–d** will exist as solvent adducts in solutions in donor solvents.

Catalytic studies

Following the computational results, we started our experimental investigations regarding catalytic dehydrogenation/dehydrocoupling of amine boranes by focusing mainly on C[1]magnesocenophane **1 a**. Indeed, this compound proved to be a very potent catalyst for dehydrogenation of dimethylamine borane **2 a** and diisopropylamine borane **2 b** (Scheme 1).

When a solution of dimethylamine borane **2 a** and 5 mol% C[1]magnesocenophane **1 a** in dme was stirred at room temperature,^[12a] dehydrogenation occurred to afford cyclic diborazane **3 a**, with $\geq 95\%$ conversion^[12b] being achieved after 16 h (Figure 5).

Similarly, diisopropylamine borane **2 b** was also dehydrogenated to give diisopropylaminoborane **4 b** in the presence of 5 mol% of **1 a**, with $\geq 95\%$ conversion after 24 h (Figure S15). When the catalyst loading was lowered for the reaction with **2 a**, 52% conversion to **3 a** was observed in the presence of



Scheme 1. Dehydrogenations of a) $\text{Me}_2\text{NH}\cdot\text{BH}_3$ (**2a**) and b) $i\text{Pr}_2\text{NH}\cdot\text{BH}_3$ (**2b**) catalyzed by **1a**.

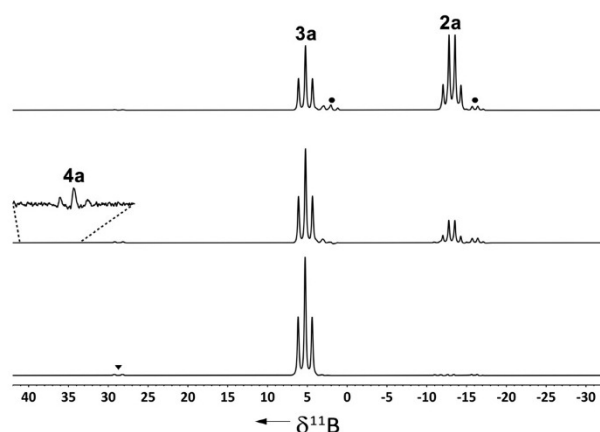
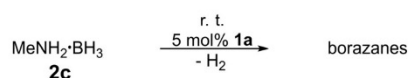


Figure 5. ^{11}B NMR spectra of the reaction of dimethylamine borane (**2a**) with 5 mol% **1a** in dme at room temperature (from top to bottom: 4, 8, 16 h; $\nabla = (\text{Me}_2\text{N})_2\text{BH}$; $\bullet = 5$).

3 mol% of **1a** after 24 h and $\geq 95\%$ conversion was achieved after 48 h. As expected, when the catalyst loading was increased, the reaction proceeded at a faster rate, giving $\geq 95\%$ conversion to **3a** after 8 h in the presence of 10 mol% of **1a** (Table 1). Interestingly, the catalytic activity of **1a** towards primary amine boranes proved to be lower. When methylamine borane **2c** was treated with 5 mol% of **1a** in dme at room temperature, dehydrocoupling occurred to give different borazane species (Scheme 2), as indicated by ^{11}B NMR spectroscopy and ESI mass spectrometry (Figures S16 and S26).^[15]



Scheme 2. Dehydrocoupling of $\text{MeNH}_2\cdot\text{BH}_3$ (**2c**) catalyzed by magnesocenophane **1a**.

However, only around 20% conversion was observed for this reaction after 24 h. When the catalyst loading was increased to 10 mol%, around 30% conversion was observed after 24 h at room temperature. This profound deviation might be due to catalyst degradation in the presence of the more reactive substrate **2c**, but the exact reason remains unclear at this point.

Table 1. Reaction parameters for the catalytic dehydrocoupling of dimethylamine borane **2a** ($c_0 = 850 \text{ mM}$) with magnesocenophanes **1a–d**, magnesocene (Cp_2Mg), and *n*-butylmagnesium ($n\text{Bu}_2\text{Mg}$) under ambient conditions.

(Pre)catalyst (loading [mol %])	Reaction time [h]	Solvent	Conversion [%]	TON/TOF [h^{-1}]
1a (5)	16	dme	≥ 95	20/1.2
1a (10)	8	dme	90	9/1.1
1a (3)	24	dme	52	17/0.7
1a (3)	48	dme	≥ 95	31/0.6
1a (5)	24	thf	42	8/0.3
1a (5)	24	Et_2O	28	6/0.2
1a (5)	24	$\text{C}_6\text{H}_4\text{F}_2$	17	4/0.2
1a (5)	24	C_6D_6	15	3/0.1
1b (5)	16	dme	76	15/0.9
1b (5)	24	dme	≥ 95	19/0.8
1c (5)	24	dme	50	10/0.4
1d (5)	24	dme	23	5/0.2
Cp_2Mg (5)	16	dme	75	14/0.9
Cp_2Mg (5)	24	dme	≥ 95	16/0.7
$n\text{Bu}_2\text{Mg}$ (5)	24	dme	≤ 5	–

In previously reported lithium- and magnesium-based systems, strong solvent effects were observed, insofar as dehydrocoupling reactions were slower in donor solvents, such as thf, but faster in non-coordinating solvents, such as aromatic hydrocarbons.^[5,16] This can be rationalized in terms of coordination of the solvent to the metal atom of the catalyst, essentially blocking binding of the substrate. In contrast, in the case of magnesocenophane **1a**, the reaction proceeded much more rapidly in dme than in benzene, toluene, or 1,2-difluorobenzene, which can primarily be attributed to the extremely low solubility of **1a** in non-coordinating solvents. Comparing coordinating solvents, the reaction is faster in dme than in thf (Table 1), which might be related to the observed reversibility of dme coordination to the magnesium atom, suggesting that thf is more tightly bound than dme (see above). In addition, it should be noted that different solvents can have a significant impact on equilibria between different species, which is believed to be important in the present catalysis (see below).

Remarkably, the present reactions proceed at room temperature, whereas previously reported magnesium (pre)catalysts **I–IV** operate only at elevated temperatures. Moreover, this represents a rare example of a main group metallocene being employed in homogeneous catalysis. It should be noted, however, that Kays' catalyst **IV** fully converts dimethylamine borane **2a** into cyclic diborazane **3a** within 150 min at 333 K at 5 mol% [Mg]. In order to benchmark our system against this, we also conducted catalytic experiments at 333 K. At this temperature, magnesocenophane **1a** catalyzes the reaction at a much faster rate, with $\geq 95\%$ conversion of **2a** into **3a** being observed after just 90 min in the presence of 5 mol% **1a** in dme ($\text{TON} = 20$; $\text{TOF} = 13.4 \text{ h}^{-1}$),^[15] making it even faster than Kays' catalyst **IV**.

To follow the reaction conveniently and to determine kinetic data, we applied in situ ^{11}B NMR spectroscopy. The reaction of **2a** and 5 mol% **1a** was conducted in an NMR tube at 323 or

333 K within the spectrometer, and spectra were acquired at appropriate intervals (Figure 6; Figures S3–S8 and S13). The results suggested pseudo-first-order kinetics for the conversion of **2a** at 323 K, as a linear fit for $\ln[2a]$ vs. t was obtained. For the reaction at 333 K, however, a significant deviation from a linear fit was observed, especially at lower substrate concentration, indicating a complex mechanism with more than one reaction route. Comparable reaction profiles were observed for the catalysis at room temperature, monitored by discontinuous ^{11}B NMR measurements (Figures S1 and S2).^[15]

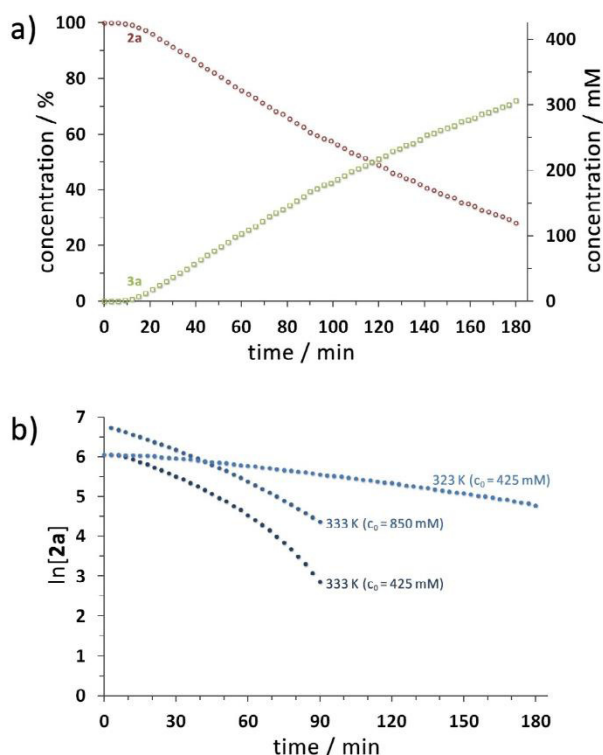


Figure 6. a) Plots of **[2a]** and **[3a]** versus time for the reaction of $\text{Me}_2\text{NH-BH}_3$ (**2a**) with 5 mol% **1a** in dme at 323 K. b) Plots of $\ln[2a]$ versus time for different reactions of $\text{Me}_2\text{NH-BH}_3$ (**2a**) with 5 mol% **1a** in dme at 323 and 333 K (reactions at 323 K were monitored until > 70% conversion; reactions at 333 K were monitored until > 90% conversion).

Having obtained these intriguing results, we also investigated the catalytic activities of magnesocenophanes **1b–d** and magnesocene (Cp_2Mg) towards dimethylamine borane **2a**. Interestingly, although these compounds also catalyze the dehydrogenation of **2a** at room temperature, they do so at slower rates (Table 1).

For the reaction of **2a** with 5 mol% Si[1]magnesocenophane **1b** in dme at room temperature, 76% conversion was observed after 16 h, whereas only 50% conversion was observed after 24 h in the case of C[2]magnesocenophane **1c**, and just 23% after 24 h in the case of Si[2]magnesocenophane **1d**. Notably, magnesocene performed similarly to Si[1]magnesocenophane **1b**, giving 75% conversion after 16 h, but it must not

be overlooked in this context that magnesocene exhibits better solubility in many solvents than [1]magnesocenophanes **1a,b**. Overall, catalytic activity is evidently strongly influenced by the ligand system. In particular, the differences between [1]- and [2]magnesocenophanes are considerable (Table 1). This indicates that the *ansa* ligand system plays an important role in the dehydrocoupling catalysis and suggests that magnesocenophanes are not simply catalyst precursors (precatalysts).

We proceeded to investigate the possible coordination of dimethylamine borane **2a** to magnesocenophanes **1a–d** computationally. Based on known coordination modes of hydridoamines to magnesocene (Figure 7, left)^[10b,d] and our DFT calculations, we predict a coordination mode whereby the amine borane binds to the magnesium atom through two B–H moieties and forms a hydrogen bond between its N–H group and the π system of one cyclopentadienyl ligand under elongation of the corresponding Mg–Cp bond (Figure 7, center).

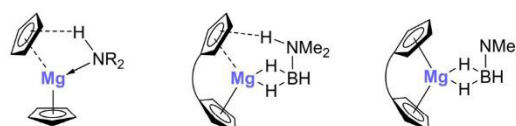


Figure 7. Coordination of hydrido-amines to magnesocene (left), of hydrido-amine boranes to magnesocenophanes (center), and of trimethylamine borane to magnesocenophanes (right).

Our computational investigation of the coordination of dimethylamine borane **2a** to magnesocenophanes **1a–d** reveals that the complexation energies roughly correlate with the dihedral angles of the Cp planes in the latter, with the largest binding energy being calculated for C[1]magnesocenophane **1a**, which is predicted to have the largest dihedral angle α , and lower binding energies being calculated for the less bent **1b–d** with smaller dihedral angles α (Table 2).

Compound	$E^{[a]}$	$[n]^{[b]}$	E [kJ mol $^{-1}$]	G^{298} [kJ mol $^{-1}$]
1a	C	1	−116.5	−63.3
1b	Si	1	−104.3	−53.2
1c	C	2	−66.2	−17.8
1d	Si	2	−61.4	−10.8

[a] E = bridging atom(s) of *ansa* bridge; [b] n = number of bridging atom(s) in *ansa* bridge.

This is in part a result of the influence of the *ansa* bridge on the $\text{Cp}\cdots\text{H-N}$ hydrogen bonds. Shorter *ansa* bridges promote stronger hydrogen bonds due to a more bent geometry of the Cp groups, whereas longer *ansa* bridging motifs result in more parallel oriented Cp ligands, disfavoring the establishment of $\text{Cp}\cdots\text{H-N}$ hydrogen bonds. Moreover, Lewis acidity of the magnesium center, which is predicted to be highest for C[1]magnesocenophane **1a**, and to decrease in **1b–d** as a function of di-

hedral angle α , favors stronger coordination of the B–H moieties to the magnesium atom. This is evident from the complexation energies for trimethylamine borane (Figure 7, right; Table 3). Stronger Mg–H–B coordination favors B–H bond acti-

Table 3. Calculated complexation energies E and G^{298} between trimethylamine borane and magnesocenophanes 1 a–d (Figure 7, right).				
Compound	$E^{[a]}$	$[n]^{[b]}$	E [kJ mol $^{-1}$]	G^{298} [kJ mol $^{-1}$]
1 a	C	1	–81.4	–32.7
1 b	Si	1	–64.5	–16.7
1 c	C	2	–51.6	–3.0
1 d	Si	2	–30.9	+15.1

[a] E =bridging atom(s) of *ansa* bridge; [b] n =number of bridging atom(s) in *ansa* bridge.

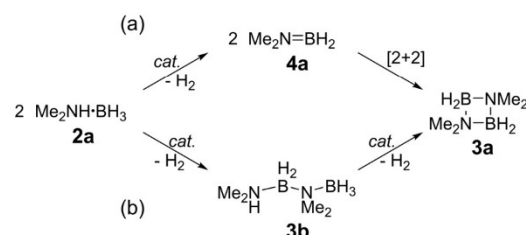
vation, which might explain the differences in catalytic performance. Assuming that, under the catalytic conditions in solution, substrate complexes (**1 a–d**)·**2 a** exist in equilibrium with the corresponding dme adducts (**1 a–d**)·dme and solvent adducts of the amine borane complexes (**1 a–d**)·dme·**2 a**, these differences in binding energies will have an important impact on such equilibria and therefore on the substrate activation, and might explain the observed differences in overall catalytic activities. It should be noted, however, that other effects, such as solubilities and ligand stabilities, must also be taken into account, and that binding energies of dme are different for each of the magnesocenophanes **1 a–d**.^[17]

Mechanistic investigations

The most intriguing aspect of the dehydrocoupling catalysis presented here is that the conversion of dimethylamine borane **2 a** into cyclic diborazane **3 a** proceeds at room temperature, unlike with previously reported magnesium-based systems, which required elevated temperatures.^[4,5] We therefore investigated the mechanism in detail, and suggest that the reaction proceeds in a ligand-assisted cooperative manner, with stepwise proton and hydride transfer from the amine borane molecule to the magnesocenophane and subsequent hydrogen elimination.

In principle, two different intermediates can be envisaged for the dehydrocoupling of dimethylamine borane **2 a** to cyclic diborazane **3 a**, namely dimethylaminoborane **4 a**, which is short-lived at room temperature and could undergo an off-metal [2+2] cycloaddition to give **3 a** (Scheme 3a), and linear diborazane **3 b**, which could undergo catalyzed ring-closing dehydrocoupling to give **3 a** (Scheme 3b).

In both pathways, the N–H and B–H bonds of substrate **2 a** have to be activated and cleaved. Therefore, selective deuteration of substrate **2 a** should provide insight into which of these bonds is broken in the rate-determining step. Investigations of kinetic isotope effects (KIEs) for starting material conversion with the deuterated substrate derivatives Me₂ND·BH₃ (**2 aND**), Me₂NH·BD₃ (**2 aBD**), and Me₂ND·BD₃ (**2 aNDBD**) gave KIEs of $k(2a)/k(2aND)=2.24$ for deuteration on nitrogen, $k(2a)/$



Scheme 3. Dehydrocoupling of Me₂NH·BH₃ (**2 a**) to give [Me₂NBH₂]₂ (**3 a**) via a) Me₂N=BH₂ (**4 a**) or b) Me₂NH–BH₂–NMe₂–BH₃ (**3 b**) as intermediates.

$k(2aBD)=1.62$ for deuteration on boron, and $k(2a)/k(2aNDBD)=3.46$ for the fully deuterated substrate (rate constants: $k(2a)=1.22(1)\times 10^{-4} s^{-1}$, $k(2aND)=5.45(1)\times 10^{-5} s^{-1}$, $k(2aBD)=7.51(9)\times 10^{-5} s^{-1}$, and $k(2aNDBD)=3.53(2)\times 10^{-5} s^{-1}$; Figure 8).

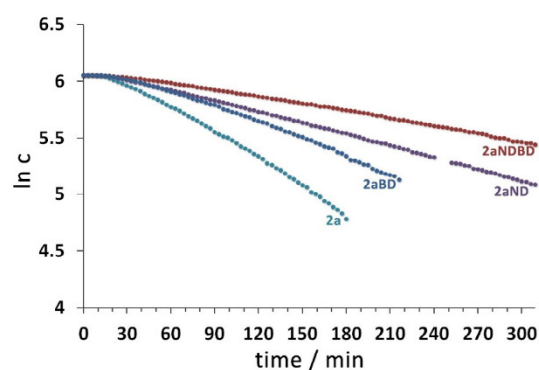
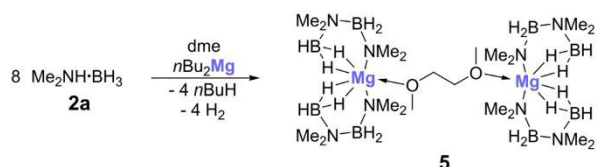


Figure 8. Plots of $\ln[2a]$, $\ln[2aND]$, $\ln[2aBD]$, and $\ln[2aNDBD]$ versus time for the reactions of Me₂NH·BH₃ (**2 a**), Me₂ND·BH₃ (**2 aND**), Me₂NH·BD₃ (**2 aBD**), and Me₂ND·BD₃ (**2 aNDBD**) with 5 mol% **1 a** in dme at 323 K (reactions were monitored until > 50% conversion in all cases).

These KIEs are different to those reported by Kays et al. for their magnesium-based catalyst **IV**, but are similar to those observed for an iron diketiminate catalyst.^[18] This suggests that cleavage of the N–H bond might occur in the rate-determining step. The results must be interpreted with caution, however, as the mechanism is complex and most likely involves different catalytic cycles (see below).

In their early work, Hill et al. succeeded in structurally characterizing a key intermediate, **I**, in the dehydrocoupling of dimethylamine borane **2 a** with dibutylmagnesium.^[4a] In the borylamido magnesium compound, the magnesium atom is complexed by two deprotonated, and hence anionic, linear diborazane moieties. This compound was shown to form cyclic diborazane **3 a** at temperatures above 333 K. We therefore investigated whether a similar intermediate plays a role in the dehydrocoupling reaction of dimethylamine borane **2 a** catalyzed by magnesocenophane **1 a**. First, we performed a reaction under the conditions normally applied for **1 a** (r.t., 16 h, dme), but using 5 mol% of dibutylmagnesium. In this experiment, virtually no formation of **3 a** was observed after 16 h by

^{11}B NMR (Table 1), although signals of a magnesium complex, similar to those described by Hill and co-workers, were observed. We therefore directly synthesized, isolated, and structurally characterized this compound, following Hill's protocol,^[4a] but using dme as solvent (Scheme 4, Figure 9).^[15]



Scheme 4. Synthesis of borylamido magnesium complex 5.

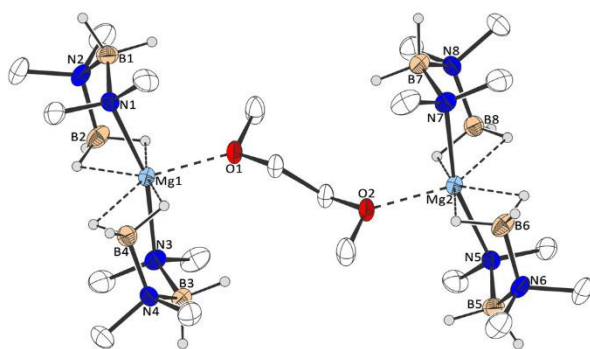
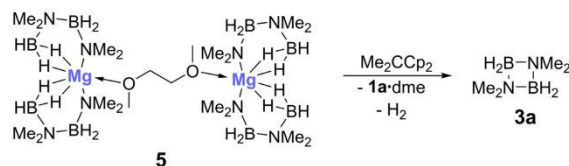


Figure 9. Molecular structure of 5 in the crystal (thermal ellipsoids at 50% probability level; hydrogen atoms except (B)–H omitted for clarity; selected bond lengths: Mg1/2–O1/2: 218.1, Mg1/2–N1/3/5/7: 215.9/216.1 pm).

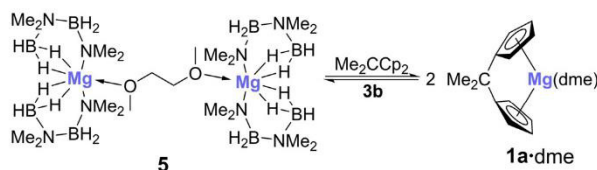
Complex 5 exhibits two crystallographically equivalent magnesium centers in a distorted pentagonal-bipyramidal configuration, in which the equatorial plane is defined by the four hydrogen atoms and the oxygen atom, with the nitrogen atoms in axial positions.^[15] The Mg–N bond lengths are very similar to those in the thf analogue, but the Mg–O bond lengths are around 10 pm shorter in the thf complex.^[4a] In this context, it is also worth noting that heptacoordinated magnesium complexes are quite rare.^[19] Compound 5 proved to be stable at room temperature under an inert atmosphere for many weeks and in organic solvents for at least several days. It does not undergo conversion to cyclic diborazane 3a, even in the presence of additional amounts of dimethylamine borane 2a, exactly how Hill and co-workers described for the thf analogue.^[4a] However, heating a solution of 5 to temperatures in excess of 333 K does slowly produce 3a, again in line with what was reported by Hill and co-workers.^[4a] We therefore conclude that this compound is not a key intermediate in the room temperature dehydrocoupling of 2a. However, when a solution of complex 5 in dme or thf was treated with 2,2-dicyclopentadienylpropane, the neutral protonated ligand of magnesocenophane 1a at room temperature, some formation of 3a was evident from the ^{11}B NMR spectrum (Scheme 5, Figure S21).^[15] Moreover, most significantly, two triplets in the ^1H NMR spectrum of the solution in thf at $\delta^1\text{H}$ = 5.60 and 5.70 ppm clearly



Scheme 5. Reaction of magnesium complex 5 with 2,2-dicyclopentadienylpropane to give cyclic diborazane 3a.

indicated the formation of magnesocenophane 1a·(thf)₂ from the reaction of complex 5 with 2,2-dicyclopentadienylpropane (Figure S22).^[15]

This clearly shows that the *ansa* ligand plays an important role in the room temperature dehydrocoupling catalysis, and that magnesocenophane 1a is formed from complex 5 and 2,2-dicyclopentadienylpropane. Under catalytic conditions, magnesium complex 5 most likely exists in equilibrium with magnesocenophane 1a (Scheme 6), as both the neutral ligand, 2,2-dicyclopentadienylpropane, as well as 1a, are observed by ^1H NMR spectroscopy. Accordingly, we believe that 1a is the relevant precatalyst and that 1a·dme·2a may be the catalytically active species in the dehydrogenation/dehydrocoupling process.

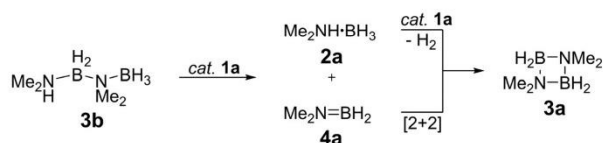


Scheme 6. Reaction of magnesium complex 5 with 2,2-dicyclopentadienylpropane to give magnesocenophane 1a.

Since linear diborazane 3b must be formed in at least small quantities through this equilibrium, we decided to directly study its reactivity towards magnesocenophane 1a under catalytic conditions. When 3b was treated with 5 mol% of 1a in dme at room temperature, dehydrocoupling to cyclic diborazane 3a was observed, but at a slower rate, giving only 63% of 3a after 16 h ($\geq 95\%$ conversion was observed after 16 h for the reaction of 2a with 5 mol% 1a under these conditions). This implies that linear diborazane 3b is most likely not the sole key intermediate in the catalysis, and that there must be a second, faster reaction route.

Interestingly, the reaction does not proceed exclusively through simple ring-closing dehydrocoupling, but also appears to proceed through a disproportionation route, as significant amounts of dimethylamine borane 2a were observed by ^{11}B NMR spectroscopy (Scheme 7, Figure S17).

Close inspection of the ^{11}B NMR spectrum of the reaction mixture obtained from dimethylamine borane 2a and 5 mol% of magnesocenophane 1a reveals four small signals, indicative of intermediates and side products formed in the reaction (Figure 5). A set of a quartet and a triplet observed at

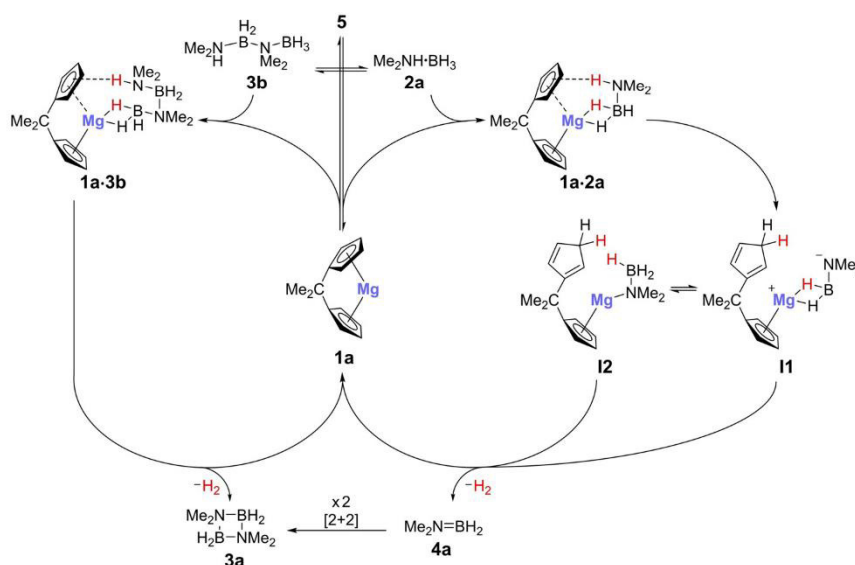


Scheme 7. Dehydrocoupling of $\text{Me}_2\text{NH}-\text{BH}_2-\text{NMe}_2-\text{BH}_3$ (**3b**) catalyzed by **1a**.

$\delta^{11}\text{B} = -15.4$ (q, $^1J_{\text{BH}} = 89$ Hz) and 3.7 ppm (t, $^1J_{\text{BH}} = 102$ Hz) corresponds to complex **5**. These signals were observed at an early stage of the reaction, did not increase with time, and then disappeared at the end of the reaction ($\geq 95\%$ conversion), consistent with the assumed equilibrium between complex **5** and magnesocenophane **1a**. A doublet observed at $\delta^{11}\text{B} = 28.7$ ppm ($^1J_{\text{BH}} = 132$ Hz) corresponds to bis(dimethylamino)borane, a well-known side product in the dehydrocoupling of **2a**,^[4] and most likely not an intermediate in the catalytic cycle. Most importantly, a low-field shifted triplet observed at $\delta^{11}\text{B} = 37.7$ ppm ($^1J_{\text{BH}} = 128$ Hz) is indicative of the formation of dimethylaminoborane **4a**, which is known to be a key intermediate in the dehydrogenation/dehydrocoupling of **2a** in many catalytic systems.^[3] Thus, this gives an important indication as to how the reaction might proceed. Because **4a** undergoes rapid, off-metal [2+2] cycloaddition at room temperature to form cyclic diborazane **3a**, it is short-lived and only observed in small amounts in the reaction mixture. Therefore, to further verify its formation, the reaction was carried out in the presence of cyclohexene as a hydroboration trapping agent. In this case, some of the formed **4a** reacted with the cyclohexene to form dimethylamino-dicyclohexylborane, which is persistent at room temperature and could be detected in the ^{11}B NMR spectrum at $\delta^{11}\text{B} = 44.2$ ppm ($\nu_{1/2} = 218$ Hz) (Figure S14).^[15] This

provides strong evidence for the presence of **4a** in the reaction solution.

Based on these findings, we propose the reaction mechanism outlined in Scheme 8. Magnesium complex **5** exists in equilibrium with magnesocenophane **1a**. Linear diborazane **3b** is formed from the reaction of complex **5** with 2,2-dicyclopentadienylpropane. Formation of magnesocenophane **1a** from **5** could be observed by ^1H NMR spectroscopy (see above), and it is important to point out that complex **5** has been reported previously,^[4a] and has been confirmed to be inactive in the ring-closing dehydrocoupling of linear diborazane **3b** to cyclic diborazane **3a** under ambient conditions. In a minor catalytic cycle (Scheme 8, left side), magnesocenophane may dehydrocouple **3b** to **3a**. This was found to occur at a slower rate than the conversion of **2a** to **3a**, and to produce **2a** in the process (see above). On the other hand, in what we believe to be the main cycle (Scheme 8, right side), **2a** is directly dehydrogenated by magnesocenophane **1a** to give dimethylaminoborane **4a**, which undergoes an off-metal [2+2] cycloaddition to form **3a**. This pathway is supported by the observation and trapping of **4a** (see above). Here, the first reaction step is protonation of one of the Cp moieties by the proton of the amine group to give intermediate **I1**. According to the observed KIEs (Figure 8), this is the rate-determining step. The resulting intermediate **I1** might rearrange to a magnesium amidoborane intermediate **I2**. Such metal amido complexes have often been implicated as intermediates in amine borane dehydrocoupling reactions.^[3] In the following step, B–H bond activation and hydrogen elimination form **4a** and regenerate **1a**. Notably, HD is observed by ^1H NMR spectroscopy ($\delta^1\text{H} = 4.50$ ppm, $^1J_{\text{HD}} = 43$ Hz), even when the fully deuterated substrate **2a**NDBD is used, and deuterated Cp carbon atoms are observed by ^{13}C NMR spectroscopy (Figures S24 and S25). This is in agreement with the proposed protonation and



Scheme 8. Simplified proposed catalytic cycle (coordinating solvent molecules omitted) for the dehydrogenation of $\text{Me}_2\text{NH}-\text{BH}_3$ (**2a**) and $\text{Me}_2\text{NH}-\text{BH}_2-\text{NMe}_2-\text{BH}_3$ (**3b**) to cyclic diborazane **3a**, catalyzed by magnesocenophane **1a**.

deprotonation of a Cp moiety of magnesocenophane **1a**. A similar ligand-assisted route with consecutive proton and hydride transfer has also been suggested by Kays and co-workers for their magnesium catalyst **IV**.^[5]

Following the experimental investigations, we turned to computational modeling of the proposed reaction pathway. To ensure that these DFT calculations were as close as possible to the experimental system, solvent coordination was considered and a dme molecule was placed on the magnesium atom in all structures. Indeed, DFT calculations at the B3LYP-D3/def2-TZVP level of theory supported the proposed catalytic cycle for dehydrogenation of dimethylamine borane **2a** and formation of dimethylaminoborane **4a** (Scheme 8, right side; Figure 10).^[11]

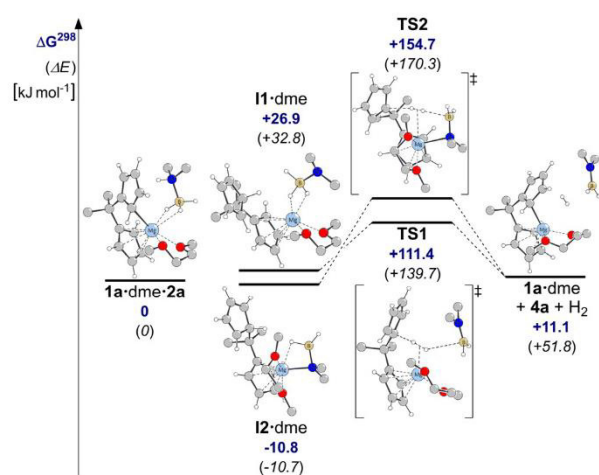


Figure 10. Calculated reaction pathways for the dehydrogenation of dimethylamine borane (**2a**) via dimethylaminoborane (**4a**), catalyzed by **1a**-dme (calculated at the B3LYP-D3/def2-TZVP level of theory^[11]; hydrogen atoms of CH₂ and CH₃ groups omitted for clarity).

It is predicted that protonation of the cyclopentadienyl moiety to give intermediate **I1**-dme is endergonic, but that the amido-magnesium intermediate **I2**-dme is lower in energy ($\Delta G^{298}(\mathbf{I1}\text{-dme}/\mathbf{I2}\text{-dme})=37.7\text{ kJ mol}^{-1}$) and exergonic with respect to the initial complex **1a**-dme-**2a**. Two different transition states, **TS1** and **TS2**, for the metal-mediated B–H bond activation, hydrogen elimination, and formation of dimethylaminoborane **4a**, starting from intermediates **I1**-dme and **I2**-dme, could be located on the potential energy surface, leading to the same product. Transition state **TS2**, connected to **I2**-dme, is higher in energy than transition state **TS1**, connected to **I1**-dme ($\Delta G^{298}(\mathbf{TS1}/\mathbf{TS2})=43.3\text{ kJ mol}^{-1}$), which suggests that the pathway via intermediate **I1**/**TS1** might be more feasible than that via intermediate **I2**/**TS2**, although neither can be ruled out completely.

When solvent coordination to the magnesium center was neglected and no dme molecule was coordinated to the magnesium atom, a similar pathway could be located on the potential energy surface (Figure S29).^[15]

Although the reaction was calculated to be slightly endergonic, the overall driving forces are the elimination of hydro-

gen and the dimerization of dimethylaminoborane **4a** to give cyclic diborazane **3a**, both of which prevent back-reactions. In this context, it is noteworthy that the reaction of dimethylamine borane **2a** with 5 mol% magnesocenophane **1a** in thf was found to proceed significantly more slowly when performed in a sealed reaction vessel (42% conversion after 24 h with 5 mol% **1a**) than in an open reaction vessel (95% conversion after 24 h with 5 mol% **1a**). Overall, the calculated reaction pathway is in agreement with our experimental observations.

Conclusions

In summary, we have reported the first magnesium-based catalyst for the dehydrocoupling of dimethylamine borane **2a** to cyclic tetramethyldiborazane **3a** that operates at room temperature. In addition, at elevated temperatures, it outperforms previously reported magnesium-based catalysts in the field,^[4,5] and represents a rare example of a main-group metallocene being employed as a catalyst. Furthermore, different [1]- and [2]magnesocenophanes have been investigated, and significant differences in the catalytic activities of these compounds have been discerned, which we believe to be a function of the tilt of the cyclopentadienyl moieties and related differences in substrate binding.

Experimental and computational investigations of the mechanism suggest a pre-equilibrium between magnesocenophane **1a** and magnesium complex **5** and clearly indicate that **1a** is the catalyst in the reaction, which is believed to operate through a ligand-assisted route involving stepwise proton and hydride transfer, with dimethylaminoborane **4a** as the key intermediate.

Overall, magnesocenophane **1a** represents the most active magnesium catalyst for amine borane dehydrogenation/dehydrocoupling reported to date, and future studies will focus on the dehydrocoupling of various other substrates.

Acknowledgements

Prof. Dr. G. Kickelbick is thanked for his continuous support. Dr. K. Hollemeyer at the Mass Spectrometry Service of Saarland University is thanked for ESI-MS measurements. S. Harling is thanked for elemental analyses. Funding by the Deutsche Forschungsgemeinschaft (DFG; SCHA 1915b/3-1) and the Fonds der Chemischen Industrie is gratefully acknowledged.

Conflict of interest

The authors declare no conflict of interest.

Keywords: amine boranes • catalysis • dehydrocoupling • magnesium • metallocenophanes

- [1] a) R. J. Keaton, J. M. Blacquiere, R. T. Baker, *J. Am. Chem. Soc.* **2007**, *129*, 1844–1845; b) B. Peng, J. Chen, *Energy Environ. Sci.* **2008**, *1*, 479–483; c) C. W. Hamilton, R. T. Baker, A. Staubit, I. Manners, *Chem. Soc. Rev.*

- 2009, 38, 279–293; d) A. Staubitz, A. P. M. Robertson, I. Manners, *Chem. Rev.* **2010**, 110, 4079–4124.
- [2] a) A. Staubitz, A. Presa Soto, I. Manners, *Angew. Chem. Int. Ed.* **2008**, 47, 6212–6215; *Angew. Chem.* **2008**, 120, 6308–6311; b) D. Marinelli, F. Fasano, B. Najjari, N. Demitri, D. Bonifazi, *J. Am. Chem. Soc.* **2017**, 139, 5503–5519; c) O. Ayhan, T. Eckert, F. A. Plamper, H. Helten, *Angew. Chem. Int. Ed.* **2016**, 55, 13321–13325; *Angew. Chem.* **2016**, 128, 13515–13519; d) T. Lorenz, A. Lik, F. A. Plamper, H. Helten, *Angew. Chem. Int. Ed.* **2016**, 55, 7236–7241; *Angew. Chem.* **2016**, 128, 7352–7357; e) A. Ledoux, P. Larini, C. Boisson, V. Monteil, J. Raynaud, E. Lacôte, *Angew. Chem. Int. Ed.* **2015**, 54, 15744–15749; *Angew. Chem.* **2015**, 127, 15970–15975; f) M. Grosche, E. Herdtweck, F. Peters, M. Wagner, *Organometallics* **1999**, 18, 4669–4672; g) D. A. Resendiz-Lara, N. E. Stubbs, M. I. Arz, N. E. Pridmore, H. A. Sparkes, I. Manners, *Chem. Commun.* **2017**, 53, 11701–11704.
- [3] a) E. M. Leitao, T. Jurca, I. Manners, *Nat. Chem.* **2013**, 5, 817–829; b) R. Waterman, *Chem. Soc. Rev.* **2013**, 42, 5629–5641; c) H. C. Johnson, T. N. Hooper, A. S. Weller, *Top. Organomet. Chem.* **2015**, 49, 153–220; d) R. L. Melen, *Chem. Soc. Rev.* **2016**, 45, 775–788; e) T. E. Stennett, S. Harder, *Chem. Soc. Rev.* **2016**, 45, 1112–1128; f) A. Rossin, M. Peruzzini, *Chem. Rev.* **2016**, 116, 8848–8872; g) D. H. A. Boom, A. R. Jupp, J. C. Slootweg, *Chem. Eur. J.* **2019**, 25, 9133–9152.
- [4] a) D. J. Liptrot, M. S. Hill, M. F. Mahon, D. J. MacDougall, *Chem. Eur. J.* **2010**, 16, 8508–8515; b) M. S. Hill, M. Hodgson, D. J. Liptrot, M. F. Mahon, *Dalton Trans.* **2011**, 40, 7783–7790; c) P. Bellham, M. D. Anker, M. S. Hill, G. Kociok-Köhn, M. F. Mahon, *Dalton Trans.* **2016**, 45, 13969–13978.
- [5] A. C. A. Ried, L. J. Taylor, A. M. Geer, H. E. L. Williams, W. Lewis, A. J. Blake, D. L. Kays, *Chem. Eur. J.* **2019**, 25, 6840–6846.
- [6] a) J. Spielmann, M. Bolte, S. Harder, *Chem. Commun.* **2009**, 6934–6936; b) D. J. Liptrot, M. S. Hill, M. F. Mahon, A. S. S. Wilson, *Angew. Chem. Int. Ed.* **2015**, 54, 13362–13365; *Angew. Chem.* **2015**, 127, 13560–13563.
- [7] D. L. Anderson, *Chemical Composition of the Mantle in Theory of the Earth*, Blackwell Scientific Publications, Boston, **1989**, Chapter 8, pp. 147–175.
- [8] a) A. Schäfer, K. Rohe, A. Grandjean, V. Huch, *Eur. J. Inorg. Chem.* **2017**, 35–38; b) W. Haider, V. Huch, A. Schäfer, *Dalton Trans.* **2018**, 47, 10425–10428; c) A. S. D. Stahlich, V. Huch, A. Grandjean, K. Rohe, K. I. Leszczyńska, D. Scheschkewitz, A. Schäfer, *Chem. Eur. J.* **2019**, 25, 173–176.
- [9] a) P. J. Shapiro, S.-J. Lee, P. Perrotin, T. Cantrell, A. Blumenfeld, B. Twamley, *Polyhedron* **2005**, 24, 1366–1381; b) P. Perrotin, P. J. Shapiro, M. Williams, B. Twamley, *Organometallics* **2007**, 26, 1823–1826; c) P. Perrotin, B. Twamley, P. J. Shapiro, *Acta Crystallogr. Sect. E* **2007**, 63, m1277–m1278.
- [10] a) M. M. Olmstead, W. J. Grigsby, D. R. Chacon, T. Hascall, P. P. Power, *Inorg. Chim. Acta* **1996**, 251, 273–284; b) A. Xia, J. E. Knox, M. J. Heeg, H. B. Schlegel, C. H. Winter, *Organometallics* **2003**, 22, 4060–4069; c) A. Jaenschke, J. Paap, U. Behrens, *Organometallics* **2003**, 22, 1167–1169; d) A. Jaenschke, U. Behrens, *Z. Naturforsch. B* **2014**, 69, 655–664.
- [11] All DFT calculations were carried out using the Gaussian 09 Revision D.01 package of programs. See the Supporting Information for further details, optimized geometries, and references.
- [12] a) Room temperature/ambient conditions correspond to about 298 K; b) the amounts of starting material and product(s) were determined by integration of the ¹¹B NMR spectra.
- [13] Fluoride ion affinities were calculated according to a literature established method from the isodesmic reactions with Et₃B/Et₃BF⁻. For more details, see, for example: H. Großekappenberg, M. Reißmann, M. Schmidtman, T. Müller, *Organometallics* **2015**, 34, 4952–4958.
- [14] Global electrophilicity indices ω were calculated following the method of Stephan et al. (Method C): A. R. Jupp, T. C. Johnstone, D. W. Stephan, *Inorg. Chem.* **2018**, 57, 14764–14771.
- [15] See the Supporting Information for further details.
- [16] R. McLellan, A. R. Kennedy, S. A. Orr, S. D. Robertson, R. E. Mulvey, *Angew. Chem. Int. Ed.* **2017**, 56, 1036–1041; *Angew. Chem.* **2017**, 129, 1056–1061.
- [17] Calculated binding energies of dme to magnesocenophanes **1a–d** (B3LYP-D3/def2-TZVP)^[11]: **1a**: $E = -139.6 \text{ kJ mol}^{-1}$, $G^{298} = -87.1 \text{ kJ mol}^{-1}$; **1b**: $E = -127.4 \text{ kJ mol}^{-1}$, $G^{298} = -72.2 \text{ kJ mol}^{-1}$; **1c**: $E = -98.8 \text{ kJ mol}^{-1}$, $G^{298} = -44.0 \text{ kJ mol}^{-1}$; **1d**: $E = -82.2 \text{ kJ mol}^{-1}$, $G^{298} = -24.1 \text{ kJ mol}^{-1}$.
- [18] N. T. Coles, M. F. Mahon, R. L. Webster, *Organometallics* **2017**, 36, 2262–2268.
- [19] M. Seitz, A. Kaiser, S. Stempfhuber, M. Zabel, O. Reiser, *Inorg. Chem.* **2005**, 44, 4630–4636.

Manuscript received: January 9, 2020

Accepted manuscript online: February 13, 2020

Version of record online: April 28, 2020

3.2 Cross-Dehydrocoupling of Amines and Silanes Catalyzed by Magnesocenophanes

Lisa Wirtz, Jessica Lambert, Bernd Morgenstern, André Schäfer

Organometallics **2021**, *40*, 2108-2117.

DOI: 10.1021/acs.organomet.1c00245

Reprinted with the permission of L. Wirtz, J. Lambert, B. Morgenstern, A. Schäfer; Cross-Dehydrocoupling of Amines and Silanes Catalyzed by Magnesocenophanes. *Organometallics* **2021**, *40*, 2108-2117.

Copyright © (2021) American Chemical Society.

Author contribution:

Lisa Wirtz:

Lead: Investigation of amine borane dehydrocoupling, kinetic studies, determination of kinetic isotope effects, mechanistic investigations, writing, reviewing and editing of the manuscript and the supporting information;

Equal (J.L.): Synthesis and characterization of cycloalkylidene[1]magnesocenophanes, catalytic studies of amine silane cross-dehydrocoupling;

Equal (A.S.): DFT-calculations.

Jessica Lambert:

Equal (L.W.): Synthesis and characterization of cycloalkylidene[1]magnesocenophanes, catalytic studies of amine silane cross-dehydrocoupling;

Supporting: Mechanistic investigations.

Bernd Morgenstern:

Lead: X-ray analysis.

André Schäfer:

Lead: Project administration and supervision, funding acquisition;

Equal (L.W.): DFT-calculations;

Supporting: Writing, reviewing and editing of the manuscript and the supporting information.

Cross-Dehydrocoupling of Amines and Silanes Catalyzed by Magnesocenophanes

Lisa Wirtz,[†] Jessica Lambert,[†] Bernd Morgenstern, and André Schäfer*



Cite This: *Organometallics* 2021, 40, 2108–2117



Read Online

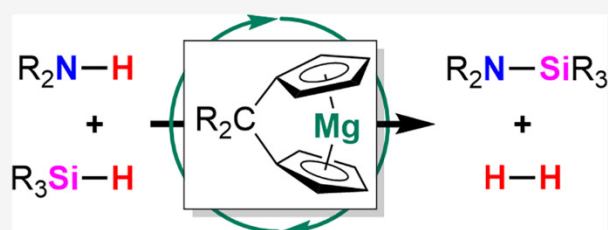
ACCESS |

Metrics & More

Article Recommendations

Supporting Information

ABSTRACT: The application of C[1]magnesocenophanes in dehydrocoupling catalysis is reported. Two new cycloalkylidene-bridged C[1]magnesocenophanes were synthesized and structurally characterized. These C[1]magnesocenophanes were used as catalysts in amine–borane dehydrocoupling and, more extensively, in amine–silane cross-dehydrocoupling. The substrate scope, involving different aliphatic, aromatic, and benzylic amines, was probed and the mechanism of this cross-dehydrocoupling catalysis was investigated.



INTRODUCTION

There has been an increasing interest in Si–N compounds in recent years, as their applications in organic chemistry and materials science have made them indispensable compounds.^{1–4} For instance, polysilazanes are used as precursors in the synthesis of Si–N-based polymers and ceramics and have found applications as ligands in organometallic chemistry.^{1–3,5–7} Due to this versatile use, an easy access to the compounds is of great interest. Established synthesis routes for the formation of Si–N bonds are often complex and produce undesired byproducts.^{2,8–10} For example, common reaction routes starting from halosilanes and amines^{2,8} or metal amides^{9,10} to give monosilazanes, disilylamines, and diamino-silanes also produce coupling products such as hydrogen halides and metal halide salts that have to be separated from the products. Dehydrocoupling reactions, on the other hand, present a more efficient method for the generation of Si–N bonds that can circumvent these difficulties, as only dihydrogen is produced as a byproduct.^{4,11} Metal-catalyzed cross-dehydrocoupling reactions of primary or secondary amines with hydrosilanes are therefore of great interest, and many different transition-metal (pre)catalysts have been developed in the past decade.^{12–16} With recent developments in s-block catalysis, the advantages of alkaline-earth-metal compounds with regard to the high occurrence in the Earth's crust of these elements and their low toxicities,¹⁷ in particular magnesium and calcium complexes, in amine–silane cross-dehydrocoupling catalysis has been brought into focus.^{18–28} Interestingly, only a handful of magnesium complexes have been employed as catalysts in the cross-dehydrocoupling catalysis of amines and silanes (Figure 1). Sadow et al. reported the use of a tris(oxazolinyl)boratomagnesium complex, I, as a (pre)catalyst for the formation of Si–N bonds, starting from primary aliphatic and aromatic amines with different silanes, giving high conversions even at room

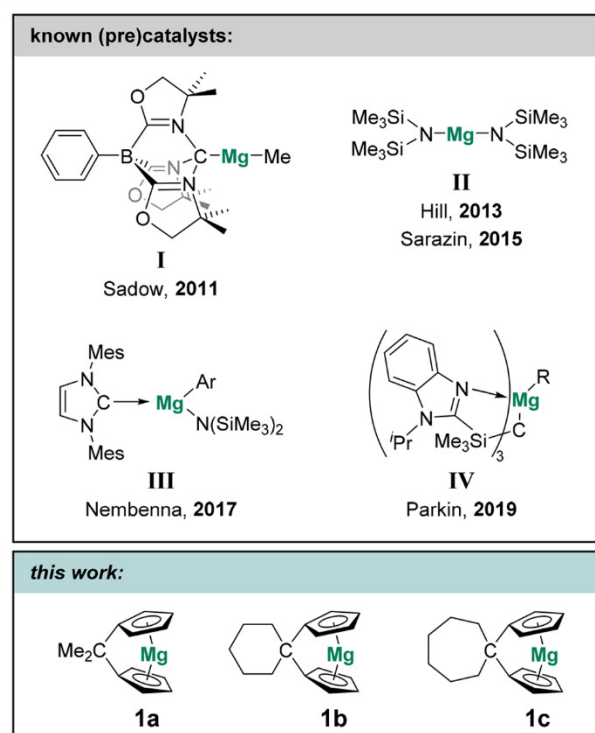


Figure 1. Selected magnesium (pre)catalysts for amine–silane cross-dehydrocoupling.

Received: April 21, 2021

Published: June 30, 2021



temperature.¹⁸ This was followed by reports of Hill et al.¹⁹ and Sarazin et al.²⁰ about the use of magnesium bis-(hexamethyldisilazide), **II**, as a readily and commercially available (pre)catalyst with a promising substrate scope. In many cases, the cross-coupling reactions proceeded under ambient conditions, giving $\geq 95\%$ conversion with a relatively low catalyst loading.^{19,20} In addition, Nembenna et al.²¹ and Parkin et al.²² showed that donor complexes of organomagnesium(II) compounds, **III** and **IV**, can also be utilized as (pre)catalysts in amine–silane cross-dehydrocoupling reactions, with Nembenna et al.'s system permitting a broader substrate scope and giving high conversions at a temperature range between room temperature and 373 K,²¹ while Parkin et al. reported the need of prolonged reaction times at temperatures of ≥ 373 K.²²

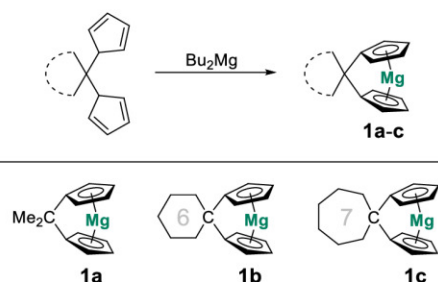
It is worth noting that although the use of transition-metal cyclopentadienide (Cp) complexes, such as metallocene- and half-sandwich-type compounds, in homogeneous catalysis is quite common,²⁹ the application of metallocene-type compounds of main-group elements as catalysts is extremely rare.³⁰ In this context, this is exemplified by the fact that compounds **I–IV** all exhibit σ -bonded alkyl, aryl, or amido ligands. However, we recently demonstrated the use of magnesocenophanes as catalysts in the dehydrocoupling of amine–boranes. In particular, a Me₂C[1]magnesocenophane proved to be a very potent catalyst in the dehydrocoupling of dimethyl- and diisopropylamine–borane.³⁰ With the resemblance between B–H and Si–H bonds, we were intrigued to extend the substrate scope of magnesocenophane-catalyzed dehydrocoupling reactions and investigate intermolecular amine–silane cross-dehydrocoupling.

Herein, we report the synthesis of two new cycloalkylidene-bridged C[1]magnesocenophanes—the first example of main-group metallocenophanes with these ligand systems—and the application of these carba[1]magnesocenophanes, **1a–c**, in amine–silane cross-dehydrocoupling catalysis.

RESULTS AND DISCUSSION

In the past, cycloalkylidene-bridged *ansa* ligands have been utilized only in transition-metal complexes, such as ytterbium, titanium, zirconium, hafnium, rhenium and iron,^{31–34} but until now have not been applied to any main-group elements. By the literature synthesis routes for 1,1-bis(cyclopentadienyl)-cyclohexane and -cycloheptane and subsequent treatment with dibutylmagnesium, a common approach in the synthesis of magnesocenophanes,³⁵ we could obtain the cyclohexylidene- and cycloheptylidene-bridged magnesocenophanes **1b,c** (Scheme 1).^{30,36,37}

Scheme 1. Synthesis of C[1]magnesocenophanes **1a–c**



1a–c are obtained as highly air-sensitive colorless solids, which are insoluble in hexane and sparingly soluble in benzene and toluene but dissolve rapidly in donor solvents such as thf and dme. Crystals, allowing for structural characterization of the solvent adducts of **1b,c** by single-crystal X-ray diffraction, were obtained from thf and dme solutions at 248 K (Figure 2).

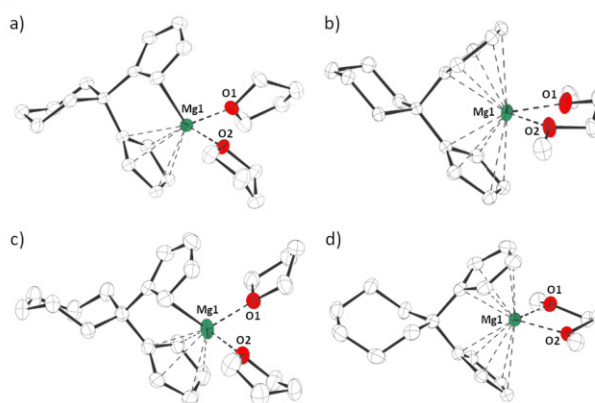


Figure 2. Molecular structures of (a) **1b**·(thf)₂, (b) **1b**·dme, (c) **1c**·(thf)₂, and (d) **1c**·dme in the crystal (displacement ellipsoids at the 50% probability level; hydrogen atoms omitted for clarity). Selected bond lengths (pm): **1b**·(thf)₂, Mg1–O1/2 202.52(22), 202.54(22), 203.39(21), 204.39(22); **1b**·dme, Mg1–O1/2 205.81(12), 206.05(12), 206.48(15), 207.73(12); **1c**·(thf)₂, Mg1–O1/2 202.00(26), 202.85(24), 203.24(16), 203.62(18), 204.20(25), 204.72(26); **1c**·dme, Mg1–O1/2 204.14(10), 210.37(11).

Not uncommon for magnesocenophanes, the coordination of donor molecules to the magnesium atom, such as thf, leads to ring slippage of one Cp ring in the solid state. Most thf complexes of magnesocenophanes show η^1/η^5 -bonded Cp groups in the solid state, whereas dme complexes usually exhibit an η^5/η^5 -bonded ligand system.³⁵ The solid state structures of **1b**·(thf)₂ and **1c**·(thf)₂ are similar to that of the previously reported **1a**·(thf)₂³⁷ and like **1b**·dme and **1c**·dme share structural features similar to those previously reported for **1a**·dme (Table 1).³⁰ Thus, the cycloalkylidene rings in the backbone of magnesocenophanes **1b,c** seem to have only a

Table 1. Selected Bond Lengths and Angles in C[1]magnesocenophanes **1a–c**^a

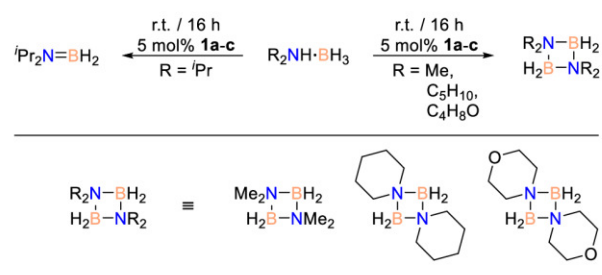
compound	Mg–Cp ^{cent} ^b (pm)	hapticity	α^c (deg)	$\delta^{b,d}$ (deg)
1a ·(thf) ₂ ³⁷	215.38(11)	η^1/η^5		
1a ·dme ³⁰	223.33(3); 225.38(3); 230.35(4)	η^5/η^5	77.8; 80.0	119.9; 121.7
1b ·(thf) ₂	213.47(9); 214.39(9)	η^1/η^5		
1b ·dme	223.46(5); 224.50(5); 225.53(5); 226.15(5)	η^5/η^5	77.7; 78.4	121.1; 122.1
1c ·(thf) ₂	212.45(11); 213.06(10); 217.76(7)	η^1/η^5		
1c ·dme	220.55(5); 224.01(5)	η^5/η^5	75.3	121.6
1c (BnNH ₂) ₂ ^c	211.13(8)	η^1/η^5		

^aMultiple values are given if more than one crystal structure was obtained, more than one molecule is found in the asymmetric unit, and/or the bond/angle is found more than once in the molecule. ^bOnly given for η^5 -bonded Cp groups. ^cDihedral angle of η^5 -Cp planes. ^dCp^{cent}–Mg–Cp^{cent} angle. ^eVide infra.

small influence on the coordination geometry around the magnesium atom in comparison to **1a**.

We recently demonstrated that $\text{Me}_2\text{C}[1]$ magnesocenophane **1a** is a potent catalyst in the dehydrocoupling of dimethylamine–borane and diisopropylamine–borane.³⁰ Therefore, the catalytic activity of the two new magnesocenophanes **1b,c** was first probed toward dimethylamine–borane and diisopropylamine–borane, and indeed was found to be similar to that of magnesocenophanes **1a**, with $\geq 95\%$ conversion after 16 h at ambient temperature in the presence of 5 mol % of **1b** or **1c**. In addition, the dehydrocoupling of piperidine–borane and morpholine–borane catalyzed by **1a–c** was investigated. Analogously to dimethylamine–borane, piperidine–borane and morpholine–borane are dehydrocoupled to give the corresponding cyclic diborazanes (morpholinyl diborazane: $\delta(^{11}\text{B})$ 2.1, $^1J_{\text{BH}} = 111$ Hz; piperidinyl diborazane: $\delta(^{11}\text{B})$ 2.7, $^1J_{\text{BH}} = 111$ Hz), in the presence of 5 mol % of **1a–c**, with $\geq 95\%$ conversion achieved after 16 h at room temperature (Scheme 2).

Scheme 2. Dehydrogenation/Dehydrocoupling of Dialkylamine–Boranes Catalyzed by C[1]magnesocenophanes **1a–c**

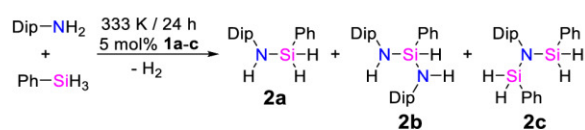


Following these promising results, we expanded the substrate spectrum and investigated intermolecular amine–silane cross-dehydrocoupling reactions catalyzed by magnesocenophanes **1a–c**, which, due to the similar electronic nature of B–H and Si–H bonds, seemed a promising target.

In the first instance, optimal reaction conditions for the amine–silane cross-dehydrocoupling reactions had to be found. We chose to use 5 mol % catalyst loading, as this is commonly reported in the literature^{18,19,21} and was found to be suitable in amine–borane dehydrocoupling. Furthermore, the performance of the catalytic dehydrocoupling of amine–boranes, catalyzed by magnesocenophanes **1a–c**, was previously found to be quite solvent dependent. Therefore, we performed the reaction of 2,6-diisopropylaniline with phenylsilane in the presence of 5 mol % of **1a–c** in different solvents (Scheme 3).

We found that reaction temperatures of 333 K were required to give 13–42% conversion after 24 h, depending on the

Scheme 3. Cross-Dehydrocoupling of 2,6-Diisopropylaniline and Phenylsilane Catalyzed by C[1]magnesocenophanes **1a–c**^{38a}

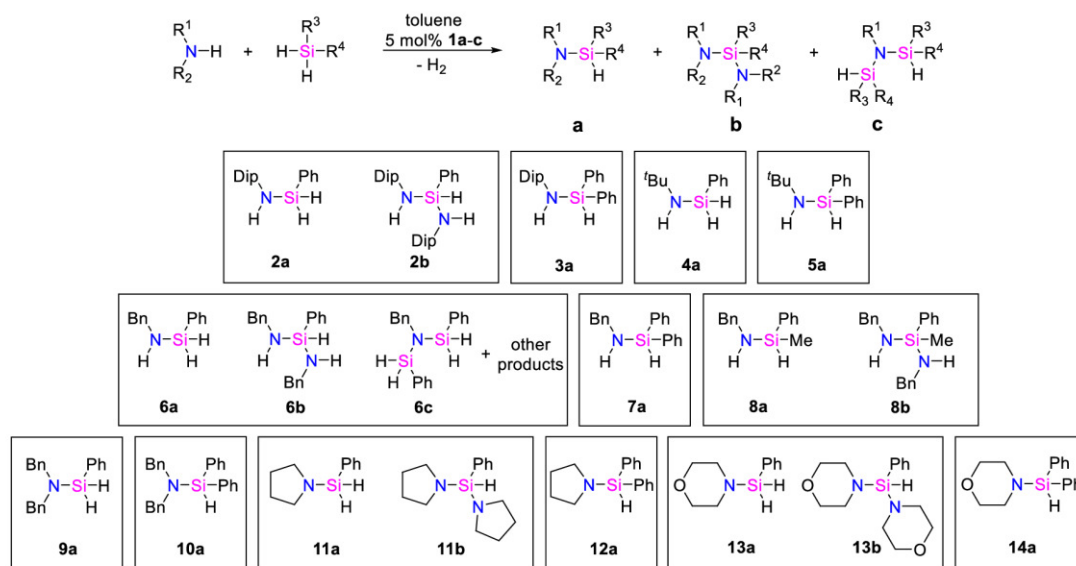


solvent and the catalyst. In addition, the ratio of formation of the different coupling products depends on the solvent and the catalyst. In most reactions, only monosilazane **2a** or a mixture of monosilazane **2a** and diaminosilane **2b** is formed. The formation of disilylamine **2c** occurs very rarely and only in the donor solvents thf and dme, whereas in other solvents disilylamine **2c** was not observed. Overall, a promising catalytic activity was observed in toluene, while the conversion was found to be much lower in thf, perhaps due to the coordinating nature of thf, which hinders substrate binding to the magnesium center. We therefore chose to conduct most of the catalytic reactions of this study in toluene.

Further investigations into a wider spectrum of amine and silane substrates, including primary and secondary aliphatic, aryl, and benzylic amines in combination with phenylsilane, diphenylsilane, and phenylmethylsilane, revealed a broad applicability of magnesocenophanes **1a–c** as cross-dehydrocoupling catalysts (Scheme 4 and Table 2). It is worth noting that we found in many cases higher conversions were observed with diphenylsilane than with phenylsilane. This is rather unusual, as many literature-known systems perform similarly with phenylsilane and diphenylsilane.^{19,21} While in several cases elevated temperatures are required, it is remarkable that the reactions with benzylamine proceeded under ambient conditions. The reactions of benzylamine with phenylsilane give a complex mixture of multiple products, including monosilazane **6a**, diaminosilane **6b**, and disilylamine **6c**. This is not uncommon, however, and was noted before by Hill et al. in the case of the precatalyst $\text{Mg}[\text{N}(\text{SiMe}_3)_2]$ (**II**).¹⁹ Notably, the best results could be achieved in the case of the reactions of benzylamine with diphenylsilane, selectively giving monosilazane **7a**, under ambient conditions, with an 80% yield after just 8 h. When all reactions with primary amines were compared, benzylamine was more reactive than aryl and aliphatic amines, while in the case of secondary amines, reactions with dialiphatic amines give higher conversions. When the catalytic activities of the magnesocenophanes **1a–c** are compared with one another, the differences are small, although **1c** seems to outperform **1a,b** in some cases. However, these differences in the catalytic activities can most likely be attributed to solubility effects and not mechanistic differences, as **1c** carries a larger cycloalkylidene group, giving a slightly higher solubility in toluene. Overall, the catalytic performance of magnesocenophanes **1a–c** is comparable to that of other magnesium catalysts in the field, in many cases.^{18,19,21} It is worth mentioning, however, that some heavier alkaline-earth-metal-based systems do catalyze the cross-dehydrocoupling of amine and silane more efficiently, at lower temperatures.^{20,24}

To gain further insight into the mechanism of the magnesocenophane-catalyzed cross-dehydrocoupling reactions, we chose the reaction of benzylamine with diphenylsilane as a model for further studies. In the first instance, it is important to understand how the amine and the silane interact with the magnesocenophane. We therefore reacted magnesocenophane **1c** independently with benzylamine and diphenylsilane in $\text{thf}-d_8$. The ^1H and ^{29}Si NMR spectra suggested no reaction between magnesocenophane **1c**(thf)₂ and diphenylsilane. On the other hand, a significant shift of the signals corresponding to the CH_2 and NH_2 moieties of benzylamine could be observed in the ^1H NMR spectrum in the case of the reaction of magnesocenophane **1c**(thf)₂ with benzylamine, while the signals of the *ansa*-ligand system remained mostly unchanged. This suggests coordination of the amine to the magnesium

Scheme 4. Cross-Dehydrocoupling of Amines and Silanes Catalyzed by C[1]magnesocenophanes 1a–c



atom in solution, giving a magnesocenophane amine complex (Scheme 5), and is in line with a previous report of magnesocene amine complexes.³⁹ We were able to obtain single crystals of this magnesocenophane bis(benzylamine) complex, **1c**·(BnNH₂)₂, as well as of a related *tert*-butylamine complex, from a thf solution at 248 K, allowing for a structural characterization by X-ray diffraction.

Similar to the aforementioned bis(thf) complexes, bis(benzylamine) complex **1c**·(BnNH₂)₂ exhibits one η^1 - and one η^5 -bonded Cp group in the solid state. The Mg–N bond lengths are shorter than those in a related magnesocene bis(benzylamine) complex, indicating a stronger bonding (Cp₂Mg·(BnNH₂)₂, Mg–N 214.61(28), 215.64(21) pm; **1c**·(BnNH₂)₂, Mg–N 210.65(23), 212.09(25) pm) (Figure 3).³⁹ This can be attributed to steric and electronic properties, as [1]magnesocenophanes have previously been discussed to possess a higher Lewis acidity and a more accessible magnesium center in comparison to the parent compound magnesocene (Cp₂Mg), due to their bent structures.³⁰

On the basis of these results, we propose that the initial step in the catalysis is the formation of a magnesocenophane amine complex. However, an important question is whether this is merely a precatalyst for some other organometallic magnesium species or a species in the catalytic cycle and thus if the *ansa*-ligand system stays coordinated to the magnesium atom during catalysis. To gain more information about this, we carried out a stoichiometric reaction of bis(benzylamine) complex **1c**·(BnNH₂)₂ with diphenylsilane and monitored it by ¹H and ²⁹Si NMR spectroscopy. The formation of a new Si–H doublet signal ($\delta(^1\text{H})$ 5.62, $^1J_{\text{SiH}} = 204.4$ Hz, $^3J_{\text{HH}} = 2.2$ Hz) was observed in the ¹H NMR spectrum, which can be attributed to monosilazane **7a**. This is further supported by the ²⁹Si{¹H} NMR spectrum giving rise to a signal corresponding to monosilazane **7a** ($\delta(^{29}\text{Si})$ –17.0). Over time, the amount of diphenylsilane decreased, while the amount of monosilazane **7a** increased. Most significantly, the characteristic resonance for the Cp protons of the magnesocenophane moiety remained almost unchanged, even after several days, and only an insignificant amount of free ligand was detected (Figure S15).

The fact that the magnesocenophane moiety can still be observed in the ¹H NMR spectrum at the end of the coupling reaction suggests that the magnesocenophanes indeed act as the catalytic species and not just as precatalysts, just as in the case of the dehydrocoupling of amine–boranes.³⁰

To get a closer insight into the kinetics of the reaction, we monitored the hydrogen evolution of the reaction as a function of pressure.³⁸ The cross-dehydrocoupling of benzylamine and diphenylsilane was carried out at ambient temperature in the presence of 2.5, 3.75, and 5 mol % of **1c** (Figure 4). As could be expected, a higher catalyst loading leads to a more rapid formation of H₂, indicating a faster reaction. Plots of c vs t , $\ln c$ vs t and $1/c$ vs t gave an almost linear fit for $1/c$ vs t (Figure S16), indicating a second-order reaction with regard to the substrates, which is not uncommon for cross-coupling reactions.^{18,24} It is worth noting that, when 5 mol % of the previously discussed magnesocenophane bis(benzylamine) complex **1c**·(BnNH₂)₂ was employed, a similar, yet slightly faster reaction was observed (Figure 4).

The fact that 5 mol % of the bis(benzylamine) complex **1c**·(BnNH₂)₂ catalyzes the cross-dehydrocoupling reaction at a similar or rather slightly faster rate supports our previous proposal that this species is formed at the start of the catalysis and is most likely part of the catalytic cycle.

Subsequently, the kinetic isotope effects (KIE) were investigated, by employing deuterated substrates, benzylamine-*d*₂ and diphenylsilane-*d*₂. The catalytic cross-dehydrocoupling was carried out with a catalyst loading of 5 mol % of **1c**. For the reaction of deuterated benzylamine⁴⁰ with undeuterated diphenylsilane a kinetic isotope effect of $\text{KIE}_{\text{ND}} = 2.36$ ($k(\text{BnNH}_2+\text{Ph}_2\text{SiH}_2) = [6.48(4)] \times 10^{-8} \text{ s}^{-1} / k(\text{BnND}_2+\text{Ph}_2\text{SiH}_2) = [2.74(5)] \times 10^{-8} \text{ s}^{-1}$) was observed, while the reaction of undeuterated benzylamine with deuterated diphenylsilane showed a kinetic isotope effect of $\text{KIE}_{\text{SD}} = 1.75$ ($k(\text{BnNH}_2+\text{Ph}_2\text{SiD}_2) = [6.48(4)] \times 10^{-8} \text{ s}^{-1} / k(\text{BnNH}_2+\text{Ph}_2\text{SiD}_2) = [3.71(8)] \times 10^{-8} \text{ s}^{-1}$). A qualitative comparison of these values suggests that the N–H bond breaking may be involved in the rate-determining step. Corresponding to this, the kinetic isotope effect observed for

Table 2. Reaction Conditions, Conversions, and Formed Products of the Cross-Dehydrocoupling of Amines and Silanes Catalyzed by C[1]magnosocenophanes 1a–c

catalyst ^a	amine/silane	T (K)/t (h)	product(s)	silane conversion (%) ^b
1a	DipNH ₂ /PhSiH ₃	333/24	DipNHSiH ₂ Ph (2a)/(DipNH) ₂ SiHPh (2b)	39 (79:21)
1b	DipNH ₂ /PhSiH ₃	333/24	DipNHSiH ₂ Ph (2a)/(DipNH) ₂ SiHPh (2b)	42 (74:26)
1c	DipNH ₂ /PhSiH ₃	333/24	DipNHSiH ₂ Ph (2a)/(DipNH) ₂ SiHPh (2b)	38 (73:27)
1c	2 equiv DipNH ₂ /PhSiH ₃	333/24	DipNHSiH ₂ Ph (2a)/(DipNH) ₂ SiHPh (2b)	64 (70:30)
1a	DipNH ₂ /Ph ₂ SiH ₂	333/24	DipNHSiHPh ₂ (3a)	52
1b	DipNH ₂ /Ph ₂ SiH ₂	333/24	DipNHSiHPh ₂ (3a)	60
1c	DipNH ₂ /Ph ₂ SiH ₂	333/24	DipNHSiHPh ₂ (3a)	81
1a	^t BuNH ₂ /PhSiH ₃	333/24	^t BuNHSiH ₂ Ph (4a)	28
1b	^t BuNH ₂ /PhSiH ₃	333/24	^t BuNHSiH ₂ Ph (4a)	17
1c	^t BuNH ₂ /PhSiH ₃	333/24	^t BuNHSiH ₂ Ph (4a)	19
1a	^t BuNH ₂ /Ph ₂ SiH ₂	333/24	^t BuNHSiHPh ₂ (5a)	57
1b	^t BuNH ₂ /Ph ₂ SiH ₂	333/24	^t BuNHSiHPh ₂ (5a)	27
1c	^t BuNH ₂ /Ph ₂ SiH ₂	333/24	^t BuNHSiHPh ₂ (5a)	94
1a	BnNH ₂ /PhSiH ₃	298/24	BnNHSiH ₂ Ph (6a)/(BnNH) ₂ SiHPh (6b)/BnN(SiH ₂ Ph) ₂ (6c) + other products	59
1b	BnNH ₂ /PhSiH ₃	298/24	BnNHSiH ₂ Ph (6a)/(BnNH) ₂ SiHPh (6b)/BnN(SiH ₂ Ph) ₂ (6c) + other products	38
1c	BnNH ₂ /PhSiH ₃	298/24	BnNHSiH ₂ Ph (6a)/(BnNH) ₂ SiHPh (6b)/BnN(SiH ₂ Ph) ₂ (6c) + other products	46
1a	BnNH ₂ /PhSiH ₃	313/24	BnNHSiH ₂ Ph (6a)/(BnNH) ₂ SiHPh (6b)/BnN(SiH ₂ Ph) ₂ (6c) + other products	82
1b	BnNH ₂ /PhSiH ₃	313/24	BnNHSiH ₂ Ph (6a)/(BnNH) ₂ SiHPh (6b)/BnN(SiH ₂ Ph) ₂ (6c) + other products	70
1c	BnNH ₂ /PhSiH ₃	313/24	BnNHSiH ₂ Ph (6a)/(BnNH) ₂ SiHPh (6b)/BnN(SiH ₂ Ph) ₂ (6c) + other products	82
1a	BnNH ₂ /Ph ₂ SiH ₂	298/8	BnNHSiHPh ₂ (7a)	90
1b	BnNH ₂ /Ph ₂ SiH ₂	298/8	BnNHSiHPh ₂ (7a)	82
1c	BnNH ₂ /Ph ₂ SiH ₂	298/8	BnNHSiHPh ₂ (7a)	84
1a	BnNH ₂ /PhMeSiH ₂	298/24	BnNHSiHPhMe (8a)	12
1b	BnNH ₂ /PhMeSiH ₂	298/24	BnNHSiHPhMe (8a)	10
1c	BnNH ₂ /PhMeSiH ₂	298/24	BnNHSiHPhMe (8a)	41
1a	BnNH ₂ /PhMeSiH ₂	333/24	BnNHSiHPhMe (8a)	66
1b	BnNH ₂ /PhMeSiH ₂	333/24	BnNHSiHPhMe (8a)/(BnNH) ₂ SiPhMe (8b)	79 (87:13)
1c	BnNH ₂ /PhMeSiH ₂	333/24	BnNHSiHPhMe (8a)/(BnNH) ₂ SiPhMe (8b)	89 (79:21)
1a	Bn ₂ NH/PhSiH ₃	333/24	Bn ₂ NSiH ₂ Ph (9a)	29
1b	Bn ₂ NH/PhSiH ₃	333/24	Bn ₂ NSiH ₂ Ph (9a)	16
1c	Bn ₂ NH/PhSiH ₃	333/24	Bn ₂ NSiH ₂ Ph (9a)	33
1a	Bn ₂ NH/Ph ₂ SiH ₂	333/48	Bn ₂ NSiHPh ₂ (10a)	10
1b	Bn ₂ NH/Ph ₂ SiH ₂	333/48	Bn ₂ NSiHPh ₂ (10a)	20
1c	Bn ₂ NH/Ph ₂ SiH ₂	333/48	Bn ₂ NSiHPh ₂ (10a)	32
1a	pyrrolidine/PhSiH ₃	333/24	(1,4-C ₄ H ₈)NSiH ₂ Ph (11a)	26
1b	pyrrolidine/PhSiH ₃	333/24	(1,4-C ₄ H ₈)NSiH ₂ Ph (11a)/((1,4-C ₄ H ₈)N) ₂ SiHPh (11b)	17 (41:59)
1c	pyrrolidine/PhSiH ₃	333/24	(1,4-C ₄ H ₈)NSiH ₂ Ph (11a)/((1,4-C ₄ H ₈)N) ₂ SiHPh (11b)	13 (26:74)
1a	pyrrolidine/Ph ₂ SiH ₂	333/24	(1,4-C ₄ H ₈)NHSiHPh ₂ (12a)	100
1b	pyrrolidine/Ph ₂ SiH ₂	333/24	(1,4-C ₄ H ₈)NHSiHPh ₂ (12a)	78
1c	pyrrolidine/Ph ₂ SiH ₂	333/24	(1,4-C ₄ H ₈)NHSiHPh ₂ (12a)	92
1a	morpholine/PhSiH ₃	333/24	(1,5-C ₄ H ₈ O)NSiH ₂ Ph (13a)/((1,5-C ₄ H ₈ O)N) ₂ SiHPh (13b)	38 (55:45)
1b	morpholine/PhSiH ₃	333/24	(1,5-C ₄ H ₈ O)NSiH ₂ Ph (13a)/((1,5-C ₄ H ₈ O)N) ₂ SiHPh (13b)	50 (54:46)
1c	morpholine/PhSiH ₃	333/24	(1,5-C ₄ H ₈ O)NSiH ₂ Ph (13a)/((1,5-C ₄ H ₈ O)N) ₂ SiHPh (13b)	37 (35:65)
1a	morpholine/Ph ₂ SiH ₂	333/24	(1,5-C ₄ H ₈ O)NSiHPh ₂ (14a)	80
1b	morpholine/Ph ₂ SiH ₂	333/24	(1,5-C ₄ H ₈ O)NSiHPh ₂ (14a)	86
1c	morpholine/Ph ₂ SiH ₂	333/24	(1,5-C ₄ H ₈ O)NSiHPh ₂ (14a)	96

^a5 mol % catalyst loading in toluene. ^bConversion estimated by integration of the ²⁹Si{¹H} NMR spectrum.

Scheme 5. Synthesis of Magnesocenophane Bis(benzylamine) Complex $1c \cdot (\text{BnNH}_2)_2$

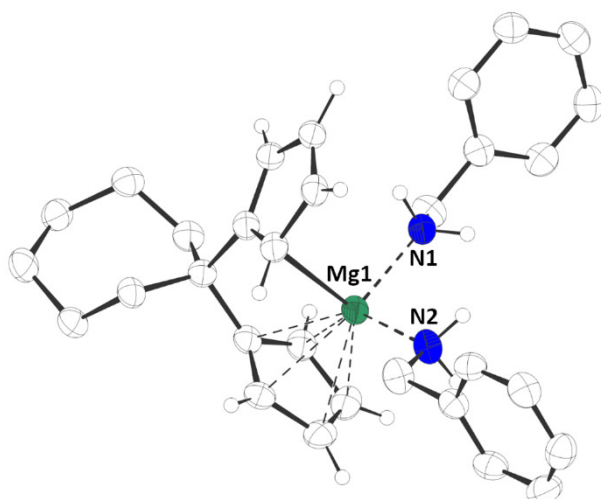
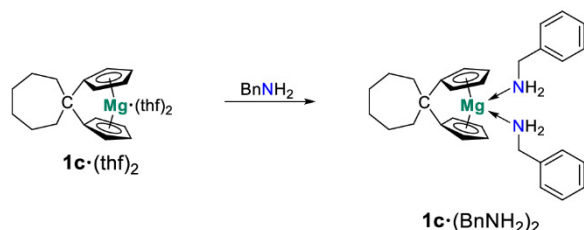


Figure 3. Molecular structure of $1c \cdot (\text{BnNH}_2)_2$ in the crystal (thermal ellipsoids at the 50% probability level; hydrogen atoms except N–H and Cp–H omitted for clarity). Selected bond lengths (pm): Mg1–N1/2 210.65(23), 212.09(25).

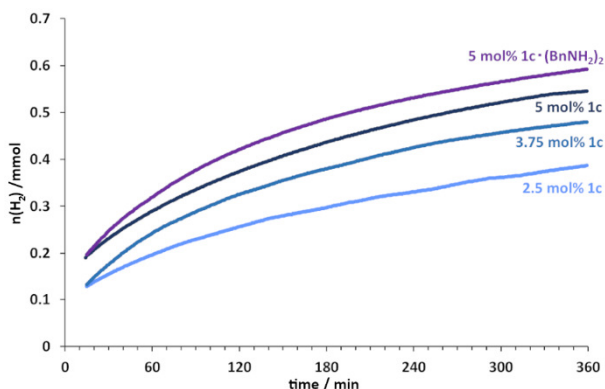


Figure 4. Plots of $n(\text{H}_2)$ versus time of the cross-dehydrocoupling reaction of benzylamine and diphenylsilane catalyzed by 2.5, 3.75, and 5 mol % of $1c$ and 5 mol % of $1c \cdot (\text{BnNH}_2)_2$.

the fully deuterated system, and thus for the reaction of deuterated benzylamine⁴⁰ with deuterated diphenylsilane, was $\text{KIE}_{\text{NDSiD}} = 2.40$ ($k(\text{BnNH}_2 + \text{Ph}_2\text{SiD}_2) = [6.48(4)] \times 10^{-8} \text{ s}^{-1} / k(\text{BnND}_2 + \text{Ph}_2\text{SiD}_2) = [2.70(4)] \times 10^{-8} \text{ s}^{-1}$), which is almost identical with KIE_{ND} (Figures S17 and S18). This is not uncommon but has been reported before for catalytic dehydrocoupling reactions of amine–boranes^{41,42} and sup-

ports the assumption that the N–H bond cleavage occurs in the rate-determining step.

On the basis of these results, we propose the following mechanism for the amine–silane cross-dehydrocoupling exemplified for magnesocenophane $1c$, benzylamine, and diphenylsilane (Scheme 6). The first step is the coordination of amine to the magnesium center, giving the bis(benzylamine) complex $1c \cdot (\text{BnNH}_2)_2$, which was structurally characterized by X-ray diffraction (*vide supra*). Subsequently, one amine molecule may be exchanged by a silane molecule, giving a mixed benzylamine–diphenylsilane magnesocenophane complex. At this point, a direct N–Si coupling step with hydrogen elimination may occur in the coordination sphere of the magnesium atom or protonation of one of the Cp groups by the N–H group may be involved. In either case, elimination of hydrogen and product monosilazane $7a$ and subsequent coordination of a new amine substrate closes the catalytic cycle. The protonation of the Cp ring by an amino group was proposed before for the mechanism of the dehydrocoupling of dimethylamine–borane, catalyzed by magnesocenophane $1a$.³⁰

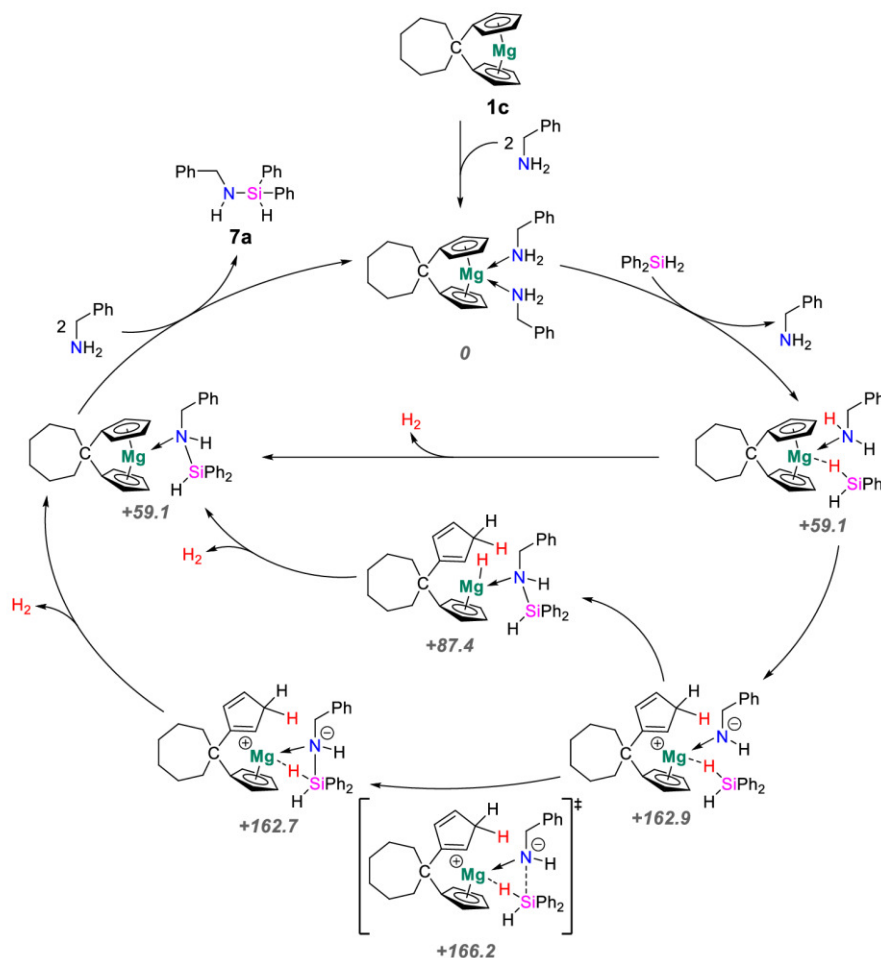
DFT calculations of the relative energies of the proposed intermediates suggest that the exchange of one amine molecule for a silane molecule is endergonic by $+59.1 \text{ kJ mol}^{-1}$ and that the corresponding product complex is energetically approximately on par. The formation of a magnesium hydride species as an intermediate may be viable ($+87.4 \text{ kJ mol}^{-1}$), but a transition state leading to an intermediate with a pentacoordinate silicon atom, which was located on the potential energy surface, is relatively high in energy for a reaction that proceeds at room temperature, suggesting that this is probably not the predominant pathway (Scheme 6). Thus, the formation of a magnesocenophane amine–silane complex as a key intermediate seems likely and a direct Si–N coupling in the coordination sphere of the magnesium atom may be the predominant route.

CONCLUSION

Overall, transition-metal Cp compounds are commonly used in homogeneous catalysis, while on the other hand, the application of metallocene-type compounds of main-group elements in homogeneous catalysis is almost unknown. In this work, we report the synthesis and solid-state structures of two new C[1]magnesocenophanes and the application of C[1]-magnesocenophanes in amine–borane dehydrocoupling, as well as amine–silane cross-dehydrocoupling. This is a rare example of main-group metallocenophanes being utilized in homogeneous catalysis and the first time of such an application in amine–silane cross-dehydrocoupling.

In addition to a substrate scope screening, the mechanism was examined by a stoichiometric reaction and kinetic investigations, assisted by DFT calculations. Significantly, a substrate complex in the form of a magnesocenophane bis(benzylamine) complex could be isolated and structurally characterized. These studies clearly suggest that magnesocenophanes $1a$ – c are not just precatalysts but are directly involved in the catalytic cycle.

This work expands the field of s-block dehydrocoupling catalysis and makes an important contribution to the application of main-group metallocene-type compounds in the catalysis.

Scheme 6. Proposed Catalytic Cycle for the Cross-Dehydrocoupling of Benzylamine and Diphenylsilane to Monosilazane **7a** Catalyzed by Magnesocenophane **1c**^a

^aRelative energies, calculated at the B3LYP-D3/def2-TZVP level of theory, are given in kJ mol⁻¹.

EXPERIMENTAL SECTION

All manipulations were carried out under an inert gas atmosphere (argon 5.0), using either Schlenk line techniques or a glovebox. 1,1-Bis(cyclopentadienyl)cyclohexane,³¹ 1,1-bis(cyclopentadienyl)cycloheptane,³² Me₂C[1]magnesocenophane **1a**,³⁰ and piperidine-borane⁴³ were synthesized according to literature procedures. All other starting materials were obtained commercially. NMR spectra were recorded on Bruker Avance III 300 and Bruker Avance III 400 spectrometers. ¹H and ¹³C NMR spectra were referenced using the solvent signals ($\delta(^1\text{H})$ (C₆H₆) 7.16, $\delta(^1\text{H})$ (CHCl₃) 7.26, $\delta(^1\text{H})$ (thf-*d*₇) 3.58; $\delta(^{13}\text{C})$ (C₆D₆) 128.06, $\delta(^{13}\text{C})$ (CDCl₃) 77.00, $\delta(^{13}\text{C})$ (thf-*d*₈) 67.57).⁴⁴ ²⁹Si NMR spectra were referenced using an external standard ($\delta(^{29}\text{Si})$ (SiMe₄) 0). MS spectra were recorded on a Q-TOF Premiere instrument from Waters, Manchester, England, in LIFDI(+) mode. The original ESI source of the instrument was replaced by a standard LIFDI source from Linden CMS, Weyhe, Germany. Single-crystal X-ray diffraction analyses were carried out at low temperatures on Bruker AXS X8 Apex CCD and Bruker AXS D8 Venture diffractometers operating with graphite-monochromated Mo K α radiation. The structure solution and refinement were performed using SHELX.⁴⁵ Crystal structures have been deposited with the Cambridge Crystallographic Data Centre (CCDC) and are available free of charge from the Cambridge Structural Database (reference

numbers: 2059653, 2059664, 2059665, 2059666, 2059668, 2059670, 2059685).

Synthesis of Cycloalkylidene[1]magnesocenophanes **1b,c**.

To a solution of 1,1-bis(cyclopentadienyl)cyclohexane (8.17 g, 38.5 mmol) or 1,1-bis(cyclopentadienyl)cycloheptane (8.06 g, 35.6 mmol) in 100 mL of hexane precooled to 273 K was added a solution of *n*-butyl-*sec*-butylmagnesium (0.7 M in hexane, 55.0 mL, 38.5 mmol/51.0 mL, 35.7 mmol). The reaction mixture was warmed to room temperature and stirred for 3 days. The product slowly precipitated and was isolated by filtration and dried *in vacuo* to obtain **1b** and **1c** as colorless solids. Yields: **1b**, 8.90 g/98%; **1c**, 7.94 g/90%.

Data for **1b** are as follows. ¹H NMR (400.13 MHz, thf-*d*₈): δ 1.41–1.49 (m, 2 H, CH₂), 1.64–1.70 (m, 4 H, CH₂), 1.74–1.80 (m, thf), 2.22–2.27 (m, 4 H, CH₂), 3.59–3.65 (m, thf), 5.58 (t, ³J_{HH} = 2.5 Hz, 4 H, Cp-H), 5.76 (t, ³J_{HH} = 2.5 Hz, 4 H, Cp-H). ¹³C{¹H} NMR (75.48 MHz, thf-*d*₈): δ 24.9 (CH₂), 26.5 (thf), 28.3 (CH₂), 37.6 (CH₂), 42.3 (CCP₂), 68.4 (thf), 95.8 (Cp), 107.9 (Cp), 139.3 (Cp). ¹H NMR (400.13 MHz, C₆D₆/thf): δ 1.30–1.42 (m, thf), 1.67–1.77 (m, 2 H, CH₂), 2.05–2.15 (m, 4 H, CH₂), 2.67–2.80 (m, 4 H, CH₂), 3.39–3.56 (m, thf), 6.01 (t, ³J_{HH} = 2.4 Hz, 4 H, Cp-H), 6.13 (t, ³J_{HH} = 2.4 Hz, 4 H, Cp-H). ¹³C{¹H} NMR (100.62 MHz, C₆D₆/thf): δ 24.6 (CH₂), 25.7 (thf), 27.8 (CH₂), 37.3 (CH₂), 42.2 (CCP₂), 68.1 (thf), 95.9 (Cp), 107.8 (Cp), 139.4 (Cp). HRMS: *m/z* calculated for C₁₆H₁₈Mg (**1b**) 234.1259 found 234.1527; *m/z* calculated for

$C_{20}H_{26}MgO$ (**1b**·thf) 306.1834, found 306.1817; m/z calculated for $C_{32}H_{36}Mg_2$ ((**1b**)₂) 468.2518, found 468.3207.

Data for **1c** are as follows. 1H NMR (400.13 MHz, thf-*d*₈): δ 1.61 (bs, 4 H, CH₂), 1.67–1.74 (m, 4 H, CH₂), 1.75–1.79 (m, thf), 2.42–2.46 (m, 4 H, CH₂), 3.59–3.64 (m, thf), 5.59 (t, $^3J_{HH}$ = 2.6 Hz, 4 H, Cp-H), 5.76 (t, $^3J_{HH}$ = 2.6 Hz, 4 H, Cp-H). $^{13}C\{^1H\}$ NMR (100.62 MHz, thf-*d*₈): δ 24.8 (CH₂), 26.4 (thf), 30.4 (CH₂), 40.0 (CH₂), 45.5 (CCP₂), 68.4 (thf), 96.2 (Cp), 108.0 (Cp), 140.7 (Cp). 1H NMR (400.13 MHz, C₆D₆/thf): δ 1.40–1.51 (m, thf), 1.70–1.75 (m, 4 H, CH₂), 1.92–2.00 (m, 4 H, CH₂), 2.72–2.78 (m, 4 H, CH₂), 3.45–3.56 (m, thf), 5.87 (t, $^3J_{HH}$ = 2.5 Hz, 4 H, Cp-H), 6.01 (t, $^3J_{HH}$ = 2.5 Hz, 4 H, Cp-H). $^{13}C\{^1H\}$ NMR (100.61 MHz, C₆D₆/thf): δ 24.4 (CH₂), 25.8 (thf), 30.1 (CH₂), 39.7 (CH₂), 45.3 (CCP₂), 68.1 (thf), 96.1 (Cp), 107.8 (Cp), 140.5 (Cp). HRMS: m/z calculated for $C_{34}H_{40}Mg_2$ ((**1c**)₂) 496.2831, found 496.3148; m/z calculated for $C_{50}H_{72}Mg_2O_4$ ((**1c**·(thf)₂)₂) 784.5131, found 784.4698.

Crystals of **1b**·(thf)₂, **1c**·(thf)₂, **1b**·dme, and **1c**·dme, suitable for single crystal X-ray diffraction, were obtained by dissolving **1b** or **1c** in the corresponding solvent and storing the solutions at 248 K.

Synthesis of Magnesocenophane–Bis(benzylamine) Complex **1c·(BnNH₂)₂.** To a solution of **1c** (255 mg, 1.03 mmol) in 3.5 mL of thf was added benzylamine (0.34 mL, 3.11 mmol), and the resulting mixture was warmed to 323 K for a few minutes. Subsequently, the mixture was slowly cooled to room temperature and storage at 248 K resulted in the crystallization of **1c**·(BnNH₂)₂ as pale needles. Yield: 240 mg/49%.

1H NMR (400.13 MHz, CD₂Cl₂): δ 1.39 (t, $^3J_{HH}$ = 7.1 Hz, 4 H, NH₂), 1.60–1.65 (m, 4 H, CH₂), 1.65–1.72 (m, 4 H, CH₂), 2.43–2.48 (m, 4 H, CH₂), 3.45 (t, $^3J_{HH}$ = 7.6 Hz, 4 H, N-CH₂-Ph), 5.77 (t, $^3J_{HH}$ = 2.6 Hz, 4 H, Cp-H), 5.89 (t, $^3J_{HH}$ = 2.6 Hz, 4 H, Cp-H), 7.13–7.17 (m, 4 H, Ph-H), 7.27–7.39 (m, 6 H, Ph-H). $^{13}C\{^1H\}$ NMR (100.62 MHz, CD₂Cl₂): δ 24.2 (CH₂), 30.2 (CH₂), 39.4 (CH₂), 45.0 (CCP₂), 46.1 (N-CH₂-Ph), 98.1 (Cp), 107.7 (Cp), 127.8 (Ph), 128.6 (Ph), 129.6 (Ph), 139.9 (Cp), 141.1 (Ph). 1H NMR (300.13 MHz, thf-*d*₈): δ 1.59–1.64 (m, 4 H, CH₂), 1.68–1.74 (m, 4 H, CH₂), 1.88 (t, $^3J_{HH}$ = 7.6 Hz, 4 H, NH₂), 2.46–2.50 (m, 4 H, CH₂), 3.55 (t, $^3J_{HH}$ = 7.6 Hz, 4 H, N-CH₂-Ph), 5.75 (t, $^3J_{HH}$ = 2.6 Hz, 4 H, Cp-H), 5.84 (t, $^3J_{HH}$ = 2.6 Hz, 4 H, Cp-H), 7.16–7.32 (m, 10 H, Ph-H). $^{13}C\{^1H\}$ NMR (75.48 MHz, 296 K, thf-*d*₈): δ 24.9 (CH₂), 30.6 (CH₂), 40.3 (CH₂), 45.5 (CCP₂), 46.9 (N-CH₂-Ph), 97.9 (Cp), 107.8 (Cp), 127.9 (Ph), 128.1 (Ph), 129.4 (Ph), 141.0 (Cp), 143.0 (Ph).

■ ASSOCIATED CONTENT

SI Supporting Information

The Supporting Information is available free of charge at <https://pubs.acs.org/doi/10.1021/acs.organomet.1c00245>.

Experimental details, NMR spectra, crystallographic details, computational details, and references (PDF)

Optimized geometries from DFT calculations (XYZ)

Accession Codes

CCDC 2059653, 2059664–2059666, 2059668, 2059670, and 2059685 contain the supplementary crystallographic data for this paper. These data can be obtained free of charge via www.ccdc.cam.ac.uk/data_request/cif, or by emailing data_request@ccdc.cam.ac.uk, or by contacting The Cambridge Crystallographic Data Centre, 12 Union Road, Cambridge CB2 1EZ, UK; fax: +44 1223 336033.

■ AUTHOR INFORMATION

Corresponding Author

André Schäfer – Saarland University, Faculty of Natural Sciences and Technology, Department of Chemistry, Campus Saarbrücken, 66123 Saarbrücken, Federal Republic of Germany; orcid.org/0000-0002-5969-6618; Email: andre.schaefer@uni-saarland.de

Authors

Lisa Wirtz – Saarland University, Faculty of Natural Sciences and Technology, Department of Chemistry, Campus Saarbrücken, 66123 Saarbrücken, Federal Republic of Germany

Jessica Lambert – Saarland University, Faculty of Natural Sciences and Technology, Department of Chemistry, Campus Saarbrücken, 66123 Saarbrücken, Federal Republic of Germany

Bernd Morgenstern – Saarland University, Faculty of Natural Sciences and Technology, Department of Chemistry, Campus Saarbrücken, 66123 Saarbrücken, Federal Republic of Germany

Complete contact information is available at:

<https://pubs.acs.org/10.1021/acs.organomet.1c00245>

Author Contributions

[†]L.W. and J.L. contributed equally.

Notes

The authors declare no competing financial interest.

■ ACKNOWLEDGMENTS

Dr. Volker Huch is thanked for assistance with X-ray crystallography. Linden ChromaSpec GmbH is thanked for TOF MS LIFDI+ measurements. Funding by the Deutsche Forschungsgemeinschaft, DFG (Emmy Noether program SCHA1915/3-1), and Fonds der Chemischen Industrie, FCI, is gratefully acknowledged.

■ DEDICATION

This paper is dedicated to Professor Dr. Ian Manners on the occasion of his 60th birthday and in acknowledgment of his pioneering work in metallocenophane and dehydrocoupling chemistry.

■ REFERENCES

- (1) Kroke, E.; Li, Y.-L.; Konetschny, C.; Lecomte, E.; Fasel, C.; Riedel, R. Silazane derived ceramics and related materials. *Mater. Sci. Eng., R* **2000**, *26*, 97–199.
- (2) Armitage, D. A.; Corriu, R. J. P.; Kendrick, T. C.; Parbhoo, B.; Tilley, T. D.; White, J. W.; Young, J. C.; Armitage, D. A. Organosilicon nitrogen compounds. In *Silicon–Heteroatom Bond*; Armitage, D. A., Corriu, R. J. P., Kendrick, T. C., Parbhoo, B., Tilley, T. D., White, J. W., Young, J. C., Eds.; Wiley: 1991.
- (3) Roth, C. A. Silylation of Organic Chemicals. *Ind. Eng. Chem. Prod. Res. Develop.* **1972**, *11*, 134–139.
- (4) Reuter, M. B.; Hageman, K.; Waterman, R. Silicon-Nitrogen Bond Formation via Heterodehydrocoupling and Catalytic N-Silylation. *Chem. - Eur. J.* **2021**, *27*, 3251–3261.
- (5) Tanabe, Y.; Murakami, M.; Kitaichi, K.; Yoshida, Y. Mild, effective and selective method for the silylation of alcohols using silazanes promoted by catalytic tetrabutylammonium fluoride. *Tetrahedron Lett.* **1994**, *35*, 8409–8412.
- (6) Tanabe, Y.; Misaki, T.; Kurihara, M.; Iida, A.; Nishii, Y. Silazanes/catalytic bases: mild, powerful and chemoselective agents for the preparation of enol silyl ethers from ketones and aldehydes. *Chem. Commun.* **2002**, 1628–1629.
- (7) Iida, A.; Horii, A.; Misaki, T.; Tanabe, Y. Anilinosilanes/TBAF Catalyst: Mild and Powerful Agent for the Silylation of Sterically Hindered Alcohols. *Synthesis* **2005**, *2005*, 2677–2682.
- (8) Fessenden, R.; Fessenden, J. S. The chemistry of silicon-nitrogen compounds. *Chem. Rev.* **1961**, *61*, 361–388.
- (9) Murugavel, R.; Palanisami, N.; Butcher, R. J. Synthesis, characterization and structures of diphenyldiaminosilanes bearing

- bulky substituents on nitrogen. *J. Organomet. Chem.* **2003**, *675*, 65–71.
- (10) Palanisami, N.; Murugavel, R. Synthesis and spectral characterization of diorganodiaminosilanes [(ArNH)₂SiPhMe] (Ar = 2,6-ⁱPr₂C₆H₃; 2,4,6-Me₃C₆H₂) and lithium silylamide [(2,6-Et₂C₆H₃NLi)(2,6-Et₂C₆H₃NH)SiPh₂]. *J. Organomet. Chem.* **2006**, *691*, 3260–3266.
- (11) Arrowsmith, M. Dehydrocouplings and other cross-couplings. *Early Main Group Metal Catalysis* **2020**, 225–250.
- (12) Liu, H. Q.; Harrod, J. F. Dehydrocoupling of Ammonia and Silanes Catalyzed by Dimethyltitanocene. *Organometallics* **1992**, *11*, 822–827.
- (13) Liu, H. Q.; Harrod, J. F. Copper(I)-catalyzed cross-dehydrocoupling reactions of silanes and amines. *Can. J. Chem.* **1992**, *70*, 107–110.
- (14) Tsuchimoto, T.; Iketani, Y.; Sekine, M. Zinc-Catalyzed Dehydrogenative N-Silylation of Indoles with Hydrosilanes. *Chem. - Eur. J.* **2012**, *18*, 9500–9504.
- (15) Königs, C. D. F.; Müller, M. F.; Aiguabella, N.; Klare, H. F. T.; Oestreich, M. Catalytic dehydrogenative Si-N coupling of pyrroles, indoles, carbazoles as well as anilines with hydrosilanes without added base. *Chem. Commun.* **2013**, *49*, 1506–1508.
- (16) Gasperini, D.; King, A. K.; Coles, N. T.; Mahon, M. F.; Webster, R. L. Seeking Heteroatom-Rich Compounds: Synthetic and Mechanistic Studies into Iron Catalyzed Dehydrocoupling of Silanes. *ACS Catal.* **2020**, *10*, 6102–6112.
- (17) Anderson, D. L. Chemical Composition of the Mantle. *Theory of the Earth*; Blackwell Scientific: Boston, 1989; Chapter 8, pp 147–175.
- (18) Dunne, J. F.; Neal, S. R.; Engelkemier, J.; Ellern, A.; Sadow, A. D. Tris(oxazolonyl)boratomagnesium-Catalyzed Cross-Dehydrocoupling of Organosilanes with Amines, Hydrazine, and Ammonia. *J. Am. Chem. Soc.* **2011**, *133*, 16782–16785.
- (19) Hill, M. S.; Liprott, D. J.; MacDougall, D. J.; Mahon, M. F.; Robinson, T. P. Hetero-dehydrocoupling of silanes and amines by heavier alkaline earth catalysis. *Chem. Sci.* **2013**, *4*, 4212–4222.
- (20) Bellini, C.; Carpentier, J.-F.; Tobisch, S.; Sarazin, Y. Barium-Mediated Cross-Dehydrocoupling of Hydrosilanes with Amines: A Theoretical and Experimental Approach. *Angew. Chem., Int. Ed.* **2015**, *54*, 7679–7683; *Angew. Chem.* **2015**, *127*, 7789–7793.
- (21) Baishya, A.; Peddarao, T.; Nembenna, S. Organomagnesium amide catalyzed cross-dehydrocoupling of organosilanes with amines. *Dalton Trans.* **2017**, *46*, 5880–5887.
- (22) Rauch, M.; Roberts, R. C.; Parkin, G. Reactivity of [Tism^{PrnBenz}]MgMe towards secondary amines and terminal alkynes: Catalytic dehydrocoupling with hydrosilanes to afford Si-N and Si-C bonds. *Inorg. Chim. Acta* **2019**, *494*, 271–279.
- (23) Buch, F.; Harder, S. The Azametallacyclopropane Ca(η^2 -Ph₃CNPh)(hmpa)₃: A Calcium Alternative to a Versatile Ytterbium-(II) Catalyst. *Organometallics* **2007**, *26*, 5132–5135.
- (24) Bellini, C.; Dorcet, V.; Carpentier, J.-F.; Tobisch, S.; Sarazin, Y. Alkaline-Earth-Catalysed Cross-Dehydrocoupling of Amines and Hydrosilanes: Reactivity Trends, Scope and Mechanism. *Chem. - Eur. J.* **2016**, *22*, 4564–4583.
- (25) Forosenko, N. V.; Basalov, I. V.; Cherkasov, A. V.; Fukin, G. K.; Shubina, E. S.; Trifonov, A. A. Amido Ca(II) complexes supported by Schiff base ligands for catalytic cross-dehydrogenative coupling of amines with silanes. *Dalton Trans.* **2018**, *47*, 12570–12581.
- (26) Li, N.; Guan, B.-T. A Dialkyl Calcium Carbene Adduct: Synthesis, Structure, and Catalytic Cross-Dehydrocoupling of Silanes with Amines. *Eur. J. Inorg. Chem.* **2019**, *2019*, 2231–2235.
- (27) Bellini, C.; Roisnel, T.; Carpentier, J.-F.; Tobisch, S.; Sarazin, Y. Sequential Barium-Catalysed N-H/H-Si Dehydrogenative Cross-Couplings: Cyclodisilanes versus Linear Oligosilanes. *Chem. - Eur. J.* **2016**, *22*, 15733–15743.
- (28) Bellini, C.; Orione, C.; Carpentier, J.-F.; Sarazin, Y. Tailored Cyclic and Linear Polycarbosilanes by Barium-Catalyzed N-H/H-Si Dehydrocoupling Reactions. *Angew. Chem., Int. Ed.* **2016**, *55*, 3744–3748; *Angew. Chem.* **2016**, *128*, 3808–3812.
- (29) Clark, T. J.; Russell, C. A.; Manners, I. Homogeneous, Titanocene-Catalyzed Dehydrocoupling of Amine-Borane Adducts. *J. Am. Chem. Soc.* **2006**, *128*, 9582–9583.
- (30) Wirtz, L.; Haider, W.; Huch, V.; Zimmer, M.; Schäfer, A. Magnescenophane-Catalyzed Amine Borane Dehydrocoupling. *Chem. - Eur. J.* **2020**, *26*, 6176–6184.
- (31) Sha, L.; Li, L.; Yuan, F. Carbon-bridged Tri(cyclopentadiene): Synthesis and Coordination with Ytterbium. *Chin. J. Chem.* **2014**, *32*, 1214–1216.
- (32) Wang, B.; Mu, B.; Deng, X.; Cui, H.; Xu, S.; Zhou, X.; Zou, F.; Li, Y.; Yang, L.; Li, Y.; Hu, Y. Synthesis and Structures of Cycloalkylidene-Bridged Cyclopentadienyl Metallocene Catalysts: Effects of the Bridges of Ansa-Metallocene Complexes on the Catalytic Activity for Ethylene Polymerization. *Chem. - Eur. J.* **2005**, *11*, 669–679.
- (33) Wang, B.; Zhu, B.; Zhang, J.; Xu, S.; Zhou, X.; Weng, L. Reactions of Doubly Bridged Bis(cyclopentadienes) with Iron Pentacarbonyl. *Organometallics* **2003**, *22*, 5543–5555.
- (34) Li, Z.; Ma, Z.-H.; Wang, H.; Han, Z.-G.; Zheng, X.-Z.; Lin, J. Synthesis and catalytic activity of monobridged bis(cyclopentadienyl)-rhenium carbonyl complexes. *Transition Met. Chem.* **2016**, *41*, 647–653.
- (35) Wirtz, L.; Schäfer, A. Main-Group Metallocenophanes. *Chem. - Eur. J.* **2021**, *27*, 1219–1230.
- (36) Cremer, C.; Jacobsen, H.; Burger, P. The metal oxo 1,2-alkyl shift: towards the aerobic oxidation of hydrocarbons. *Chimia* **1997**, *51*, 968.
- (37) Perrotin, P.; Shapiro, P. J.; Williams, M.; Twamley, B. In Search of a Versatile Pathway to ansa-Chromocene Complexes. Synthesis and Characterization of the Highly Unstable ansa-Chromocene Carbonyl Complex Me₂C(C₅H₄)₂CrCO. *Organometallics* **2007**, *26*, 1823–1826.
- (38) (a) See the [Supporting Information](#) for further details. (b) Tracking of hydrogen evolution via pressure measurements was carried out using the *Man on the Moon X103* kit.
- (39) Xia, A.; Knox, J. E.; Heeg, M. J.; Schlegel, H. B.; Winter, C. H. Synthesis, Structure, and Properties of Magnescene Amine Adducts. Structural Distortions Arising from N-H...C₅H₅⁻ Hydrogen Bonding and Molecular Orbital Calculations Thereof. *Organometallics* **2003**, *22*, 4060–4069.
- (40) Deuterated benzylamine used in KIE experiments had a deuteration degree of 75–80%. Higher deuteration degrees could not be achieved, which is in agreement with previous literature reports.^{46–48} KIEs should therefore be interpreted in a qualitative manner.
- (41) Sewell, L. J.; Huertos, M. A.; Dickinson, M. E.; Weller, A. S.; Lloyd-Jones, G. C. Dehydrocoupling of Dimethylamine Borane Catalyzed by Rh(PCy₃)₂H₂Cl. *Inorg. Chem.* **2013**, *52*, 4509–4516.
- (42) Maier, T. M.; Sandl, S.; Shenderovich, I. G.; Jacobi von Wangelin, A.; Weigand, J. J.; Wolf, R. Amine-Borane Dehydrogenation and Transfer Hydrogenation Catalyzed by α -Diimine Cobaltates. *Chem. - Eur. J.* **2019**, *25*, 238–245.
- (43) Veeraraghavan Ramachandran, P.; Kulkarni, A. S.; Zhao, Y.; Mei, J. Amine-boranes bearing borane-incompatible functionalities: application to selective amine protection and surface functionalization. *Chem. Commun.* **2016**, *52*, 11885–11888.
- (44) Fulmer, G. R.; Miller, A. J. M.; Sherden, N. H.; Gottlieb, H. E.; Nudelman, A.; Stoltz, B. M.; Bercaw, J. E.; Goldberg, K. I. NMR Chemical Shifts of Trace Impurities: Common Laboratory Solvents, Organics, and Gases in Deuterated Solvents Relevant to the Organometallic Chemist. *Organometallics* **2010**, *29*, 2176–2179.
- (45) Sheldrick, G. M. A short history of SHELX. *Acta Crystallogr., Sect. A: Found. Crystallogr.* **2008**, *64*, 112–122.
- (46) Cristian, L.; Nica, S.; Pavel, O. D.; Mihailciuc, C.; Almasan, V.; Coman, S. M.; Hardacre, C.; Parvulescu, V. I. Novel ruthenium-terpyridyl complex for direct oxidation of amines to nitriles. *Catal. Sci. Technol.* **2013**, *3*, 2646–2653.
- (47) Hawthorne, M. F. The Question of Hydrogen Bonded Transition States in Nucleophilic Aromatic Substitution Reactions. *J. Am. Chem. Soc.* **1954**, *76*, 6358–6360.

(48) Ross, S. D.; Finkelstein, M.; Petersen, R. C. Nucleophilic Displacement Reactions in Aromatic Systems. V. The Mechanism of the Reaction of 2,4-Dinitrochlorobenzene with Primary Amines in Chloroform. *J. Am. Chem. Soc.* **1959**, *81*, 5336–5342.

3.3 Constrained Geometry *ansa*-Half-Sandwich Complexes of Magnesium – Versatile s-Block Catalysts

Lisa Wirtz, Kinza Yasmin Ghulam, Bernd Morgenstern, André Schäfer

ChemCatChem **2022**, *14*, e202201007.

DOI: 10.1002/cctc.202201007

The above cited article was published as an “Open Access” article under the terms of Creative Commons Attribution-NonCommercial-NoDerivs License.

Copyright © (2022) The Authors. Published by Wiley-VCH Verlag GmbH & Co. KGaA.

Author contribution:

Lisa Wirtz:

Lead: Synthesis and characterization of **1a-d**, investigation of catalytic reactions, mechanistic investigations, DFT-calculations, writing, reviewing and editing of the manuscript and supporting information.

Kinza Yasmin Ghulam:

Supporting: Synthesis and characterization of **1b**.

Bernd Morgenstern:

Lead: X-ray analysis.

André Schäfer:

Lead: Project administration and supervision, funding acquisition;

Supporting: Writing, reviewing and editing of the manuscript and supporting information.

Constrained Geometry *ansa*-Half-Sandwich Complexes of Magnesium – Versatile *s*-Block Catalysts

Lisa Wirtz,^[a] Kinza Yasmin Ghulam,^[a] Bernd Morgenstern,^[a] and André Schäfer*^[a]

The synthesis, characterization and catalytic application of a series of constrained geometry *ansa*-half-sandwich complexes of magnesium is reported. These versatile *s*-block catalysts were

applied in different dehydrocoupling and hydroelementation reactions, demonstrating a broad applicability with particularly remarkable performance in dehydrocoupling reactions.

Introduction

ansa-Half-sandwich ligands are quite popular in transition metal chemistry.^[1–4] For example, complexes of group 3 and 4 metals have been known since the early 1990s and are often used in homogenous catalysis, such as olefin polymerization, and are even applied in industrial processes.^[3,5,6] Different types of these so-called constrained geometry catalysts (CGCs) are known, which exhibit different *ansa* bridging motifs and various cyclopentadienyl, indenyl or fluorenyl groups.^[3,7] In contrast, such *ansa*-half-sandwich ligands have only rarely found application in main-group chemistry.^[8–10] In 2001 and 2003, Cowley and coworkers reported constrained geometry *ansa*-half-sandwich complexes of group 13 and group 15 compounds, followed by a report from our group about related heavy group 14 *N*-heterocyclic half-sandwich complexes.^[8,9,11] The first constrained geometry alkaline earth metal complex of this type, containing calcium as the central atom, was reported by Tamm and coworkers in 2008.^[12] Subsequently, magnesium complexes of this type have also been described, but – until now – have not been structurally authenticated, and in general, such constrained geometry *ansa*-half-sandwich complexes of main group elements have seen only little application in homogenous catalysis.^[10,13]

In general, the interest in *s*-block based catalysts has grown tremendously over the past decades,^[14–16] due to the attractive properties of these metals for catalytic applications, which are their high natural abundances in the earth's crust, their associated low carbon footprint and their low toxicity, high biocompatibility respectively.^[17,18] Thus, there is considerable interest in magnesium based catalysts with a broad applicability spectrum, and since magnesium can be considered a “green”

metal in catalysis for the afore mentioned reasons, transformations with no or minimal by-product are of particular interest. One such reaction type for the formation of new E–E bonds (E = *p*-block element) with a particularly high atom economy is dehydrocoupling, which generates dihydrogen as the only by-product, while providing easy and straight forward access to a number of inorganic *p*-block compounds.^[19–23] There are several examples of such reactions catalyzed by magnesium. For instance, magnesium compounds have been employed in dehydrocoupling reactions of amine-boranes,^[24–29] and in cross-dehydrocoupling reactions of amines with silanes.^[25,30–32] Furthermore, magnesium-based catalysts have also been employed in hydroelementation reactions, pioneered by the groups of Hill, Harder, Sadow and others.^[15,33] For example, magnesium-catalyzed hydroborations are a well-established area^[14,33–38] as is the important reaction type of hydroamination, such as intramolecular ring-closing hydroamination for the preparation of *N*-heterocycles.^[13,39–47] Furthermore, interest in atom-economical C–C bond formation in organic chemistry has increased. The field was formerly dominated by transition metal catalysts, but more recently, main group and in particular *s*-block based catalysts are now being established.^[48,49]

Inspired by these aspects and our continued interest in main-group Cp complexes and their application in homogenous catalysis, we were intrigued to develop a magnesium-based catalyst system that could be employed in a wide variety of reaction types. Herein, we report the syntheses and characterization of four constrained geometry *ansa*-half-sandwich complexes of magnesium and their versatile applications as catalysts in different dehydrocoupling and hydroelementation reactions.

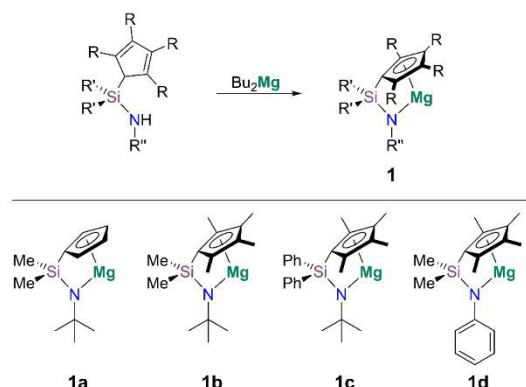
Results and Discussion

Synthesis and Characterization of *ansa*-Half-Sandwich Magnesium Complexes

Literature known *ansa*-half-sandwich ligands^[50–53] were reacted with dibutylmagnesium to obtain the corresponding *ansa*-half-sandwich magnesium complexes **1a–d** (Scheme 1). Similar to magnesocenophanes,^[24,25,54–56] **1a–d** possess Lewis acidic magnesium atoms and crystallized as solvent adducts from donor

[a] L. Wirtz, K. Y. Ghulam, Dr. B. Morgenstern, Dr. A. Schäfer
 Faculty of Natural Science and Technology
 Department of Chemistry
 Saarland University
 Campus Saarbrücken
 66123 Saarbrücken (Germany)
 E-mail: andre.schaefer@uni-saarland.de

© 2022 The Authors. ChemCatChem published by Wiley-VCH GmbH. This is an open access article under the terms of the Creative Commons Attribution Non-Commercial NoDerivs License, which permits use and distribution in any medium, provided the original work is properly cited, the use is non-commercial and no modifications or adaptations are made.



Scheme 1. Synthesis of magnesium complexes 1 a–d.

solvent (Figure 1, S14–S18). In case of 1 a–c, mono dme adducts are observed in the solid state, with the dme molecule coordinated to the magnesium atom *via* both oxygen atoms and the magnesium atom exhibiting an η^5 coordination mode to the Cp group. In case of *N*-phenyl complex 1 d, two dme molecules are coordinated to the magnesium atom in the solid state, with one bonded *via* both and one only *via* one oxygen atom. Consequently, the magnesium atom exhibits an η^1 coordination to the Cp ligand. Although this solid-state structure does not necessarily reflect the situation in solution, it highlights the coordinative flexibility of this Cp-based ligand system, which can adapt to and compensate for the electronic and steric situation at the central atom. Noteworthy, similar η^1 ring slippage structures were observed for

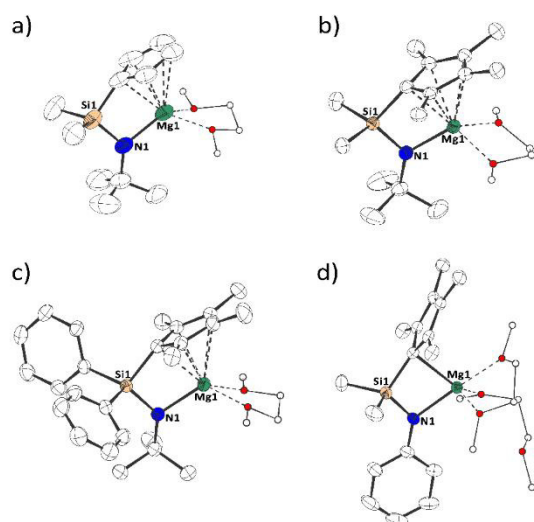


Figure 1. Molecular structures of a) 1 a·dme, b) 1 b·dme, c) 1 c·dme, and d) 1 d·(dme)₂ in the crystal (displacement ellipsoids for 50% probability level; hydrogen atoms omitted for clarity; dme molecules drawn as ball-and-stick models).

[1]magnesocenophane thf and amine complexes in the past.^[24,25,57]

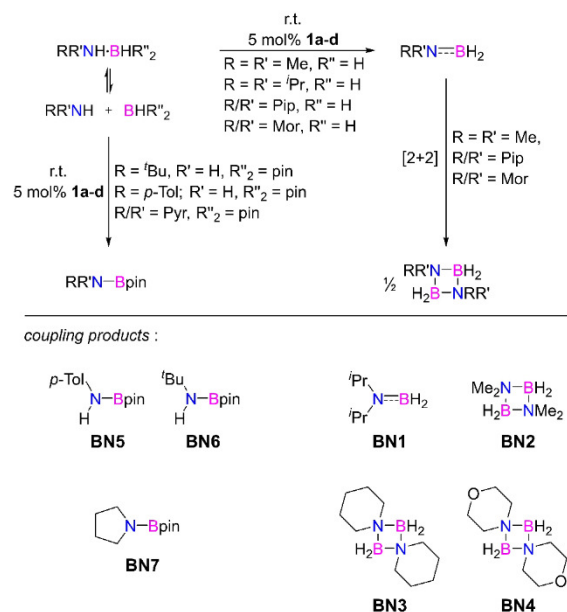
The Mg–O^{dme} bonds are 203.98(41) to 210.66(11) pm, which is slightly longer than the Mg–O^{thf} bonds in 1 a·(thf)₂ (202.67(31) to 204.98(33) pm; Table S1) and in line with what was previously observed in dme and thf adducts of [1]magnesocenophanes.^[24,25] Corresponding to this, DFT calculations indicate stronger binding of thf than dme (Table S2).^[24,25,57] The Mg–Cp^{cent} bond distances in 1 a–c·(dme) are 215.05(6) to 220.36(7) pm (Table S1), which is again similar to the distances in dme complexes of [1]magnesocenophanes. Regarding electronic properties, DFT calculations predict fluoride ion affinities (FIA)^[58] and global electrophilicity indices (GEI)^[59] slightly below those for previously reported [1]magnesocenophanes, but still indicate a pronounced Lewis acidic character of the magnesium center.^[24,60]

Dehydrocoupling Catalysis

Amine-Borane Dehydrocoupling

Recently, we demonstrated that [1]magnesocenophanes are potent catalysts in the dehydrocoupling of amine-boranes.^[24,25] While many magnesium based catalysts require elevated temperatures to operate,^[26–29] [1]magnesocenophanes were able to catalyze the dehydrocoupling reactions of different dialkylamine-boranes at room temperature.^[24,25] We therefore started our investigations into the catalytic abilities of *ansa*-half-sandwich magnesium complexes 1 a–d by testing their performance in the dehydrocoupling of amine-boranes. The dehydrocoupling of dimethylamine-borane to cyclic tetramethyldiborazane takes place at room temperature with 5 mol% of 1 a–d, giving up to 87% conversion after just 8 h. Analogously, the dehydrocoupling of piperidine-borane, morpholine-borane and diisopropylamine-borane gave quantitative or near quantitative conversions with 5 mol% of 1 a–d after 8 h at room temperature (Scheme 2; Table 1).

This is significantly faster than the previously reported [1]magnesocenophane-catalyzed reactions, which required approx. twice the reaction time to attain similar conversions, and by far the best performance for a magnesium catalyst.^[26–29] After these promising results, we choose to expand the substrate scope and investigate the intermolecular dehydrocoupling of amines with pinacolborane, for which only few metal catalysts have been reported so far.^[61–68] Since it is well known that such reaction can also occur without any catalyst in some cases,^[69] we carried out control experiments with pinacolborane and the corresponding amines in the absence of any metal catalyst. Pinacolborane and *tert*-butylamine respectively pyrrolidine were stirred in dme at room temperature for 1 h, whereupon ~20% of the respective dehydrocoupling products were observed by ¹¹B NMR spectroscopy. The corresponding control experiment between *p*-toluidine and pinacolborane gave a conversion of ~50%. Following these blank experiments, *tert*-butylamine, pyrrolidine and *p*-toluidine were reacted with pinacolborane in dme for 1 h in the presence of 5 mol% of 1 a–d. This addition of



Scheme 2. Amine-borane dehydrocoupling catalyzed by 1 a–d.

5 mol% catalyst resulted in the doubling to quadrupling of the conversions under identical reaction conditions, thus a strong catalytic effect could be observed (Scheme 2; Table 1).

Overall, this is roughly on a par with a β -diketiminato magnesium system reported by Hill and coworkers,^[62] and somewhat faster than alkali-metal amide catalysts, reported by Panda and coworkers.^[63] Interestingly, 1 a–d all performed relatively similarly in the dehydrocoupling of dialkylamineboranes and amines with pinacolborane, indicating no strong effects of the different substitution patterns on the catalytic performance. Mechanistically we assume that the amine-borane dehydrogenation/dehydrocoupling reactions catalyzed by 1 a–d follow a similar pathway as with the related magnesocenophane systems, previously reported.^[24,25]

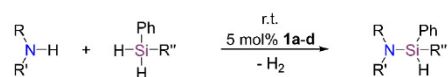
Amine Silane Cross-Dehydrocoupling

Recently, we reported the utilization of C-[1]magnesocenophanes in amine silane cross-dehydrocoupling.^[25] Therefore, following the successful application of the title compounds 1 a–d in amine-borane dehydrocoupling, we expanded the substrate scope to silanes and investigate the possibility for catalytic Si–N bond formations. Remarkably, the cross-dehydrocoupling between diphenylsilane and methylphenylsilane with different primary and secondary amines with 5 mol% of catalyst loading, gave quantitative or near quantitative conversions in most cases after just 1 h at room temperature (Scheme 3, Table 2). Only the cross-dehydrocoupling of *tert*-butylamine and dibenzylamine with diphenylsilane yielded lower conversions, or required longer reaction times respectively, presumably due to the higher steric demand

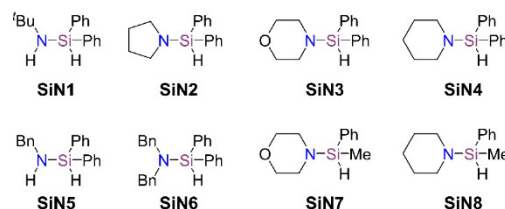
Table 1. Summary of catalysts, substrates, formed coupling products and conversions of the amine-borane dehydrocoupling reactions catalyzed by 1 a–d, corresponding to Scheme 2.^[a]

catalyst	substrate(s)	product	conversion
1 a	^t Pr ₂ NH·BH ₃	BN1	≥ 95%
1 b·dme	^t Pr ₂ NH·BH ₃	BN1	≥ 95%
1 c·dme	^t Pr ₂ NH·BH ₃	BN1	≥ 95%
1 d·dme	^t Pr ₂ NH·BH ₃	BN1	≥ 95%
1 a	Me ₂ NH·BH ₃	BN2	82%
1 b·dme	Me ₂ NH·BH ₃	BN2	87%
1 c·dme	Me ₂ NH·BH ₃	BN2	80%
1 d·dme	Me ₂ NH·BH ₃	BN2	78%
1 a	PipNH·BH ₃	BN3	≥ 95%
1 b·dme	PipNH·BH ₃	BN3	91%
1 c·dme	PipNH·BH ₃	BN3	87%
1 d·dme	PipNH·BH ₃	BN3	≥ 95%
1 a	MorNH·BH ₃	BN4	≥ 95%
1 b·dme	MorNH·BH ₃	BN4	≥ 95%
1 c·dme	MorNH·BH ₃	BN4	91%
1 d·dme	MorNH·BH ₃	BN4	92%
–	<i>p</i> -TolNH + HBpin	BN5	50%
1 a	<i>p</i> -TolNH + HBpin	BN5	≥ 95%
1 b·dme	<i>p</i> -TolNH + HBpin	BN5	≥ 95%
1 c·dme	<i>p</i> -TolNH + HBpin	BN5	≥ 95%
1 d·dme	<i>p</i> -TolNH + HBpin	BN5	≥ 95%
–	^t BuNH ₂ + HBpin	BN6	19%
1 a	^t BuNH ₂ + HBpin	BN6	67%
1 b·dme	^t BuNH ₂ + HBpin	BN6	70%
1 c·dme	^t BuNH ₂ + HBpin	BN6	76%
1 d·dme	^t BuNH ₂ + HBpin	BN6	48%
–	PyrNH + HBpin	BN7	20%
1 a	PyrNH + HBpin	BN7	94%
1 b·dme	PyrNH + HBpin	BN7	95%
1 c·dme	PyrNH + HBpin	BN7	≥ 95%
1 d·dme	PyrNH + HBpin	BN7	72%

[a] Conditions: BN1–BN4: dme; room temperature; 8 h; 5 mol% catalyst loading; BN5–BN7: dme; room temperature; 1 h; 5 mol% catalyst loading.



coupling products:



Scheme 3. Amine silane cross-dehydrocoupling catalyzed by 1 a–d.

of those amines. Furthermore, catalysts 1 a–d performed relatively equally in case of SiN2,3,4,5,7,8, while 1 a and 1 d showed lower catalytic performance in the afore mentioned coupling reaction yielding SiN1 and SiN6. Particularly surprise is

Table 2. Summary of catalysts, substrates, formed coupling products and conversions of the amine silane cross-dehydrocoupling reactions catalyzed by **1a–d**, corresponding to Scheme 3.^[a]

catalyst	substrates	product	conversion
1a	^t BuNH ₂ /Ph ₂ SiH ₂	SiN1	50 %
1b·dme	^t BuNH ₂ /Ph ₂ SiH ₂	SiN1	65 %
1c·dme	^t BuNH ₂ /Ph ₂ SiH ₂	SiN1	66 %
1d·dme	^t BuNH ₂ /Ph ₂ SiH ₂	SiN1	31 %
1a	PyrNH/Ph ₂ SiH ₂	SiN2	≥ 95 %
1b·dme	PyrNH/Ph ₂ SiH ₂	SiN2	≥ 95 %
1c·dme	PyrNH/Ph ₂ SiH ₂	SiN2	≥ 95 %
1d·dme	PyrNH/Ph ₂ SiH ₂	SiN2	≥ 95 %
1a	MorNH/Ph ₂ SiH ₂	SiN3	≥ 95 %
1b·dme	MorNH/Ph ₂ SiH ₂	SiN3	≥ 95 %
1c·dme	MorNH/Ph ₂ SiH ₂	SiN3	≥ 95 %
1d·dme	MorNH/Ph ₂ SiH ₂	SiN3	≥ 95 %
1a	PipNH/Ph ₂ SiH ₂	SiN4	≥ 95 %
1b·dme	PipNH/Ph ₂ SiH ₂	SiN4	≥ 95 %
1c·dme	PipNH/Ph ₂ SiH ₂	SiN4	≥ 95 %
1d·dme	PipNH/Ph ₂ SiH ₂	SiN4	≥ 95 %
1a	BnNH ₂ /Ph ₂ SiH ₂	SiN5	89 %
1b·dme	BnNH ₂ /Ph ₂ SiH ₂	SiN5	92 %
1c·dme	BnNH ₂ /Ph ₂ SiH ₂	SiN5	89 %
1d·dme	BnNH ₂ /Ph ₂ SiH ₂	SiN5	≥ 95 %
1a	Bn ₂ NH/Ph ₂ SiH ₂	SiN6	51 %
1b·dme	Bn ₂ NH/Ph ₂ SiH ₂	SiN6	87 %
1c·dme	Bn ₂ NH/Ph ₂ SiH ₂	SiN6	88 %
1d·dme	Bn ₂ NH/Ph ₂ SiH ₂	SiN6	0 %
1a	MorNH/MePhSiH ₂	SiN7	≥ 95 %
1b·dme	MorNH/MePhSiH ₂	SiN7	≥ 95 %
1c·dme	MorNH/MePhSiH ₂	SiN7	≥ 95 %
1d·dme	MorNH/MePhSiH ₂	SiN7	≥ 95 %
1a	PipNH/MePhSiH ₂	SiN8	≥ 95 %
1b·dme	PipNH/MePhSiH ₂	SiN8	≥ 95 %
1c·dme	PipNH/MePhSiH ₂	SiN8	≥ 95 %
1d·dme	PipNH/MePhSiH ₂	SiN8	≥ 95 %

[a] Conditions: **SiN1–SiN5, SiN7, SiN8**: C₆D₆; room temperature; 1 h; 5 mol% catalyst loading; **SiN6**: C₆D₆; room temperature; 16 h; 5 mol% catalyst loading.

the fact that **1d** repeatedly and reproducibly gave almost no coupling product **SiN6** in the reaction of dibenzylamine with diphenylsilane. To preclude that this originates from poor solubility of **1d·dme**, we repeated the reaction in thf under otherwise identical conditions, but still only observed 10% conversion. Increased reaction times of up to 24 h and increased catalyst loadings of 10 mol% did not yield significantly higher conversions. The reason for this remains unclear, but it might be more related to electronic than steric reasons. In all cases, catalysts **1a–d** gave selectively the mono coupling products, but no diaminosilanes and/or disilylamines.

While several magnesium-based systems are known to catalyze amine silane cross-dehydrocoupling reactions at room temperature, they typically require reaction times of 15 h to 24 h.^[30–32] Thus, the performance of **1a–d** is quite remarkable, as they give near quantitative conversions after just 1 h in many cases. Although, some heavier alkaline earth metal compounds do catalyze the cross-dehydrocoupling of amines and silanes

more efficiently,^[70,71] *ansa*-half-sandwich magnesium complexes **1a–d**, in particular **1b** and **1c**, are among the most potent magnesium-based catalysts for amine silane cross-dehydrocoupling.

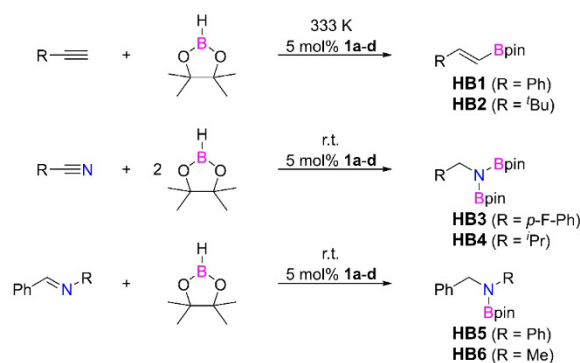
As the *ansa*-half-sandwich complexes **1a–d** are structural related to [1]magnesianocenes, we assume that the mechanism is similar to what we suggested before, based on experimental and theoretical investigations.^[25] Most likely, the initial step involves the formation of a bis(amine) complex of the type **1a–d**·(amine)₂. Such a complex could be observed spectroscopically, when **1a** was treated with two equivalents of pyrrolidine, giving **1a**·(pyrrolidine)₂.^[60] Most importantly, no formation of free ligand was detected by ¹H/¹³C{¹H}/²⁹Si{¹H} NMR spectroscopy in this experiment, indicating that no metal-ligand cleavage takes place and that **1a**, **1a**·(pyrrolidine)₂ respectively, is most likely involved in the catalysis and that **1a** is not just a precatalyst. Furthermore, addition of two equivalents of diphenylsilane to this magnesium amine complex, resulted in dehydrocoupling and formation of coupling product **SiN2**, while magnesium complex **1a** remained intact.

Hydroelementation Catalysis

Hydroboration

In general, hydroelementation reactions are of great interest for a variety of reasons, including the synthetically straight forward possibility to incorporate functional group across different unsaturated chemical bonds, combined with their high atom economy. One of the most popular hydroelementation reactions are hydroborations, for which different magnesium-based catalysts have been reported in the past.^[14,33–38] Accordingly, we probed the possibility of using *ansa*-half-sandwich complexes **1a–d** as catalysts for hydroboration reactions of alkynes, nitriles and imines with pinacolborane (Scheme 4; Table 3).

A catalyst loading of 5 mol% is commonly reported in literature^[14,33,72,73] and has also been used successfully for dehydrocoupling reactions with **1a–d**, which is why we performed our investigation with this loading. The hydroboration of phenyl and *tert*-butyl alkyne with equimolar



Scheme 4. Hydroboration of alkynes, nitriles and imines catalyzed by **1a–d**.

Table 3. Summary of catalysts, substrates, formed hydroboration products and conversions of the hydroboration reactions catalyzed by **1a–d**, corresponding to Scheme 4.^[a]

catalyst	substrate + n HBpin	product	conversion
–	PhC≡CH (n = 1)	HB1	0%
MgBr ₂	PhC≡CH (n = 1)	HB1	0%
1a	PhC≡CH (n = 1)	HB1	81%
1b ·dme	PhC≡CH (n = 1)	HB1	62%
1c ·dme	PhC≡CH (n = 1)	HB1	64%
1d ·dme	PhC≡CH (n = 1)	HB1	75%
–	^t BuC≡CH (n = 1)	HB2	4%
MgBr ₂	^t BuC≡CH (n = 1)	HB2	20%
1a	^t BuC≡CH (n = 1)	HB2	81%
1b ·dme	^t BuC≡CH (n = 1)	HB2	76%
1c ·dme	^t BuC≡CH (n = 1)	HB2	88%
1d ·dme	^t BuC≡CH (n = 1)	HB2	79%
–	<i>p</i> -F-PhC≡N (n = 2)	HB3	0%
MgBr ₂	<i>p</i> -F-PhC≡N (n = 2)	HB3	0%
1a	<i>p</i> -F-PhC≡N (n = 2)	HB3	63%
1b ·dme	<i>p</i> -F-PhC≡N (n = 2)	HB3	≥ 95%
1c ·dme	<i>p</i> -F-PhC≡N (n = 2)	HB3	≥ 95%
1d ·dme	<i>p</i> -F-PhC≡N (n = 2)	HB3	≥ 95%
–	^t PrC≡N (n = 2)	HB4	0%
MgBr ₂	^t PrC≡N (n = 2)	HB4	0%
1a	^t PrC≡N (n = 2)	HB4	39%
1b ·dme	^t PrC≡N (n = 2)	HB4	≥ 95%
1c ·dme	^t PrC≡N (n = 2)	HB4	≥ 95%
1d ·dme	^t PrC≡N (n = 2)	HB4	≥ 95%
–	PhHC=NPh (n = 1)	HB5	0%
MgBr ₂	PhHC=NPh (n = 1)	HB5	0%
1a	PhHC=NPh (n = 1)	HB5	66%
1b ·dme	PhHC=NPh (n = 1)	HB5	76%
1c ·dme	PhHC=NPh (n = 1)	HB5	66%
1d ·dme	PhHC=NPh (n = 1)	HB5	60%
–	PhHC=NMe (n = 1)	HB6	19%
MgBr ₂	PhHC=NMe (n = 1)	HB6	19%
1a	PhHC=NMe (n = 1)	HB6	79%
1b ·dme	PhHC=NMe (n = 1)	HB6	70%
1c ·dme	PhHC=NMe (n = 1)	HB6	72%
1d ·dme	PhHC=NMe (n = 1)	HB6	54%

[a] Conditions: C₆D₆ (MgBr₂ in thf); room temperature or 333 K; 24 h; 5 mol% catalyst loading.

amounts of pinacolborane was carried out at 333 K for 24 h. The reactions gave conversions of 62% to 88%, under selective formation of the anti-Markovnikov *syn*-product. For comparison, Ma and coworkers reported the application of a β-diketiminato magnesium complex in the catalytic hydroboration of terminal alkynes. The authors used 5 mol% of catalyst loading and temperatures above 373 K to obtain 99% conversion after six hours,^[72] and Cavallo, Rueping and coworkers utilize 7 mol% of dibutylmagnesium as a precatalyst and obtained 83% conversion after 18 hours at 353 K in the hydroboration of terminal alkynes.^[74] Thus, *ansa*-half-sandwich magnesium complexes **1a–d** operate at comparable temperatures. Subsequently, the hydroboration of nitriles and imines were investigated and found to be feasible at room temperature. With a catalyst loading of 5 mol%, conversions of up to 76% to ≥ 95% were achievable after 24 h at room temperature, depending on the catalyst. Noteworthy, magnesium complex **1a**, carrying the

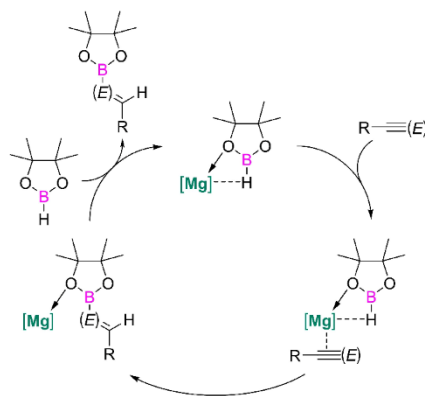
non-methylated Cp ring, performed significantly poorer in some of these reactions, possibly due to lower stability and corresponding catalyst degradation. Overall, the catalytic performance in these hydroboration reactions is remarkable for a magnesium-based system, as some other systems use higher catalyst loadings of 10 mol%,^[72,75] while also requiring elevated temperatures of 333 K to 343 K.^[33,36–38,72,75,76] However, an exception worth mentioning is a magnesium-based system reported by Hill and coworkers, which operates in a temperature range between 298 K and 343 K and gives high conversions within under 1 h in some cases.^[73] Noteworthy, control experiments under identical conditions but without any metal compound or using 5 mol% of MgBr₂ showed little to no conversions (Table 3).

Different mechanisms for metal catalyzed hydroborations have been proposed in the literature. These often involve B–H oxidative addition to the metal center of the catalyst. However, in case of a magnesium(II) compound, this is not plausible. More likely, **1a–d** act as Lewis acids, activating the B–H moiety.^[72,75,77] The Lewis acidic magnesium center may coordinate the pinacolborane *via* one of the oxygen atoms, while formation of a Mg–H–B multicenter bonding interaction activates the B–H bond and enables the transfer to the unsaturated C=C/C≡N/C=N moieties (Scheme 5).

Hydroamination

Following these promising results in hydroboration catalysis, we expanded our investigations of hydroelementation catalysis to other *p*-block element hydrides and targeted hydroaminations. The well-known intramolecular hydroamination of α-(*o*)-aminoalkenes is of great importance for the synthesis of *N*-heterocycles and has therefore been investigated extensively in the past decades, but still represents a challenge for metal catalysis, especially for *s*-block-based catalyst systems.^[78–80]

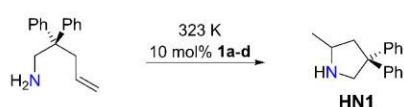
When 2,2-diphenyl-4-penten-1-amine is treated with 10 mol% of **1a–d** at 323 K for 24 h, full conversion (≥ 95%) to


Scheme 5. Proposed mechanism for the hydroboration of alkynes and nitriles catalyzed by **1a–d** (E=CH, N).

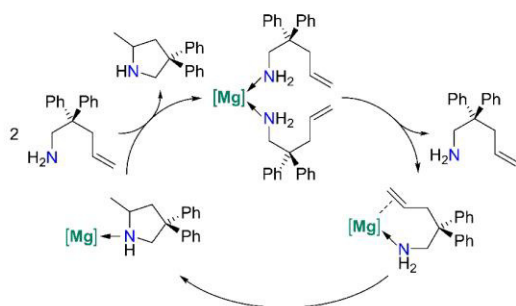
the intramolecular hydroamination product is observed (Scheme 6).

Higher catalyst loading of 10 mol% and elevated temperatures are not unusual for this reaction and are commonly reported in the literature. For instance, Sadow and coworkers used loading of 10 mol% of magnesium-based catalysts, which gave quantitative conversion in the intramolecular hydroamination of 2,2-diphenyl-4-penten-1-amine after 1 h to 24 h at temperatures of room temperature and 323 K to 333 K.^[43–45] Cano and coworkers had reported a related *ansa*-half-sandwich magnesium complex, that catalyzed the ring-closing hydroamination of 2,2-diphenyl-4-penten-1-amine at 333 K,^[13] and Hultsch and coworkers reported this hydroamination at room temperature using different magnesium based catalysts.^[39–42] Furthermore, it must also be mentioned that Harder and coworkers have reported some highly active magnesium catalysts for this reaction, giving quantitative conversions after 45 min to 12 h at room temperature.^[46,47] Their reported calcium-complex is even more efficient, as it needs only five minutes to reach full conversions.^[47] Never the less, **1a–d** performed quite competitively for a magnesium-based system.

Interestingly, the higher catalyst loading of 10 mol% enables an NMR characterization of the magnesium complexes in the catalytic reaction mixture. Most significantly, after the catalytic transformation is complete, the *ansa*-half-sandwich complexes **1a–d** are intact, as for instance indicated by the typical resonances for the Si–CH₃, N–C(CH₃)₃ and Cp–H groups in case of **1a** (Figure S13). This is an important finding, as it clearly indicates that **1a–d** are most likely catalysts and not just precatalysts. Mechanistically, we assume that a bis(amine) complex – as discussed before (*vide infra*) – forms and that by dissociation of one of the amines and coordination/activation of the C=C double bond moiety, the N–H transfer can occur in



Scheme 6. Ring-closing hydroamination of 2,2-diphenyl-4-penten-1-amine to 2-methyl-4,4-diphenylpyrrolidine catalyzed by **1a–d**.



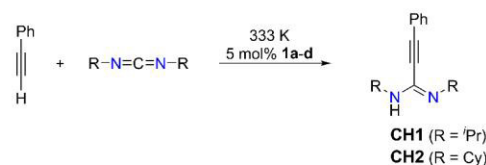
Scheme 7. Proposed mechanism for the cyclic hydroamination of 2,2-diphenyl-4-penten-1-amine to 2-methyl-4,4-diphenylpyrrolidine catalyzed by **1a–d**.

the coordination sphere of the magnesium atom (Scheme 7). Such a mechanism was proposed for the intramolecular hydroamination by alkaline-earth metal complexes by Tobisch, backed up by DFT calculations.^[81]

Hydroacetylenation

Following the promising results of **1a–d** in different dehydrocoupling and hydroelementation scenarios, we also investigated their catalytic abilities in the addition of terminal alkynes to carbodiimides, as this C–H activation/C–C bond formation reaction could in principle also be regarded as a type of hydroelementation (hydrocarboration). A catalyst loading of 5 mol% of **1a–d** yielded 54% to 62% conversion after 24 h at 333 K, for the reaction of phenylacetylene with *N,N'*-dicyclohexylcarbodiimide. Changing the carbodiimide to *N,N'*-diisopropylcarbodiimide gave 60% to 80% at the same reaction conditions (Scheme 8; Table 4). **1a–d** all performed relatively equally in these transformations.

For comparison, Coles and coworkers reported of a magnesium compound, that promoted the catalytic addition of phenylacetylene to *N,N'*-diisopropylcarbodiimide, giving conversions of ca. 50% after 24 h at 323 K.^[48] This is somewhat comparable to the catalytic performance of **1a–d**. Noteworthy however, Hill and coworkers reported a magnesium compound that was able to catalyze this reaction at room temperature, with conversions in the range of 60% after 24 h. Furthermore, some heavier alkaline earth metal compounds have been shown to possess an even higher catalytic activity.^[49]



Scheme 8. Hydroacetylenation of phenylacetylene and carbodiimides catalyzed by **1a–d**.

Table 4. Summary of catalysts, substrates, formed products and conversions of the hydroacetylenation reactions catalyzed by **1a–d**, corresponding to Scheme 8.^[a]

catalyst	substrate + PhC≡CH	product	Conversion
1a	PrN=C=NPr	CH1	79%
1b ·dme	PrN=C=NPr	CH1	73%
1c ·dme	PrN=C=NPr	CH1	78%
1d ·dme	PrN=C=NPr	CH1	63%
1a	CyN=C=NCy	CH2	62%
1b ·dme	CyN=C=NCy	CH2	54%
1c ·dme	CyN=C=NCy	CH2	61%
1d ·dme	CyN=C=NCy	CH2	56%

[a] Conditions: C₆D₆; 333 K; 24 h; 5 mol% catalyst loading.

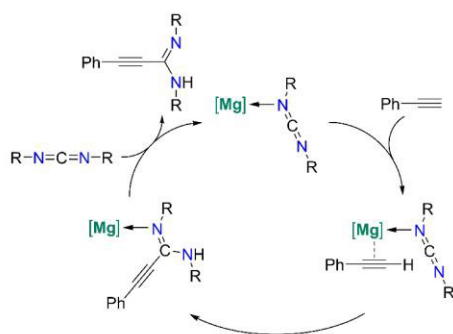
We assume that a similar mechanism is in operation for **1 a–d** as was previously described by Coles *et al.* and Hill *et al.* for their systems (Scheme 9).^[48,49,82]

Following coordination of the carbodiimide to the electrophilic magnesium center, the phenylacetylene may coordinate to the magnesium center as well and then undergo the addition reaction upon C–H activation in the coordination sphere of the magnesium center. Noteworthy, the stoichiometric reaction of **1 b**·(dme) with *N,N'*-diisopropylcarbodiimide resulted in the formation of the postulated complex, along uncoordinated dme, as indicated by ¹H/¹³C{¹H}/²⁹Si{¹H} NMR spectroscopy and importantly, no free ligand was detected,^[60] suggesting that **1 a–d** are catalysts for this reaction and not just precatalysts.

Conclusion

In this work, we reported the syntheses and characterization of four constrained geometry *ansa*-half-sandwich complexes of magnesium, **1 a–d**. We used these compounds as homogenous catalysts in different high atom economy scenarios, more specifically dehydrocoupling and hydroelementation transformations, including B–N and Si–N (cross-) dehydrocoupling, hydroborations, hydroaminations and hydroacetylenations. In amine-borane dehydrocoupling, as well as in amine silane cross-dehydrocoupling, **1 a–d** are among the best magnesium-based systems, as they operate at room temperature and generally give high conversions after short reaction times. In hydroboration reactions, these compounds have also been found to be useful catalysts that can readily catalyze the hydroboration of multiple substrates, such as alkynes, nitriles and imines. Furthermore, we could also successfully use **1 a–d** in the ring-closing hydroamination of an α - ω -aminoalkene. Finally, their catalytic capabilities in the addition of a terminal alkyne to carbodiimides was demonstrated.

Thus, this work significantly expands the field of application of cyclopentadienyl magnesium compounds in homogenous catalysis, reporting a new kind of magnesium catalyst that possesses a broad application scope in different catalytic transformations.



Scheme 9. Proposed mechanism for the hydroacetylenation of phenylacetylene and carbodiimides catalyzed by **1 a–d**.

Experimental Section

General Details

All manipulations were carried out under an argon inert gas atmosphere (argon 5.0), using either Schlenk line techniques or a glovebox. NMR spectra were recorded on Bruker Avance III 300 and Bruker Avance III 400 spectrometers. ¹H and ¹³C NMR spectra were referenced using the solvent signals ($\delta^1\text{H}$ (CHCl₃)=7.26, $\delta^1\text{H}$ (C₆HD₆)=7.16, $\delta^1\text{H}$ (thf-d₇)=3.58; $\delta^{13}\text{C}$ (C₆D₆)=128.06, $\delta^{13}\text{C}$ (CDCl₃)=77.16, $\delta^{13}\text{C}$ (thf-d₈)=67.57). ¹¹B and ²⁹Si NMR spectra were referenced using external standards ($\delta^{11}\text{B}$ (BF₃·OEt₂)=0, $\delta^{29}\text{Si}$ (SiMe₄)=0). Crystal structures have been deposited with the Cambridge Crystallographic Data Centre (CCDC) and are available free of charge from the Cambridge Structural Database (reference numbers: 2193652, 2193656, 2193657, 2193660, 2193661).

Synthesis and Characterization of Magnesium Complexes **1 a–d**

1 a

To a solution of (C₅H₅)SiMe₂NHtBu (4.19 g, 21.4 mmol) in hexane (~125 mL) precooled to 273 K was added a solution of *n*-butyl-*sec*-butylmagnesium (0.7 M in hexane, 30.1 mL, 21.1 mmol). The cooling bath was removed, and the mixture was heated to 333 K for 20 h. The precipitated product was isolated by filtration and dried *in vacuo* to obtain **1 a** as colorless solid. Yield: 4.04 g/88%.

¹H NMR (400.13 MHz, thf-d₈): δ (in ppm): 6.13 (t, ³J_{HH}=2.3 Hz, 2 H; Cp-H), 5.99 (t, ³J_{HH}=2.3 Hz, 2 H; Cp-H), 1.04 (s, 9 H; C(CH₃)₃), 0.25 (s, 6 H; Si-CH₃); ¹³C{¹H} NMR (100.62 MHz, thf-d₈): δ (in ppm): 117.5 (Cp), 111.4 (Cp), 108.8 (Cp), 51.6 (C(CH₃)₃), 37.9 (C(CH₃)₃), 4.7 (Si-CH₃); ²⁹Si{¹H} NMR (79.49 MHz, thf-d₈): δ (in ppm): -22.6.

1 b·dme

To a solution of (C₅Me₄H)SiMe₂NHtBu (4.42 g, 17.6 mmol) in hexane (~125 mL) was added a solution of *n*-butyl-*sec*-butylmagnesium (0.7 M in hexane, 25.1 mL, 17.6 mmol). The mixture was stirred for two days at 333 K and subsequently 2 days at room temperature. The solvent was removed *in vacuo* to give a yellow oil. The oil was diluted with dme and stored at 248 K to obtained **1 b**·dme as colorless crystals. Yield: 1.96 g/31%.

¹H NMR (400.13 MHz, thf-d₈): δ (in ppm): 3.42 (dme), 3.27 (dme), 2.13 (s, 6 H, Cp-CH₃), 1.94 (s, 6 H, Cp-CH₃), 1.09 (s, 9 H, C(CH₃)₃), 0.32 (s, 6 H, Si-CH₃); ¹³C{¹H} NMR (100.62 MHz, thf-d₈): δ (in ppm): 116.6 (Cp), 114.4 (Cp), 108.3 (Cp), 72.8 (dme), 59.0 (dme), 51.5 (C(CH₃)₃), 38.0 (C(CH₃)₃), 15.0 (Cp-CH₃), 12.2 (Cp-CH₃), 8.9 (Si-CH₃); ²⁹Si{¹H} NMR (79.49 MHz, thf-d₈): δ (in ppm): -22.1.

1 c·dme

To a solution of (C₅Me₄H)SiPh₂NHtBu (7.89 g, 21.0 mmol) in hexane (~125 mL) and dme (~5 mL) was added a solution of *n*-butyl-*sec*-butylmagnesium (0.7 M in hexane, 30.0 mL, 21.0 mmol). The mixture was stirred for one day at 333 K. The precipitated product was isolated by filtration as a pale-yellow solid and dried *in vacuo*. Yield: 3.06 g/30%.

¹H NMR (400.13 MHz, thf-d₈): δ (in ppm): 7.78–7.71 (m, 4 H, Ph-H), 7.17–7.07 (m, 6 H, Ph-H), 3.42 (dme), 3.27 (dme), 1.93 (s, 6 H, Cp-CH₃), 1.67 (s, 6 H, Cp-CH₃), 1.30 (s, 9 H, C(CH₃)₃); ¹³C{¹H} NMR (100.62 MHz, thf-d₈): δ (in ppm): 148.1 (Ph), 137.6 (Ph), 136.4 (Ph), 127.4 (Ph), 127.1 (Ph), 118.4 (Cp), 115.0 (Cp), 105.3 (Cp), 72.8 (dme),

59.0 (dme), 51.5 (C(CH₃)₃), 38.5 (C(CH₃)₃), 15.2 (Cp-CH₃), 12.3 (Cp-CH₃); ²⁹Si{¹H} NMR (79.49 MHz, thf-*d*₆): δ (in ppm): -30.8.

1 d · dme

To a solution of (C₂Me₂H)SiMe₂NHPH (4.37 g, 20.3 mmol) in toluene (~100 mL) and dme (~5 mL) was added a solution of *n*-butyl-*sec*-butylmagnesium (0.7 M in hexane, 29.0 mL, 20.3 mmol). The mixture was stirred for one day at 333 K. The precipitated crude product was isolated by filtration and dried *in vacuo*. The crude product was diluted with dme and the solution was stored at 248 K to obtain the product as colorless crystals. Yield: 1.05 g/16%.

¹H NMR (400.13 MHz, thf-*d*₆): δ (in ppm): 6.74–6.68 (m, 2 H, Ph-H), 6.20–6.16 (m, 2 H, Ph-H), 6.09–6.04 (m, 1 H, Ph-H), 3.42 (dme), 3.27 (dme), 2.14 (s, 6 H, Cp-CH₃), 2.01 (s, 6 H, Cp-CH₃), 0.52 (s, 6 H, Si-CH₃); ¹³C{¹H} NMR (100.62 MHz, thf-*d*₆): δ (in ppm): 159.4 (Ph), 129.1 (Ph), 116.4 (Ph), 116.2 (Cp), 111.7 (Cp), 109.1 (Cp), 72.8 (dme), 59.1 (dme), 14.6 (Cp-CH₃), 12.0 (Cp-CH₃), 4.0 (Si-CH₃); ²⁹Si{¹H} NMR (79.49 MHz, thf-*d*₆): δ (in ppm): -17.7.

Acknowledgements

Support and funding by the Deutsche Forschungsgemeinschaft, DFG, (Emmy Noether program SCHA1915/3-1/2) is gratefully acknowledged. Instrumentation and technical assistance for this work were provided by the Service Center X-ray Diffraction, with financial support from Saarland University and the Deutsche Forschungsgemeinschaft (INST 256/506-1). Open Access funding enabled and organized by Projekt DEAL.

Conflict of Interest

The authors declare no conflict of interest.

Data Availability Statement

The data that support the findings of this study are available in the supplementary material of this article.

Keywords: Magnesium · half-sandwich complexes · constrained geometry complexes · dehydrocoupling · hydroelementation

- [1] P. J. Shapiro, E. Bunel, W. P. Schaefer, J. E. Bercaw, *Organometallics* **1990**, *9*, 867–869.
- [2] W. E. Piers, P. J. Shapiro, E. E. Bunel, J. E. Bercaw, *Synlett* **1990**, *1990*, 74–84.
- [3] J. Okuda, *Chem. Ber.* **1990**, *123*, 1649–1651.
- [4] M. C. Baier, M. A. Zuideveld, S. Mecking, *Angew. Chem. Int. Ed.* **2014**, *53*, 9722–9744; *Angew. Chem.* **2014**, *126*, 9878–9902.
- [5] J. Cano, K. Kunz, *J. Organomet. Chem.* **2007**, *692*, 4411–4423.
- [6] A. L. McKnight, R. M. Waymouth, *Chem. Rev.* **1998**, *98*, 2587–2598.
- [7] H. Braunschweig, F. M. Breitling, *Coord. Chem. Rev.* **2006**, *250*, 2691–2720.
- [8] J. M. Pietryga, J. D. Gorden, C. L. B. Macdonald, A. Voigt, R. J. Wiecek, A. H. Cowley, *J. Am. Chem. Soc.* **2001**, *123*, 7713–7714.
- [9] R. J. Wiecek, C. L. B. Macdonald, J. N. Jones, J. M. Pietryga, A. H. Cowley, *Chem. Commun.* **2003**, 430–431.
- [10] M. Weger, P. Pahl, F. Schmidt, B. S. Soller, P. J. Altmann, A. Pöthig, G. Gemmecker, W. Eisenreich, B. Rieger, *Macromolecules* **2019**, *52*, 7073–7080.
- [11] I.-A. Bischoff, B. Morgenstern, A. Schäfer, *Chem. Commun.* **2022**, *58*, 8934–8937.
- [12] T. K. Panda, C. G. Hrib, P. G. Jones, J. Jenter, P. W. Roesky, M. Tamm, *Eur. J. Inorg. Chem.* **2008**, *2008*, 4270–4279.
- [13] C. Gallegos, R. Camacho, M. Valiente, T. Cuenca, J. Cano, *Catal. Sci. Technol.* **2016**, *6*, 5134–5143.
- [14] M. Magre, M. Szweczyk, M. Rueping, *Chem. Rev.* **2022**, *122*, 8261–8312.
- [15] R. Rochat, M. J. Lopez, H. Tsurugi, K. Mashima, *ChemCatChem* **2016**, *8*, 10–20.
- [16] M. M. D. Roy, A. A. Omaña, A. S. S. Wilson, M. S. Hill, S. Aldrige, E. Rivard, *Chem. Rev.* **2021**, *121*, 12784–12965.
- [17] D. L. Anderson, in *Chemical Composition of the Mantle (Chapter 8), Theory of the Earth*, Blackwell Scientific, Boston, **1989**, pp. 147–175.
- [18] P. Nuss, M. J. Eckelman, *PLoS One* **2014**, *9*, e101298.
- [19] B. Peng, J. Chen, *Energy Environ. Sci.* **2008**, *1*, 479–483.
- [20] M. B. Reuter, K. Hageman, R. Waterman, *Chem. Eur. J.* **2021**, *27*, 3251–3261.
- [21] M. Arrowsmith, in: *Dehydrocoupling, Other Cross-couplings (Chapter 9), Early Main Group Metal Catalysis: Concepts and Reactions* (Edl: S. Harder), Wiley-VCH, Weinheim, **2020**, pp. 225–250.
- [22] E. M. Leitao, T. Jurca, I. Manners, *Nat. Chem.* **2013**, *5*, 817–829.
- [23] R. L. Melen, *Chem. Soc. Rev.* **2016**, *45*, 775–788.
- [24] L. Wirtz, W. Haider, V. Huch, M. Zimmer, A. Schäfer, *Chem. Eur. J.* **2020**, *26*, 6176–6184.
- [25] L. Wirtz, J. Lambert, B. Morgenstern, A. Schäfer, *Organometallics* **2021**, *40*, 2108–2117.
- [26] D. J. Liptrot, M. S. Hill, M. F. Mahon, D. J. MacDougall, *Chem. Eur. J.* **2010**, *16*, 8508–8515.
- [27] M. S. Hill, M. Hodgson, D. J. Liptrot, M. F. Mahon, *Dalton Trans.* **2011**, *40*, 7783–7790.
- [28] P. Bellham, M. D. Anker, M. S. Hill, G. Kociok-Köhn, M. F. Mahon, *Dalton Trans.* **2016**, *45*, 13969–13978.
- [29] A. C. A. Ried, L. J. Taylor, A. M. Geer, H. E. L. Williams, W. Lewis, A. J. Blake, D. L. Kays, *Chem. Eur. J.* **2019**, *25*, 6840–6846.
- [30] J. F. Dunne, S. R. Neal, J. Engelkemier, A. Ellern, A. D. Sadow, *J. Am. Chem. Soc.* **2011**, *133*, 16782–16785.
- [31] M. S. Hill, D. J. Liptrot, D. J. MacDougall, M. F. Mahon, T. P. Robinson, *Chem. Sci.* **2013**, *4*, 4212–4222.
- [32] A. Baishya, T. Peddaraio, S. Nembenna, *Dalton Trans.* **2017**, *46*, 5880–5887.
- [33] I. Banerjee, T. K. Panda, *Appl. Organomet. Chem.* **2021**, *35*, e6333.
- [34] S. Rej, A. Das, T. K. Panda, *Adv. Synth. Catal.* **2021**, *363*, 4818–4840.
- [35] K. Watanabe, J. H. Pang, R. Takita, S. Chiba, *Chem. Sci.* **2022**, *13*, 27–38.
- [36] D. Hayrapetyan, A. Y. Khalimon, *Chem. Asian J.* **2020**, *15*, 2575–2587.
- [37] D. Mukherjee, S. Shirase, T. P. Spaniol, K. Mashima, J. Okuda, *Chem. Commun.* **2016**, *52*, 13155–13158.
- [38] S. Schnitzler, T. P. Spaniol, J. Okuda, *Inorg. Chem.* **2016**, *55*, 12997–13006.
- [39] P. Horrillo-Martínez, K. C. Hultzsich, *Tetrahedron Lett.* **2009**, *50*, 2054–2056.
- [40] X. Zhang, T. J. Emge, K. C. Hultzsich, *Organometallics* **2010**, *29*, 5871–5877.
- [41] X. Zhang, T. J. Emge, K. C. Hultzsich, *Angew. Chem. Int. Ed.* **2012**, *51*, 394–398; *Angew. Chem.* **2012**, *124*, 406–410.
- [42] X. Zhang, S. Tobisch, K. C. Hultzsich, *Chem. Eur. J.* **2015**, *21*, 7841–7857.
- [43] J. F. Dunne, D. B. Fulton, A. Ellern, A. D. Sadow, *J. Am. Chem. Soc.* **2010**, *132*, 17680–17683.
- [44] S. R. Neal, A. Ellern, A. D. Sadow, *J. Organomet. Chem.* **2011**, *696*, 228–234.
- [45] N. Eedugurala, M. Hovey, H.-A. Ho, B. Jana, N. L. Lampland, A. Ellern, A. D. Sadow, *Organometallics* **2015**, *34*, 5566–5575.
- [46] B. Freitag, C. A. Fischer, J. Penafiel, G. Ballmann, H. Elsen, C. Färber, D. F. Piesik, S. Harder, *Dalton Trans.* **2017**, *46*, 11192–11200.
- [47] P. C. Stegner, J. Eyslein, G. M. Ballmann, J. Langer, J. Schmidt, S. Harder, *Dalton Trans.* **2021**, *50*, 3178–3185.
- [48] R. J. Schwamm, M. P. Coles, *Organometallics* **2013**, *32*, 5277–5280.
- [49] M. Arrowsmith, M. R. Crimmin, M. S. Hill, S. L. Lomas, M. S. Heng, P. B. Hitchcock, G. Kociok-Köhn, *Dalton Trans.* **2014**, *43*, 14249–14256.
- [50] H. G. Alt, K. Föttinger, W. Millius, *J. Organomet. Chem.* **1999**, *572*, 21–30.
- [51] D. W. Carpenetti, L. Kloppenburg, J. T. Kupec, J. L. Petersen, *Organometallics* **1996**, *15*, 1572–1581.

- [52] J. Pinkas, M. Horáček, V. Varga, K. Mach, K. Szarka, A. Vargová, R. Gyepes, *Polyhedron* **2020**, *188*, 114704.
- [53] Z. Hou, T. Koizumi, M. Nishiura, Y. Wakatsuki, *Organometallics* **2001**, *20*, 3323–3328.
- [54] a) C. Cremer, H. Jacobsen, P. Burger, *Chimia* **1997**, *51*, 650–653; b) C. Cremer, H. Jacobsen, P. Burger, *Chimia* **1997**, *51*, 968.
- [55] P. Perrotin, P. J. Shapiro, M. Williams, B. Twamley, *Organometallics* **2007**, *26*, 1823–1826.
- [56] P. Perrotin, B. Twamley, P. J. Shapiro, *Acta Crystallogr. Sect. E* **2007**, *63*, m1277–m1278.
- [57] L. Wirtz, A. Schäfer, *Chem. Eur. J.* **2021**, *27*, 1219–1230.
- [58] Fluoride ion affinities (FIA) were calculated according to a literature established method from the isodesmic reactions with Et₃B/Et₃BF⁻. For more details see for example: H. Großekappenberg, M. Reißmann, M. Schmidtman, T. Müller, *Organometallics* **2015**, *34*, 4952–4958.
- [59] Global electrophilicity indices ω were calculated following the method of Stephan and coworkers (Method C): A. R. Jupp, T. C. Johnstone, D. W. Stephan, *Inorg. Chem.* **2018**, *57*, 14764–14771.
- [60] See supporting information for further details.
- [61] C. M. Vogels, P. E. O'Connor, T. E. Phillips, K. J. Watson, M. P. Shaver, P. G. Hayes, S. A. Westcott, *Can. J. Chem.* **2001**, *79*, 1898–1905.
- [62] D. J. Liptrot, M. S. Hill, M. F. Mahon, A. S. S. Wilson, *Angew. Chem. Int. Ed.* **2015**, *54*, 13362–13365; *Angew. Chem.* **2015**, *127*, 13560–13563.
- [63] A. Harinath, S. Anga, T. K. Panda, *RSC Adv.* **2016**, *6*, 35648–35653.
- [64] S. Kaufmann, P. W. Roesky, *Eur. J. Inorg. Chem.* **2021**, *2021*, 2899–2905.
- [65] A. G. M. Barrett, M. R. Crimmin, M. S. Hill, P. B. Hitchcock, P. A. Procopiou, *Organometallics* **2007**, *26*, 4076–4079.
- [66] Z. Yang, M. Zhong, X. Ma, K. Nijesh, S. De, P. Parameswaran, H. W. Roesky, *J. Am. Chem. Soc.* **2016**, *138*, 2548–2551.
- [67] J. D. Erickson, T. Y. Lai, D. J. Liptrot, M. M. Olmstead, P. P. Power, *Chem. Commun.* **2016**, *52*, 13656–13659.
- [68] Y. Wang, P. Xu, X. Xu, *Chin. Chem. Lett.* **2021**, *32*, 4002–4005.
- [69] E. A. Romero, J. L. Peltier, R. Jassar, G. Bertrand, *Chem. Commun.* **2016**, *52*, 10563–10565.
- [70] C. Bellini, J.-F. Carpentier, S. Tobisch, Y. Sarazin, *Angew. Chem. Int. Ed.* **2015**, *54*, 7679–7683; *Angew. Chem.* **2015**, *127*, 7789–7793.
- [71] C. Bellini, V. Dorcet, J.-F. Carpentier, S. Tobisch, Y. Sarazin, *Chem. Eur. J.* **2016**, *22*, 4564–4583.
- [72] J. Li, M. Luo, X. Sheng, H. Hua, W. Yao, S. A. Pullarkat, L. Xu, M. Ma, *Org. Chem. Front.* **2018**, *5*, 3538–3547.
- [73] M. Arrowsmith, M. S. Hill, G. Kociok-Köhn, *Chem. Eur. J.* **2013**, *19*, 2776–2783.
- [74] M. Magre, B. Maity, A. Falconnet, L. Cavallo, M. Rueping, *Angew. Chem. Int. Ed.* **2019**, *58*, 7025–7029; *Angew. Chem.* **2019**, *131*, 7099–7103.
- [75] C. Weetman, M. D. Anker, M. Arrowsmith, M. S. Hill, G. Kociok-Köhn, D. J. Liptrot, M. F. Mahon, *Chem. Sci.* **2016**, *7*, 628–641.
- [76] K. Manna, P. Ji, F. X. Greene, W. Lin, *J. Am. Chem. Soc.* **2016**, *138*, 7488–7491.
- [77] M. R. Crimmin, M. S. Hill, in *Homogeneous Catalysis with Organometallic Complexes of Group 2, Topics in Organometallic Chemistry*, Springer, Berlin Heidelberg, **2013**, pp. 191–242.
- [78] T. E. Müller, K. C. Hultsch, M. Yus, F. Foubelo, M. Tada, *Chem. Rev.* **2008**, *108*, 3795–3892.
- [79] L. Huang, M. Arndt, K. Gooßen, H. Heydt, L. J. Gooßen, *Chem. Rev.* **2015**, *115*, 2596–2697.
- [80] J. Huo, G. He, W. Chen, X. Hu, Q. Deng, D. Chen, *BMC Chem. Biol.* **2019**, *13*, 89.
- [81] S. Tobisch, *Chem. Eur. J.* **2015**, *21*, 6765–6779.
- [82] R. J. Schwamm, B. M. Day, N. E. Mansfield, W. Knowelden, P. B. Hitchcock, M. P. Coles, *Dalton Trans.* **2014**, *43*, 14302–14314.

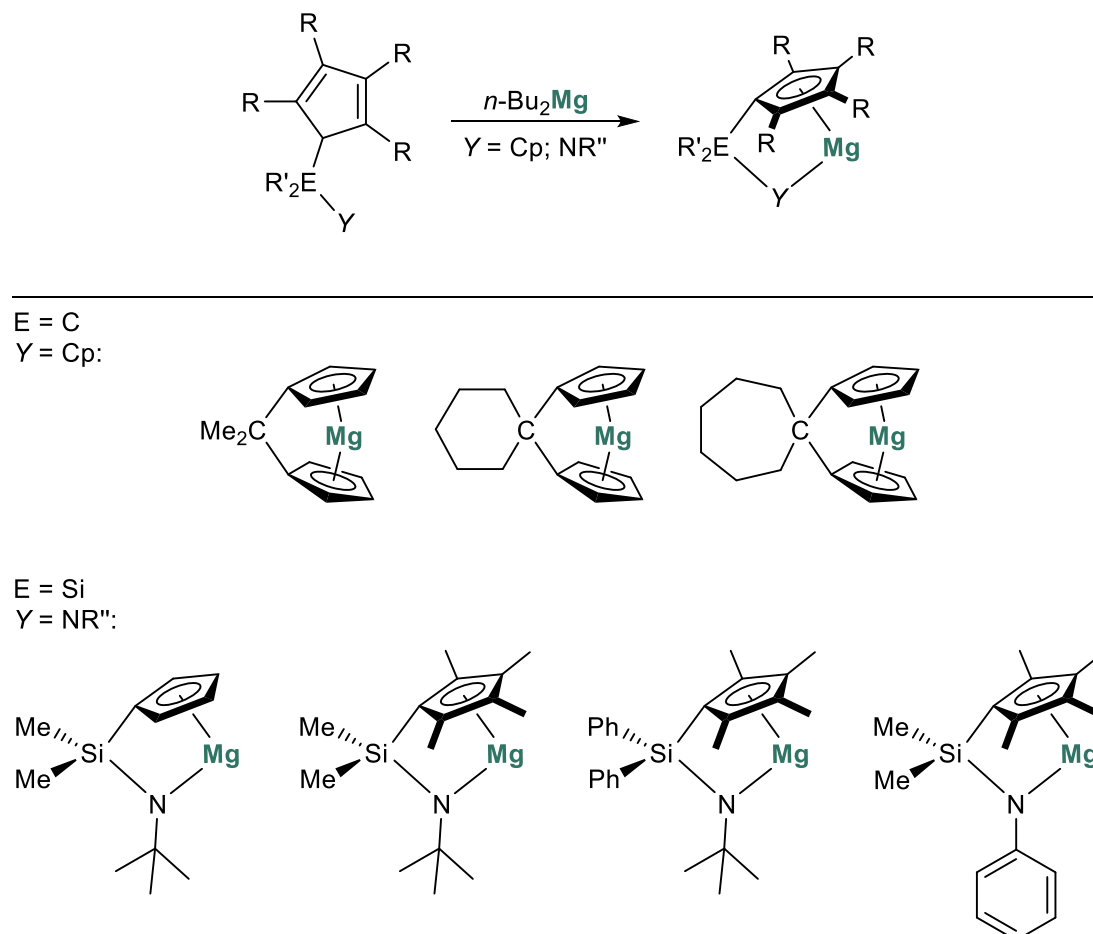
Manuscript received: August 9, 2022

Revised manuscript received: September 20, 2022

Version of record online: October 26, 2022

4. Conclusion

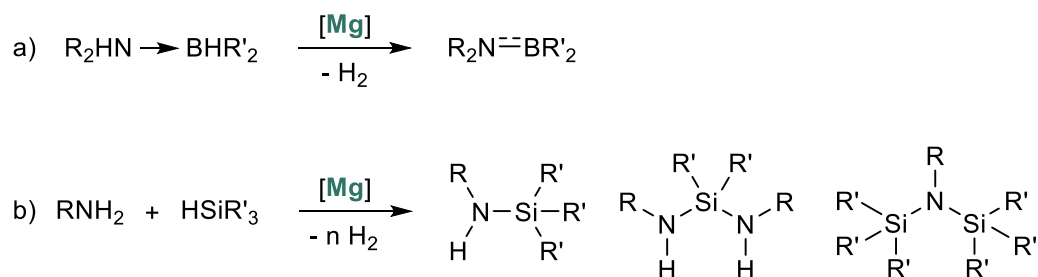
The synthesis and characterization of three C[1]magnesocenophanes as well as four constrained geometry *ansa*-half-sandwich magnesium complexes was successful (Scheme 27).



Scheme 27: Overview of cyclopentadienyl magnesium complexes obtained as part of this doctoral thesis.

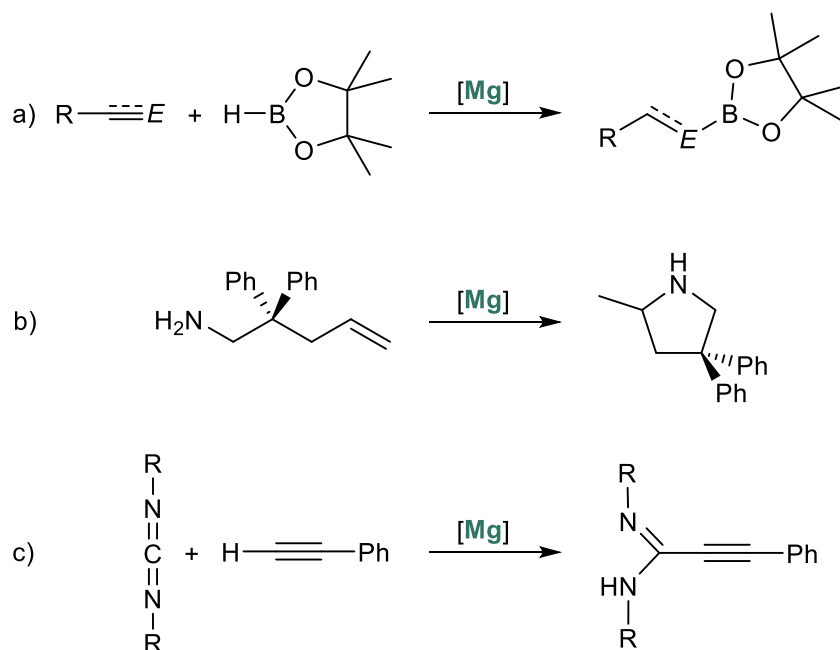
The successfully obtained magnesocenophanes and *ansa*-half-sandwich complexes were spectroscopically characterized by multi nuclear NMR spectroscopy. The structural characterization of the complexes was carried out by single crystal X-ray diffraction. Furthermore, the magnesium complexes were investigated by DFT calculations. The computed fluoride ion affinities (FIA) and the global electrophilicity indices (GEI) predict the magnesium atom to exhibit significant Lewis acidity. Following the characterization of these complexes, they were

used as catalysts in dehydrocoupling reactions (Scheme 28) and, in case of the *ansa*-half-sandwich complexes, also in hydroelementation reactions (Scheme 29).



Scheme 28: a) Dehydrogenation of amine boranes and b) cross-dehydrocoupling of amines and silanes catalyzed by magnesocenophanes and *ansa*-half-sandwich complexes.

Initially, the catalytic activity of the cyclopentadienyl magnesium complexes was tested in amine borane and in amine silane dehydrocoupling reactions (Scheme 28), starting with experiments to investigate the optimal reaction conditions, in which a strong impact of the used solvent was found. Subsequently, the substrate scope was broadened and in many cases high conversions were obtained at ambient conditions. This is remarkable, since many magnesium-based systems reported before needed high temperatures in similar dehydrocoupling applications. For a more in-depth understanding, kinetic studies and DFT calculations were performed to gain insight into the mechanism. Thereby, a strong influence of the *ansa*-ligand on the catalytic activity was revealed. In particular, the performance of [2]magnesocenophanes is less effective compared to [1]magnesocenophanes, indicating a strong ligand effect on the catalytic activity. In addition, it was demonstrated that the *ansa*-ligands play a central role through stepwise protonation and deprotonation of the Cp ring during the catalytic cycle. Following the promising application of the magnesocenophanes in dehydrocoupling/dehydrogenation reactions, the *ansa*-half-sandwich magnesium complexes were also employed in different hydroelementation reactions (Scheme 29).



Scheme 29: a) Hydroboration reactions, b) hydroamination reaction of 2,2-diphenylpent-4-en-1-amine and c) hydroacetylenation reaction of phenylacetylene and carbodiimides catalyzed by *ansa*-half-sandwich magnesium complexes.

The applicability of the four constrained geometry *ansa*-half-sandwich magnesium complexes in hydroelementation reactions were first probed in the hydroboration of alkynes, nitriles and imines with pinacolborane. After the successful application of the magnesium complexes in the hydroboration, the substrate spectrum was expanded to hydroamination and hydroacetylenation reactions. The *ansa*-half-sandwich magnesium complexes all showed good performance in the ring closing hydroamination of 2,2-diphenylpent-4-en-1-amine. Furthermore, the four compounds succeeded in the addition of phenylacetylene to different carbodiimides. Mechanistic investigations of these systems revealed intact catalyst system at the end of the reaction, indicating that these species are catalysts and not just precatalysts.

Noticeably, the utilization of cyclopentadienyl magnesium complexes in dehydrocoupling reactions described in this doctoral thesis, is the only example of magnesocenophanes and *ansa*-half-sandwich magnesium complexes in dehydrogenation catalysis. Most significantly, until now, the cyclopentadienyl magnesium complexes, especially the *ansa*-half-sandwich complexes, show by far the best performance for any magnesium catalysts in this field. The additional application of the *ansa*-half-sandwich complexes in hydroelementation reactions expanded the utilization of cyclopentadienyl magnesium complexes in homogeneous catalysis. Overall, the magnesium-based cyclopentadienyl complexes are promising catalysts and potent alternatives to transition metal-based catalysts.

5. References

- [1] T. J. Kealy, P. L. Pauson, *Nature* **1951**, *168*, 1039–1040.
- [2] S. A. Miller, J. A. Tebboth, J. F. Tremaine, *J. Chem. Soc.* **1952**, 632–635.
- [3] G. B. Kauffman, *J. Chem. Educ.* **1983**, *60*, 185.
- [4] P. L. Pauson, *J. Organomet. Chem.* **2001**, 637–639, 3–6.
- [5] H. Werner, *Angew. Chem. Int. Ed.* **2012**, *51*, 6052–6058.
- [6] P. Štěpnička, *Dalton Trans.* **2022**, *51*, 8085–8102.
- [7] E. O. Fischer, W. Pfab, *Z. Naturforsch. B* **1952**, *7*, 377–379.
- [8] E. O. Fischer, W. Hafner, *Z. Naturforsch. B* **1954**, *9*, 503–505.
- [9] P. Schüler, H. Görls, S. Kriek, M. Westerhausen, *Chem. Eur. J.* **2021**, *27*, 15508–15515.
- [10] G. Wilkinson, F. A. Cotton, *Chem. Ind.-Lond.* **1954**, 307–308.
- [11] K. Ziegler, H. Froitzheim-Kühlhorn, K. Hafner, *Chem. Ber.* **1956**, *89*, 434–443.
- [12] E. O. Fischer, H. P. Hofmann, *Chem. Ber.* **1959**, *92*, 482–486.
- [13] C.-H. Wong, T.-Y. Lee, K.-J. Chao, S. Lee, *Acta Cryst. B* **1972**, *28*, 1662–1665.
- [14] E. O. Fischer, G. Stölzle, *Chem. Ber.* **1961**, *94*, 2187–2193.
- [15] A. W. Duff, P. B. Hitchcock, M. F. Lappert, R. G. Taylor, J. A. Segal, *J. Organomet. Chem.* **1985**, *293*, 271–283.
- [16] D. J. Burkey, T. P. Hanusa, J. C. Huffman, *Adv. Funct. Mater.* **1994**, *4*, 1–8.
- [17] N. Bachmann, L. Wirtz, B. Morgenstern, C. Müller, A. Schäfer, *Acta Cryst. E* **2022**, *78*, 287–290.
- [18] D. J. Burkey, R. A. Williams, T. P. Hanusa, *Organometallics* **1993**, *12*, 1331–1337.
- [19] P. B. Duval, C. J. Burns, D. L. Clark, D. E. Morris, B. L. Scott, J. D. Thompson, E. L. Werkema, L. Jia, R. A. Andersen, *Angew. Chem. Int. Ed.* **2001**, *40*, 3357–3361.
- [20] G. B. Deacon, F. Jaroschik, P. C. Junk, R. P. Kelly, *Organometallics* **2015**, *34*, 2369–2377.
- [21] M. G. Gardiner, C. L. Raston, C. H. L. Kennard, *Organometallics* **1991**, *10*, 3680–3686.
- [22] C. D. Sofield, R. A. Andersen, *J. Organomet. Chem.* **1995**, *501*, 271–276.
- [23] F. Weber, M. Schultz, C. D. Sofield, R. A. Andersen, *Organometallics* **2002**, *21*, 3139–3146.
- [24] M. del Mar Conejo, R. Fernández, E. Gutiérrez-Puebla, Á. Monge, C. Ruiz, E. Carmona, *Angew. Chem. Int. Ed.* **2000**, *39*, 1949–1951.
- [25] M. del Mar Conejo, R. Fernández, D. del Río, E. Carmona, A. Monge, C. Ruiz, A. M. Márquez, J. Fernández Sanz, *Chem. Eur. J.* **2003**, *9*, 4452–4461.
- [26] M. J. Harvey, K. T. Quisenberry, T. P. Hanusa, V. G. Young Jr., *Eur. J. Inorg. Chem.* **2003**, 3383–3390.
- [27] C. P. Morley, P. Jutzi, C. Krueger, J. M. Wallis, *Organometallics* **1987**, *6*, 1084–1090.
- [28] R. A. Williams, K. F. Tesh, T. P. Hanusa, *J. Am. Chem. Soc.* **1991**, *113*, 4843–4851.
- [29] M. Westerhausen, M. Hartmann, G. Heckmann, W. Schwarz, *J. Organomet. Chem.* **1997**, *541*, 261–268.
- [30] M. Westerhausen, M. Hartmann, N. Makropoulos, B. Wieneke, M. Wieneke, W. Schwarz, D. Stalke, *Z. Naturforsch. B* **1998**, *53*, 117–125.
- [31] M. Westerhausen, M. Hartmann, W. Schwarz, *J. Organomet. Chem.* **1995**, *501*, 359–367.
- [32] P.-J. Sinnema, P. J. Shapiro, B. Höhn, T. E. Bitterwolf, B. Twamley, *Organometallics* **2001**, *20*, 2883–2888.
- [33] D. P. Daniels, G. B. Deacon, D. Harakat, F. Jaroschik, P. C. Junk, *Dalton Trans.* **2012**, *41*, 267–277.
- [34] K. M. Kane, P. J. Shapiro, A. Vij, R. Cubbon, A. L. Rheingold, *Organometallics* **1997**, *16*, 4567–4571.

- [35] C. Müller, J. Warzen, V. Huch, B. Morgenstern, I.-A. Bischoff, M. Zimmer, A. Schäfer, *Chem. Eur. J.* **2021**, *27*, 6500–6510.
- [36] A. Hammel, W. Schwarz, J. Weidlein, *J. Organomet. Chem.* **1989**, *378*, 347–361.
- [37] L. M. Engelhardt, P. C. Junk, C. L. Raston, A. H. White, *J. Chem. Soc., Chem. Commun.* **1988**, 1500–1501.
- [38] H. Schumann, J. Gottfriedsen, M. Glanz, S. Dechert, J. Demtschuk, *J. Organomet. Chem.* **2001**, *617–618*, 588–600.
- [39] R. A. Andersen, R. Blom, C. J. Burns, H. V. Volden, *J. Chem. Soc., Chem. Commun.* **1987**, 768–769.
- [40] R. A. Andersen, J. M. Boncella, C. J. Burns, R. Blom, A. Haaland, H. V. Volden, *J. Organomet. Chem.* **1986**, *312*, C49–C52.
- [41] C. J. Burns, R. A. Andersen, *J. Organomet. Chem.* **1987**, *325*, 31–37.
- [42] J. Vollet, E. Baum, H. Schnöckel, *Organometallics* **2003**, *22*, 2525–2527.
- [43] H. Sitzmann, T. Dezember, M. Ruck, *Angew. Chem. Int. Ed.* **1998**, *37*, 3113–3116.
- [44] R. Zerger, G. Stucky, *J. Organomet. Chem.* **1974**, *80*, 7–17.
- [45] G. B. Deacon, C. M. Forsyth, F. Jaroschik, P. C. Junk, D. L. Kay, T. Maschmeyer, A. F. Masters, J. Wang, L. D. Field, *Organometallics* **2008**, *27*, 4772–4778.
- [46] H. Schumann, S. Schutte, H.-J. Kroth, D. Lentz, *Angew. Chem. Int. Ed.* **2004**, *43*, 6208–6211.
- [47] C. Ruspic, J. R. Moss, M. Schürmann, S. Harder, *Angew. Chem. Int. Ed.* **2008**, *47*, 2121–2126.
- [48] L. Orzechowski, D. F.-J. Piesik, C. Ruspic, S. Harder, *Dalton Trans.* **2008**, 4742–4746.
- [49] Y. Schulte, H. Weinert, C. Wölper, S. Schulz, *Organometallics* **2020**, *39*, 206–216.
- [50] X. Shi, G. Qin, Y. Wang, L. Zhao, Z. Liu, J. Cheng, *Angew. Chem. Int. Ed.* **2019**, *58*, 4356–4360.
- [51] S. Harder, F. Feil, *Organometallics* **2002**, *21*, 2268–2274.
- [52] S. J. Pratten, M. K. Cooper, M. J. Aroney, *J. Organomet. Chem.* **1990**, *381*, 147–153.
- [53] S. Baguli, S. Mondal, C. Mandal, S. Goswami, D. Mukherjee, *Chem. Asian J.* **2022**, *17*, e202100962.
- [54] P. Jutzi, N. Burford, *Chem. Rev.* **1999**, *99*, 969–990.
- [55] A. Togni, R. L. Halterman, *Metallocenes: Synthesis Reactivity Applications*, Wiley-VCH, Weinheim, **1998**.
- [56] A. Jaenschke, J. Paap, U. Behrens, *Organometallics* **2003**, *22*, 1167–1169.
- [57] T. P. Hanusa, *Organometallics* **2002**, *21*, 2559–2571.
- [58] A. Almenningen, O. Bastiansen, A. Haaland, *J. Chem. Phys.* **1964**, *40*, 3434–3437.
- [59] E. Weiss, E. O. Fischer, *Z. Anorg. Allg. Chem.* **1955**, *278*, 219–224.
- [60] W. Bünder, E. Weiss, *J. Organomet. Chem.* **1975**, *92*, 1–6.
- [61] M. M. Olmstead, W. J. Grigsby, D. R. Chacon, T. Hascall, P. P. Power, *Inorg. Chim. Acta* **1996**, *251*, 273–284.
- [62] A. Jaenschke, J. Paap, U. Behrens, *Z. Anorg. Allg. Chem.* **2008**, *634*, 461–469.
- [63] A. Xia, M. J. Heeg, C. H. Winter, *J. Am. Chem. Soc.* **2002**, *124*, 11264–11265.
- [64] K. Fichtel, K. Hofmann, U. Behrens, *Organometallics* **2004**, *23*, 4166–4168.
- [65] L. Abis, F. Calderazzo, C. Maichle-Mössmer, G. Pampaloni, J. Strähle, G. Tripepi, *J. Chem. Soc., Dalton Trans.* **1998**, 841–846.
- [66] M. E. Smith, R. A. Andersen, *J. Am. Chem. Soc.* **1996**, *118*, 11119–11128.
- [67] A. D. Bond, R. A. Layfield, J. A. MacAllister, M. McPartlin, J. M. Rawson, D. S. Wright, *Chem. Commun.* **2001**, 1956–1957.
- [68] C. Dohmeier, C. Robl, M. Tacke, H. Schnöckel, *Angew. Chem. Int. Ed.* **1991**, *30*, 564–565.
- [69] M. Mitsuhara, M. Ogasawara, H. Sugiura, *J. Cryst. Growth* **1998**, *183*, 38–42.
- [70] K. V. Salazar, S. G. Pattillo, M. Trkula, *Fusion Technol.* **2000**, *38*, 69–73.
- [71] M. Putkonen, T. Sajavaara, L. Niinistö, *J. Mater. Chem.* **2000**, *10*, 1857–1861.
- [72] T. F. Kuech, P.-J. Wang, M. A. Tischler, R. Potemski, G. J. Scilla, F. Cardone, *J. Cryst. Growth* **1988**, *93*, 624–630.
- [73] M. J. Benac, A. H. Cowley, R. A. Jones, A. F. Tasch, *Chem. Mater.* **1989**, *1*, 289–290.

- [74] M. Vehkamäki, T. Hatanpää, T. Hänninen, M. Ritala, M. Leskelä, *Electrochem. Solid-State Lett.* **1999**, *2*, 504–506.
- [75] M. Vehkamäki, T. Hänninen, M. Ritala, M. Leskelä, T. Sajavaara, E. Rauhala, J. Keinonen, *Chem. Vap. Deposition* **2001**, *7*, 75–80.
- [76] K. A. Allen, B. G. Gowenlock, W. E. Lindsell, *J. Polym. Sci.* **1974**, *12*, 1131–1133.
- [77] Y. Li, H. Deng, W. Brittain, M. S. Chisholm, *Polym. Bull. (Berlin)* **1999**, *42*, 635–639.
- [78] S. Mortara, D. Fregonese, S. Bresadola, *Macromol. Chem. Phys.* **2001**, *202*, 2630–2633.
- [79] L. Wirtz, A. Schäfer, *Chem. Eur. J.* **2021**, *27*, 1219–1230.
- [80] R. L. N. Hailes, A. M. Oliver, J. Gwyther, G. R. Whittell, I. Manners, *Chem. Soc. Rev.* **2016**, *45*, 5358–5407.
- [81] U. T. Mueller-Westerhoff, *Angew. Chem. Int. Ed.* **1986**, *25*, 702–717.
- [82] R. A. Musgrave, A. D. Russell, I. Manners, *Organometallics* **2013**, *32*, 5654–5667.
- [83] D. E. Herbert, U. F. J. Mayer, I. Manners, *Angew. Chem. Int. Ed.* **2007**, *46*, 5060–5081.
- [84] P. J. Shapiro, *Coord. Chem. Rev.* **2002**, *231*, 67–81.
- [85] M. A. Bau, S. Wiesler, S. L. Younas, J. Streuff, *Chem. Eur. J.* **2019**, *25*, 10531–10545.
- [86] W. Röhl, H.-H. Brintzinger, B. Rieger, R. Zolk, *Angew. Chem. Int. Ed.* **1990**, *29*, 279–280.
- [87] S. Collins, W. J. Gauthier, D. A. Holden, B. A. Kuntz, N. J. Taylor, D. G. Ward, *Organometallics* **1991**, *10*, 2061–2068.
- [88] B. Rieger, A. Reinmuth, W. Röhl, H. H. Brintzinger, *J. Mol. Catal.* **1993**, *82*, 67–73.
- [89] B. Wang, *Coord. Chem. Rev.* **2006**, *250*, 242–258.
- [90] J. M. Nelson, H. Rengel, I. Manners, *J. Am. Chem. Soc.* **1993**, *115*, 7035–7036.
- [91] I. Manners, *Chem. Commun.* **1999**, 857–865.
- [92] R. D. A. Hudson, *J. Organomet. Chem.* **2001**, *637–639*, 47–69.
- [93] V. Bellas, M. Rehahn, *Angew. Chem. Int. Ed.* **2007**, *46*, 5082–5104.
- [94] D. E. Herbert, U. F. J. Mayer, J. B. Gilroy, M. J. López-Gómez, A. J. Lough, J. P. H. Charmant, I. Manners, *Chem. Eur. J.* **2009**, *15*, 12234–12246.
- [95] U. F. J. Mayer, J. B. Gilroy, D. O'Hare, I. Manners, *J. Am. Chem. Soc.* **2009**, *131*, 10382–10383.
- [96] S. Baljak, A. D. Russell, S. C. Binding, M. F. Haddow, D. O'Hare, I. Manners, *J. Am. Chem. Soc.* **2014**, *136*, 5864–5867.
- [97] R. A. Musgrave, R. L. N. Hailes, V. T. Annibale, I. Manners, *Chem. Sci.* **2019**, *10*, 9841–9852.
- [98] R. L. N. Hailes, R. A. Musgrave, A. F. R. Kilpatrick, A. D. Russell, G. R. Whittell, D. O'Hare, I. Manners, *Chem. Eur. J.* **2019**, *25*, 1044–1054.
- [99] R. A. Musgrave, A. D. Russell, P. R. Gamm, R. L. N. Hailes, K. Lam, H. A. Sparkes, J. C. Green, W. E. Geiger, I. Manners, *Organometallics* **2021**, *40*, 1945–1955.
- [100] J. M. Nelson, A. J. Lough, I. Manners, *Angew. Chem. Int. Ed.* **1994**, *33*, 989–991.
- [101] U. Vogel, A. J. Lough, I. Manners, *Angew. Chem. Int. Ed.* **2004**, *43*, 3321–3325.
- [102] B. Bagh, G. Schatte, J. C. Green, J. Müller, *J. Am. Chem. Soc.* **2012**, *134*, 7924–7936.
- [103] M. Tamm, A. Kunst, E. Herdtweck, *Chem. Commun.* **2005**, 1729–1731.
- [104] H. Braunschweig, C. J. Adams, T. Kupfer, I. Manners, R. M. Richardson, G. R. Whittell, *Angew. Chem. Int. Ed.* **2008**, *47*, 3826–3829.
- [105] C. Cremer, H. Jacobsen, P. Burger, *Chimia* **1997**, *51*, 650–653.
- [106] C. Cremer, H. Jacobsen, P. Burger, *Chimia* **1997**, *51*, 968.
- [107] P. Perrotin, P. J. Shapiro, M. Williams, B. Twamley, *Organometallics* **2007**, *26*, 1823–1826.
- [108] P. Perrotin, B. Twamley, P. J. Shapiro, *Acta Cryst. E* **2007**, *63*, m1277–m1278.
- [109] P. J. Shapiro, S.-J. Lee, P. Perrotin, T. Cantrell, A. Blumenfeld, B. Twamley, *Polyhedron* **2005**, *24*, 1366–1381.
- [110] W. Haider, V. Huch, A. Schäfer, *Dalton Trans.* **2018**, *47*, 10425–10428.
- [111] H.-R. H. Damrau, A. Geyer, M.-H. Proscenc, A. Weeber, F. Schaper, H.-H. Brintzinger, *J. Organomet. Chem.* **1998**, *553*, 331–343.

- [112] M. Schultz, C. D. Sofield, M. D. Walter, R. A. Andersen, *New J. Chem.* **2005**, *29*, 919–927.
- [113] M. Westerhausen, N. Makropoulos, B. Wieneke, K. Karaghiosoff, H. Nöth, H. Schwenk-Kircher, J. Knizek, T. Seifert, *Eur. J. Inorg. Chem.* **1998**, 965–971.
- [114] A. Antiñolo, R. Fernández-Galán, N. Molina, A. Otero, I. Rivilla, A. M. Rodríguez, *J. Organomet. Chem.* **2009**, *694*, 1959–1970.
- [115] M. Rieckhoff, U. Pieper, D. Stalke, F. T. Edelmann, *Angew. Chem. Int. Ed.* **1993**, *32*, 1079–1081.
- [116] M. Könemann, G. Erker, R. Fröhlich, S. Kotila, *Organometallics* **1997**, *16*, 2900–2908.
- [117] G. J. Matare, K. M. Kane, P. J. Shapiro, A. Vij, *J. Chem. Crystallogr.* **1998**, *28*, 731–734.
- [118] N. Leyser, K. Schmidt, H.-H. Brintzinger, *Organometallics* **1998**, *17*, 2155–2161.
- [119] G. J. Matare, D. M. Foo, K. M. Kane, R. Zehnder, M. Wagener, P. J. Shapiro, T. Concolino, A. L. Rheingold, *Organometallics* **2000**, *19*, 1534–1539.
- [120] B. Twamley, G. J. Matare, P. J. Shapiro, A. Vij, *Acta Cryst. E* **2001**, *57*, m402–m403.
- [121] P.-J. Sinnema, B. Höhn, R. L. Hubbard, P. J. Shapiro, B. Twamley, A. Blumenfeld, A. Vij, *Organometallics* **2002**, *21*, 182–191.
- [122] S. Fox, J. P. Dunne, M. Tacke, J. F. Gallagher, *Inorg. Chim. Acta* **2004**, *357*, 225–234.
- [123] E. D. Brady, S. C. Chmely, K. C. Jayaratne, T. P. Hanusa, V. G. Young, *Organometallics* **2008**, *27*, 1612–1616.
- [124] M. Kessler, S. Hansen, C. Godemann, A. Spannenberg, T. Beweries, *Chem. Eur. J.* **2013**, *19*, 6350–6357.
- [125] R. E. Cramer, P. N. Richmann, J. W. Gilje, *J. Organomet. Chem.* **1991**, *408*, 131–136.
- [126] D. J. Burkey, E. K. Alexander, T. P. Hanusa, *Organometallics* **1994**, *13*, 2773–2786.
- [127] B. Blom, G. Klatt, D. Gallego, G. Tan, M. Driess, *Dalton Trans.* **2015**, *44*, 639–644.
- [128] H. Lehmkuhl, K. Mehler, R. Benn, A. Ruffińska, C. Krüger, *Chem. Ber.* **1986**, *119*, 1054–1069.
- [129] S. C. Sockwell, T. P. Hanusa, J. C. Huffman, *J. Am. Chem. Soc.* **1992**, *114*, 3393–3399.
- [130] S. Ghosh, E. Glöckler, C. Wölper, A. Tjaberings, A. H. Gröschel, S. Schulz, *Organometallics* **2020**, *39*, 4221–4231.
- [131] M. J. Harvey, T. P. Hanusa, V. G. Young, *J. Organomet. Chem.* **2001**, *626*, 43–48.
- [132] D. F. Gaines, K. M. Coleson, J. C. Calabrese, *J. Am. Chem. Soc.* **1979**, *101*, 3979–3980.
- [133] M. del Mar Conejo, R. Fernández, E. Carmona, E. Gutiérrez-Puebla, Á. Monge, *Organometallics* **2001**, *20*, 2434–2436.
- [134] D. Naglav, B. Tobey, A. Neumann, D. Bläser, C. Wölper, S. Schulz, *Organometallics* **2015**, *34*, 3072–3078.
- [135] O. Michel, H. M. Dietrich, R. Litlabø, K. W. Törnroos, C. Maichle-Mössmer, R. Anwander, *Organometallics* **2012**, *31*, 3119–3127.
- [136] P. J. Shapiro, E. Bunel, W. P. Schaefer, J. E. Bercaw, *Organometallics* **1990**, *9*, 867–869.
- [137] W. E. Piers, P. J. Shapiro, E. E. Bunel, J. E. Bercaw, *Synlett* **1990**, *1990*, 74–84.
- [138] J. Okuda, *Chem. Ber.* **1990**, *123*, 1649–1651.
- [139] H. Braunschweig, F. M. Breitling, *Coord. Chem. Rev.* **2006**, *250*, 2691–2720.
- [140] A. L. McKnight, R. M. Waymouth, *Chem. Rev.* **1998**, *98*, 2587–2598.
- [141] J. Cano, K. Kunz, *J. Organomet. Chem.* **2007**, *692*, 4411–4423.
- [142] M. C. Baier, M. A. Zuideveld, S. Mecking, *Angew. Chem. Int. Ed.* **2014**, *53*, 9722–9744.
- [143] P. Jutzi, J. Kleimeier, T. Redeker, H.-G. Stammler, B. Neumann, *J. Organomet. Chem.* **1995**, *498*, 85–89.
- [144] A. Garcés, L. F. Sánchez-Barba, C. Alonso-Moreno, M. Fajardo, J. Fernández-Baeza, A. Otero, A. Lara-Sánchez, I. López-Solera, A. M. Rodríguez, *Inorg. Chem.* **2010**, *49*, 2859–2871.

- [145] M. Honrado, A. Otero, J. Fernández-Baeza, L. F. Sánchez-Barba, A. Garcés, A. Lara-Sánchez, J. Martínez-Ferrer, S. Sobrino, A. M. Rodríguez, *Organometallics* **2015**, *34*, 3196–3208.
- [146] N. Eedugurala, M. Hovey, H.-A. Ho, B. Jana, N. L. Lampland, A. Ellern, A. D. Sadow, *Organometallics* **2015**, *34*, 5566–5575.
- [147] M. Weger, P. Pahl, F. Schmidt, B. S. Soller, P. J. Altmann, A. Pöthig, G. Gemmecker, W. Eisenreich, B. Rieger, *Macromolecules* **2019**, *52*, 7073–7080.
- [148] C. Gallegos, R. Camacho, M. Valiente, T. Cuenca, J. Cano, *Catal. Sci. Technol.* **2016**, *6*, 5134–5143.
- [149] T. K. Panda, C. G. Hrib, P. G. Jones, J. Jenter, P. W. Roesky, M. Tamm, *Eur. J. Inorg. Chem.* **2008**, 4270–4279.
- [150] P. G. Jones, F. Aal, C. Hrib, M. Tamm, *CSD Communication* **2019**, DOI: 10.5517/ccdc.csd.cc23f08v.
- [151] M. Röper, *Chem. Unserer Zeit* **2006**, *40*, 126–135.
- [152] D. L. Anderson, *Chemical Composition of the Mantle. In: Theory of the Earth*, Blackwell Scientific, Boston, **1989**.
- [153] V. Koß, *Die Erdkruste. In: Umweltchemie*, Springer, Berlin, Heidelberg, **1997**.
- [154] P. Nuss, M. J. Eckelman, *PLoS ONE* **2014**, *9*, e101298.
- [155] W. Haider, M. D. Calvin-Brown, I.-A. Bischoff, V. Huch, B. Morgenstern, C. Müller, T. Sergeieva, D. M. Andrada, A. Schäfer, *Inorg. Chem.* **2022**, *61*, 1672–1684.
- [156] M. J. Ogier, *Ann. Chim. Phys.* **1880**, *5*, 5–66.
- [157] E. W. Corcoran, L. G. Sneddon, *J. Am. Chem. Soc.* **1984**, *106*, 7793–7800.
- [158] E. W. Corcoran, L. G. Sneddon, *J. Am. Chem. Soc.* **1985**, *107*, 7446–7450.
- [159] R. L. Melen, *Chem. Soc. Rev.* **2016**, *45*, 775–788.
- [160] E. M. Leitao, T. Jurca, I. Manners, *Nat. Chem.* **2013**, *5*, 817–829.
- [161] T. J. Clark, K. Lee, I. Manners, *Chem. Eur. J.* **2006**, *12*, 8634–8648.
- [162] R. Waterman, *Chem. Soc. Rev.* **2013**, *42*, 5629–5641.
- [163] A. E. Nako, S. J. Gates, N. Schädel, A. J. P. White, M. R. Crimmin, *Chem. Commun.* **2014**, *50*, 9536–9538.
- [164] M. Arrowsmith, *Dehydrocouplings and Other Cross-Couplings. In: Early Main Group Metal Catalysis*, Wiley-VCH, Weinheim, **2020**.
- [165] D. Marinelli, F. Fasano, B. Najjari, N. Demitri, D. Bonifazi, *J. Am. Chem. Soc.* **2017**, *139*, 5503–5519.
- [166] O. Ayhan, T. Eckert, F. A. Plamper, H. Helten, *Angew. Chem. Int. Ed.* **2016**, *55*, 13321–13325.
- [167] T. Lorenz, A. Lik, F. A. Plamper, H. Helten, *Angew. Chem. Int. Ed.* **2016**, *55*, 7236–7241.
- [168] A. Ledoux, P. Larini, C. Boisson, V. Monteil, J. Raynaud, E. Lacôte, *Angew. Chem. Int. Ed.* **2015**, *54*, 15744–15749.
- [169] D. A. Resendiz-Lara, N. E. Stubbs, M. I. Arz, N. E. Pridmore, H. A. Sparkes, I. Manners, *Chem. Commun.* **2017**, *53*, 11701–11704.
- [170] M. Grosche, E. Herdtweck, F. Peters, M. Wagner, *Organometallics* **1999**, *18*, 4669–4672.
- [171] R. J. Keaton, J. M. Blacquiere, R. T. Baker, *J. Am. Chem. Soc.* **2007**, *129*, 1844–1845.
- [172] C. W. Hamilton, R. T. Baker, A. Staubitz, I. Manners, *Chem. Soc. Rev.* **2009**, *38*, 279–293.
- [173] A. Staubitz, A. P. M. Robertson, I. Manners, *Chem. Rev.* **2010**, *110*, 4079–4124.
- [174] B. Peng, J. Chen, *Energy Environ. Sci.* **2008**, *1*, 479–483.
- [175] L. J. Sewell, G. C. Lloyd-Jones, A. S. Weller, *J. Am. Chem. Soc.* **2012**, *134*, 3598–3610.
- [176] A. Rossin, M. Peruzzini, *Chem. Rev.* **2016**, *116*, 8848–8872.
- [177] S. Bhunya, T. Malakar, G. Ganguly, A. Paul, *ACS Catal.* **2016**, *6*, 7907–7934.
- [178] T. J. Clark, C. A. Russell, I. Manners, *J. Am. Chem. Soc.* **2006**, *128*, 9582–9583.
- [179] M. M. Hansmann, R. L. Melen, D. S. Wright, *Chem. Sci.* **2011**, *2*, 1554–1559.
- [180] T. E. Stennett, S. Harder, *Chem. Soc. Rev.* **2016**, *45*, 1112–1128.

- [181] D. H. A. Boom, A. R. Jupp, J. C. Slootweg, *Chem. Eur. J.* **2019**, *25*, 9133–9152.
- [182] J. Spielmann, M. Bolte, S. Harder, *Chem. Commun.* **2009**, 6934–6936.
- [183] D. J. Liptrot, M. S. Hill, M. F. Mahon, D. J. MacDougall, *Chem. Eur. J.* **2010**, *16*, 8508–8515.
- [184] P. Bellham, M. S. Hill, G. Kociok-Köhn, D. J. Liptrot, *Chem. Commun.* **2013**, *49*, 1960–1962.
- [185] D. J. Liptrot, M. S. Hill, M. F. Mahon, A. S. S. Wilson, *Angew. Chem. Int. Ed.* **2015**, *54*, 13362–13365.
- [186] A. C. A. Ried, L. J. Taylor, A. M. Geer, H. E. L. Williams, W. Lewis, A. J. Blake, D. L. Kays, *Chem. Eur. J.* **2019**, *25*, 6840–6846.
- [187] M. S. Hill, M. Hodgson, D. J. Liptrot, M. F. Mahon, *Dalton Trans.* **2011**, *40*, 7783–7790.
- [188] P. Bellham, M. D. Anker, M. S. Hill, G. Kociok-Köhn, M. F. Mahon, *Dalton Trans.* **2016**, *45*, 13969–13978.
- [189] M. M. D. Roy, A. A. Omaña, A. S. S. Wilson, M. S. Hill, S. Aldridge, E. Rivard, *Chem. Rev.* **2021**, *121*, 12784–12965.
- [190] Y. Tanabe, M. Murakami, K. Kitaichi, Y. Yoshida, *Tetrahedron Lett.* **1994**, *35*, 8409–8412.
- [191] Y. Tanabe, T. Misaki, M. Kurihara, A. Iida, Y. Nishii, *Chem. Commun.* **2002**, 1628–1629.
- [192] A. Iida, A. Horii, T. Misaki, Y. Tanabe, *Synthesis* **2005**, *2005*, 2677–2682.
- [193] C. A. Roth, *Ind. Eng. Chem. Prod. Res. Dev.* **1972**, *11*, 134–139.
- [194] E. Kroke, Y.-L. Li, C. Konetschny, E. Lecomte, C. Fasel, R. Riedel, *Mater. Sci. Eng., R* **2000**, *26*, 97–199.
- [195] R. Fessenden, J. S. Fessenden, *Chem. Rev.* **1961**, *61*, 361–388.
- [196] R. Murugavel, N. Palanisami, R. J. Butcher, *J. Organomet. Chem.* **2003**, *675*, 65–71.
- [197] N. Palanisami, R. Murugavel, *J. Organomet. Chem.* **2006**, *691*, 3260–3266.
- [198] M. B. Reuter, K. Hageman, R. Waterman, *Chem. Eur. J.* **2021**, *27*, 3251–3261.
- [199] K. Kuciński, G. Hreczycho, *ChemCatChem* **2017**, *9*, 1868–1885.
- [200] V. Verma, A. Koperniku, P. M. Edwards, L. L. Schafer, *Chem. Commun.* **2022**, *58*, 9174–9189.
- [201] H. Q. Liu, J. F. Harrod, *Organometallics* **1992**, *11*, 822–827.
- [202] H. Q. Liu, J. F. Harrod, *Can. J. Chem.* **1992**, *70*, 107–110.
- [203] T. Tsuchimoto, Y. Iketani, M. Sekine, *Chem. Eur. J.* **2012**, *18*, 9500–9504.
- [204] C. D. F. Königs, M. F. Müller, N. Aiguabella, H. F. T. Klare, M. Oestreich, *Chem. Commun.* **2013**, *49*, 1506–1508.
- [205] D. Gasperini, A. K. King, N. T. Coles, M. F. Mahon, R. L. Webster, *ACS Catal.* **2020**, *10*, 6102–6112.
- [206] J. F. Dunne, S. R. Neal, J. Engelkemier, A. Ellern, A. D. Sadow, *J. Am. Chem. Soc.* **2011**, *133*, 16782–16785.
- [207] M. S. Hill, D. J. Liptrot, D. J. MacDougall, M. F. Mahon, T. P. Robinson, *Chem. Sci.* **2013**, *4*, 4212–4222.
- [208] C. Bellini, J.-F. Carpentier, S. Tobisch, Y. Sarazin, *Angew. Chem. Int. Ed.* **2015**, *54*, 7679–7683.
- [209] A. Baishya, T. Peddarao, S. Nembenna, *Dalton Trans.* **2017**, *46*, 5880–5887.
- [210] M. Rauch, R. C. Roberts, G. Parkin, *Inorg. Chim. Acta* **2019**, *494*, 271–279.
- [211] F. Buch, S. Harder, *Organometallics* **2007**, *26*, 5132–5135.
- [212] C. Bellini, V. Dorcet, J.-F. Carpentier, S. Tobisch, Y. Sarazin, *Chem. Eur. J.* **2016**, *22*, 4564–4583.
- [213] C. Bellini, T. Roisnel, J.-F. Carpentier, S. Tobisch, Y. Sarazin, *Chem. Eur. J.* **2016**, *22*, 15733–15743.
- [214] C. Bellini, C. Orione, J.-F. Carpentier, Y. Sarazin, *Angew. Chem. Int. Ed.* **2016**, *55*, 3744–3748.
- [215] N. V. Forosenko, I. V. Basalov, A. V. Cherkasov, G. K. Fukin, E. S. Shubina, A. A. Trifonov, *Dalton Trans.* **2018**, *47*, 12570–12581.
- [216] N. Li, B.-T. Guan, *Eur. J. Inorg. Chem.* **2019**, *2019*, 2231–2235.

- [217] D. T. Hurd, *J. Am. Chem. Soc.* **1948**, *70*, 2053–2055.
- [218] H. C. Brown, B. C. S. Rao, *J. Am. Chem. Soc.* **1956**, *78*, 2582–2588.
- [219] H. C. Brown, B. C. S. Rao, *J. Am. Chem. Soc.* **1956**, *78*, 5694–5695.
- [220] H. Brown, B. C. Rao, *J. Org. Chem.* **1957**, *22*, 1136–1137.
- [221] H. C. Brown, B. C. S. Rao, *J. Am. Chem. Soc.* **1959**, *81*, 6423–6428.
- [222] H. C. Brown, B. C. S. Rao, *J. Am. Chem. Soc.* **1959**, *81*, 6428–6434.
- [223] H. C. Brown, *Tetrahedron* **1961**, *12*, 117–138.
- [224] A. D. Sadow, *Alkali and Alkaline Earth Element-Catalyzed Hydroboration Reactions. In: Early Main Group Metal Catalysis*, Wiley-VCH, Weinheim, **2020**.
- [225] D. Männig, H. Nöth, *Angew. Chem. Int. Ed.* **1985**, *24*, 878–879.
- [226] K. Burgess, M. J. Ohlmeyer, *Chem. Rev.* **1991**, *91*, 1179–1191.
- [227] N. Miyaura, A. Suzuki, *Chem. Rev.* **1995**, *95*, 2457–2483.
- [228] X. He, J. F. Hartwig, *J. Am. Chem. Soc.* **1996**, *118*, 1696–1702.
- [229] T. Ohmura, Y. Yamamoto, N. Miyaura, *J. Am. Chem. Soc.* **2000**, *122*, 4990–4991.
- [230] J. Y. Wu, B. Moreau, T. Ritter, *J. Am. Chem. Soc.* **2009**, *131*, 12915–12917.
- [231] R. J. Ely, J. P. Morken, *J. Am. Chem. Soc.* **2010**, *132*, 2534–2535.
- [232] K. Semba, T. Fujihara, J. Terao, Y. Tsuji, *Chem. Eur. J.* **2012**, *18*, 4179–4184.
- [233] A. A. Oluyadi, S. Ma, C. N. Muhoro, *Organometallics* **2013**, *32*, 70–78.
- [234] L. Zhang, D. Peng, X. Leng, Z. Huang, *Angew. Chem. Int. Ed.* **2013**, *52*, 3676–3680.
- [235] J. V. Obligacion, P. J. Chirik, *Org. Lett.* **2013**, *15*, 2680–2683.
- [236] N. Eedugurala, Z. Wang, U. Chaudhary, N. Nelson, K. Kandel, T. Kobayashi, I. I. Slowing, M. Pruski, A. D. Sadow, *ACS Catal.* **2015**, *5*, 7399–7414.
- [237] G. Zhang, H. Zeng, J. Wu, Z. Yin, S. Zheng, J. C. Fettinger, *Angew. Chem. Int. Ed.* **2016**, *55*, 14369–14372.
- [238] S. Bagherzadeh, N. P. Mankad, *Chem. Commun.* **2016**, *52*, 3844–3846.
- [239] Z. Huang, D. Liu, J. Camacho-Bunquin, G. Zhang, D. Yang, J. M. López-Encarnación, Y. Xu, M. S. Ferrandon, J. Niklas, O. G. Poluektov, J. Jellinek, A. Lei, E. E. Bunel, M. Delferro, *Organometallics* **2017**, *36*, 3921–3930.
- [240] S. R. Tamang, M. Findlater, *J. Org. Chem.* **2017**, *82*, 12857–12862.
- [241] D. Wei, B. Carboni, J.-B. Sortais, C. Darcel, *Adv. Synth. Catal.* **2018**, *360*, 3649–3654.
- [242] C. C. Chong, R. Kinjo, *ACS Catal.* **2015**, *5*, 3238–3259.
- [243] A. R. Bazkiaei, M. Findlater, A. E. V. Gorden, *Org. Biomol. Chem.* **2022**, *20*, 3675–3702.
- [244] K. N. Harrison, T. J. Marks, *J. Am. Chem. Soc.* **1992**, *114*, 9220–9221.
- [245] A. S. Dudnik, V. L. Weidner, A. Motta, M. Delferro, T. J. Marks, *Nat. Chem.* **2014**, *6*, 1100–1107.
- [246] S. Chen, D. Yan, M. Xue, Y. Hong, Y. Yao, Q. Shen, *Org. Lett.* **2017**, *19*, 3382–3385.
- [247] V. L. Weidner, C. J. Barger, M. Delferro, T. L. Lohr, T. J. Marks, *ACS Catal.* **2017**, *7*, 1244–1247.
- [248] D. Yan, P. Dai, S. Chen, M. Xue, Y. Yao, Q. Shen, X. Bao, *Org. Biomol. Chem.* **2018**, *16*, 2787–2791.
- [249] S. Patnaik, A. D. Sadow, *Angew. Chem. Int. Ed.* **2019**, *58*, 2505–2509.
- [250] T. J. Hadlington, M. Hermann, G. Frenking, C. Jones, *J. Am. Chem. Soc.* **2014**, *136*, 3028–3031.
- [251] Z. Yang, M. Zhong, X. Ma, S. De, C. Anusha, P. Parameswaran, H. W. Roesky, *Angew. Chem. Int. Ed.* **2015**, *54*, 10225–10229.
- [252] Z. Yang, M. Zhong, X. Ma, K. Nijesh, S. De, P. Parameswaran, H. W. Roesky, *J. Am. Chem. Soc.* **2016**, *138*, 2548–2551.
- [253] A. Bismuto, M. J. Cowley, S. P. Thomas, *ACS Catal.* **2018**, *8*, 2001–2005.
- [254] W. Liu, Y. Ding, D. Jin, Q. Shen, B. Yan, X. Ma, Z. Yang, *Green Chem.* **2019**, *21*, 3812–3815.
- [255] Q. Shen, X. Ma, W. Li, W. Liu, Y. Ding, Z. Yang, H. W. Roesky, *Chem. Eur. J.* **2019**, *25*, 11918–11923.
- [256] A. Harinath, J. Bhattacharjee, T. K. Panda, *Adv. Synth. Catal.* **2019**, *361*, 850–857.

- [257] A. Harinath, I. Banerjee, J. Bhattacharjee, T. K. Panda, *New J. Chem.* **2019**, *43*, 10531–10536.
- [258] N. Sarkar, S. Bera, S. Nembenna, *J. Org. Chem.* **2020**, *85*, 4999–5009.
- [259] K. Hobson, C. J. Carmalt, C. Bakewell, *Inorg. Chem.* **2021**, *60*, 10958–10969.
- [260] K. Nakaya, S. Takahashi, A. Ishii, K. Boonpalit, P. Surawatanawong, N. Nakata, *Dalton Trans.* **2021**, *50*, 14810–14819.
- [261] V. B. Saptal, R. Wang, S. Park, *RSC Adv.* **2020**, *10*, 43539–43565.
- [262] W. K. Shin, H. Kim, A. K. Jaladi, D. K. An, *Tetrahedron* **2018**, *74*, 6310–6315.
- [263] Y. Wu, C. Shan, J. Ying, J. Su, J. Zhu, L. L. Liu, Y. Zhao, *Green Chem.* **2017**, *19*, 4169–4175.
- [264] H. Kim, J. H. Lee, H. Hwang, D. K. An, *New J. Chem.* **2020**, *44*, 11330–11335.
- [265] P. Ghosh, A. J. von Wangelin, *Org. Chem. Front.* **2020**, *7*, 960–966.
- [266] D. Bedi, A. Brar, M. Findlater, *Green Chem.* **2020**, *22*, 1125–1128.
- [267] C. Yu, C. Guo, L. Jiang, M. Gong, Y. Luo, *Organometallics* **2021**, *40*, 1201–1206.
- [268] R. Rochat, M. J. Lopez, H. Tsurugi, K. Mashima, *ChemCatChem* **2016**, *8*, 10–20.
- [269] K. Revunova, G. I. Nikonov, *Dalton Trans.* **2015**, *44*, 840–866.
- [270] M. S. Hill, D. J. Liptrot, C. Weetman, *Chem. Soc. Rev.* **2016**, *45*, 972–988.
- [271] K. Kuciński, G. Hreczycho, *Green Chem.* **2020**, *22*, 5210–5224.
- [272] D. Hayrapetyan, A. Y. Khalimon, *Chem. Asian J.* **2020**, *15*, 2575–2587.
- [273] S. Rej, A. Das, T. K. Panda, *Adv. Synth. Catal.* **2021**, *363*, 4818–4840.
- [274] K. Watanabe, J. H. Pang, R. Takita, S. Chiba, *Chem. Sci.* **2022**, *13*, 27–38.
- [275] M. Magre, M. Szewczyk, M. Rueping, *Curr. Opin. Green Sustainable Chem.* **2021**, *32*, 100526.
- [276] M. Arrowsmith, T. J. Hadlington, M. S. Hill, G. Kociok-Köhn, *Chem. Commun.* **2012**, *48*, 4567–4569.
- [277] J. Li, M. Luo, X. Sheng, H. Hua, W. Yao, S. A. Pullarkat, L. Xu, M. Ma, *Org. Chem. Front.* **2018**, *5*, 3538–3547.
- [278] D. Mukherjee, S. Shirase, T. P. Spaniol, K. Mashima, J. Okuda, *Chem. Commun.* **2016**, *52*, 13155–13158.
- [279] M. K. Barman, A. Baishya, S. Nembenna, *Dalton Trans.* **2017**, *46*, 4152–4156.
- [280] S. Yadav, R. Dixit, M. K. Bisai, K. Vanka, S. S. Sen, *Organometallics* **2018**, *37*, 4576–4584.
- [281] Y. Li, H. Pan, Y. Lu, Y. Luo, Y. Dang, Y. Wang, S. Xia, Y. Li, Y. Xia, *Dalton Trans.* **2022**, *51*, 3616–3624.
- [282] K. Manna, P. Ji, F. X. Greene, W. Lin, *J. Am. Chem. Soc.* **2016**, *138*, 7488–7491.
- [283] M. D. Anker, M. Arrowsmith, P. Bellham, M. S. Hill, G. Kociok-Köhn, D. J. Liptrot, M. F. Mahon, C. Weetman, *Chem. Sci.* **2014**, *5*, 2826–2830.
- [284] M. D. Anker, M. S. Hill, J. P. Lowe, M. F. Mahon, *Angew. Chem. Int. Ed.* **2015**, *54*, 10009–10011.
- [285] M. D. Anker, C. E. Kefalidis, Y. Yang, J. Fang, M. S. Hill, M. F. Mahon, L. Maron, *J. Am. Chem. Soc.* **2017**, *139*, 10036–10054.
- [286] M. Rauch, G. Parkin, *J. Am. Chem. Soc.* **2017**, *139*, 18162–18165.
- [287] X. Cao, W. Wang, K. Lu, W. Yao, F. Xue, M. Ma, *Dalton Trans.* **2020**, *49*, 2776–2780.
- [288] X. Cao, J. Li, A. Zhu, F. Su, W. Yao, F. Xue, M. Ma, *Org. Chem. Front.* **2020**, *7*, 3625–3632.
- [289] V. Vasilenko, C. K. Blasius, H. Wadepohl, L. H. Gade, *Chem. Commun.* **2020**, *56*, 1203–1206.
- [290] M. Ma, J. Li, X. Shen, Z. Yu, W. Yao, S. A. Pullarkat, *RSC Adv.* **2017**, *7*, 45401–45407.
- [291] D. Mukherjee, A. Ellern, A. D. Sadow, *Chem. Sci.* **2014**, *5*, 959–964.
- [292] N. L. Lampland, M. Hovey, D. Mukherjee, A. D. Sadow, *ACS Catal.* **2015**, *5*, 4219–4226.
- [293] A. Falconnet, M. Magre, B. Maity, L. Cavallo, M. Rueping, *Angew. Chem. Int. Ed.* **2019**, *58*, 17567–17571.
- [294] M. Szewczyk, M. Magre, V. Zubar, M. Rueping, *ACS Catal.* **2019**, *9*, 11634–11639.

- [295] M. Magre, M. Szewczyk, M. Rueping, *Org. Lett.* **2020**, *22*, 3209–3214.
- [296] Y. K. Jang, M. Magre, M. Rueping, *Org. Lett.* **2019**, *21*, 8349–8352.
- [297] M. Magre, E. Paffenholz, B. Maity, L. Cavallo, M. Rueping, *J. Am. Chem. Soc.* **2020**, *142*, 14286–14294.
- [298] M. Arrowsmith, M. S. Hill, T. Hadlington, G. Kociok-Köhn, C. Weetman, *Organometallics* **2011**, *30*, 5556–5559.
- [299] J. Intemann, M. Lutz, S. Harder, *Organometallics* **2014**, *33*, 5722–5729.
- [300] C. Weetman, M. S. Hill, M. F. Mahon, *Polyhedron* **2016**, *103*, 115–120.
- [301] M. Arrowsmith, M. S. Hill, G. Kociok-Köhn, *Chem. Eur. J.* **2013**, *19*, 2776–2783.
- [302] C. Weetman, M. S. Hill, M. F. Mahon, *Chem. Commun.* **2015**, *51*, 14477–14480.
- [303] C. Weetman, M. D. Anker, M. Arrowsmith, M. S. Hill, G. Kociok-Köhn, D. J. Liptrot, M. F. Mahon, *Chem. Sci.* **2016**, *7*, 628–641.
- [304] C. Weetman, M. S. Hill, M. F. Mahon, *Chem. Eur. J.* **2016**, *22*, 7158–7162.
- [305] Y. Yang, M. D. Anker, J. Fang, M. F. Mahon, L. Maron, C. Weetman, M. S. Hill, *Chem. Sci.* **2017**, *8*, 3529–3537.
- [306] M. Rauch, S. Ruccolo, G. Parkin, *J. Am. Chem. Soc.* **2017**, *139*, 13264–13267.
- [307] M. Magre, B. Maity, A. Falconnet, L. Cavallo, M. Rueping, *Angew. Chem. Int. Ed.* **2019**, *58*, 7025–7029.
- [308] C. Bakewell, *Dalton Trans.* **2020**, *49*, 11354–11360.
- [309] J.-J. Brunet, D. Neibecker, F. Niedercorn, *J. Mol. Catal.* **1989**, *49*, 235–259.
- [310] T. E. Müller, M. Beller, *Chem. Rev.* **1998**, *98*, 675–704.
- [311] K. C. Hultzsich, *Org. Biomol. Chem.* **2005**, *3*, 1819–1824.
- [312] T. E. Müller, K. C. Hultzsich, M. Yus, F. Foubelo, M. Tada, *Chem. Rev.* **2008**, *108*, 3795–3892.
- [313] P. Horrillo-Martínez, K. C. Hultzsich, *Tetrahedron Lett.* **2009**, *50*, 2054–2056.
- [314] X. Zhang, T. J. Emge, K. C. Hultzsich, *Organometallics* **2010**, *29*, 5871–5877.
- [315] S. Streiff, F. Jérôme, *Chem. Soc. Rev.* **2021**, *50*, 1512–1521.
- [316] C. Michon, M.-A. Abadie, F. Medina, F. Agbossou-Niedercorn, *J. Organomet. Chem.* **2017**, *847*, 13–27.
- [317] K. C. Hultzsich, *Adv. Synth. Catal.* **2005**, *347*, 367–391.
- [318] I. Aillaud, J. Collin, J. Hannedouche, E. Schulz, *Dalton Trans.* **2007**, 5105–5118.
- [319] F. Alonso, I. P. Beletskaya, M. Yus, *Chem. Rev.* **2004**, *104*, 3079–3160.
- [320] I. Bytschkov, S. Doye, *Eur. J. Org. Chem.* **2003**, *2003*, 935–946.
- [321] J. F. Hartwig, *Pure Appl. Chem.* **2004**, *76*, 507–516.
- [322] S. Hong, T. J. Marks, *Acc. Chem. Res.* **2004**, *37*, 673–686.
- [323] M. Nobis, B. Drießen-Hölscher, *Angew. Chem. Int. Ed.* **2001**, *40*, 3983–3985.
- [324] F. Pohlki, S. Doye, *Chem. Soc. Rev.* **2003**, *32*, 104–114.
- [325] P. W. Roesky, *Angew. Chem. Int. Ed.* **2009**, *48*, 4892–4894.
- [326] P. W. Roesky, T. E. Müller, *Angew. Chem. Int. Ed.* **2003**, *42*, 2708–2710.
- [327] J. Seayad, A. Tillack, C. G. Hartung, M. Beller, *Adv. Synth. Catal.* **2002**, *344*, 795–813.
- [328] R. A. Widenhoefer, X. Han, *Eur. J. Org. Chem.* **2006**, 4555–4563.
- [329] D. A. Patton, M. E. Cremeens, *Rev. J. Chem.* **2014**, *4*, 1–20.
- [330] M. R. Gagne, S. P. Nolan, T. J. Marks, *Organometallics* **1990**, *9*, 1716–1718.
- [331] M. R. Gagne, C. L. Stern, T. J. Marks, *J. Am. Chem. Soc.* **1992**, *114*, 275–294.
- [332] S. M. Coman, V. I. Parvulescu, *Org. Process Res. Dev.* **2015**, *19*, 1327–1355.
- [333] J. Hannedouche, E. Schulz, *Chem. Eur. J.* **2013**, *19*, 4972–4985.
- [334] J.-S. Ryu, G. Y. Li, T. J. Marks, *J. Am. Chem. Soc.* **2003**, *125*, 12584–12605.
- [335] F. Lauterwasser, P. G. Hayes, S. Bräse, W. E. Piers, L. L. Schafer, *Organometallics* **2004**, *23*, 2234–2237.
- [336] Y. Chapurina, R. Guillot, D. Lyubov, A. Trifonov, J. Hannedouche, E. Schulz, *Dalton Trans.* **2013**, *42*, 507–520.
- [337] T. Spallek, R. Anwander, *Dalton Trans.* **2016**, *45*, 16393–16403.
- [338] M. R. Bürgstein, H. Berberich, P. W. Roesky, *Organometallics* **1998**, *17*, 1452–1454.
- [339] A. Zulys, M. Dochnahl, D. Hollmann, K. Löhnwitz, J.-S. Herrmann, P. W. Roesky, S. Blechert, *Angew. Chem. Int. Ed.* **2005**, *44*, 7794–7798.

- [340] H. Kim, Y. K. Kim, J. H. Shim, M. Kim, M. Han, T. Livinghouse, P. H. Lee, *Adv. Synth. Catal.* **2006**, *348*, 2609–2618.
- [341] M. R. Gagne, L. Brard, V. P. Conticello, M. A. Giardello, C. L. Stern, T. J. Marks, *Organometallics* **1992**, *11*, 2003–2005.
- [342] S. Kaufmann, P. W. Roesky, *Eur. J. Inorg. Chem.* **2021**, *2021*, 2899–2905.
- [343] V. Rodriguez-Ruiz, R. Carlino, S. Bezzenine-Lafollée, R. Gil, D. Prim, E. Schulz, J. Hannedouche, *Dalton Trans.* **2015**, *44*, 12029–12059.
- [344] B. Schlummer, J. F. Hartwig, *Org. Lett.* **2002**, *4*, 1471–1474.
- [345] A. Ates, C. Quinet, *Eur. J. Org. Chem.* **2003**, 1623–1626.
- [346] C. Quinet, P. Jourdain, C. Hermans, A. Ates, I. Lucas, I. E. Markó, *Tetrahedron* **2008**, *64*, 1077–1087.
- [347] G. Rousseau, R. Lebeuf, K. Schenk, F. Castet, F. Robert, Y. Landais, *Chem. Eur. J.* **2014**, *20*, 14771–14782.
- [348] T. Ogata, A. Ujihara, S. Tsuchida, T. Shimizu, A. Kaneshige, K. Tomioka, *Tetrahedron Lett.* **2007**, *48*, 6648–6650.
- [349] J. Deschamp, C. Olier, E. Schulz, R. Guillot, J. Hannedouche, J. Collin, *Adv. Synth. Catal.* **2010**, *352*, 2171–2176.
- [350] Z. Chen, L. Wu, H. Fang, T. Zhang, Z. Mao, Y. Zou, X. Zhang, M. Yan, *Adv. Synth. Catal.* **2017**, *359*, 3894–3899.
- [351] X. Peng, A. Kaga, H. Hirao, S. Chiba, *Org. Chem. Front.* **2016**, *3*, 609–613.
- [352] A. Kaga, X. Peng, H. Hirao, S. Chiba, *Chem. Eur. J.* **2015**, *21*, 19112–19118.
- [353] X. Peng, B. M. K. Tong, H. Hirao, S. Chiba, *Angew. Chem. Int. Ed.* **2014**, *53*, 1959–1962.
- [354] J. Deschamp, J. Collin, J. Hannedouche, E. Schulz, *Eur. J. Org. Chem.* **2011**, *2011*, 3329–3338.
- [355] P. Horrillo-Martínez, K. C. Hultsch, F. Hampel, *Chem. Commun.* **2006**, 2221–2223.
- [356] S. Datta, P. W. Roesky, S. Blechert, *Organometallics* **2007**, *26*, 4392–4394.
- [357] S. Datta, M. T. Gamer, P. W. Roesky, *Organometallics* **2008**, *27*, 1207–1213.
- [358] J. Jenter, R. Köppe, P. W. Roesky, *Organometallics* **2011**, *30*, 1404–1413.
- [359] A. G. M. Barrett, M. R. Crimmin, M. S. Hill, P. B. Hitchcock, G. Kociok-Köhn, P. A. Procopiou, *Inorg. Chem.* **2008**, *47*, 7366–7376.
- [360] A. G. M. Barrett, M. R. Crimmin, M. S. Hill, P. A. Procopiou, *Proc. R. Soc. A* **2010**, *466*, 927–963.
- [361] M. Arrowsmith, M. S. Hill, G. Kociok-Köhn, *Organometallics* **2009**, *28*, 1730–1738.
- [362] B. Liu, T. Roisnel, J.-F. Carpentier, Y. Sarazin, *Chem. Eur. J.* **2013**, *19*, 2784–2802.
- [363] B. Liu, T. Roisnel, J.-F. Carpentier, Y. Sarazin, *Chem. Eur. J.* **2013**, *19*, 13445–13462.
- [364] N. Romero, S.-C. Roşca, Y. Sarazin, J.-F. Carpentier, L. Vendier, S. Mallet-Ladeira, C. Dinoi, M. Etienne, *Chem. Eur. J.* **2015**, *21*, 4115–4125.
- [365] M. Arrowsmith, M. S. Hill, G. Kociok-Köhn, *Organometallics* **2011**, *30*, 1291–1294.
- [366] F. Buch, S. Harder, *Z. Naturforsch. B* **2008**, *63*, 169–177.
- [367] J. S. Wixey, B. D. Ward, *Dalton Trans.* **2011**, *40*, 7693–7696.
- [368] J. S. Wixey, B. D. Ward, *Chem. Commun.* **2011**, *47*, 5449–5451.
- [369] T. D. Nixon, B. D. Ward, *Chem. Commun.* **2012**, *48*, 11790–11792.
- [370] C. Qi, F. Hasenmaile, V. Gandon, D. Lebœuf, *ACS Catal.* **2018**, *8*, 1734–1739.
- [371] A. Mukherjee, S. Nembenna, T. K. Sen, S. P. Sarish, P. Kr. Ghorai, H. Ott, D. Stalke, S. K. Mandal, H. W. Roesky, *Angew. Chem. Int. Ed.* **2011**, *50*, 3968–3972.
- [372] P. C. Stegner, C. A. Fischer, D. T. Nguyen, A. Rösch, J. Penafiel, J. Langer, M. Wiesinger, S. Harder, *Eur. J. Inorg. Chem.* **2020**, *2020*, 3387–3394.
- [373] M. R. Crimmin, M. Arrowsmith, A. G. M. Barrett, I. J. Casely, M. S. Hill, P. A. Procopiou, *J. Am. Chem. Soc.* **2009**, *131*, 9670–9685.
- [374] M. Arrowsmith, M. R. Crimmin, A. G. M. Barrett, M. S. Hill, G. Kociok-Köhn, P. A. Procopiou, *Organometallics* **2011**, *30*, 1493–1506.
- [375] M. Arrowsmith, M. S. Hill, G. Kociok-Köhn, *Organometallics* **2014**, *33*, 206–216.
- [376] X. Zhang, T. J. Emge, K. C. Hultsch, *Angew. Chem. Int. Ed.* **2012**, *51*, 394–398.
- [377] X. Zhang, S. Tobisch, K. C. Hultsch, *Chem. Eur. J.* **2015**, *21*, 7841–7857.

- [378] J. F. Dunne, D. B. Fulton, A. Ellern, A. D. Sadow, *J. Am. Chem. Soc.* **2010**, *132*, 17680–17683.
- [379] S. R. Neal, A. Ellern, A. D. Sadow, *J. Organomet. Chem.* **2011**, *696*, 228–234.
- [380] B. Freitag, C. A. Fischer, J. Penafiel, G. Ballmann, H. Elsen, C. Färber, D. F. Piesik, S. Harder, *Dalton Trans.* **2017**, *46*, 11192–11200.
- [381] P. C. Stegner, J. Eyselein, G. M. Ballmann, J. Langer, J. Schmidt, S. Harder, *Dalton Trans.* **2021**, *50*, 3178–3185.
- [382] B. Schmid, S. Frieß, A. Herrera, A. Linden, F. W. Heinemann, H. Locke, S. Harder, R. Dorta, *Dalton Trans.* **2016**, *45*, 12028–12040.
- [383] J. E. Baldwin, *J. Chem. Soc., Chem. Commun.* **1976**, 734–736.
- [384] R. M. Beesley, C. K. Ingold, J. F. Thorpe, *J. Chem. Soc., Trans.* **1915**, *107*, 1080–1106.
- [385] S. Tobisch, *Chem. Eur. J.* **2011**, *17*, 14974–14986.
- [386] M. Arrowsmith, M. R. Crimmin, M. S. Hill, S. L. Lomas, M. S. Heng, P. B. Hitchcock, G. Kociok-Köhn, *Dalton Trans.* **2014**, *43*, 14249–14256.
- [387] G. Himbert, W. Schwickerath, *Liebigs Ann. Chem.* **1984**, *1984*, 85–97.
- [388] G. Himbert, W. Schwickerath, G. Maas, *Liebigs Ann. Chem.* **1985**, *1985*, 1389–1397.
- [389] R. J. Schwamm, B. M. Day, N. E. Mansfield, W. Knowelden, P. B. Hitchcock, M. P. Coles, *Dalton Trans.* **2014**, *43*, 14302–14314.
- [390] A. D. Sadow, T. D. Tilley, *J. Am. Chem. Soc.* **2003**, *125*, 7971–7977.
- [391] U. Rosenthal, P. Arndt, W. Baumann, V. V. Burlakov, A. Spannenberg, *J. Organomet. Chem.* **2003**, *670*, 84–96.
- [392] U. Rosenthal, V. V. Burlakov, M. A. Bach, T. Beweries, *Chem. Soc. Rev.* **2007**, *36*, 719–728.
- [393] R. Kubiak, I. Prochnow, S. Doye, *Angew. Chem. Int. Ed.* **2009**, *48*, 1153–1156.
- [394] B.-T. Guan, Z. Hou, *J. Am. Chem. Soc.* **2011**, *133*, 18086–18089.
- [395] J. Oyamada, Z. Hou, *Angew. Chem. Int. Ed.* **2012**, *51*, 12828–12832.
- [396] B.-T. Guan, B. Wang, M. Nishiura, Z. Hou, *Angew. Chem. Int. Ed.* **2013**, *52*, 4418–4421.
- [397] W. Yi, J. Zhang, M. Li, Z. Chen, X. Zhou, *Inorg. Chem.* **2011**, *50*, 11813–11824.
- [398] Y. Wu, S. Wang, L. Zhang, G. Yang, X. Zhu, Z. Zhou, H. Zhu, S. Wu, *Eur. J. Org. Chem.* **2010**, *2010*, 326–332.
- [399] Z. Du, W. Li, X. Zhu, F. Xu, Q. Shen, *J. Org. Chem.* **2008**, *73*, 8966–8972.
- [400] S. Zhou, S. Wang, G. Yang, Q. Li, L. Zhang, Z. Yao, Z. Zhou, H. Song, *Organometallics* **2007**, *26*, 3755–3761.
- [401] W.-X. Zhang, M. Nishiura, Z. Hou, *J. Am. Chem. Soc.* **2005**, *127*, 16788–16789.
- [402] A. Samzadeh-Kermani, *J. Heterocycl. Chem.* **2020**, *57*, 248–256.
- [403] G. F. Schmidt, G. Süss-Fink, *J. Organomet. Chem.* **1988**, *356*, 207–211.
- [404] F. M. Sroor, C. G. Hrib, L. Hilfert, S. Busse, F. T. Edelman, *New J. Chem.* **2015**, *39*, 7595–7601.
- [405] Y. Zhao, X. Ma, B. Yan, C. Ni, X. He, Y. Peng, Z. Yang, *J. Organomet. Chem.* **2021**, *946–947*, 121879.
- [406] C. Ni, X. Ma, Z. Yang, H. W. Roesky, *Eur. J. Inorg. Chem.* **2022**, *2022*, e202100929.
- [407] R. J. Schwamm, M. P. Coles, *Organometallics* **2013**, *32*, 5277–5280.
- [408] H. Pellissier, *Org. Biomol. Chem.* **2017**, *15*, 4750–4782.
- [409] H. Helten, B. Dutta, J. R. Vance, M. E. Sloan, M. F. Haddow, S. Sproules, D. Collison, G. R. Whittell, G. C. Lloyd-Jones, I. Manners, *Angew. Chem. Int. Ed.* **2013**, *52*, 437–440.

6. Supporting Information

6.1 Magnesocenophane-Catalyzed Amine Borane Dehydrocoupling

Chemistry–A European Journal

Supporting Information

Magnesocenophane-Catalyzed Amine Borane Dehydrocoupling

Lisa Wirtz, Wasim Haider, Volker Huch, Michael Zimmer, and André Schäfer^{*[a]}

SUPPORTING INFORMATION

Experimental Procedures	S3	—	S4
Reaction Monitoring	S5	—	S10
NMR spectra	S11	—	S17
MS spectra	S18		
XRD data	S19	—	S20
Computational Details	S21	—	S34
References	S35		

SUPPORTING INFORMATION

Experimental Procedures

All manipulations were carried out under an argon inert gas atmosphere (argon 5.0), using either Schlenk line techniques or a glovebox. $\text{Me}_2\text{NH}\cdot\text{BH}_3$ was purchased from ABCR and used as received. $\text{Me}_2\text{NH}_2\text{Cl}$ was purchased from Alfa Aesar and used as received. 2,2-dicyclopentadienylpropane,¹ magnesocene and magnesocenophanes, **1b-d**,² diisopropylamine borane, **2b**,³ and methylamine borane, **2c**,⁴ linear diborazane, **3b**,⁵ and N-deuterated derivative of dimethylamine borane, **2aND**⁶ were synthesized according to literature known procedures.

NMR spectra were recorded on Bruker Avance III 300 and Bruker Avance III 400 spectrometers. ^1H and ^{13}C NMR spectra were referenced using the solvent signals.⁷ ^{11}B NMR spectra were referenced using an external standard ($\delta^{11}\text{B}(\text{BF}_3\cdot\text{OEt}_2) = 0$). Mass spectrometry was performed on a Bruker Solarix FT-ICR MS 7 Tesla spectrometer. Single crystal X-ray diffraction analysis was carried out at low temperatures on a Bruker AXS X8 Apex CCD diffractometer and on a Bruker AXS D8 Venture diffractometer operating with graphite monochromated Mo K α radiation. Structure solution and refinement were performed using SHELX.⁸

Synthesis of C[1]magnesocenophane 1a:

This compound had been described before,⁹ and was synthesized by a modified procedure:

To a solution of 24.0 g (139 mmol) 2,2-dicyclopentadienylpropane in hexane was added 199 mL of a solution of *n*-butyl-sec-butylmagnesium (139 mmol, 0.7 M in hexane) at 273 K. The mixture was allowed to warm to room temperature and subsequently stirred over night at 333 K. After filtration, the precipitate was washed with small portions of cold hexane and dried *in vacuo*.

Yield: 16.9 g / 56%.

$\delta^1\text{H}$ (400.13 MHz, $\text{C}_6\text{D}_6/\text{dme}$) = 2.35 (s, 6 H, CH_3), 6.02 (t, $^3J_{\text{HH}} = 2.5$ Hz, 4 H, Cp-H), 6.08 (t, $^3J_{\text{HH}} = 2.5$ Hz, 4 H, Cp-H);

$\delta^1\text{H}$ (400.13 MHz, $\text{C}_6\text{D}_6/\text{thf}$) = 1.39 (THF), 2.27 (s, 6 H, CH_3), 3.51 (THF), 6.07 (t, $^3J_{\text{HH}} = 2$ Hz, 4 H, Cp-H), 6.15 (t, $^3J_{\text{HH}} = 2$ Hz, 4 H, Cp-H);

$\delta^1\text{H}$ (400.13 MHz, thf-D8) = 1.71 (s, 6 H, CH_3), 5.60 (t, $^3J_{\text{HH}} = 2$ Hz, 4 H, Cp-H), 5.76 (t, $^3J_{\text{HH}} = 2$ Hz, 4 H, Cp-H);

$\delta^{13}\text{C}\{^1\text{H}\}$ (100.62 MHz, $\text{C}_6\text{D}_6/\text{dme}$) = 27.6 (CH_3), 38.5 ($\text{C}-\text{CH}_3$), 96.0 (Cp), 107.1 (Cp);

$\delta^{13}\text{C}\{^1\text{H}\}$ (100.62 MHz, $\text{C}_6\text{D}_6/\text{thf}$) = 25.7 (THF), 29.1 (CH_3), 37.8 ($\text{C}-\text{CH}_3$), 68.1 (THF), 95.7 (Cp), 108.1 (Cp), 141.3 (Cp);

$\delta^{13}\text{C}\{^1\text{H}\}$ (100.62 MHz, thf-D8) = 29.2 (CH_3), 37.8 ($\text{C}-\text{CH}_3$), 95.6 (Cp), 108.2 (Cp), 141.3 (Cp).

Synthesis of 2aBD:

Note: $\text{Me}_2\text{NH}\cdot\text{BD}_3$, **2aBD**, cannot be synthesized by treatment of $\text{Me}_2\text{NH}_2\text{Cl}$ with NaBD_4 .⁶

Dimethylammoniumchlorid was N-deuterated by repeatedly stirring it in D_2O . Full N-deuteration was confirmed by ^1H NMR spectroscopy. 1.50 g (18.0 mmol) of N-deuterated dimethylammoniumchlorid and 0.75 g (17.9 mmol) of sodium borodeuteride were added to a Schlenk flask and cooled to 273 K. 75 mL of precooled thf were added and the solution was stirred for 1 h at 273 K and subsequently allowed to warm to room temperature and stirred over night. The mixture was filtered, all volatiles were removed *in vacuo* and the crude was stirred in water for 5 h to allow for N-D/H exchange. The product was subsequently extracted with dichloromethane and dried *in vacuo*.

Yield: 0.44 g / 40%.

$\delta^1\text{H}$ (400.13 MHz, C_6D_6) = 1.78 (d, 6 H, CH_3), 2.82 (br s, 1 H, NH);

$\delta^{13}\text{C}\{^1\text{H}\}$ (100.62 MHz, C_6D_6) = 43.8 (CH_3);

$\delta^{11}\text{B}$ (128.38 MHz, C_6D_6) = -13.4 (m, BD_3).

Synthesis of 2aNDBD:

Dimethylammoniumchlorid was N-deuterated by repeatedly stirring it in D_2O . Full N-deuteration was confirmed by ^1H NMR spectroscopy. 2.0 g (23.9 mmol) of N-deuterated dimethylammoniumchlorid and 1.0 g (23.9 mmol) of sodium borodeuteride were added to a Schlenk flask and cooled to 273 K. 100 mL of precooled thf were added and the solution was stirred for 1 h at 273 K and subsequently allowed to warm to room temperature and stirred over night. All volatiles were removed *in vacuo* and the product was sublimed from the crude *in vacuo* at 313 K.

Yield: 0.22 g / 15%.

$\delta^1\text{H}$ (400.13 MHz, C_6D_6) = 1.70 (s, 6 H, CH_3);

$\delta^{13}\text{C}\{^1\text{H}\}$ (100.62 MHz, C_6D_6) = 43.7 (CH_3);

$\delta^{11}\text{B}$ (128.38 MHz, C_6D_6) = -13.2 (m, BD_3).

SUPPORTING INFORMATION

Synthesis of magnesium complex 5:

The thf derivative of this compound had been described before.¹⁰ Complex **5** was synthesized by following the corresponding procedure, but using toluene/dme 10:1 as solvent.

$\delta^1\text{H}$ (400.13 MHz, C_6D_6) = 1.35 - 2.01 (m, 20 H, BH), 2.17 (s, 24 H, N-CH_3), 2.21 (s, 24 H, N-CH_3), 3.15 (s, 6 H, O-CH_3), 3.36 (s, 4 H, O-CH_2);

$\delta^{13}\text{C}\{^1\text{H}\}$ (100.62 MHz, C_6D_6) = 52.0 (CH_3), 59.6 (dme- CH_3), 72.0 (dme- CH_2);

$\delta^{11}\text{B}$ (128.38 MHz, C_6D_6) = -16.6 (t, $^1J_{\text{BH}} = 86$ Hz, BH_2), 2.9 (q, $^1J_{\text{BH}} = 106$ Hz, BH_3);

$\delta^{11}\text{B}$ (128.38 MHz, dme) = -15.4 (q, $^1J_{\text{BH}} = 89$ Hz), 3.7 (t, $^1J_{\text{BH}} = 102$ Hz).

Elemental analysis for $\text{C}_{20}\text{H}_{78}\text{B}_8\text{Mg}_2\text{N}_8\text{O}_2$: calculated: C: 40.17%, H: 13.15%, N: 18.74%; found: C: 40.10%, H: 12.81%, N: 18.59%.

Catalytic dehydrocoupling:

In a typical run, the reaction was performed in a glovebox using a 5 mL volume vial. Magnesocenophane **1a** (5 mol%: 8.0 mg, 0.04 mmol) was added to a solution of the corresponding amine borane (**2a**: 50 mg, 0.85 mmol; **2b**: 95 mg, 0.83 mmol; **2c**: 37 mg, 0.82 mmol) in 1 mL dme and the mixture was stirred at ambient conditions for a given amount of time.

For NMR measurements, a sample of approximately 0.3 mL was added to a NMR tube, diluted with approximately 0.3 mL of C_6D_6 , and analyzed by ^{11}B NMR spectroscopy.

For discontinuous monitoring of the reaction, the reaction was performed at approximately three times the scale, and aliquots were taken at the corresponding points in time and analyzed by ^{11}B NMR spectroscopy.

The following signals were observed for the different species in dme: $\delta^{11}\text{B}$ (128 MHz, dme) = -21.0 (**2b** ($i\text{Pr}_2\text{NH}\cdot\text{BH}_3$), q, $^1J_{\text{BH}} = 98.0$ Hz); -18.0 (**2c** ($\text{MeNH}_2\cdot\text{BH}_3$), q, $^1J_{\text{BH}} = 96.0$ Hz); -13.3 (**2a** ($\text{Me}_2\text{NH}\cdot\text{BH}_3$), q, $^1J_{\text{BH}} = 98.0$ Hz); -5.3 ($([\text{MeNHBH}_2]_3)$, t, $^1J_{\text{BH}} = 106$ Hz); 5.4 (**3a** ($[\text{Me}_2\text{NBH}_2]_2$), t, $^1J_{\text{BH}} = 114$ Hz); 28.8 ($([\text{Me}_2\text{N}]_2\text{BH})$, d, $^1J_{\text{BH}} = 132$ Hz); 35.1 (**4b** ($i\text{Pr}_2\text{N}=\text{BH}_2$), t, $^1J_{\text{BH}} = 127$ Hz); 37.7 (**4a** ($\text{Me}_2\text{N}=\text{BH}$)₂, t, $^1J_{\text{BH}} = 128$ Hz).

SUPPORTING INFORMATION

Reaction Monitoring

For continuous monitoring of the reaction at elevated temperatures by ^{11}B NMR spectroscopy, dme solutions of **2a** and 5 mol% of **1a** were charged into NMR tubes and analyzed by *in-situ* ^{11}B NMR spectroscopy at 323 K and 333 K (spectrometer temperature), with ^{11}B NMR spectra being recorded at regular intervals of 3 min. In all cases, conversions were determined by integration of **2a** vs **3a**. In some cases, a slight deviation from a linear fit for $\ln c/T$ is observed for the first few data points. This might arise from the sample warming up in the preheated spectrometer.

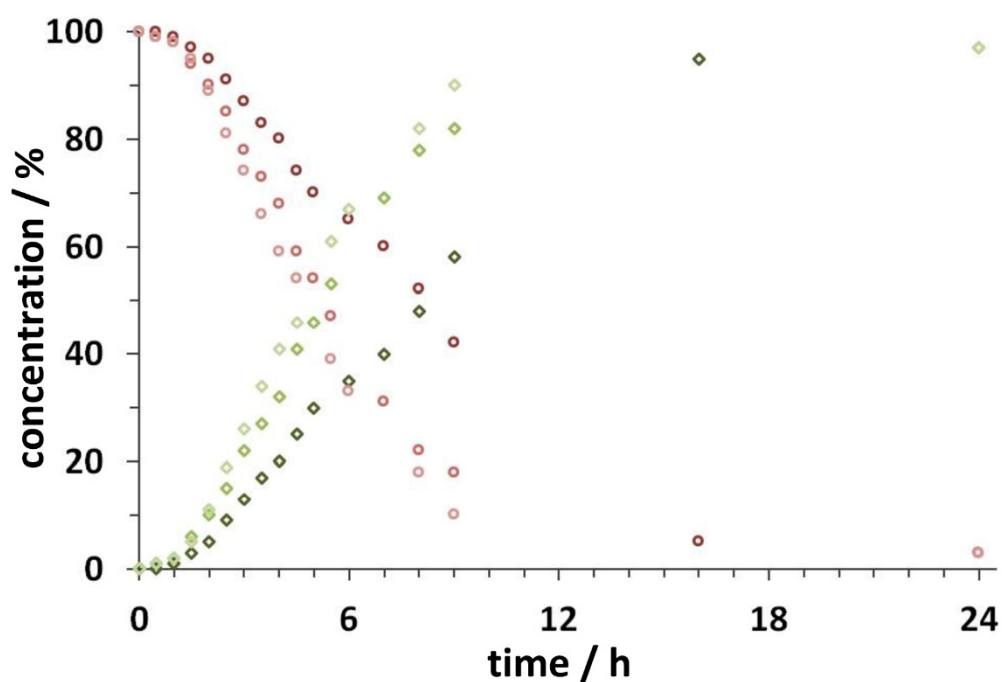


Figure S1. Relative concentration of **2a** (○) ($c_0 = 850$ mM) and **3a** (◇) vs time, for reactions catalyzed by 5 mol% (■), 7.5 mol% (◆) and 10 mol% (◻) of **1a** in dme at r.t., as determined by discontinuous ^{11}B NMR measurements.

SUPPORTING INFORMATION

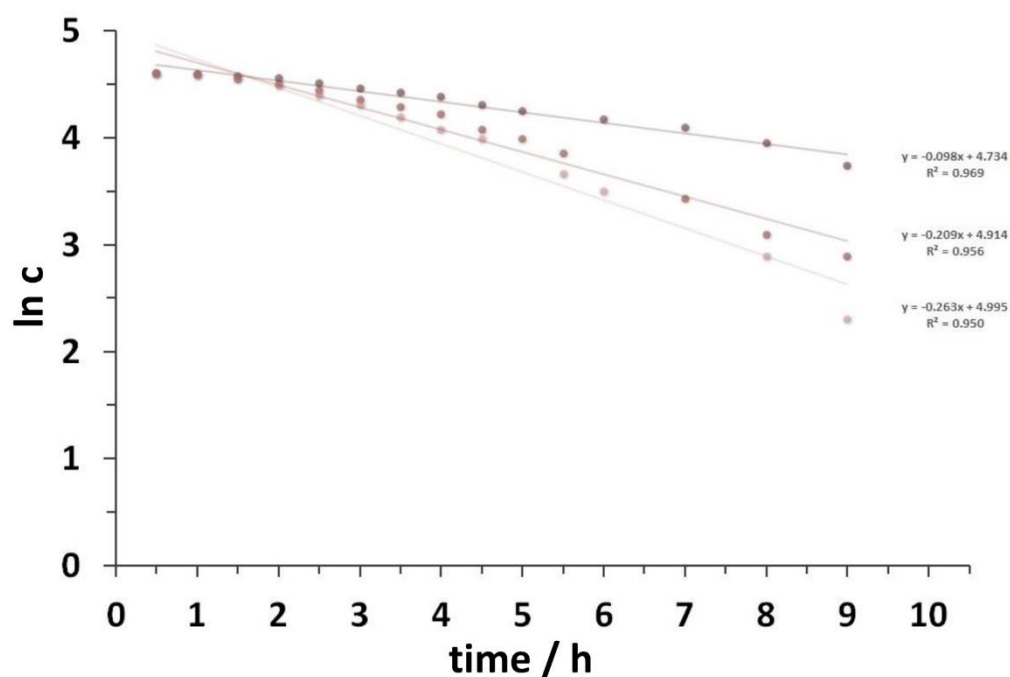


Figure S2. Plots of $\ln[2a]$ (for relative concentrations in %, $c_0 = 850$ mM) vs time, for reactions catalyzed by 5 mol% (■), 7.5 mol% (●) and 10 mol% (▲) of **1a** in dme at r. t., as determined by discontinuous ^{11}B NMR measurements.

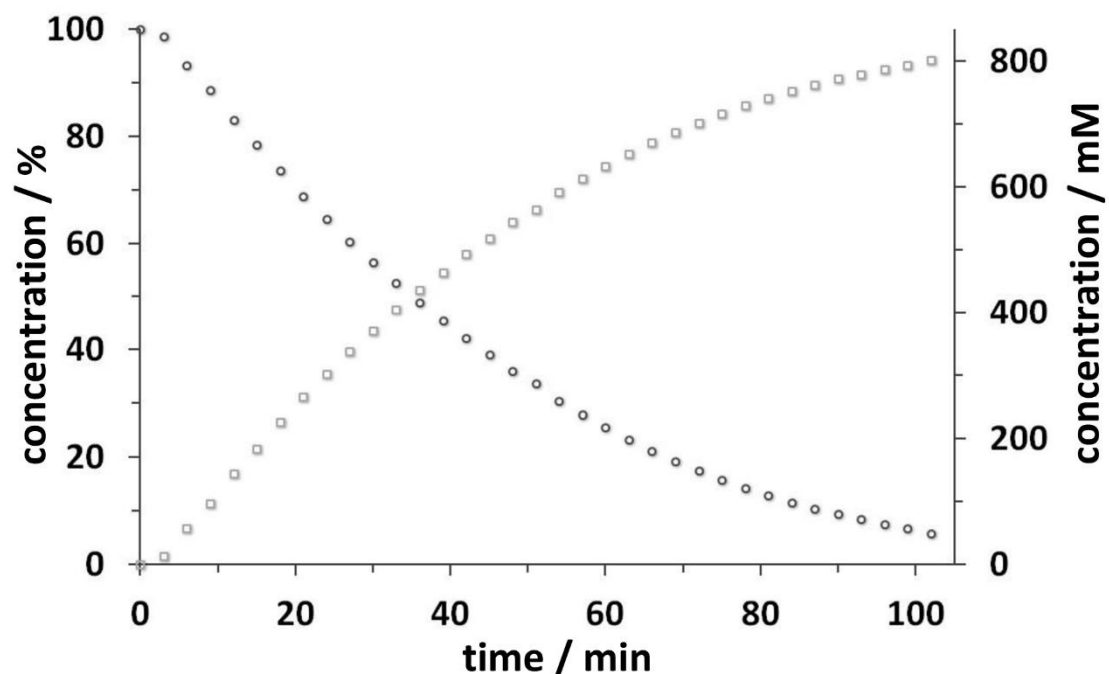


Figure S3. Plot of concentration of **2a** (○) ($c_0 = 850$ mM) and **3a** (□) vs time, for reactions catalyzed by 5 mol% of **1a** in dme at 333 K, as determined by *in-situ* ^{11}B NMR measurements.

SUPPORTING INFORMATION

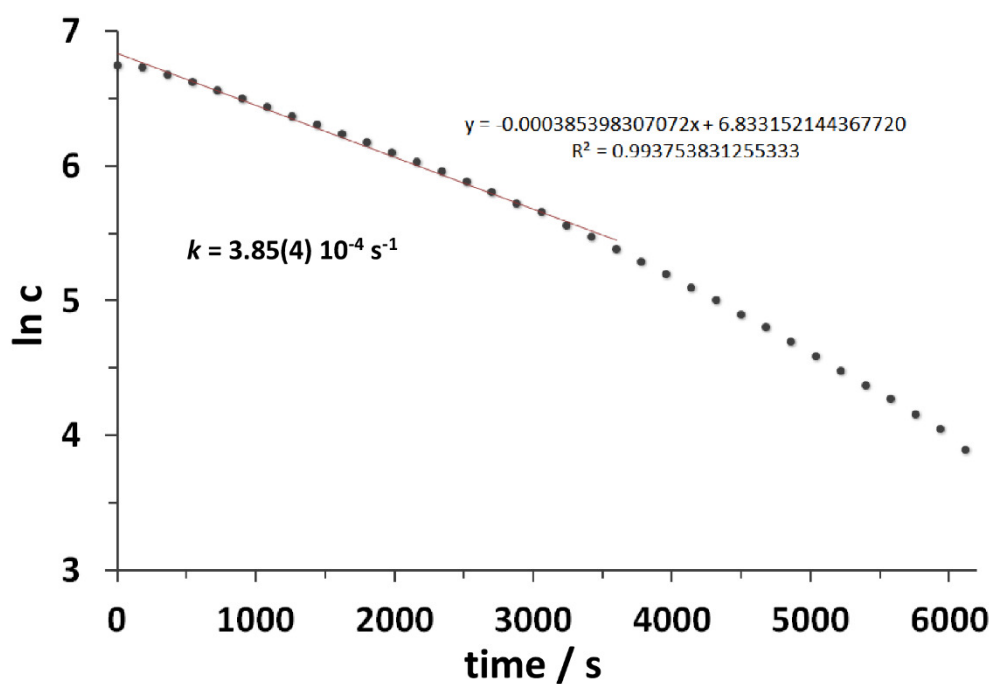


Figure S4. Plot of $\ln[2\mathbf{a}]$ (for concentrations in mmol L^{-1} estimated from the known starting concentrations of $c_0 = 850 \text{ mM}$ for $2\mathbf{a}$) vs time, for reactions catalyzed by 5 mol% of $1\mathbf{a}$ in dme at 333 K, as determined by *in-situ* ^{11}B NMR measurements. Rate constant $k(2\mathbf{a})$ was determined by a linear fitting for 0 - 60 min (error of the rate constant was estimated from R^2).

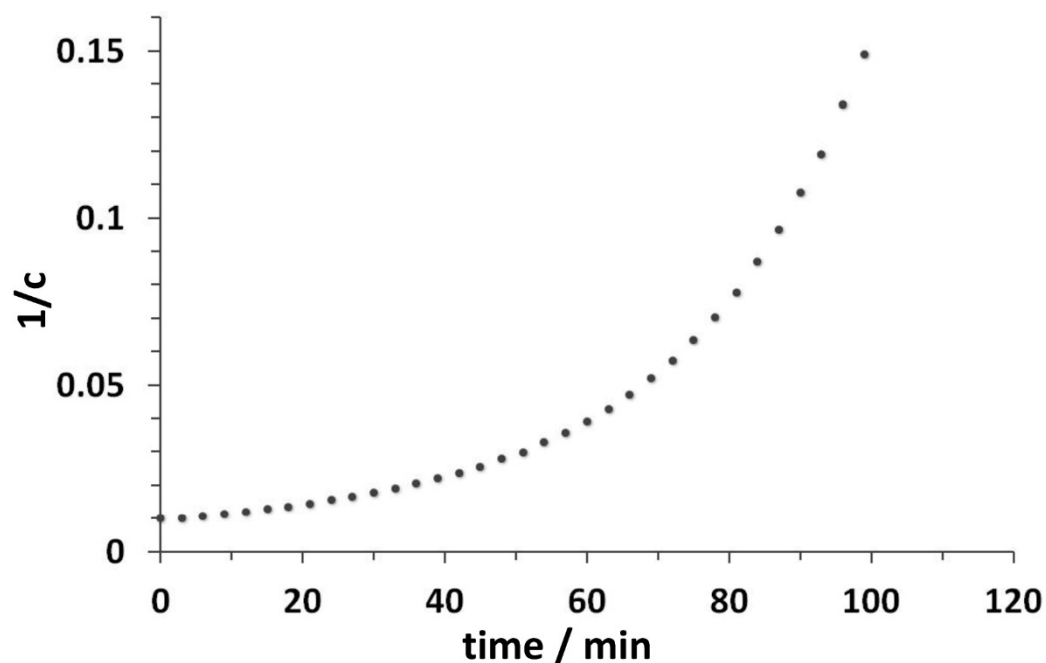


Figure S5. Plot of $1/[2\mathbf{a}]$ (for relative concentrations in %, $c_0 = 850 \text{ mM}$) vs time, for reactions catalyzed by 5 mol% of $1\mathbf{a}$ in dme at 333 K, as determined by *in-situ* ^{11}B NMR measurements.

SUPPORTING INFORMATION

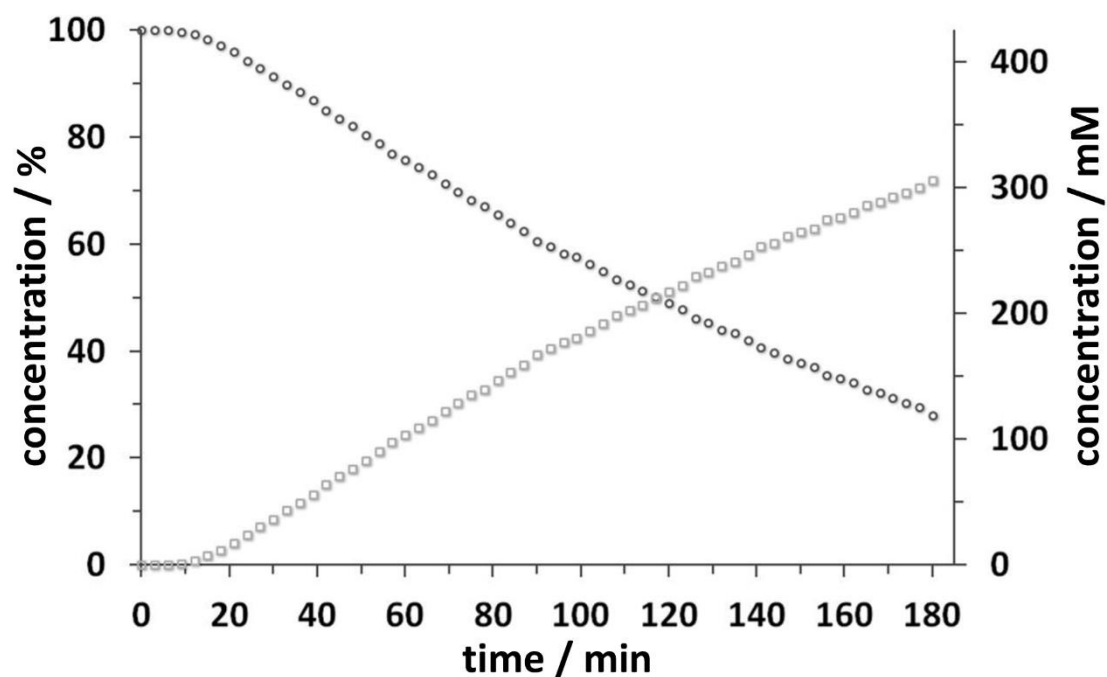


Figure S6. Plot of concentration of **2a** (O) ($c_0 = 425$ mM) and **3a** (□) vs time, for reactions catalyzed by 5 mol% of **1a** in dme at 323 K, as determined by *in-situ* ^{11}B NMR measurements.

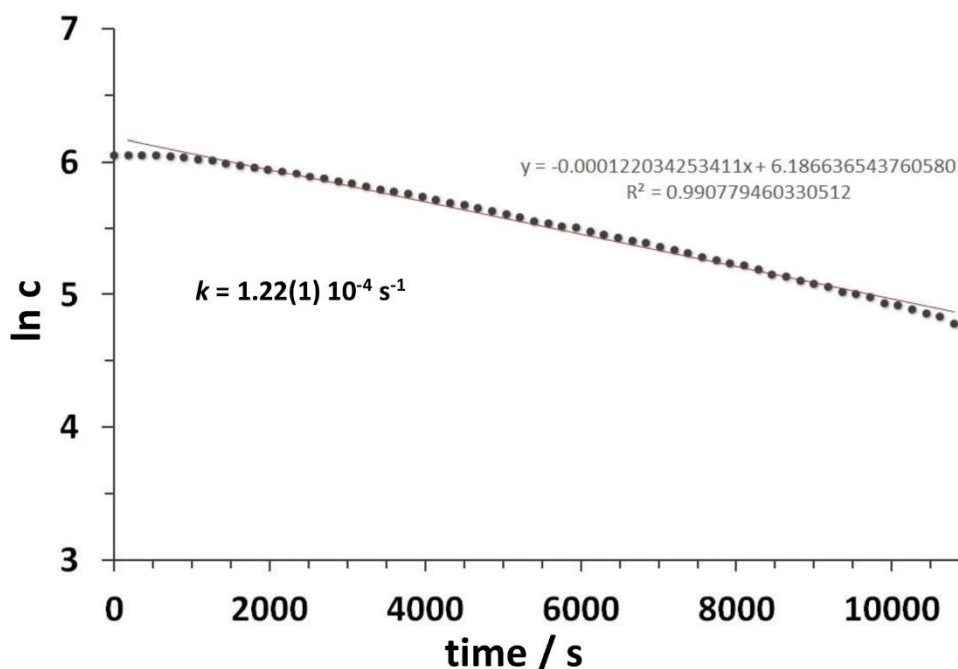


Figure S7. Plot of $\ln[2a]$ (for concentrations in mmol L^{-1} estimated from the known starting concentrations of $c_0 = 425$ mM for **2a**) vs time, for reactions catalyzed by 5 mol% of **1a** in dme at 323 K, as determined by *in-situ* ^{11}B NMR measurements. Rate constant $k(2a)$ was determined by a linear fitting for 3-180 min (error of the rate constant was estimated from R^2).

SUPPORTING INFORMATION

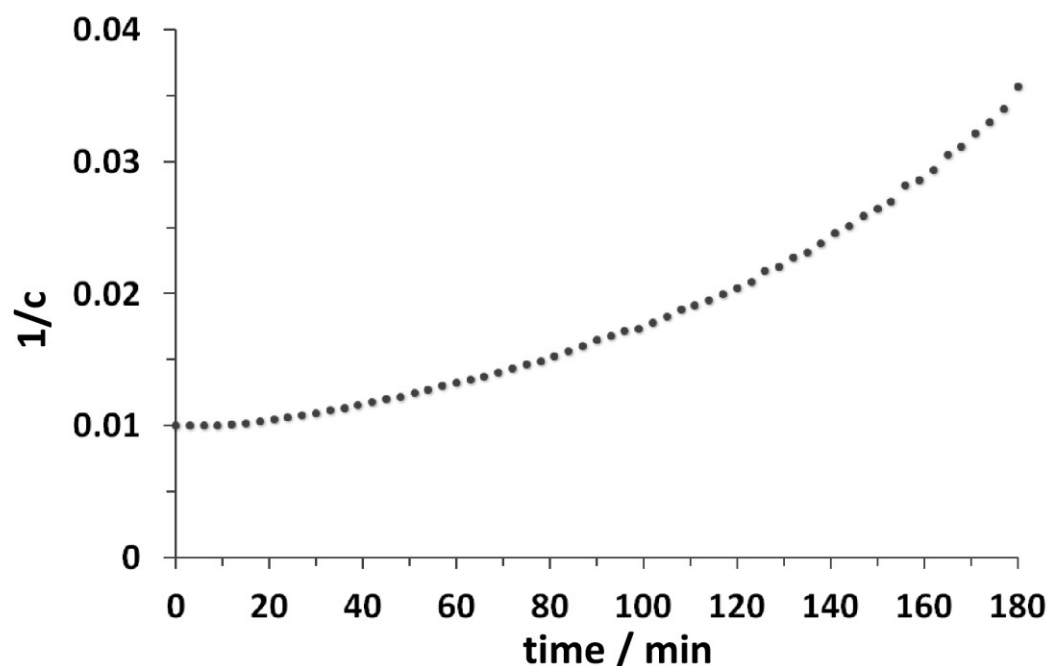


Figure S8. Plot of $1/[2a]$ (for relative concentrations in %, $c_0 = 425$ mM) vs time, for reactions catalyzed by 5 mol% of **1a** in dme at 323 K, as determined by *in-situ* ^{11}B NMR measurements.

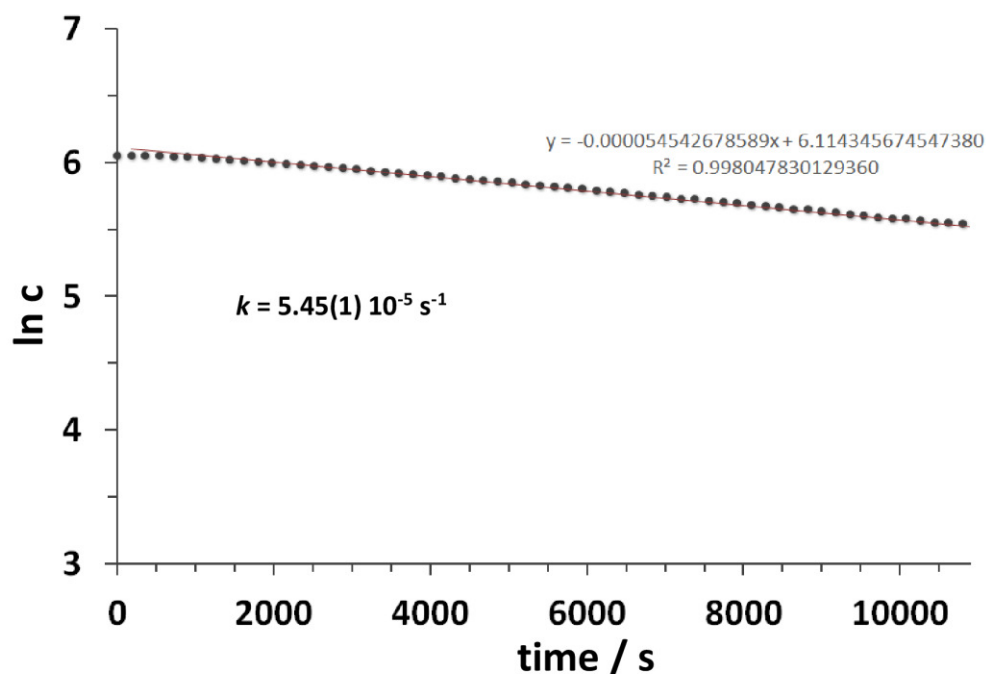


Figure S9. Plot of $\ln[2aND]$ (for concentrations in mmol L^{-1} estimated from the known starting concentrations of $c_0 = 425$ mM for **2aND**) vs time, for reactions catalyzed by 5 mol% of **1a** in dme at 323 K, as determined by *in-situ* ^{11}B NMR measurements. Rate constant $k(2aND)$ was determined by a linear fitting for 3-309 min (error of the rate constant was estimated from R^2).

SUPPORTING INFORMATION

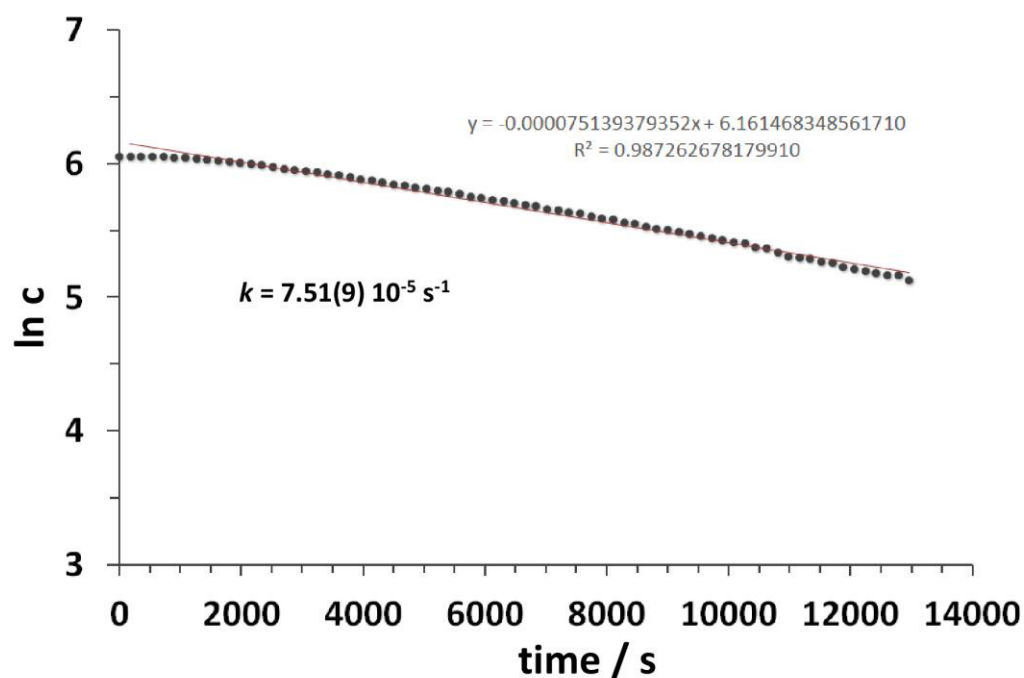


Figure S10. Plot of $\ln[2\mathbf{aBD}]$ (for concentrations in mmol L^{-1} estimated from the known starting concentrations of $c_0 = 425 \text{ mM}$ for **2aBD**) vs time, for reactions catalyzed by 5 mol% of **1a** in dme at 323 K, as determined by *in-situ* ^{11}B NMR measurements. Rate constant $k(2\mathbf{aBD})$ was determined by a linear fitting for 3-216 min (error of the rate constant was estimated from R^2).

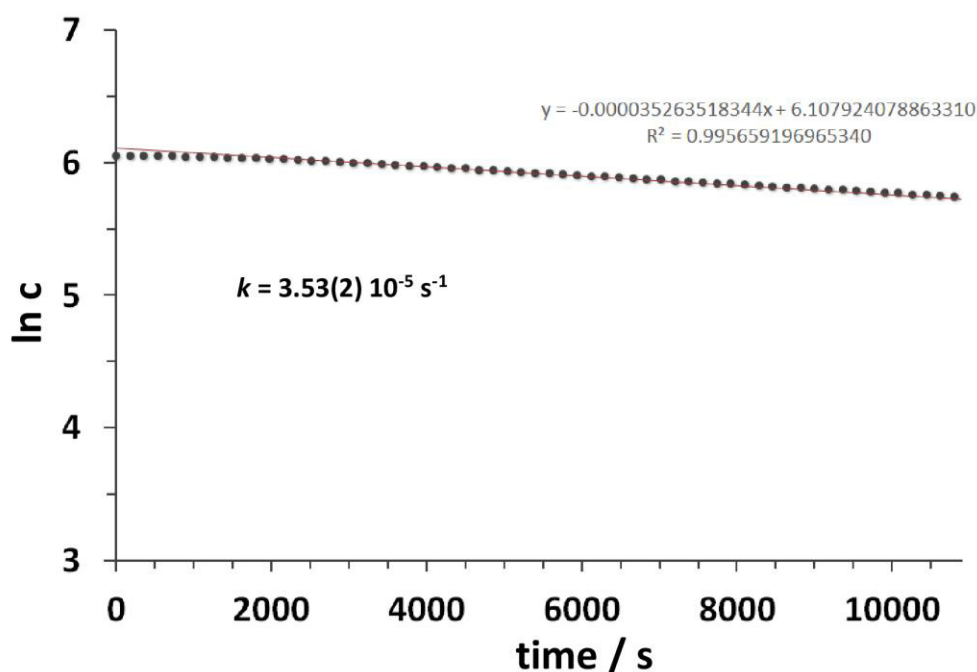


Figure S11. Plot of $\ln[2\mathbf{aNDBD}]$ (for concentrations in mmol L^{-1} estimated from the known starting concentrations of $c_0 = 425 \text{ mM}$ for **2aBD**) vs time, for reactions catalyzed by 5 mol% of **1a** in dme at 323 K, as determined by *in-situ* ^{11}B NMR measurements. Rate constant $k(2\mathbf{aBD})$ was determined by a linear fitting for 3-360 min (error of the rate constant was estimated from R^2).

SUPPORTING INFORMATION

NMR spectra

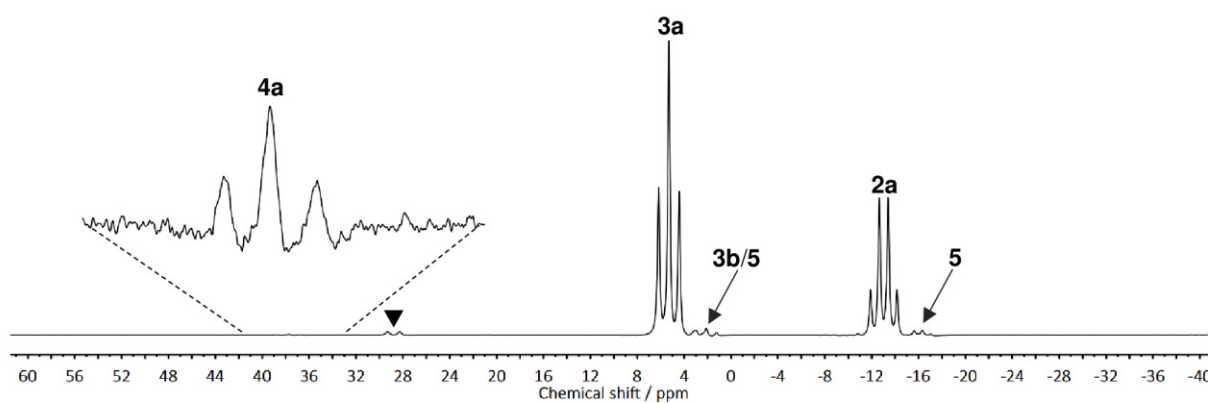


Figure S12. ^{11}B NMR spectrum (128.38 MHz, 293 K, $\text{C}_6\text{D}_6/\text{dme}$) of the reaction mixture of **2a** with 3 mol% of **1a** at r.t. after 24 h (▼ $[\text{Me}_2\text{N}]_2\text{BH}$).

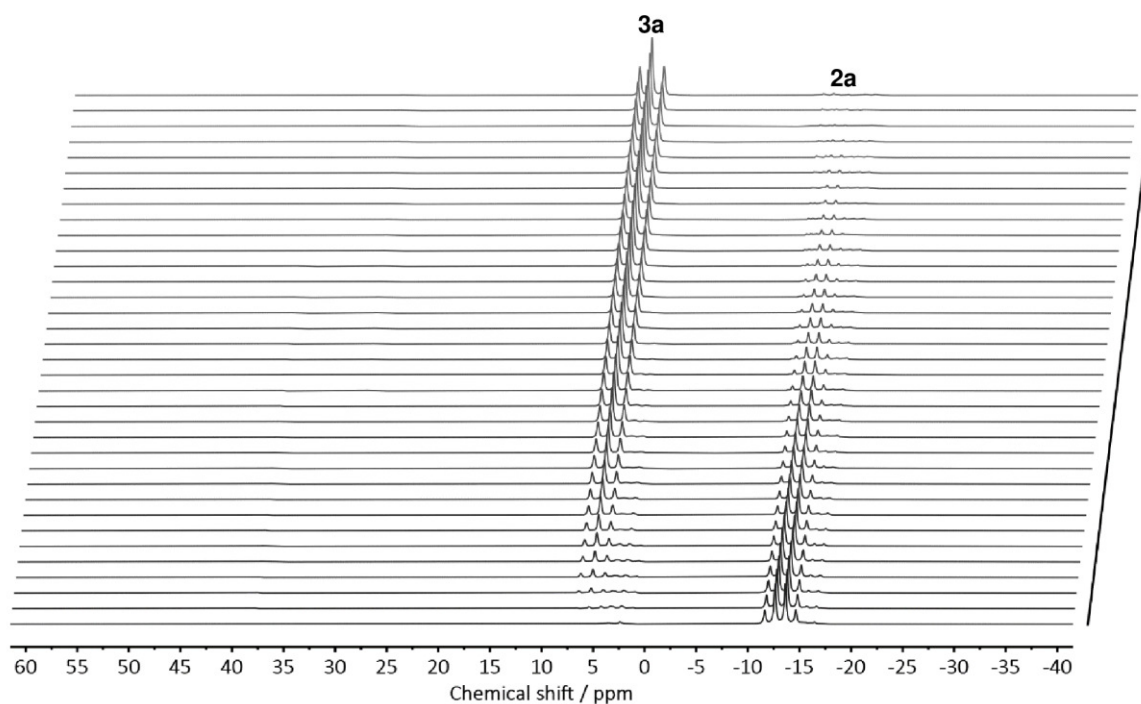


Figure S13. ^{11}B NMR spectra (96.29 MHz, 333 K, dme) of *in-situ* NMR monitoring of the reaction mixture of **2a** with 5 mol% of **1a** at 333 K in interval of 3 min (▼ $[\text{Me}_2\text{N}]_2\text{BH}$).

SUPPORTING INFORMATION

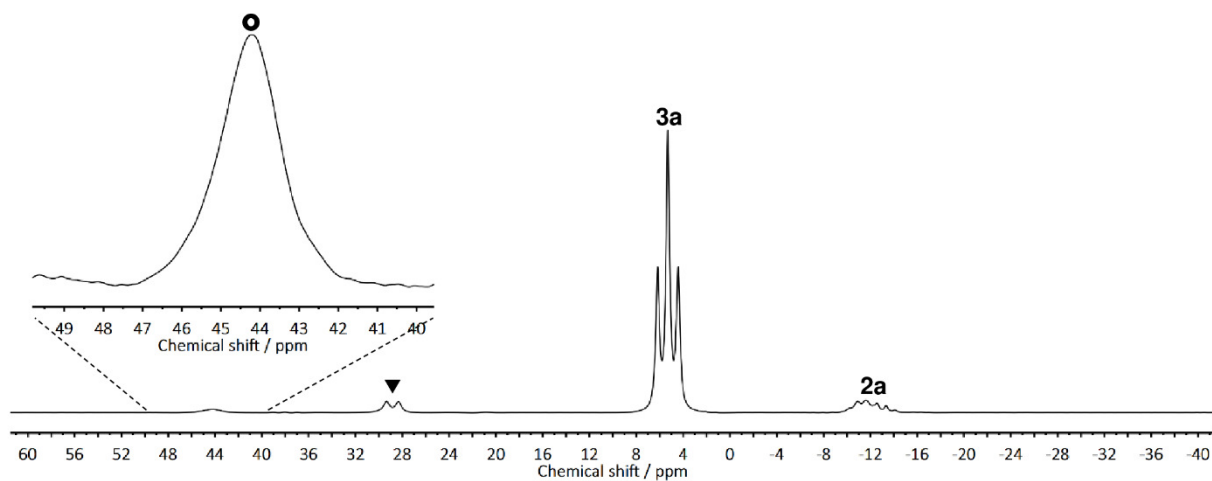


Figure S14. ^{11}B NMR spectrum (128.38 MHz, 293 K, $\text{C}_6\text{D}_6/\text{thf}$) of the reaction mixture of **2a** with 5 mol% of **1a** at r.t. after 24 h in the presence of cyclohexene (● $\text{Me}_2\text{N}=\text{BCy}_2$; ▼ $[\text{Me}_2\text{N}]_2\text{BH}$).

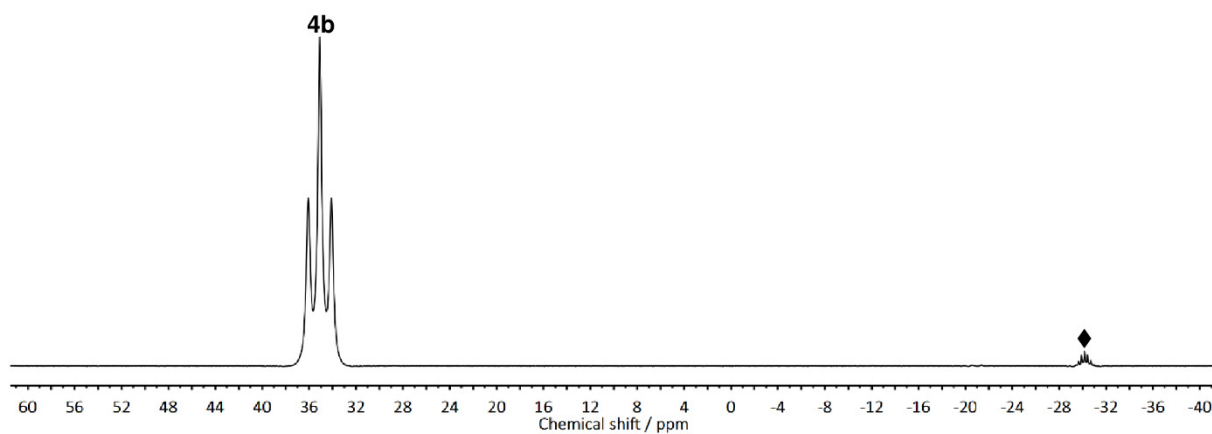


Figure S15. ^{11}B NMR spectrum (128.38 MHz, 293 K, $\text{C}_6\text{D}_6/\text{dme}$) of the reaction mixture of **2b** with 5 mol% of **1a** at r.t. after 24 h (◆ BH_4^-).

SUPPORTING INFORMATION

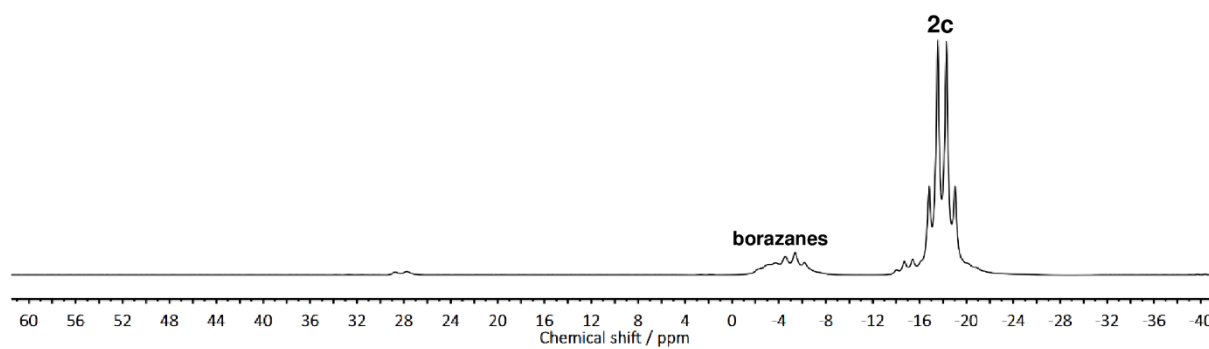


Figure S16. ^{11}B NMR spectrum (128.38 MHz, 293 K, $\text{C}_6\text{D}_6/\text{dme}$) of the reaction mixture of **2c** with 5 mol% of **1a** at r.t. after 24 h.

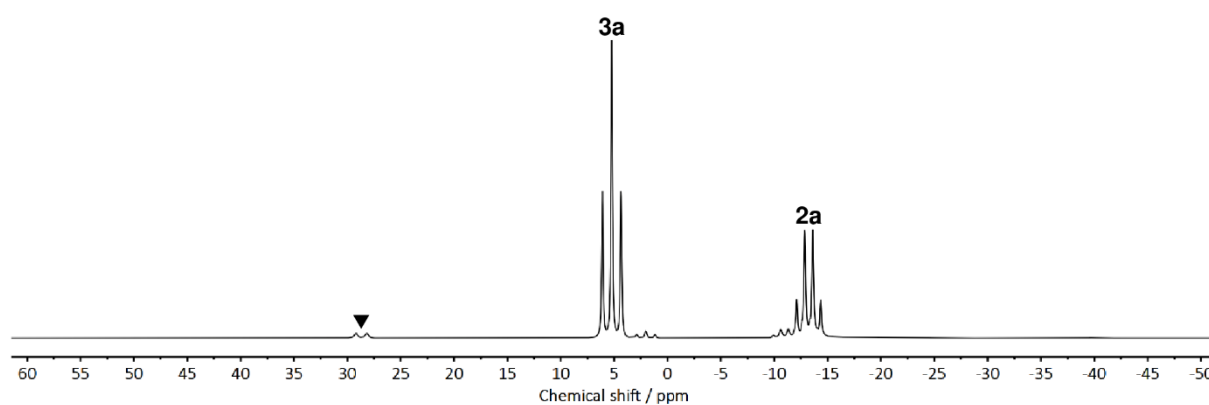


Figure S17. ^{11}B NMR spectrum (128.38 MHz, 294 K, $\text{C}_6\text{D}_6/\text{dme}$) of the reaction mixture of **3b** with 5 mol% of **1a** at r.t. after 16 h (▼ $[\text{Me}_2\text{N}]_2\text{BH}$).

SUPPORTING INFORMATION

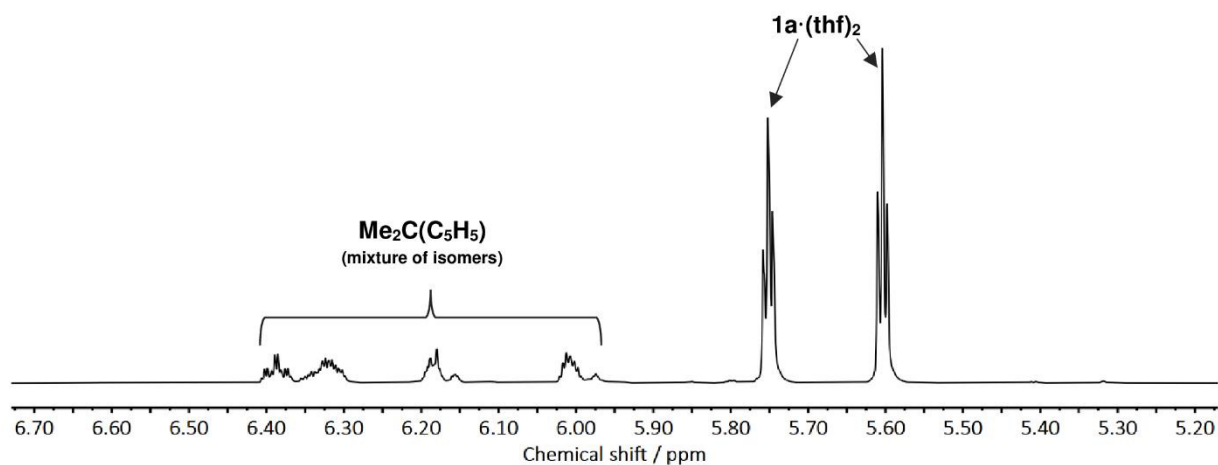


Figure S18. Part of the ^1H NMR spectrum (400.13 MHz, 293 K, thf-D8) of the reaction mixture of 1 eq **1a** with 1 eq **2a** at r.t. after 48 h.

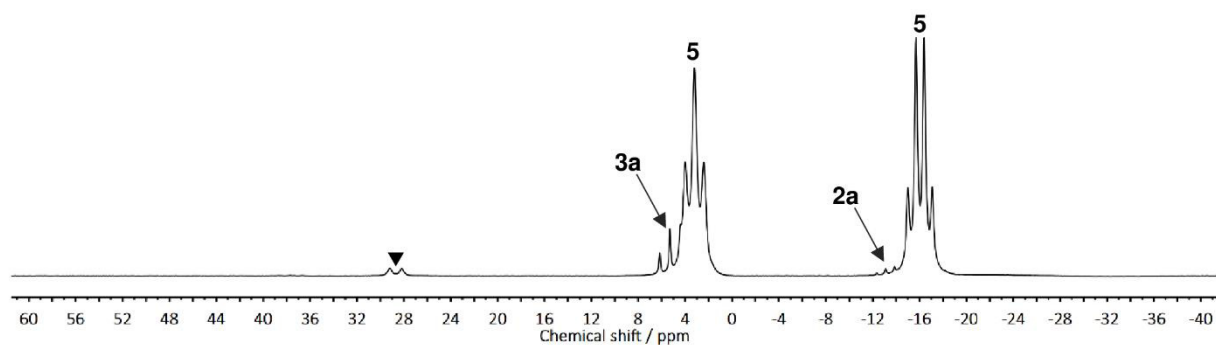


Figure S19. ^{11}B NMR spectrum (128.38 MHz, 293 K, thf-D8) of the reaction mixture of 1 eq **1a** with 1 eq **2a** at r.t. after 48 h (\blacktriangledown [Me₂N]₂BH).

SUPPORTING INFORMATION

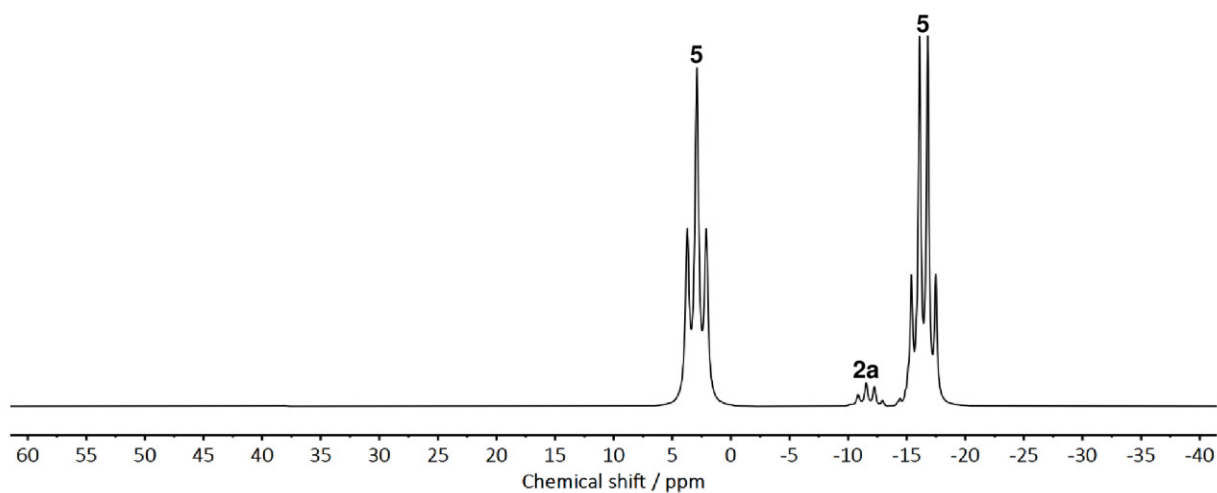


Figure S20. ^{11}B NMR spectrum (128.38 MHz, 293 K, C_6D_6) of magnesium complex **5**.

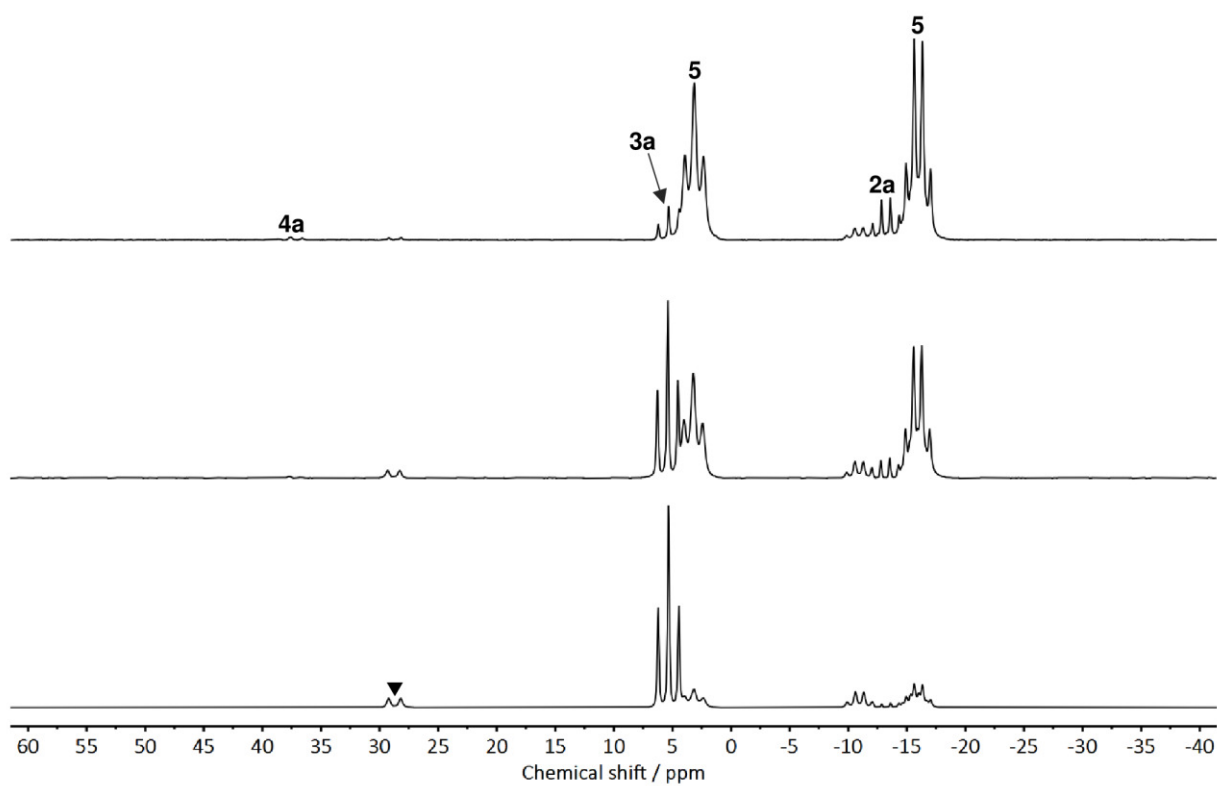


Figure S21. ^{11}B NMR spectra (128.38 MHz, 293 K, dme) of a mixture of magnesium complex **5** and 2,2-dicyclopentadienylpropane at r.t. after 1 h (top), 24 h (center) and 96 h (bottom) (▼ $[\text{Me}_2\text{N}]_2\text{BH}$).

SUPPORTING INFORMATION

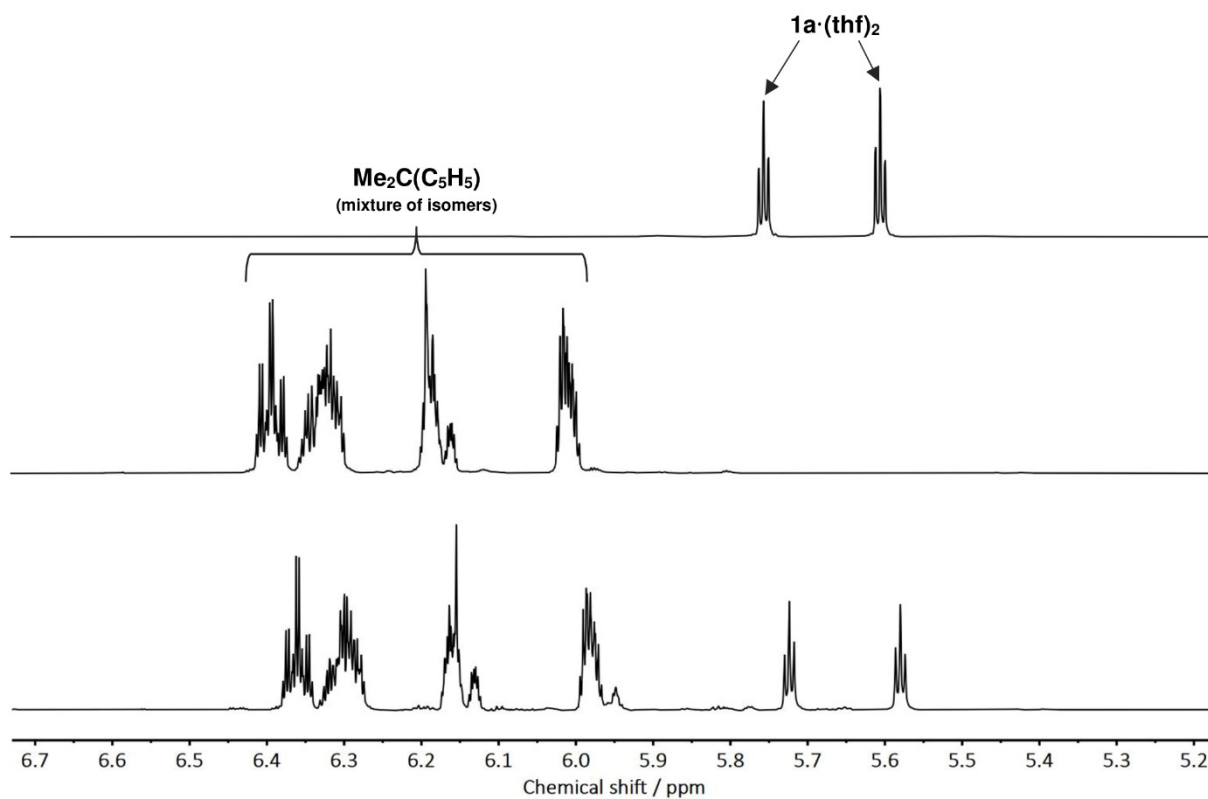


Figure S22. Part of the ^1H NMR spectra (400.13 MHz, 294 K, thf-D_8) of 2,2-dicyclopentadienylpropane (top), C[1]magnesocenophane-bis(thf), $1\text{a}\cdot(\text{thf})_2$, (center), and of a mixture of magnesium complex 5 and 2,2-dicyclopentadienylpropane (bottom) at r.t. after 2 h.

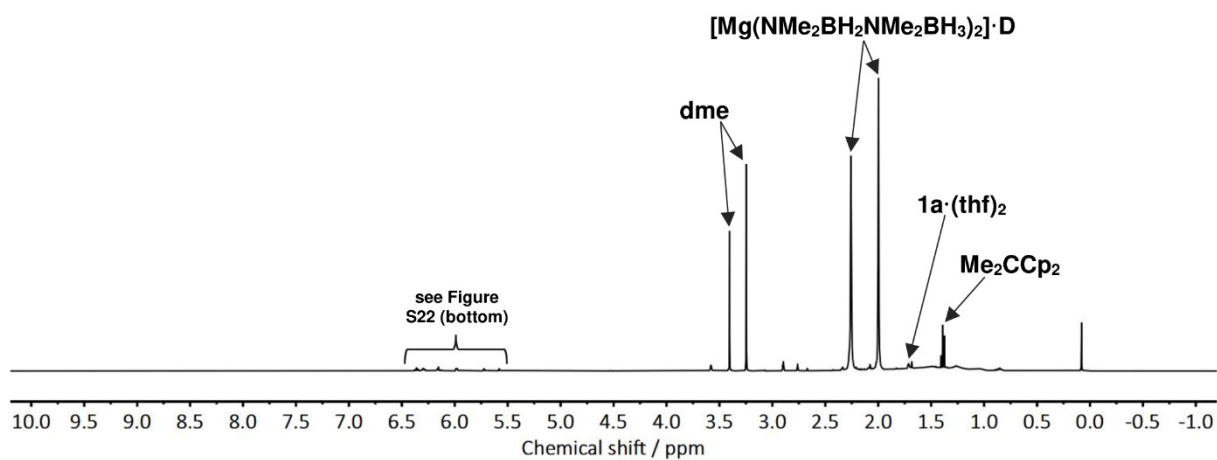


Figure S23. ^1H NMR spectrum (400.13 MHz, 294 K, thf-D_8) of a mixture of magnesium complex 5 and 2,2-dicyclopentadienylpropane at r.t. after 2 h.

SUPPORTING INFORMATION

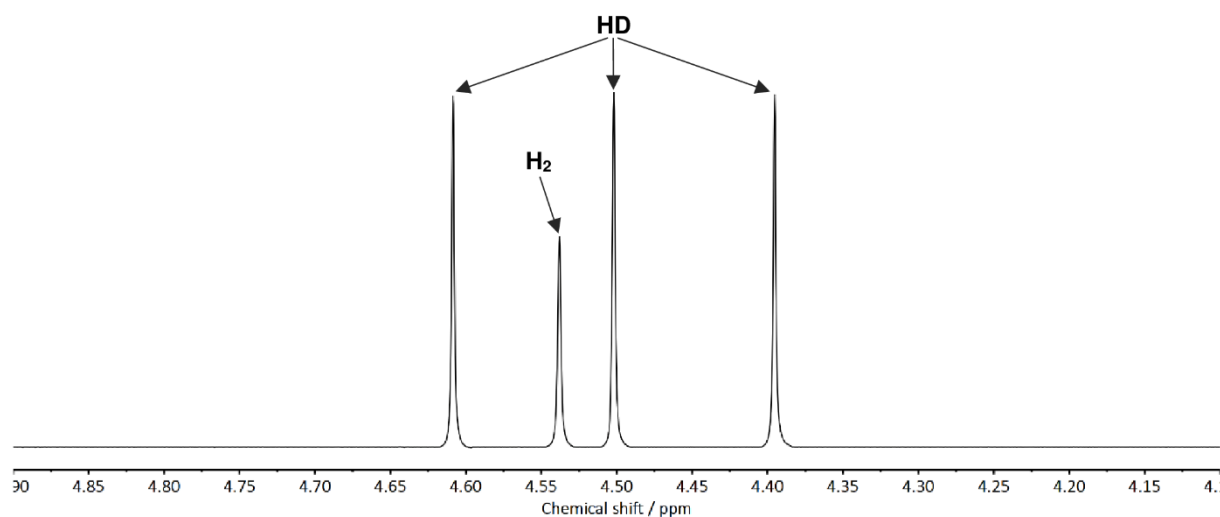


Figure S24. Part of the ^1H NMR spectrum (400.13 MHz, 294 K, thf-D8) of the reaction mixture of **2aNDBD** with 10 mol% of **1a** at r.t. after 96 h.

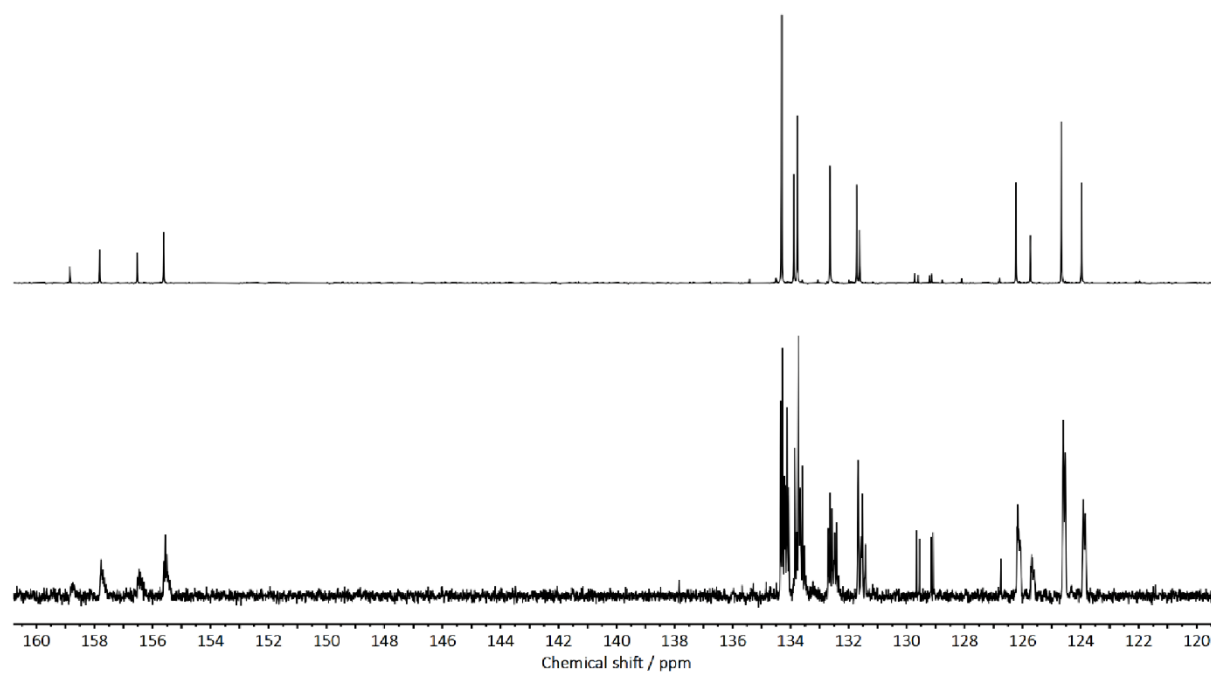


Figure S25. Part of the ^{13}C NMR spectra (100.62 MHz, 293 K, thf-D8) of 2,2-dicyclopentadienylpropane (top), and of the reaction mixture of **2aNDBD** with 10 mol% of **1a** at r.t. after 96 h (bottom).

SUPPORTING INFORMATION

MS spectra

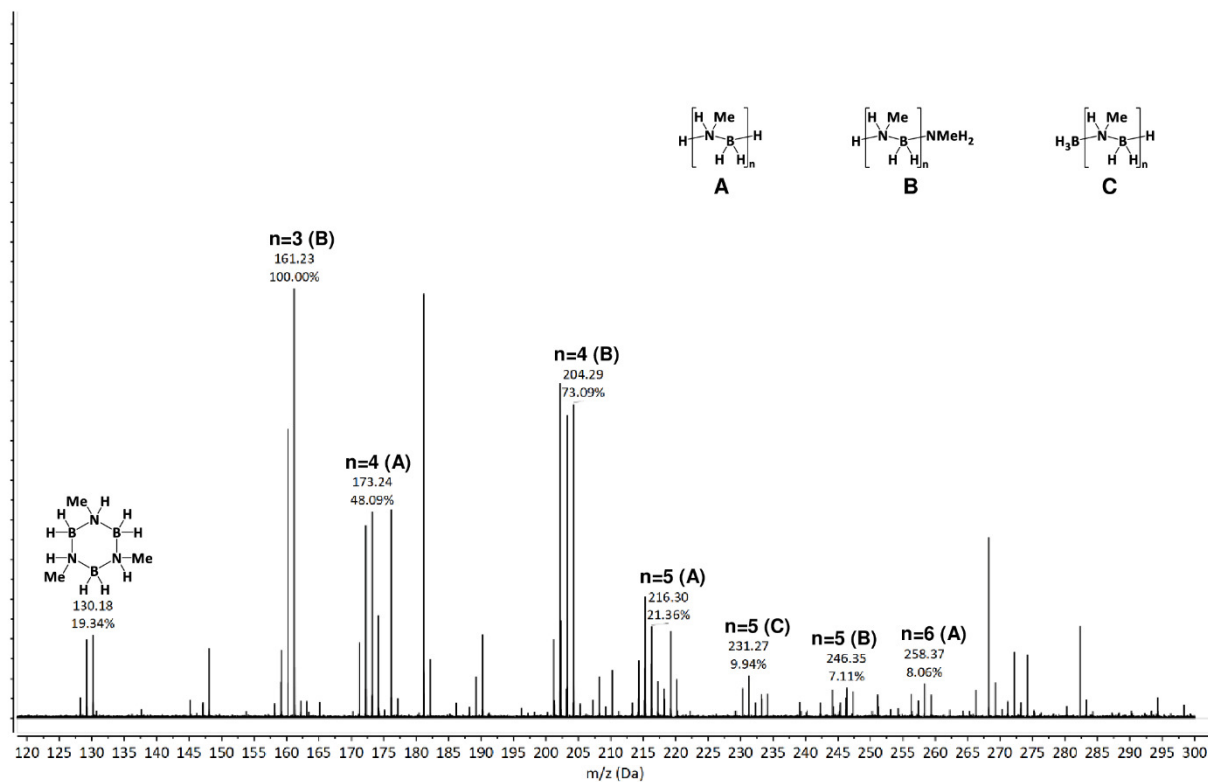


Figure S26. MS spectrum (ESI) of the reaction mixture of **2c** with 10 mol% of **1a** after 72 h

SUPPORTING INFORMATION

XRD data

Crystal structure data has been deposited with the Cambridge Crystallographic Data Centre (CCDC) and is available free of charge from the Cambridge Structural Database.

crystal structure data of 1a·dme

(this compound was crystallized in two different modification)

CCDC code:	1921397	1971379
empirical formula	C ₁₇ H ₂₄ MgO ₂	C ₁₇ H ₂₄ MgO ₂
formula weight	284.67	189.78
temperature	212(2) K	132(2) K
wavelength	0.71073 Å	0.71073 Å
crystal system	monoclinic	orthorhombic
space group	C2/c	Pbca
unit cell dimensions	a = 9.5539(9) Å α = 90° b = 13.3525(9) Å β = 97.564(3)° c = 12.4343(8) Å γ = 90°	a = 14.3619(4) Å α = 90° b = 14.5325(5) Å β = 90° c = 15.0215(5) Å γ = 90°
volume	1572.4(2) Å ³	3135.20(17) Å ³
Z	4	12
density (calculated)	1.202 mg m ⁻³	1.206 Mg/m ³
absorption coefficient	0.112 mm ⁻¹	0.112 mm ⁻¹
F(000)	616	1232
crystal size	0.273 x 0.184 x 0.174 mm ³	0.382 x 0.376 x 0.344 mm ³
theta range for data collection	2.637 to 32.665°	2.411 to 30.396°
index ranges	-11 ≤ h ≤ 14, -19 ≤ k ≤ 20, -18 ≤ l ≤ 18	-20 ≤ h ≤ 20, -15 ≤ k ≤ 20, -21 ≤ l ≤ 21
reflections collected	16705	31413
independent reflections	2888 [R(int) = 0.0358]	4684 [R(int) = 0.0236]
completeness to theta = 25.242°	100.0%	99.8%
absorption correction	semi-empirical from equivalents	semi-empirical from equivalents
max. and min. transmission	0.7464 and 0.7216	0.7460 and 0.7152
refinement method	full-matrix least-squares on F ²	full-matrix least-squares on F ²
data / restraints / parameters	2888 / 0 / 140	4684 / 0 / 185
goodness-of-fit on F ²	1.034	1.051
final R indices [I > 2σ(I)]	R1 = 0.0532, wR2 = 0.1404	R1 = 0.0346, wR2 = 0.0840
R indices (all data)	R1 = 0.0780, wR2 = 0.1602	R1 = 0.0487, wR2 = 0.0915
extinction coefficient	n/a	n/a
largest diff. peak and hole	0.238 and -0.551 e.Å ⁻³	0.362 and -0.221 e.Å ⁻³

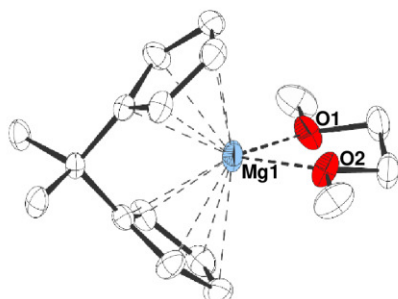


Figure S27. Molecular structure of 1a·dme in the crystal (thermal ellipsoids at 30% probability level; hydrogen atoms omitted for clarity; selected bond length and angles: Mg1-O1/O2: 205.3 pm, Mg1-Cp^{centroid}: 230.4 pm, α = 80.1°).

SUPPORTING INFORMATION

crystal structure data of **5**

CCDC code:	1971378
empirical formula	C ₂₀ H ₇ B ₈ Mg ₂ N ₈ O ₂
formula weight	598.00
temperature	173(2) K
wavelength	0.71073 Å
crystal system	monoclinic
space group	<i>P</i> 2 ₁ / <i>c</i>
unit cell dimensions	a = 8.6472(4) Å α = 90° b = 9.4595(6) Å β = 93.600(2)° c = 23.9567(16) Å γ = 90°
volume	1955.7(2) Å ³
Z	2
density (calculated)	1.015 mg m ⁻³
absorption coefficient	0.090 mm ⁻¹
F(000)	668
crystal size	0.318 x 0.201 x 0.138 mm ³
theta range for data collection	2.315 to 33.271°
index ranges	-13 ≤ h ≤ 12, -11 ≤ k ≤ 14, -34 ≤ l ≤ 36
reflections collected	24493
independent reflections	7446 [R(int) = 0.0362]
completeness to theta = 25.242°	99.9%
absorption correction	semi-empirical from equivalents
max. and min. transmission	0.7465 and 0.7035
refinement method	full-matrix least-squares on F ²
data / restraints / parameters	7446 / 0 / 336
goodness-of-fit on F ²	1.027
final R indices [I > 2σ(I)]	R1 = 0.0452, wR2 = 0.1026
R indices (all data)	R1 = 0.0701, wR2 = 0.1140
extinction coefficient	n/a
largest diff. peak and hole	0.262 and -0.234 e.Å ⁻³

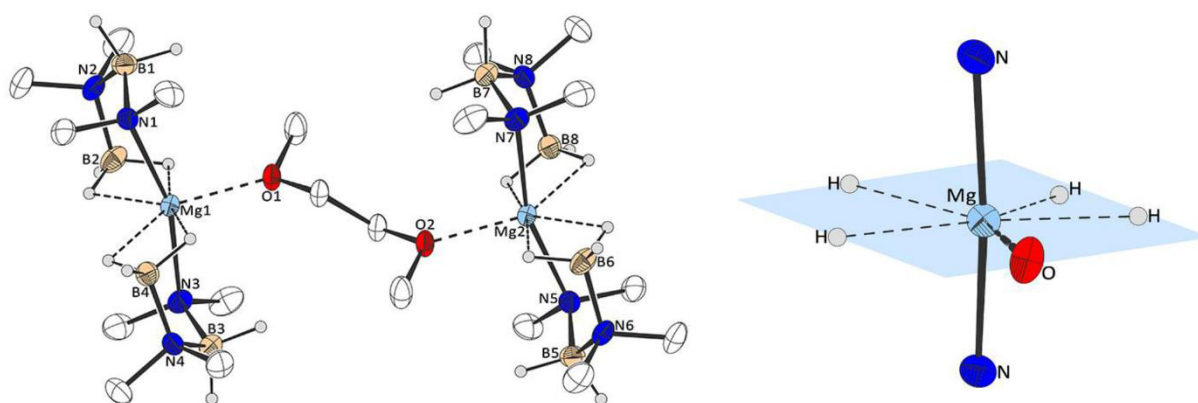


Figure S28. Molecular structure of magnesium complex **5** (left) and of coordination environment of magnesium in **5** (right) in the crystal (thermal ellipsoids at 50% probability level; hydrogen atoms except for (B)-H omitted for clarity; selected bond length: Mg1/2-O1/2: 218.1 pm, Mg1/2-N1/3/5/7: 216.1 pm / 215.9 pm).

SUPPORTING INFORMATION

Computational Details

All calculations were performed using the Gaussian 09, Revision D.01 package of programs.¹¹ All geometry optimizations have been carried out at the B3LYP-D3¹²/def2-TZVP¹³ level of theory. Every optimized structure was confirmed to be either a minimum or a maximum on the potential energy surface by a subsequent frequency analysis (all positive eigenvalues for minima, one negative eigenvalue for maxima (transition state)) All transition states were verified to be connected to the corresponding minima by calculations along the intrinsic reaction coordinate.

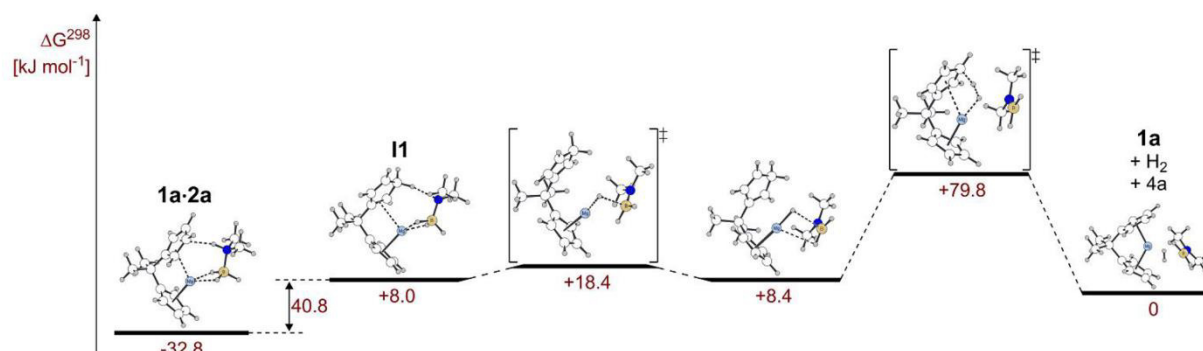
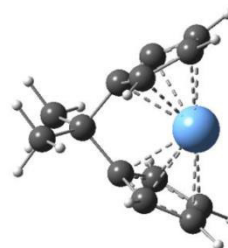


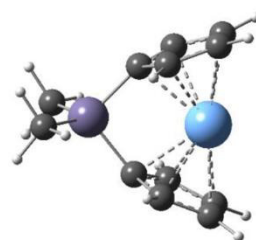
Figure S29. Calculated reaction pathway for the dehydrogenation reaction of dimethylamine borane, **2a**, with magnesocenophane, **1a**, without solvent coordination.

optimized geometry of **1a**

Mg	0.00000000	1.39696500	0.00000000
C	0.00000000	-1.54543800	0.00000000
C	1.20375100	-0.57238400	0.00000400
C	-1.20375100	-0.57238400	-0.00000400
C	1.62587400	0.16403700	-1.13915500
C	-1.62587400	0.16403700	1.13915500
C	2.24721400	1.36448900	-0.71281100
C	-2.24721400	1.36448900	0.71281100
C	-1.62587700	0.16404400	-1.13915900
C	1.62587700	0.16404300	1.13915900
C	-2.24721400	1.36449500	-0.71280800
C	2.24721400	1.36449500	0.71280800
H	1.43358900	-0.09937400	-2.16689100
H	-1.43358900	-0.09937400	2.16689100
C	0.00000300	-2.43862400	-1.24534700
C	-0.00000300	-2.43862400	1.24534700
H	2.72675900	2.09524200	-1.34546600
H	-2.72675900	2.09524200	1.34546600
H	-1.43358800	-0.09935100	-2.16689800
H	1.43358800	-0.09935100	2.16689800
H	-2.72675500	2.09525300	-1.34545900
H	2.72675500	2.09525300	1.34545900
H	-0.88609200	-3.07573100	-1.25256500
H	0.88609200	-3.07575600	-1.25254500
H	0.00002000	-1.86210100	-2.16950400
H	0.88609200	-3.07573100	1.25256500
H	-0.88609200	-3.07575600	1.25254500
H	-0.00002000	-1.86210100	2.16950400

optimized geometry of **1b**

Mg	1.45066400	-0.00000800	0.00000000
C	1.66313100	-2.23195100	-0.71283000
C	1.66313100	-2.23195500	0.71282900
C	0.40191000	-1.74897900	-1.13855300
H	2.45344100	-2.60614600	-1.34565800
C	0.40191200	-1.74898700	1.13855700
H	2.45344200	-2.60615300	1.34565400
C	-0.39469600	-1.42146100	0.00000300
H	0.11425400	-1.59657000	-2.16846100
H	0.11425700	-1.59658500	2.16846600
C	0.40192900	1.74898500	-1.13855800
C	-0.39468100	1.42146400	-0.00000300
C	1.66315400	2.23194000	-0.71282900
H	0.11427200	1.59659300	-2.16846800
C	0.40192900	1.74897500	1.13855400
C	1.66315400	2.23193500	0.71282900
H	2.45346700	2.60613300	-1.34565400
H	0.11427100	1.59657600	2.16846200

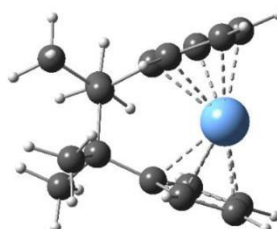


SUPPORTING INFORMATION

H	2.45346700	2.60612200	1.34565700
C	-2.68176100	0.00002200	1.55568100
H	-3.32031900	0.88508000	1.59655800
H	-3.32030900	-0.88504300	1.59657700
H	-2.05573000	0.00003600	2.45059500
C	-2.68176300	-0.00001000	-1.55568000
H	-3.32035100	-0.88504000	-1.59653200
H	-3.32028300	0.88508400	-1.59660000
H	-2.05573300	-0.00006100	-2.45059400
Si	-1.63787200	0.00001000	0.00000000

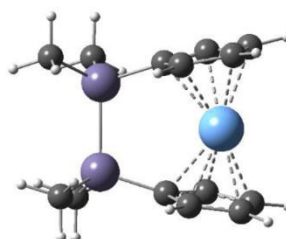
optimized geometry of 1c

C	0.08349600	-1.44526900	-0.03551700
C	1.78859900	-0.85720400	-1.75453400
C	2.51381900	-1.59843300	0.48416100
C	0.08292100	1.44539400	0.03532200
C	1.78823100	0.85768700	1.75450600
C	2.51336000	1.59925000	-0.48410100
Mg	-1.73881900	-0.00025700	0.00066000
C	-0.56839800	-1.65880100	1.20772000
C	-0.84365900	-1.82207600	-1.04637600
H	1.12767100	-0.25370600	-2.37429000
H	2.81089100	-0.53128400	-1.93755100
H	1.71062800	-1.89045700	-2.09507500
H	3.49996800	-1.13763200	0.39570200
H	2.57123600	-2.59589700	0.04500300
H	2.28698200	-1.72251400	1.54133100
C	-0.84421600	1.82240400	1.04614700
C	-0.56920700	1.65819200	-1.20790800
H	1.12740300	0.25398000	2.37416800
H	2.81059200	0.53200000	1.93755700
H	1.70999700	1.89088900	2.09513400
H	3.49967200	1.13884100	-0.39539800
H	2.57030100	2.59678900	-0.04505400
H	2.28665500	1.72310400	-1.54132600
H	-0.15084300	-1.46405800	2.18168600
C	-1.88458300	-2.12324800	0.97215400
H	-2.60476200	-2.40166100	1.72571200
C	-2.06096600	-2.22717700	-0.43474100
C	-2.06179000	2.22672500	0.43445700
H	-2.92869300	2.62017000	0.94206900
C	-1.88551200	2.12222600	-0.97239900
H	-2.60591400	2.39995600	-1.72599700
H	-0.15170900	1.46313600	-2.18183100
H	-0.67475300	-1.78350900	-2.10975400
H	-0.67514500	1.78444700	2.10952200
H	-2.92781400	-2.62064400	-0.94243200
C	1.43854300	-0.77791900	-0.25691800
C	1.43827500	0.77844000	0.25684500



optimized geometry of 1d

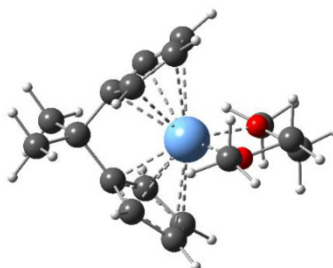
Si	1.49585900	1.19319100	0.10085200
Si	1.49589000	-1.19318900	-0.10062700
C	-0.28687300	1.75530900	-0.04402700
C	2.15382800	1.70788300	1.79351000
C	2.52547900	1.98847800	-1.26609400
C	-0.28686000	-1.75528000	0.04400700
C	2.15402400	-1.70766800	-1.79328900
C	2.52539800	-1.98862100	1.26631200
Mg	-1.83886300	-0.00001000	-0.00010100
C	-1.06743100	1.81686400	-1.23787200
C	-1.19579400	1.97950900	1.03361600
H	1.56905600	1.25759700	2.59884900
H	3.19025200	1.38870600	1.92336400
H	2.11374800	2.79303600	1.91512800
H	3.56278800	1.64763100	-1.22757800
H	2.52006000	3.07696000	-1.17090000
H	2.13158600	1.73629800	-2.25310800
C	-1.19564500	-1.97951000	-1.03374500
C	-1.06755900	-1.81688000	1.23776000
H	1.56929000	-1.25731900	-2.59862100
H	3.19043300	-1.38839000	-1.92301200
H	2.11403200	-2.79280800	-1.91504700
H	3.56267600	-1.64765900	1.22799900
H	2.52010100	-3.07708600	1.17090200
H	2.13133800	-1.73667900	2.25331800
C	-0.69223800	1.68093300	-2.24142000
C	-2.41953800	2.06801400	-0.90127700
H	-3.23661000	2.19728800	-1.59438800
C	-2.50050500	2.16818800	0.51459400
C	-2.50041200	-2.16822600	-0.51488100
H	-3.38834400	-2.39200200	-1.08602100
C	-2.41961800	-2.06806200	0.90100000
H	-3.23676900	-2.19736500	1.59401200
H	-0.69249400	-1.68098000	2.24136100
H	-0.93488200	1.99552500	2.08101900
H	-0.93460500	-1.99552900	-2.08111600
H	-3.38851100	2.39195300	1.08562600



SUPPORTING INFORMATION

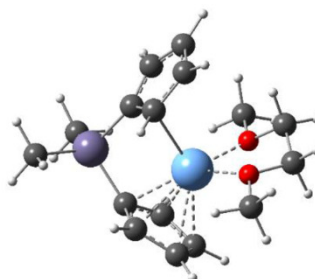
optimized geometry of 1a-dme

Mg	0.32566600	0.00000000	0.00000000
O	1.99565000	0.57042600	1.18448500
O	1.99564800	-0.57042500	-1.18448500
C	-2.59748200	0.00000000	0.00000100
C	-1.65150300	1.05711700	-0.58813900
C	-1.65150200	-1.05711700	0.58814000
C	-0.96485400	2.04853700	0.16122300
C	-0.96485400	-2.04853700	-0.16122300
C	0.10205600	2.55494100	-0.62428800
C	0.10205600	-2.55494200	0.62428700
C	-0.97470900	-0.94870200	1.83338200
C	-0.97471000	0.94870100	-1.83338200
C	0.09222300	-1.87756300	1.85517600
C	0.09222200	1.87756300	-1.85517600
C	3.21406400	0.61080400	0.44489000
C	3.21406200	-0.61080700	-0.44488900
C	1.87434800	1.56424100	2.20375300
C	1.87434600	-1.56423900	-2.20375500
H	-1.21967200	2.37528500	1.15744400
H	-1.21967300	-2.37528500	-1.15744400
H	0.90039600	1.41455300	2.66190700
H	0.90039300	-1.41454900	-2.66190900
C	-3.49641700	0.60671700	1.08584600
C	-3.49641800	-0.60671700	-1.08584400
H	0.76932500	3.35747900	-0.34518600
H	0.76932500	-3.35747900	0.34518500
H	-1.23809500	-0.27909500	2.63741800
H	-1.23809700	0.27909400	-2.63741800
H	0.76907000	-2.04353200	2.67981700
H	0.76906800	2.04353200	-2.67981800
H	3.24711500	1.52722800	-0.15370500
H	4.07119700	0.58530800	1.12451300
H	3.24711100	-1.52723100	0.15370500
H	4.07119600	-0.58531300	-1.12451300
H	2.66348900	1.42895200	2.94723300
H	1.92411100	2.56511700	1.77029600
H	2.66348700	-1.42894800	-2.94723500
H	1.92410900	-2.56511600	-1.77030000
H	-4.13336000	-0.16387200	1.52442900
H	-4.13139800	1.38467300	0.65777200
H	-2.92014500	1.05791400	1.89255100
H	-4.13336100	0.16387200	-1.52442700
H	-4.13139900	-1.38467200	-0.65777000
H	-2.92014700	-1.05791400	-1.89255000



optimized geometry of 1b-dme

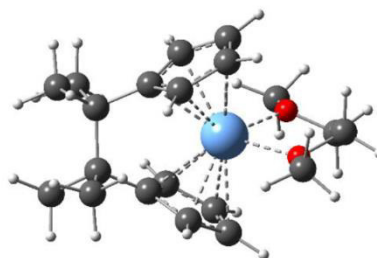
Mg	-0.54055000	-0.41486900	-0.03170900
O	-2.51850000	-0.53057600	-0.82866700
O	-1.66611500	0.73687500	1.31019100
C	1.32304100	1.17555600	-0.63982400
C	-0.48463400	2.13274900	-1.73861400
C	0.31378200	0.96414800	-1.65926400
H	0.35795200	0.19903800	-2.42882900
C	1.07340700	2.45818700	-0.11116200
H	1.62552800	2.91187700	0.70123300
C	-0.02285000	3.04127400	-0.78086000
C	1.47424700	-1.52185700	0.40130900
C	0.72059900	-1.57021200	1.61228700
H	0.97083900	-1.05063000	2.52605300
C	-0.40645400	-2.40447500	1.43046100
C	-0.37141300	-2.88966900	0.10385100
C	0.77427600	-2.34891200	-0.52600400
H	1.06751900	-2.52617400	-1.55066700
C	-2.88144600	1.21654600	0.72555700
H	-2.63915600	2.02058900	0.02626300
C	-3.51635500	0.04205600	0.01787100
C	-2.98930100	-1.57595000	-1.67903500
H	-2.13492500	-1.92177900	-2.25461400
C	-1.09658700	1.61333200	2.29328700
H	-0.13959400	1.18273800	2.57234100
C	3.53620200	0.55741900	1.39438500
C	3.74768700	-0.59525500	-1.46787000
H	-1.29066400	2.29671100	-2.44084100
H	-0.43518600	4.02266900	-0.58671700
H	-1.14250300	-2.65444800	2.17986900
H	-1.07220600	-3.58424400	-0.33479300
H	-3.55399300	1.58495200	1.50558600
H	-4.36876000	0.37982300	-0.57946400
H	-3.85465900	-0.71223000	0.73676500
H	-3.38612100	-2.40463600	-1.08701200
H	-3.75971500	-1.19004300	-2.35087200
H	-1.75817400	1.66163600	3.16188600
H	-0.93201600	2.60029300	1.86278700
H	4.25233100	-0.18601700	1.75111100
H	4.08759500	1.46402600	1.13511000
H	2.86638500	0.80223300	2.22175500
H	3.19163600	-0.99299800	-2.31999400
H	4.32189500	0.26397900	-1.82188500
H	4.44765000	-1.36495900	-1.13391000
Si	2.57690400	-0.08885600	-0.08722100



SUPPORTING INFORMATION

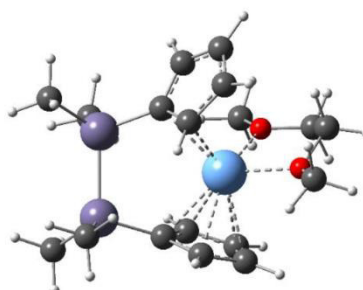
optimized geometry of 1c-dme

C	-1.18832700	1.40380200	-0.29017100
C	-2.85304100	0.46950300	-1.89571200
C	-3.62803300	1.65069700	0.12287300
C	-1.18834300	-1.40380200	0.29018800
C	-2.85308300	-0.46949300	1.89569400
C	-3.62804400	-1.65067700	-0.12290600
Mg	0.73949200	-0.00000800	0.00001100
C	-0.58525200	1.91384000	0.88809200
C	-0.28500800	1.68026400	-1.35457100
H	-2.16177600	-0.22497600	-2.36913900
H	-3.86297700	0.08387100	-2.02671300
H	-2.79333500	1.41627300	-2.43388000
H	-4.61101900	1.17348300	0.11471600
H	-3.67954500	2.53325800	-0.51725600
C	-3.42236100	1.99702700	1.13371900
C	-0.28503800	-1.68025300	1.35460300
C	-0.58525300	-1.91384900	-0.88806300
H	-2.16182400	0.22498400	2.36913500
H	-3.86302000	-0.08385800	2.02667400
H	-2.79338900	-1.41626400	2.43386100
H	-4.61102400	-1.17345300	-0.11476300
H	-3.67957300	-2.53323800	0.51722100
H	-3.42235900	-1.99700700	-1.13374900
H	-1.00962900	1.89161900	1.87634100
C	0.64928000	2.51641300	0.54697800
H	1.31866700	3.01429300	1.23197200
C	0.83408300	2.37629600	-0.83690400
C	0.83406000	-2.37629000	0.83695700
H	1.68109700	-2.72149300	1.40913300
C	0.64927600	-2.51641900	-0.54692700
H	1.31867300	-3.01430600	-1.23190700
H	-1.00961600	-1.89163700	-1.87831700
O	2.48948800	0.09170200	1.31305100
O	2.48945800	-0.09172200	-1.31307500
C	3.70595100	0.39814500	0.64248200
C	3.70594500	-0.39813800	-0.64253700
C	2.41347100	0.54689800	2.66134800
H	1.42563800	0.27502000	3.02432200
C	2.41341300	-0.54691700	-2.66137000
H	1.42558000	-0.27502300	-3.02432900
H	-0.44484300	1.45074800	-2.39563600
H	-0.44486600	-1.45072700	2.39566300
H	1.68112700	2.72150500	-1.40906700
H	3.74812800	1.47236600	0.43350900
H	4.56367400	0.11337700	1.26030200
H	3.74815600	-1.47235800	-0.43356700
H	4.56364500	-0.11334800	-1.26037800
H	3.18010600	0.05328100	3.26455000
H	2.53471500	1.63108700	2.71337400
H	3.18004600	-0.05331200	-3.26458400
H	2.53464200	-1.63110800	-2.71339700
C	-2.53288400	-0.69944000	0.40615200
C	-2.53287000	0.69945000	-0.40616400



optimized geometry of 1d-dme

Si	2.16096100	1.30493500	0.12679900
Si	2.64376600	-0.98008300	-0.21886100
C	0.39925200	1.58910900	-0.41320300
C	2.30839400	1.69676400	1.97648100
C	3.33513000	2.45911900	-0.80489400
C	1.03104600	-1.83220500	0.17663000
C	3.11146300	-1.36195300	-2.00900900
C	4.01553500	-1.59630400	0.92544000
Mg	-0.92900200	-0.45249900	-0.03845600
C	-0.21879900	1.10677000	-1.63295600
C	-0.41629700	2.66551300	0.02592900
H	1.76012300	0.97190400	2.58254500
H	3.35159600	1.67213100	2.29984000
H	1.91482900	2.69203700	2.19911700
H	4.37515300	2.29851100	-0.50814400
H	3.08107500	3.50383700	-0.60815900
H	3.26120700	2.29647700	-1.88217800
C	0.15632500	-2.50088600	-0.72888300
C	0.36638200	-1.83006300	1.43829400
H	2.34253300	-1.01943200	-2.70457700
H	4.04645100	-0.86770400	-2.28200200
H	3.24312800	-2.43737600	-2.15433500
H	4.95187000	-1.06176800	0.74644700
H	4.19718700	-2.66296400	0.77129700
H	3.74339500	-1.45168700	1.97318400
H	0.24277800	0.42313000	-2.33572400
C	-1.35276300	1.90321400	-1.89954600
H	-1.99701300	1.81409000	-2.76309100
C	-1.47363500	2.85377400	-0.87275300
C	-0.99894400	-2.91836000	-0.03129900
H	-1.83966500	-3.44984600	-0.44995600
C	-0.87193000	-2.49973100	1.30998900
H	-1.59194900	-2.66548100	2.09771100
H	0.76151100	-1.41494000	2.35406300
O	-2.95424700	-0.74326000	-0.76357500
O	-2.15865900	0.47878900	1.39503400
C	-3.87961200	0.17887400	-0.18557900
C	-3.55818300	0.23640400	1.28934000
C	-3.21752800	-1.07178400	-2.12727800
H	-2.40983700	-1.72472000	-2.44933200
C	-1.70270100	0.84444500	2.69588800

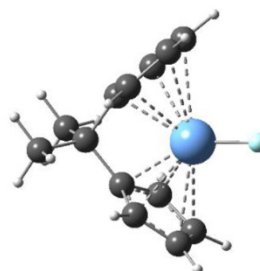


SUPPORTING INFORMATION

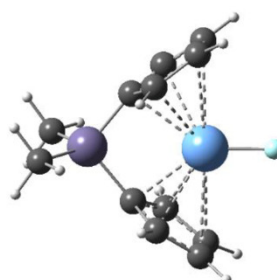
H	-0.63673400	1.03227700	2.61063400
H	-0.24882600	3.24670500	0.92251400
H	0.35877100	-2.67934800	-1.77472000
H	-2.25797300	3.59358500	-0.78479000
H	-3.74093100	1.15999600	-0.64754300
H	-4.90628300	-0.16940900	-0.33577700
H	-3.80254400	-0.70929600	1.78517100
H	4.11825800	1.04884400	1.76175800
H	-4.17234500	-1.59806100	-2.20543000
H	-3.23078400	-0.17191800	-2.74430200
H	-2.20638100	1.75725300	3.02136000
H	-1.88578600	0.03478700	3.40753200

optimized geometry of 1a-F⁻

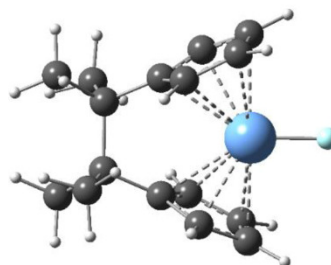
Mg	0.00000300	1.25931500	-0.00000300
C	-2.60874200	0.92982400	0.70124200
C	-2.60874200	0.92982000	-0.70124800
C	-1.74300300	-0.10129100	1.13928600
C	-3.14417200	1.61786200	1.33845800
C	-1.74300300	-0.10129700	-1.13928600
C	-3.14417200	1.61785500	-1.33846700
C	-1.21430300	-0.76617100	0.00000200
H	-1.52244700	-0.33915300	2.16900900
H	-1.52244600	-0.33916500	-2.16900700
C	1.74300400	-0.10129200	1.13928600
C	1.21430600	-0.76617400	0.00000200
C	2.60873900	0.92982600	0.70124300
H	1.52244800	-0.33915400	2.16900900
C	1.74300400	-0.10129800	-1.13928500
C	2.60873900	0.92982300	-0.70124700
H	3.14416700	1.61786600	1.33845800
H	1.52244800	-0.33916600	-2.16900700
H	3.14416700	1.61785900	-1.33846700
C	0.00000100	-1.70145500	0.00000500
C	0.00000000	-2.60450800	-1.24215600
H	0.88909200	-3.24017600	-1.24826000
H	-0.88909500	-3.24017400	-1.24826000
H	0.00000000	-2.02628800	-2.16516300
C	-0.00000100	-2.60450200	1.24217100
H	-0.88909500	-3.24016700	1.24827800
H	0.88909200	-3.24016900	1.24827800
H	0.00000000	-2.02627600	2.16517400
F	-0.00000200	3.06209400	-0.00000800

optimized geometry of 1b-F⁻

Mg	1.31279000	-0.00014100	0.00000000
C	1.22664600	-2.69924400	-0.70286600
C	1.22664900	-2.69924100	0.70286500
C	0.13590300	-1.91953000	-1.13996100
H	1.96436500	-3.16946700	-1.33654800
C	0.13590200	-1.91953200	1.13996000
H	1.96436900	-3.16946200	1.33654700
C	-0.58325700	-1.44089400	0.00000000
H	-0.12672800	-1.72472100	-2.17099500
H	-0.12672900	-1.72472400	2.17099400
C	0.13624900	1.91950100	-1.13996100
C	-0.58300200	1.44100200	0.00000000
C	1.22714200	2.69900200	-0.70286500
H	-0.12642300	1.72474400	-2.17099400
C	0.13625000	1.91949900	1.13996100
C	1.22714200	2.69900200	0.70286600
H	1.96496100	3.16907000	-1.33654600
H	-0.12642100	1.72474200	2.17099500
H	1.96496100	3.16907000	1.33654600
C	-2.83448800	0.00025300	1.54564800
H	-3.47128600	0.88788800	1.58010800
H	-3.47138400	-0.88731000	1.58015200
H	-2.21327600	0.00024200	2.44442300
C	-2.83448700	0.00025300	-1.54564900
H	-3.47138300	-0.88731000	-1.58015400
H	-3.47128700	0.88788700	-1.58010700
H	-2.21327500	0.00024500	-2.44442400
Si	-1.75203500	0.00016000	0.00000000
F	3.11496100	-0.00020900	0.00000000

optimized geometry of 1c-F⁻

Mg	1.76315900	0.00002300	0.00000500
C	-0.33720800	1.42682400	-0.07243900
C	0.25230200	1.77581400	1.16639000
C	0.59127500	1.80686600	-1.08206100
C	1.51347600	2.36783500	0.92537600
H	-0.17865900	1.61775400	2.14266000
C	1.71981100	2.39884800	-0.46510200
H	0.45839500	1.68802500	-2.14583700
H	2.21445900	2.69709300	1.67734100
H	2.61110500	2.73869300	-0.96826800
C	0.25236100	-1.77582900	-1.16643200
C	1.51355100	-2.36781300	-0.92541600
C	-0.33715800	-1.42684400	0.07239600
H	-0.17859500	-1.61777800	-2.14270300
C	1.71987900	-2.39883200	0.46506100
H	2.21454100	-2.69705400	-1.67738200
C	0.59132600	-1.80687800	1.08201800
H	2.61117600	-2.73866300	0.96823100
H	0.45843700	-1.68804900	2.14579500
C	-1.68295800	-0.75512600	0.29105300

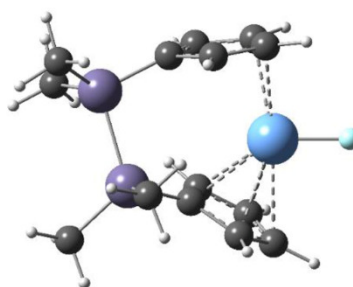


SUPPORTING INFORMATION

C	-1.68299200	0.75508000	-0.29108500
C	-2.00747100	-0.75885700	1.79835400
H	-3.02486600	-0.41380800	1.98708400
H	-1.92691400	-1.77601700	2.18508600
H	-1.32421300	-0.13331300	2.36886200
C	-2.77986500	-1.61204200	-0.37900700
H	-2.82890600	-2.58424200	0.11645900
H	-3.76554500	-1.14306400	-0.29903600
H	-2.57086400	-1.79742400	-1.43091900
C	-2.77986500	1.61192100	0.37912700
H	-2.82893200	2.58417300	-0.11623400
H	-3.76553700	1.14294200	0.29917700
H	-2.57078200	1.79718600	1.43104900
C	-2.00761300	0.75892000	-1.79836900
H	-3.02498800	0.41380100	-1.98706400
H	-1.92718400	1.77612600	-2.18500500
H	-1.32433600	0.13350600	-2.36899300
F	3.58679300	0.00005800	0.00005000

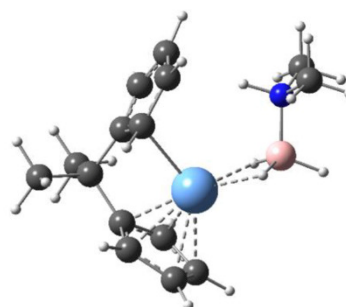
optimized geometry of 1d·F

Mg	-2.15432600	0.34547800	-0.13671200
C	-0.52603400	-1.43622200	0.19336000
C	-1.03892200	-1.05335800	1.47039900
C	-1.61875000	-2.04811400	-0.49920100
C	-2.39819700	-1.42683100	1.55135200
H	-0.47778900	-0.55082300	2.24334300
C	-2.75217500	-2.04649000	0.33158500
H	-1.58059200	-2.43435600	-1.50749500
H	-3.06204200	-1.23540400	2.38166500
H	-3.74494000	-2.35961600	0.04894700
C	-0.02296300	1.96101400	-1.23172500
C	-1.32391300	2.43356700	-0.98795300
C	0.67249500	1.84379200	0.00508800
H	0.37175800	1.70333500	-2.20570000
C	-1.46094100	2.60711900	0.42430800
H	-2.07658400	2.67402000	-1.72444500
C	-0.23203100	2.25260400	1.01498700
H	-2.32396900	3.02754300	0.92198800
H	-0.03427700	2.23807000	2.07821600
C	2.70732300	0.77499500	2.05816300
H	3.55744900	0.10533300	2.21244800
H	3.01166000	1.78570100	2.34502400
H	1.90796700	0.46134500	2.73265600
C	3.60338600	1.19940700	-0.84311700
H	3.99570800	2.18233800	-0.56674600
H	4.41408800	0.46982700	-0.75770400
H	3.30141800	1.24433100	-1.89216000
C	2.21100600	-2.84273000	0.38358200
H	1.76226300	-3.79138100	0.07498300
H	3.25729800	-2.83860100	0.06301500
H	2.19240400	-2.80503000	1.47532100
C	1.30470800	-1.57504900	-2.23877100
H	2.33277000	-1.59385500	-2.60948700
H	0.81963500	-2.50770200	-2.54064400
H	0.78067900	-0.75088800	-2.72646700
Si	2.12240100	0.73918100	0.25419300
Si	1.25147500	-1.37301500	-0.35229000
F	-3.83746700	0.64905900	-0.75835600



optimized geometry of 1a·2a

Mg	0.04881800	1.04287000	0.31390000
C	-1.23624100	-1.67144500	1.27488300
C	-1.33507300	-2.32808300	0.04568600
C	0.03574100	-1.02389100	1.32662800
H	-1.94952800	-1.70822400	2.08743600
C	-0.12964700	-2.12146700	-0.67021900
H	-2.17738600	-2.91273600	-0.30008900
C	0.74540000	-1.36325100	0.11552500
H	0.50748500	-0.69971300	2.24713900
H	0.07867700	-2.50009100	-1.65911200
C	2.24700000	1.37291300	1.01184400
C	2.22122000	0.58491000	-0.16680500
C	1.76017400	2.67135400	0.70573100
H	2.54264400	1.03489900	1.99203600
C	1.74206000	1.42349300	-1.21162600
C	1.45485500	2.70255000	-0.67540900
H	1.70087800	3.50524100	1.38795000
H	1.58255400	1.12859600	-2.23654700
H	1.10243700	3.55898200	-1.22869700
C	2.19256800	-0.94466900	-0.20212900
C	2.62104900	-1.46186400	-1.58094800
H	3.63263900	-1.12249600	-1.80910900
H	2.60983100	-2.55291800	-1.60039000
H	1.95935500	-1.10972800	-2.37238900
C	3.14275300	-1.53853600	0.85377600
H	3.09410100	-2.62850300	0.82724400
H	4.17222800	-1.22807700	0.66186600
H	2.87411000	-1.22380400	1.86149600
H	-1.76325100	1.80593500	0.80046000
H	-1.36547400	1.22253200	-1.11305100
B	-2.22729500	1.55196800	-0.31088400
H	-2.82824600	2.50408500	-0.71854400
N	-3.18423100	0.29299800	-0.14612300
H	-2.58038100	-0.49160300	0.17403000
C	-3.77365800	-0.12294200	-1.44174500
H	-4.39255900	-1.00945800	-1.30368400
H	-4.37600700	0.69274000	-1.83816400
H	-2.96704700	-0.35170900	-2.13368200

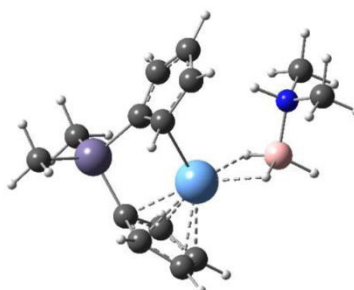


SUPPORTING INFORMATION

C	-4.22177100	0.50199800	0.88967100
H	-4.84313700	1.35003600	0.60634900
H	-4.83867000	-0.39118600	0.99098400
H	-3.73355700	0.71551000	1.83776800

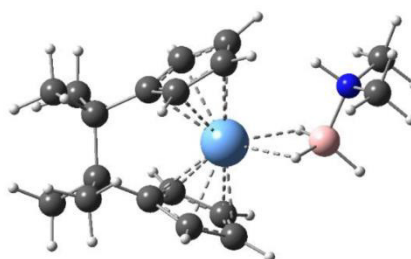
optimized geometry of 1b·2a

Mg	0.06445500	1.01384900	-0.25400600
C	1.41074100	-1.67700000	-1.49594100
C	1.56713900	-2.36680600	-0.27974600
C	0.16244700	-1.01429100	-1.46333200
H	2.09413600	-1.69085900	-2.33407600
C	0.42198800	-2.13960800	0.50667000
H	2.41153600	-2.98557100	-0.00444400
C	-0.49070000	-1.33041400	-0.20881300
H	-0.32544300	-0.58961100	-2.33392700
H	0.25543800	-2.53291100	1.49966200
C	-2.01450800	1.68753500	-1.09926200
C	-2.20477500	0.99396200	0.13367200
C	-1.32214000	2.89818700	-0.85288700
H	-2.32336100	1.33390500	-2.07207500
C	-1.62001500	1.82228900	1.14200100
C	-1.08350100	2.98290300	0.54075700
H	-1.06576200	3.64807400	-1.58580100
H	-1.56754800	1.58410900	2.19433700
H	-0.59693100	3.79973500	1.05139100
C	2.63059600	-1.44984700	1.99237500
H	-3.63852400	-1.15281000	2.29012300
H	-2.56335100	-2.53772400	2.06402700
H	-1.92834600	-1.02372500	2.71196600
C	-3.47791900	-1.59608200	-0.98115400
H	-3.42013500	-2.68675500	-0.98829900
H	-4.50193700	-1.30558800	-0.73473200
H	-3.26382000	-1.24695000	-1.99357900
H	1.90622500	1.73774900	-0.68515000
H	1.46373700	1.09844900	1.20021900
B	2.34280700	1.44871600	0.42572100
H	2.94053900	2.38276700	0.87834300
N	3.29931400	0.19183600	0.23771900
H	2.71090100	-0.57763200	-0.13381600
C	3.85037300	-0.27974400	1.53100000
H	4.47003100	-1.16271700	1.37463500
H	4.44376500	0.51664400	1.97687000
H	3.02340200	-0.53229100	2.18979000
C	4.36720600	0.44207300	-0.75790400
H	4.98425900	1.27235300	-0.41819400
H	4.98205500	-0.44947900	-0.88287800
H	3.90634000	0.70157700	-1.70806900
Si	-2.25673800	-0.87087900	0.24675000



optimized geometry of 1c·2a

C	-0.45396400	-1.31638000	-0.11931000
C	-1.90380700	-1.35265600	1.91989400
C	-2.63421300	-2.48626800	-0.15170100
C	-1.77203300	1.32587600	-0.01829900
C	-3.25030500	-0.03529200	-1.50816800
C	-3.90839000	0.38537600	0.82361900
Mg	0.48879100	0.84153500	-0.15158600
C	0.03791800	-1.06691500	-1.45155800
C	0.60208600	-1.97808900	0.55992600
H	-1.36799700	-0.53425000	2.39783300
H	-2.91621100	-1.38175300	2.31730800
H	-1.42334800	-2.28251700	2.22114600
H	-3.68850300	-2.49339500	0.13526000
H	-2.16626900	-3.37903500	0.26562000
H	-2.56942700	-2.56245300	-1.23547100
C	-1.25182000	2.05200400	-1.12124600
C	-1.16761600	1.87471600	1.14718800
H	-2.50030700	-0.32830900	-2.23892100
H	-4.04590800	-0.77850800	-1.53730500
H	-3.67845600	0.91457000	-1.83055200
H	-4.57171600	-0.48054800	0.87952200
H	-4.47902900	1.21630000	0.40548600
H	-3.62417300	0.66636200	1.83549600
H	-0.53136400	-0.66911300	-2.27536700
C	1.33913200	-1.60096700	-1.56456300
H	1.94467300	-1.58446700	-2.45948600
C	1.68161200	-2.17250300	-0.32576300
C	-0.33267900	3.02125100	-0.64379800
H	0.21548400	3.72720400	-1.24785900
C	-0.28533300	2.91353700	0.76127900
H	0.31274200	3.51555700	1.42714300
H	-1.35890600	1.57438900	2.16386900
H	0.57585400	-2.32476700	1.58023200
H	-1.49465400	1.88763800	-2.15819900
H	2.57706300	-2.74024000	-0.10419900
B	2.83867100	1.22283000	0.33463100
H	2.01052500	0.91254300	1.17933300
H	3.43916800	2.19906700	0.68192300
H	2.34541400	1.40085500	-0.77071400
N	3.81102100	-0.02929100	0.19352900
H	3.18393700	-0.80600000	-0.07878900
C	4.43797800	-0.39957100	1.48326000
H	3.65183900	-0.61049700	2.20457600
H	5.06675800	-1.28188600	1.35949100
H	5.03935400	0.43520800	1.83924700
C	4.81287800	0.15067500	-0.88170800
H	5.43597500	-0.73954900	-0.97288700
H	4.29135200	0.32947200	-1.81910300

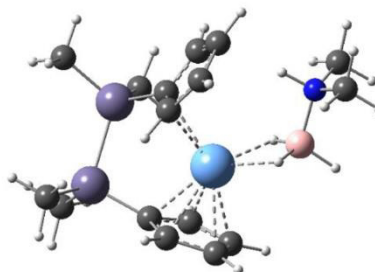


SUPPORTING INFORMATION

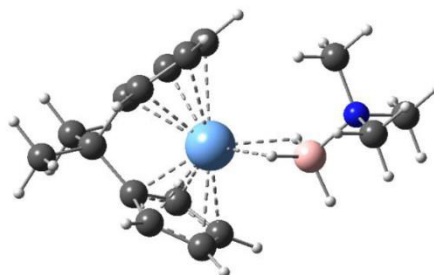
H	5.43424900	1.01319800	-0.64649700
C	-2.68558700	0.111110100	-0.07991300
C	-1.90654200	-1.22966400	0.38302800

optimized geometry of 1d·2a

C	-0.16916200	-1.32076100	0.33235100
C	1.29380600	-1.71563900	-2.31481700
C	2.24953500	-3.21904700	0.18747400
C	1.65146000	1.70286800	0.01283500
C	3.62307000	0.17574200	1.79109000
C	4.22926100	0.53205500	-1.21709600
Mg	-0.60457700	0.99935700	0.16025400
C	-0.44955600	-0.83883800	1.67124700
C	-1.31989800	-2.07314500	-0.04312800
H	0.89994100	-0.78334000	-2.72609200
H	2.24145800	-1.92870100	-2.81437700
H	0.59499400	-2.51629300	-2.57079100
H	3.23140900	-3.41250500	-0.25265000
H	1.59279100	-4.05623300	-0.06193700
H	2.36455300	-3.19682800	1.27320900
C	1.06592300	2.37324200	1.12491200
C	0.95980800	2.17781100	-1.14502600
H	2.85722100	0.01376300	2.55236100
H	4.32907100	-0.65542000	1.85295200
H	4.15856900	1.09497600	2.04135600
H	4.91057700	-0.32189500	-1.24373100
H	4.81411300	1.42732700	-0.99181800
H	3.80572900	0.65239200	-2.21650400
H	0.26391600	-0.34955900	2.32238000
C	-1.71677100	-1.29226100	2.06358500
H	-2.19012600	-1.09860500	3.01534000
C	-2.24684300	-2.06865400	1.01064400
C	0.05073300	3.24349900	0.66060800
H	-0.56115700	3.89100900	1.26959400
C	-0.00892200	3.12717100	-0.74751600
H	-0.68530600	3.65816300	-1.39901700
H	1.15586900	1.87385500	-2.16293800
H	-1.44021000	-2.59437300	-0.98288000
H	1.35133100	2.23991800	2.15756300
H	-3.18299400	-2.61345700	1.03762600
B	-2.93556900	1.29267500	-0.53348300
H	-2.05258600	0.92561800	-1.29396700
H	-3.50419000	2.24621900	-0.98553300
H	-2.52131900	1.54237100	0.59022700
N	-3.93047600	0.06043700	-0.37495700
H	-3.35871900	-0.69969000	0.03308600
C	-4.44074000	-0.41930800	-1.67959100
H	-3.59503800	-0.69502000	-2.30512700
H	-5.08829700	-1.28522200	-1.53800900
H	-4.99765700	0.38314200	-2.16059600
C	-5.02641700	0.34348100	0.58000300
H	-5.66571900	-0.53266700	0.69246800
H	-4.59093400	0.60202000	1.54229700
H	-5.61247700	1.18362800	0.21115800
Si	1.52268600	-1.59061300	-0.44016000
Si	2.86656900	0.28757000	0.06572800

optimized geometry of 1a·(Me₃NBH₃)

Mg	0.06770200	0.21927400	0.00580800
C	3.01969300	-0.23202100	-0.00903600
C	2.24755600	1.09676800	-0.00131600
C	1.88833100	-1.27266100	-0.00189700
C	1.60034600	1.65491600	-1.13549400
C	1.12740800	-1.62971000	1.14167200
C	0.57298500	2.52291200	-0.69528700
C	-0.10261700	-2.18630200	0.71940100
C	1.10987600	-1.62721500	-1.13485300
C	1.61071400	1.64679900	1.14258600
C	-0.11365400	-2.18467600	-0.69464200
C	0.57915100	2.51766500	0.71798400
H	1.81985200	1.42435300	-2.16601500
H	1.41637800	-1.46922900	2.16817000
C	3.89764000	-0.36629200	-1.25950800
C	3.91647100	-0.36963800	1.22766700
H	-0.07320600	3.11478400	-1.32452300
H	-0.85398300	-2.61033700	1.36824100
H	1.38393500	-1.46659600	-2.16546300
H	1.83912600	1.40815000	2.16931700
H	-0.87539200	-2.60725100	-1.33168100
H	-0.06107800	3.10525600	1.35729800
H	4.39419100	-1.33863000	-1.27113100
H	4.65992900	0.41503000	-1.26958400
H	3.32235400	-0.27752600	-2.18004600
H	4.67904100	0.41145900	1.22782200
H	4.41276100	-1.34218400	1.22950200
H	3.35533200	-0.28267100	2.15705700
H	-1.76931700	0.56773200	-1.02108400
H	-1.75828800	0.53129700	1.00544300
B	-2.36380600	0.86648700	0.00057500
H	-2.63507700	2.03223200	0.02628800
N	-3.75409400	0.03266600	-0.00371900
C	-3.51085800	-1.43427700	-0.07276300
H	-2.97310400	-1.65991800	-0.98841900
H	-2.89244900	-1.72945300	0.76910100
H	-4.46122300	-1.97005300	-0.05219200
C	-4.56085700	0.45127700	-1.18388700
H	-5.51062000	-0.08597500	-1.19629700
H	-4.73954500	1.52210100	-1.12866300

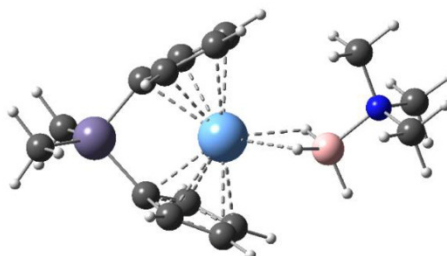


SUPPORTING INFORMATION

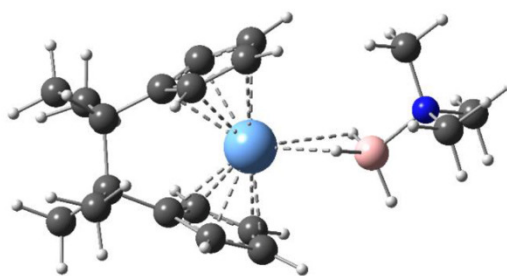
H	-4.00004200	0.23066600	-2.08889400
C	-4.50659800	0.34694200	1.24282300
H	-4.66629100	1.42086000	1.29784600
H	-5.46542500	-0.17405100	1.24143300
H	-3.91610900	0.03064200	2.09923300

optimized geometry of 1b·(Me₃NBH₃)

Mg	-0.04767800	0.20447400	-0.00922500
C	2.07089800	1.36528000	-0.00117500
C	1.71105900	-1.43129900	0.00225100
C	1.34905900	1.80857700	-1.14858800
C	0.88187700	-1.70413500	1.12927000
C	0.19947200	2.51657300	-0.73343000
C	-0.38280600	-2.14879300	0.68318500
C	0.91595800	-1.71584900	-1.14547500
C	1.32784500	1.82035900	1.12790300
C	-0.36037500	-2.15714000	-0.73338700
C	0.18595200	2.52406000	0.68362100
H	1.62044100	1.61019900	-2.17546300
H	1.16528400	-1.57185800	2.16328500
C	4.17771600	-0.33419500	-1.52172700
C	4.14050100	-0.32403300	1.57936400
H	-0.52776900	2.99042700	-1.37410700
H	-1.19390500	-2.47689100	1.31396400
H	1.22852100	-1.58918000	-2.17169900
H	1.58060100	1.63443500	2.16186000
H	-1.15151700	-2.49080900	-1.38842500
H	-0.55225100	3.00540200	1.30559100
H	4.69411000	-1.29636300	-1.54938800
H	4.92870100	0.45846200	-1.55272400
H	3.57288400	-0.25428400	-2.42763300
H	4.88907500	0.47022000	1.62451300
H	4.65781800	-1.28504500	1.62456700
H	3.51373800	-0.24070100	2.46992300
H	-1.93178300	0.40318400	-0.87472700
H	-2.08899400	0.60302100	1.13582500
B	-2.60145400	0.82167100	0.05791000
H	-2.86748700	1.98014800	-0.09845700
N	-4.00134800	-0.00574600	0.00950800
C	-3.79006900	-1.44983900	0.29775700
H	-3.07484000	-1.85114000	-0.41272200
H	-3.38118400	-1.55199500	1.29860600
H	-4.73708100	-1.98750900	0.22526000
C	-4.60622200	0.14163500	-1.34298000
H	-5.57425500	-0.36114700	-1.37794100
H	-4.72803300	1.19979300	-1.56075800
H	-3.93560700	-0.29739900	-2.07759800
C	-4.92647800	0.56433800	1.02740400
H	-5.09657900	1.61411900	0.80299700
H	-5.87355600	0.02174900	1.01783900
H	-4.46355600	0.48204600	2.00783600
Si	3.11069700	-0.18528200	0.01572900

optimized geometry of 1c·(Me₃NBH₃)

C	1.70045100	1.41309900	0.03500100
C	3.24413300	0.63664200	1.83000000
C	4.15908800	1.33002300	-0.35227500
C	1.39655700	-1.41773600	-0.06232400
C	3.22299900	-1.00967500	-1.70864000
C	3.77223500	-1.86056200	0.53772200
Mg	-0.38091300	0.22003300	-0.06664700
C	1.13359400	1.70188900	-1.23175200
C	0.80409100	1.93885100	1.00655300
H	2.48181200	0.11078500	2.40192500
H	4.21044200	0.19176900	2.06322900
H	3.26844600	1.66867200	2.18207700
H	5.08761800	0.76759500	-0.22546300
H	4.29554200	2.30907500	0.11048600
H	3.99970900	1.49501100	-1.41619200
C	0.48451100	-1.70912500	-1.11092300
C	0.68832500	-1.60923700	1.15087400
H	2.65517300	-0.33089600	-2.34175800
H	4.28119000	-0.79356600	-1.84631600
H	3.04737500	-2.02455700	-2.06804000
H	4.80606300	-1.50952100	0.49632600
H	3.73735000	-2.85078900	0.07962500
H	3.49180800	-1.97729400	1.58281400
H	1.55210700	1.44057500	-2.18933000
C	-0.09398500	2.38309600	-1.04637600
H	-0.74692800	2.74083800	-1.82677400
C	-0.29355900	2.54021300	0.34353700
C	-0.76492300	-2.07082500	-0.55041900
H	-1.63180400	-2.38407900	-1.10824800
C	-0.63683300	-2.00634900	0.85651300
H	-1.39394800	-2.24885500	1.58679700
H	1.08238100	-1.46976500	2.14391400
H	0.92968200	1.89655100	2.07595200
H	0.69373900	-1.66383300	-2.16681000
H	-1.12846400	3.03235200	0.81460400
C	2.96603600	0.61321200	0.31490900
C	2.82438000	-0.91050300	-0.22393600
H	-2.32458600	0.44768100	0.69351000
H	-2.67791900	0.55441400	-1.29913400
B	-3.08020900	0.82221500	-0.19027100
H	-3.35181700	1.98367300	-0.05244100
N	-4.45824600	-0.02015700	0.03909500
C	-5.48003500	0.46350700	-0.92861300
H	-6.41293000	-0.08807500	-0.79689400

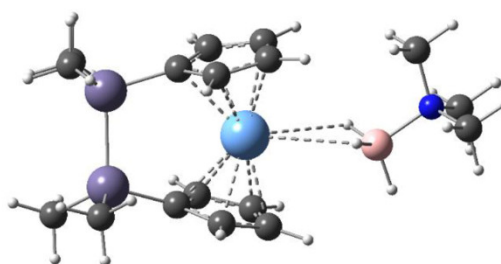


SUPPORTING INFORMATION

H	-5.64854900	1.52452000	-0.76324000
H	-5.10364400	0.31841900	-1.93831400
C	-4.23334400	-1.47472800	-0.17295600
H	-3.89208000	-1.63067700	-1.19247500
H	-3.46273400	-1.81718700	0.51099800
H	-5.15928600	-2.02725600	-0.00255600
C	-4.94804700	0.20429600	1.42608200
H	-5.08723300	1.27117200	1.58217500
H	-5.89176300	-0.32174600	1.58299700
H	-4.20106900	-0.16191500	2.12615200

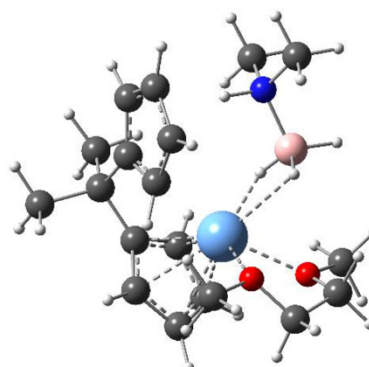
optimized geometry of 1d·(Me₃NBH₃)

C	1.37601500	1.74487600	-0.09171200
C	3.56421400	1.41174800	2.00492100
C	4.33769000	1.83681900	-0.95520600
C	1.07054900	-1.68077000	0.03543500
C	3.44049700	-1.75574300	-1.88623300
C	3.88816300	-2.28336900	1.12355300
Mg	-0.45808000	0.18999000	-0.06625400
C	0.69185000	1.82069900	-1.34025600
C	0.43389900	2.14766800	0.90091300
H	2.86217500	0.95206100	2.70440500
H	4.55882900	1.02051600	2.23019000
H	3.57129900	2.48785600	2.19577000
H	5.33109400	1.40165700	-0.82064800
H	4.40943900	2.91305900	-0.78001800
H	4.04758600	1.68612000	-1.99727500
C	0.14279900	-1.89835300	-1.02338800
C	0.30210800	-1.65033100	1.23554900
H	2.86891300	-1.20759500	-2.63857400
H	4.49601500	-1.51926300	-2.03817500
H	3.30078700	-2.82387100	-2.07078400
H	4.95358100	-2.04863800	1.05943900
H	3.76455600	-3.35672500	0.95982200
H	3.56040400	-2.05965300	2.14110900
C	1.11238200	1.57175900	-2.30364100
C	-0.63302300	2.26661100	-1.11985100
H	-1.38819900	2.43262300	-1.87164300
C	-0.79288500	2.47257800	0.27543400
C	-1.16138100	-2.00566100	-0.48631300
H	-2.06365500	-2.18551100	-1.04718500
C	-1.06181100	-1.85239600	0.92135300
H	-1.87523100	-1.89049100	1.62845400
H	0.69328400	-1.49119700	2.22962500
H	0.62671100	2.20117700	1.96188200
H	0.39230400	-1.96644400	-2.07144100
H	-1.69071300	2.81687000	0.76169500
H	-3.07167300	0.49619900	0.94356500
H	-3.15675300	0.41503700	-1.06704400
B	-3.69841100	0.79185200	-0.05085100
H	-3.98627400	1.96319300	-0.08318900
N	-5.11697800	-0.02852700	0.04544100
C	-5.96712600	0.31956100	-1.12261100
H	-6.91554300	-0.22047900	-1.07676300
H	-6.14926100	1.39124200	-1.11780000
H	-5.43527400	0.05695400	-2.03386600
C	-4.86215700	-1.49202800	0.04882100
H	-4.36807800	-1.76431300	-0.87962500
H	-4.20565900	-1.73493700	0.87984100
H	-5.80134000	-2.04153500	0.14233100
C	-5.82014200	0.35176400	1.29838200
H	-5.98332600	1.42667700	1.29713900
H	-6.77676400	-0.17043100	1.37095100
H	-5.19118500	0.09201700	2.14629500
Si	3.08133700	1.04854900	0.21462900
Si	2.89165400	-1.29179400	-0.13865500



optimized geometry of 1a·dme·2a

Mg	0.78760000	-0.22378500	-0.06599600
C	-1.57060100	0.86167700	2.23095600
C	-2.81729400	1.18820600	1.70240000
C	-1.07549900	-0.26784500	1.51319100
H	-1.07076200	1.36473100	3.04720500
C	-3.12307600	0.25551900	0.66519700
H	-3.44787400	2.01000300	2.01618400
C	-2.07387300	-0.65726500	0.56192200
H	-0.37963600	-0.97918200	1.93490900
H	-4.01906400	0.26747900	0.06154900
C	0.49101700	-2.65714400	0.14129300
C	-0.52275300	-2.12757600	-0.69583100
C	1.73898500	-2.53588500	-0.51686800
H	0.33788800	-3.09558000	1.11492400
C	0.12180700	-1.67496500	-1.87841200
C	1.50714100	-1.94183300	-1.77067200
H	2.69110600	-2.88137500	-0.14163100
H	-0.36409000	-1.23234700	-2.73308000
H	2.25308700	-1.73410900	-2.52152100
C	-1.98087300	-1.90333200	-0.31540300
C	-2.84370300	-1.74497300	-1.57706500
H	-2.73890600	-2.61737800	-2.22476600
H	-3.89692500	-1.64225600	-1.31125700
H	-2.55876600	-0.85958800	-2.14732700
C	-2.51454400	-3.11709600	0.47813800
H	-3.56000000	-2.95505800	0.74710200
H	-2.43795600	-4.03251200	-0.11371600
H	-1.95561700	-3.25859100	1.40304500
H	0.74722100	2.17457300	0.22512400
H	0.06780400	1.14341900	-1.38475200

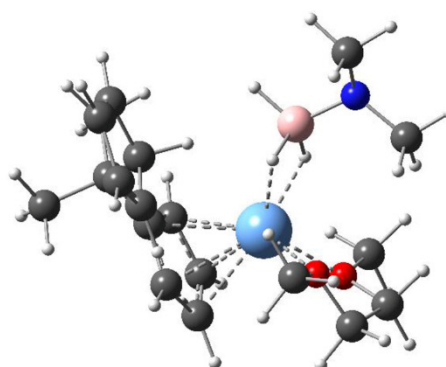


SUPPORTING INFORMATION

B	0.14897400	2.22791600	-0.82645400
H	0.64922800	3.02146700	-1.58660800
N	-1.34409600	2.67292200	-0.51541000
H	-1.74242000	2.00169900	0.16467900
C	-2.20989600	2.63243200	-1.71507500
H	-3.23301000	2.89720800	-1.44790100
H	-1.82461600	3.33091000	-2.45702900
H	-2.19756900	1.62415100	-2.11927900
C	-1.39470900	3.99628800	0.14516800
H	-0.96838700	4.74463800	-0.52153700
H	-2.42518300	4.25667300	0.38823000
H	-0.81102100	3.94862500	1.06105200
O	2.16965600	0.13795100	1.65739900
C	2.02118200	-0.54969300	2.90550200
H	0.99650000	-0.41034400	3.23198000
H	2.23200100	-1.61481600	2.77971200
H	2.69951200	-0.11999300	3.64632400
C	3.53715800	0.26658200	1.26197200
H	4.12423100	0.68925400	2.08320900
H	3.93416400	-0.72021700	1.00173300
C	3.58167900	1.18464000	0.06847500
H	3.25301300	2.19486100	0.33536400
H	4.60412800	1.22937200	-0.32147400
O	2.70264300	0.63379200	-0.89923400
C	2.88250600	1.14598600	-2.21893500
H	2.79432500	2.23374200	-2.22444500
H	3.85960700	0.84045000	-2.60377300
H	2.09427800	0.71920300	-2.83117300

optimized geometry of I1·dme

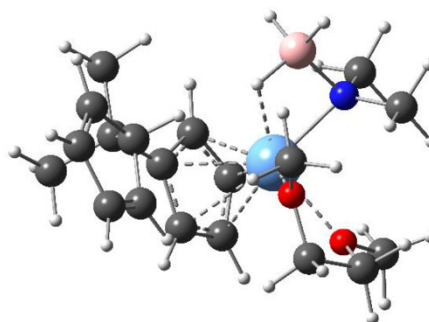
Mg	1.02058500	-0.53633300	-0.23198000
C	-3.72591600	1.08504700	2.00947900
C	-4.39985400	1.72328100	0.87928600
C	-2.70776100	0.33896300	1.54980400
H	-4.01182000	1.20542500	3.04565000
C	-3.79167000	1.35152600	-0.25918600
H	-5.23947000	2.39931700	0.96367500
C	-2.62429800	0.44845400	0.04937200
H	-2.04247600	-0.25593600	2.15106700
H	-4.04266300	1.68980200	-1.25196900
C	-0.64434000	-2.08086400	0.66467900
C	-1.17940600	-1.58314100	-0.55573700
C	0.54804100	-2.79045500	0.39092900
H	-1.09971400	-2.00061100	1.63742000
C	-0.28326700	-1.98986300	-1.58005300
C	0.77256300	-2.73551500	-1.00199500
H	1.16439700	-3.29784500	1.11738600
H	-0.37969300	-1.76852300	-2.62946600
H	1.59531200	-3.18719200	-1.53440400
C	-2.52704900	-0.89515400	-0.76105200
C	-2.72671500	-0.57929900	-2.25218900
H	-2.62046100	-1.48533600	-2.84955200
H	-3.72858500	-0.19061700	-2.43054800
H	-2.00156400	0.15485200	-2.60639500
C	-3.64934300	-1.85144300	-0.31272900
H	4.62425400	-1.36734300	-0.40572100
H	-3.64620400	-2.74977600	-0.93284100
H	-3.52016200	-2.15846700	0.72442500
H	0.30264600	1.20131300	-0.37464600
H	-0.04649300	1.47229600	-2.29962000
B	0.85825900	1.48291300	-1.50316300
H	1.63408500	0.54365000	-1.77335600
N	1.60236400	2.78033100	-1.40483800
H	-1.71700800	1.01506600	-0.20319100
C	0.75081900	3.93388100	-1.20441000
H	0.28522300	3.95784600	-0.19849100
H	1.31675800	4.86544200	-1.32196200
H	-0.05695200	3.93153000	-1.93730600
C	2.73833900	2.80140900	-0.51962700
H	3.28919700	3.74524600	-0.60276400
H	2.46811700	2.67452700	0.55015600
H	3.42750000	1.99389100	-0.77993400
O	1.66682400	0.19449700	1.67221000
C	0.75255500	0.64670700	2.67353900
H	-0.06791600	1.13001500	2.15071500
H	0.37446400	-0.19626200	3.25720800
H	1.24797300	1.36670100	3.32861600
C	2.84119000	-0.44902300	2.16417000
H	3.23912100	0.09237000	3.02675100
H	2.59733200	-1.47382700	2.46184200
C	3.84624000	-0.42827500	1.03504000
H	4.19117900	0.59307000	0.85048500
H	4.70525800	-1.06224100	1.27647500
O	3.17759400	-0.92312800	-0.12174000
C	3.99742100	-1.00547300	-1.28864800
H	4.38410800	-0.02024400	-1.55892200
H	4.82329900	-1.70041100	-1.11639900
H	3.36396800	-1.37414300	-2.09073800



SUPPORTING INFORMATION

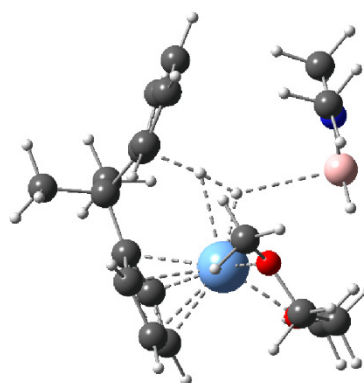
optimized geometry of I2-dme

Mg	-1.03154100	-0.32797500	0.01519000
C	3.62058000	2.13564100	-0.35561300
C	4.43943600	1.58110900	0.72303400
C	2.55171800	1.34450900	-0.54735500
H	3.84996200	3.04186300	-0.89999700
C	3.86313200	0.45464100	1.17380900
H	5.35258400	2.02501700	1.09485900
C	2.58189700	0.19323700	0.42255400
H	1.76534800	1.50152200	-1.26462800
H	4.22424500	-0.16358500	1.98036300
C	0.46628300	-0.75780700	-1.90643500
C	0.99776800	-1.43056900	-0.76879200
C	-0.78685500	-1.32102000	-2.22636700
H	0.96691100	0.00071800	-2.48552000
C	0.03436100	-2.40063800	-0.39042500
C	-1.06569600	-2.32888200	-1.28105700
H	-1.42498700	-1.01242900	-3.03944800
H	0.10393900	-3.06684400	0.45203700
H	-1.94471500	-2.95446900	-1.24776700
C	2.38769500	-1.25373800	-0.16524000
C	2.58582100	-2.26319300	0.97728800
H	2.42358000	-3.27852700	0.61424000
H	3.60244300	-2.21508500	1.36627400
H	1.88998300	-2.07979200	1.79783300
C	3.44723200	-1.51997600	-1.25050400
H	4.45453700	-1.39497600	-0.84707200
H	3.34690100	-2.53955700	-1.62635900
H	3.33204500	-0.83874300	-2.09290900
H	-0.72325600	-1.87833900	2.73435000
H	-0.09458000	-0.24905600	1.82512700
B	-1.01992500	-0.73075900	2.50740000
H	-1.11960300	-0.05707000	3.51216100
N	-2.34355800	-0.65981700	1.61464000
H	1.75951500	0.32290500	1.13986500
C	-3.18381300	0.48175400	1.97377100
H	-4.04326500	0.56839000	1.30028400
H	-3.56174700	0.39646500	3.00071700
H	-2.60825000	1.40457100	1.91287100
C	-3.13550600	-1.88988700	1.66460000
H	-3.49967200	-2.09612900	2.68008700
H	-4.00424700	-1.82149000	0.99968000
H	-2.52542800	-2.73269300	1.34731500
O	-0.63088100	1.78127700	0.22538800
C	-0.04385100	2.52843600	1.30301800
H	0.11745700	1.82500300	2.11333500
H	0.90442200	2.96157500	0.98183000
H	-0.73491500	3.30878600	1.63111000
C	-1.08361300	2.55314000	-0.89085700
H	-0.96546900	3.62012900	-0.69781700
H	-0.48139100	2.27868900	-1.75947900
C	-2.53712700	2.20691700	-1.13029100
H	-3.17225700	2.58176500	-0.31964200
H	-2.87953600	2.63410700	-2.07972400
O	-2.59337700	0.78833300	-1.16945700
C	-3.83794100	0.23743800	-1.58121700
H	-4.64548900	0.56138300	-0.91883300
H	-4.06484000	0.53371800	-2.60937000
H	-3.73226700	-0.84316000	-1.52848400



optimized geometry of TS1

Mg	1.05305400	-0.65453500	-0.11395800
C	-2.78830800	1.05138900	1.83040200
C	-3.38162900	1.53703600	0.62777900
C	-2.15759300	-0.14551300	1.55193600
H	-2.83637300	1.53509800	2.79682800
C	-3.11880500	0.63182300	-0.38212400
H	-3.92870700	2.46351900	0.52405000
C	-2.28103300	-0.42404600	0.13957100
H	-1.67654000	-0.78518900	2.27478400
H	-3.40954400	0.74081500	-1.41589900
C	0.04064900	-2.52709900	0.89844400
C	-0.63772900	-2.29005900	-0.32517700
C	1.38612800	-2.88948900	0.62026900
H	-0.39893500	-2.48428100	1.88074500
C	0.31386700	-2.50275500	-1.36044000
C	1.55174800	-2.88180900	-0.77988900
H	2.13204300	-3.16651000	1.35018800
H	0.12526200	-2.41241700	-2.41780700
H	2.45879100	-3.11653100	-1.31514900
C	-2.08526500	-1.81921400	-0.48600100
C	-2.44852900	-1.77064000	-1.97727300
H	-2.27058700	-2.73842500	-2.44925600
H	-3.50304200	-1.52453800	-2.10114500
H	-1.86387700	-1.01630800	-2.50789500
C	-3.02214800	-2.83193300	0.20519400
H	-4.05891900	-2.50083100	0.11712000
H	-2.92551800	-3.82177500	-0.24956400
H	-2.78862600	-2.92020600	1.26579300
H	-0.16865000	0.59825600	-0.67769600
H	0.84399000	2.56788600	-2.59420500
B	0.84256900	2.80409300	-1.42250300
H	1.77206600	2.49968000	-0.73739700
N	-0.20211300	3.50889100	-0.85118100
H	-1.03348500	0.25754700	-0.33629200
C	-1.39653100	3.90531400	-1.58355900
H	-2.26374200	3.34940900	-1.21668800

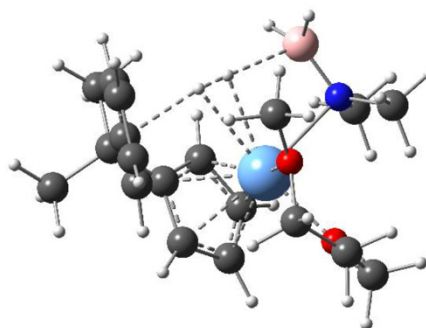


SUPPORTING INFORMATION

H	-1.59066700	4.97505500	-1.45159500
H	-1.26766800	3.70025400	-2.64410700
C	-0.31683800	3.73268900	0.58117800
H	-0.53028400	4.78542400	0.79407600
H	-1.12948200	3.12440200	0.99372800
H	0.61319200	3.45591000	1.07477400
O	1.83271700	0.42270800	1.51616700
C	1.19402000	0.47135000	2.80040200
H	0.13227300	0.60676300	2.60628200
H	1.36203000	-0.46044400	3.34612800
H	1.58420300	1.31754600	3.36973600
C	3.25799400	0.31509400	1.54454200
H	3.67544900	1.00297600	2.28445700
H	3.53821100	-0.71057100	1.80607100
C	3.74995300	0.68428600	0.16200900
H	3.60193100	1.74989100	-0.02856200
H	4.81061600	0.43542000	0.05732000
O	2.97600600	-0.07351500	-0.76932700
C	3.30243700	0.15162900	-2.14545500
H	3.12286100	1.19456500	-2.41060000
H	4.34481000	-0.11896700	-2.32854600
H	2.64809500	-0.49357600	-2.72697600

optimized geometry of TS2

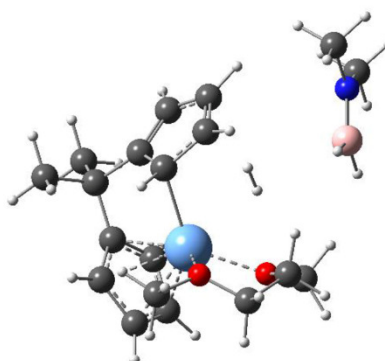
Mg	-0.81956700	-0.29819400	-0.04817900
C	2.98953000	2.36661500	-0.61739500
C	3.48924900	2.24201100	0.69801400
C	2.44961000	1.13002500	-1.00140400
H	3.02092300	3.26016500	-1.22707800
C	3.27694300	0.92323700	1.11632700
H	3.94585400	3.02677000	1.28448600
C	2.62373900	0.20666700	0.06559000
H	2.06733100	0.89682100	-1.98381200
H	3.57466300	0.51144600	2.06907000
C	0.47010700	-1.39696800	-1.76434400
C	1.04435800	-1.68770100	-0.49480600
C	-0.80880600	-1.98783700	-1.83601800
H	0.95577200	-0.86633900	-2.56535100
C	0.07253000	-2.43072100	0.22542400
C	-1.07315300	-2.61186900	-0.60215600
H	-1.47003600	-1.94995000	-2.68770600
H	0.19621200	-2.83059700	1.21823700
H	-1.95234600	-3.18374400	-0.35095100
C	2.45308100	-1.31088800	-0.04099800
C	2.77353800	-1.99556000	1.29719800
H	2.66193100	-3.07781800	1.20708400
H	3.80303000	-1.78482400	1.58617000
H	2.12524900	-1.65366400	2.10458000
C	3.45849700	-1.85337300	-1.08662900
H	4.47622000	-1.60459100	-0.78035300
H	3.37189600	-2.93941700	-1.18449100
H	3.28692900	-1.40433000	-2.06388300
H	-0.62661500	-1.19623800	3.27420500
H	0.51284700	0.13152100	1.85721400
B	-1.10655300	-0.18199400	2.88530900
H	-0.88324500	0.86256100	3.40714800
N	-2.18652000	-0.26003600	1.91673000
H	1.17397800	0.32950100	1.41997400
C	-3.08931800	0.90037400	1.82164800
H	-3.66812300	0.85456400	0.89849900
H	-3.78724000	0.91848400	2.66453200
H	-2.51201600	1.81917200	1.81969000
C	-2.95104700	-1.52194000	1.87903900
H	-3.66165800	-1.56317100	2.71096000
H	-3.51062800	-1.60296200	0.94625000
H	-2.27310500	-2.36601300	1.94857100
O	-0.71102000	1.81587900	0.04539800
C	0.04412400	2.70558200	0.90646000
H	-0.01223400	2.29331200	1.90679100
H	1.08160400	2.75517200	0.57630600
H	-0.43183900	3.68890800	0.88577900
C	-0.93066800	2.31222900	-1.27963000
H	-0.86867500	3.40112900	-1.29740000
H	-0.16050600	1.90980000	-1.94131500
C	-2.31827300	1.85802800	-1.67171300
H	-3.08646700	2.41487300	-1.12439500
H	-2.47850700	1.98456700	-2.74676300
O	-2.40732300	0.47381400	-1.32206700
C	-3.58023000	-0.17867100	-1.80195200
H	-4.47541600	0.30538700	-1.40038400
H	-3.60842400	-0.15508400	-2.89405500
H	-3.53027800	-1.20986000	-1.46568900



SUPPORTING INFORMATION

optimized geometry of 1a·dme + 4a + H₂

Mg	-0.96478200	0.67129300	0.15063400
C	1.25465200	-1.02694000	-1.28271700
C	1.62774200	-2.13045100	-0.53750500
C	-0.17779700	-0.91293800	-1.21904500
H	1.91048700	-0.37857300	-1.84663400
C	0.45087200	-2.74897900	-0.01906500
H	2.63826300	-2.46259800	-0.35034700
C	-0.65905200	-2.03962800	-0.44754400
H	-0.75353600	-0.47099700	-2.03033300
H	0.44119100	-3.60007600	0.64608000
C	-3.27452400	0.10945200	-0.14876800
C	-2.62875100	-0.95236900	0.52883700
C	-3.26712900	1.25956000	0.68366500
H	-3.70305700	0.05623000	-1.13688200
C	-2.22556900	-0.44758500	1.79336200
C	-2.62163300	0.91083800	1.88925300
H	-3.72290700	2.21222100	0.45949600
H	-1.68860500	-1.00116100	2.54715500
H	-2.49304500	1.55280700	2.74777000
C	-2.13010900	-2.25808700	-0.09017200
C	-2.29702700	-3.41432800	0.90620300
H	-3.35018800	-3.53967300	1.16470900
H	-1.93343400	-4.34860600	0.47396300
H	-1.74042300	-3.23391500	1.82565700
C	-2.92895400	-2.59944900	-1.36250500
H	-2.56979200	-3.54149900	-1.77977600
H	-3.99526600	-2.69696500	-1.14335300
H	-2.80583500	-1.83552500	-2.13096900
H	0.94441400	-0.46234000	2.11858800
H	3.61493800	1.31043800	1.07783200
B	4.03097100	0.86578700	0.04937100
H	3.88137400	1.45548300	-0.98004500
N	4.71995700	-0.33226500	0.05830800
H	1.15759000	-0.84653300	1.51235600
C	4.91632700	-1.13229600	1.25830500
H	4.39801300	-2.09193400	1.17076900
H	5.98045400	-1.33408800	1.41878500
H	4.52247900	-0.60661200	2.12492200
C	5.23580200	-0.96748800	-1.14616900
H	6.31009500	-1.15729100	-1.05291900
H	4.73604100	-1.92453400	-1.32192800
H	5.06509200	-0.32576200	-2.00714800
O	-0.77539800	2.21184900	-1.39027300
C	-1.78505700	2.42303100	-2.37726200
H	-2.21166500	1.44955300	-2.60078000
H	-2.56879000	3.07983800	-1.99062200
H	-1.34261200	2.85369700	-3.27881800
C	-0.11804400	3.39941500	-0.95591800
H	0.34524000	3.91108400	-1.80579800
H	-0.84676400	4.06828300	-0.48398300
C	0.93463900	2.96952900	0.03790300
H	1.72441000	2.38981800	-0.44188200
H	1.37423200	3.84368500	0.52267100
O	0.26890200	2.14672700	1.00765300
C	0.77238000	2.22844900	2.34437700
H	1.80442700	1.87968500	2.38638800
H	0.70299400	3.25930400	2.69980400
H	0.13637800	1.59094800	2.95220600



SUPPORTING INFORMATION

References

- [1] S. Liu, A. M. Invergo, J. P. McInnis, A. R. Mouat, A. Motta, T. L. Lohr, M. Delferro, T. J. Marks, *Organometallics* **2017**, *36*, 4403-4421.
- [2] a) P. Perrotin, B. Twamley, P. J. Shapiro, *Acta Cryst. E* **2007**, *63*, m1277-m1278. b) P. J. Shapiro, S.-J. Lee, P. Perrotin, T. Cantrell, A. Blumenfeld, B. Twamley, *Polyhedron* **2005**, *24*, 1366-1381. c) W. Haider, V. Huch, A. Schäfer, *Dalton Trans.* **2018**, *47*, 10425-10428.
- [3] C. A. Jaska, K. Temple, A. J. Lough, I. Manners, *J. Am. Chem. Soc.* **2003**, *125*, 9424-9434.
- [4] Y. Duan, R. Bai, J. Tian, L. Chen, X. Yan, *Synth. Commun.* **2014**, *44*, 2555-2564.
- [5] H. C. Johnson, A. P. M. Robertson, A. B. Chaplin, L. J. Sewell, A. L. Thompson, M. F. Haddow, I. Manners, A. S. Weller, *J. Am. Chem. Soc.* **2011**, *133*, 11076-11079.
- [6] A. C. A. Ried, L. J. Taylor, A. M. Geer, H. E. L. Williams, W. Lewis, A. J. Blake, D. L. Kays, *Chem. Eur. J.* **2019**, *25*, 6840-6846.
- [7] G. R. Fulmer, A. J. M. Miller, N. H. Sherden, H. E. Gottlieb, A. Nudelman, Brian M. Stoltz, J. E. Bercaw, K. I. Goldberg, *Organometallics* **2010**, *29*, 2176-2179.
- [8] G. Sheldrick, *Acta Cryst. A* **2008**, *64*, 112-122.
- [9] P. Perrotin, P. J. Shapiro, M. Williams, B. Twamley, *Organometallics* **2007**, *26*, 1823-1826.
- [10] D. J. Liptrot, M. S. Hill, M. F. Mahon, D. J. MacDougall, *Chem. Eur. J.* **2010**, *16*, 8508-8515.
- [11] Gaussian 09, Revision D.01, M. J. Frisch, G. W. Trucks, H. B. Schlegel, G. E. Scuseria, M. A. Robb, J. R. Cheeseman, G. Scalmani, V. Barone, G. A. Petersson, H. Nakatsuji, X. Li, M. Caricato, A. Marenich, J. Bloino, B. G. Janesko, R. Gomperts, B. Mennucci, H. P. Hratchian, J. V. Ortiz, A. F. Izmaylov, J. L. Sonnenberg, D. Williams-Young, F. Ding, F. Lipparini, F. Egidi, J. Goings, B. Peng, A. Petrone, T. Henderson, D. Ranasinghe, V. G. Zakrzewski, J. Gao, N. Rega, G. Zheng, W. Liang, M. Hada, M. Ehara, K. Toyota, R. Fukuda, J. Hasegawa, M. Ishida, T. Nakajima, Y. Honda, O. Kitao, H. Nakai, T. Vreven, K. Throssell, J. A. Montgomery, Jr., J. E. Peralta, F. Ogliaro, M. Bearpark, J. J. Heyd, E. Brothers, K. N. Kudin, V. N. Staroverov, T. Keith, R. Kobayashi, J. Normand, K. Raghavachari, A. Rendell, J. C. Burant, S. S. Iyengar, J. Tomasi, M. Cossi, J. M. Millam, M. Klene, C. Adamo, R. Cammi, J. W. Ochterski, R. L. Martin, K. Morokuma, O. Farkas, J. B. Foresman, D. J. Fox, Gaussian, Inc., Wallingford CT, **2016**.
- [12] a) A. D. Becke, *J. Chem. Phys.* **1993**, *98*, 5648-5652; b) C. Lee, W. Yang, R. G. Parr, *Phys. Rev. B* **1988**, *37*, 785-789; c) S. H. Vosko, L. Wilk, M. Nusair, *Can. J. Phys.* **1980**, *58*, 1200-1211; d) P. J. Stephens, F. J. Devlin, C. F. Chabalowski, M. J. Frisch, *J. Phys. Chem.* **1994**, *98*, 11623-11627; e) S. Grimme, J. Antony, S. Ehrlich, H. Krieg, *J. Chem. Phys.* **2010**, *132*, 154104.
- [13] a) F. Weigend, R. Ahlrichs, *Phys. Chem. Chem. Phys.* **2005**, *7*, 3297-3305; b) F. Weigend, *Phys. Chem. Chem. Phys.* **2006**, *8*, 1057-1065.

6.2 Cross-Dehydrocoupling of Amines and Silanes Catalyzed by Magnesocenophanes

Supplementary Information

for

**Cross-Dehydrocoupling of Amines and Silanes
Catalyzed by Magnesocenophanes**

Lisa Wirtz[§], Jessica Lambert[§], Bernd Morgenstern, and André Schäfer*

Saarland University, Faculty of Natural Sciences and Technology, Department of Chemistry, Campus Saarbrücken, 66123 Saarbrücken,
Federal Republic of Germany

Experimental Details	S3 – S9
NMR Spectra	S10 – S15
Kinetic Plots	S16 – S17
XRD Data	S18 – S24
Computational Details	S25
References	S26

Experimental Details

Synthesis of magnesocenophane-*tert*-butylamine-complex (**1a**·(*t*BuNH₂)₂):

In a Schlenk flask **1a** (1.00 g; 5.14 mmol) was dissolved in 20 mL of thf and *tert*-butylamine (22.0 mL; 208 mmol) was added. The mixture was stirred for approximately 15 min and subsequently stored at 248 K to obtain **1a**·(*t*BuNH₂)₂ as colorless crystals.

Yield: 1.57 g / 90%.

¹H NMR (400.13 MHz, thf-*d*₆): δ = 1.03 (s, 18 H, C(CH₃)₃), 1.21 (bs, 3 H, NH₂), 1.70 (s, 6 H, C-CH₃), 5.66 (t, ³J_{HH} = 2.6 Hz, 4 H, Cp-*H*), 5.77 (t, ³J_{HH} = 2.6 Hz, 4 H, Cp-*H*). ¹³C{¹H} NMR (100.62 MHz, thf-*d*₆): δ = 29.6 (C(CH₃)₂), 32.3 (C(CH₃)₃), 37.6 (C(CH₃)₂), 48.4 (C(CH₃)₃), 97.0 (Cp), 108.6 (Cp), 141.7 (Cp).

Deuteration of benzylamine

The deuteration of benzylamine was carried out according to a modified literature procedure.¹ Benzylamine (2.0 mL; 18.3 mmol) was stirred in D₂O (8.0 mL; 443 mmol) over night. The solution was extracted with Dichloromethane, dried over MgSO₄ and the volatiles were removed in vacuo. The procedure was repeated several times to obtain a deuteration degree of 75-80%.

General procedure for catalytic amine borane dehydrocoupling

In a closed 5 mL volume vial in a glovebox, 5 mol% catalyst and the corresponding amine borane (Me₂NH·BH₃: 849 μmol; ⁱPr₂NH·BH₃: 695 μmol; (C₅H₁₀)NH·BH₃: 808 μmol; (C₄H₈O)NH·BH₃: 817 μmol) were dissolved in 1 mL of dme and stirred for 16 h. Conversions were determined by integration of the ¹¹B NMR spectra.

The signals observed for tetramethyldiborazane,² diisopropylaminoborane,² and piperidinyldiborazane³ were in agreement with literature data.

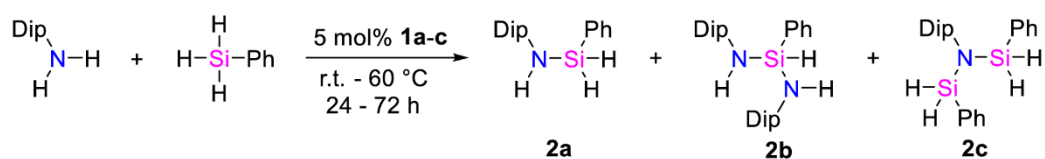
Morpholinylidiborazane:

¹H NMR (300.13 MHz, C₆D₆): δ = 2.09-3.50 (m, BH₂), 2.50 (t, ³J_{HH} = 4.7 Hz, 4 H, CH₂), 3.45 (t, ³J_{HH} = 4.7 Hz, 4 H, CH₂). ¹¹B NMR (96.29 MHz, C₆D₆): δ = 2.1 (t, ¹J_{BH} = 115 Hz, BH₂). ¹³C{¹H} NMR (75.48 MHz, C₆D₆): δ = 59.0 (CH₂), 64.3 (CH₂).

General procedure for catalytic amine silane cross-dehydrocoupling

In a closed Schlenk tube, 5 mol% catalyst, 2.06 mmol (1 eq) amine, 2.06 mmol (1 eq) silane and 2 mL of the respective solvent were stirred for the time and temperature indicated. Subsequently, 0.3 mL of the sample was removed, 0.3 mL of deuterated benzene were added, and the sample was examined by NMR spectroscopy. The conversion was determined by integration of the ²⁹Si{¹H} NMR spectrum. Signals were assigned based on the literature.

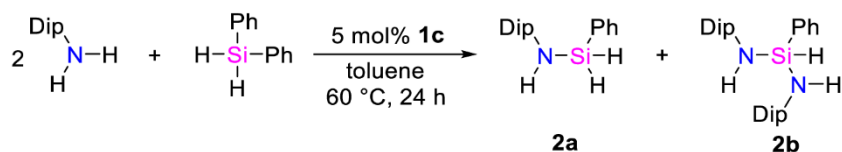
Diisopropylphenylamine + Phenylsilane



Conversion of PhSiH ₃ :	Catalyst	Solvent	Temp (K)	Time (h)	Yield (%) (Ratio)	
Catalyst 1a :	C ₇ H ₈		298 K	24 h	1% (100:0:0)	
	C ₇ H ₈		333 K	24 h	39% (79:21:0)	
	thf		298 K	24 h	4% (100:0:0)	
	thf		333 K	24 h	13% (82:0:18)	
	dme		298 K	24 h	13% (68:20:11)	
	dme		333 K	24 h	38% (31:54:15)	
	C ₆ H ₄ F ₂		298 K	24 h	6% (100:0:0)	
	C ₆ H ₄ F ₂		333 K	24 h	38% (75:25:0)	
	CH ₂ Cl ₂		298 K	24 h	13% (100:0:0)	
	Catalyst 1b :	C ₇ H ₈		298 K	24 h	8% (100:0:0)
		C ₇ H ₈		298 K	72 h	11% (100:0:0)
		C ₇ H ₈		333 K	24 h	42% (74:26:0)
		thf		298 K	24 h	1% (100:0:0)
		thf		333 K	24 h	15% (93:0:7)
dme			298 K	24 h	5% (100:0:0)	
dme			333 K	24 h	25% (51:34:15)	
C ₆ H ₄ F ₂			298 K	24 h	3% (100:0:0)	
C ₆ H ₄ F ₂			333 K	24 h	38% (78:22:0)	
CH ₂ Cl ₂			298 K	24 h	4% (100:0:0)	
Catalyst 1c :	C ₇ H ₈		298 K	24 h	14% (100:0:0)	
	C ₇ H ₈		298 K	72 h	13% (100:0:0)	
	C ₇ H ₈		333 K	24 h	38% (73:27:0)	
	thf		298 K	24 h	7% (100:0:0)	
	thf		333 K	24 h	33% (58:23:19)	
	dme		298 K	24 h	16% (46:54:0)	
	dme		333 K	24 h	35% (26:58:16)	
	C ₆ H ₄ F ₂		298 K	24 h	5% (100:0:0)	
	C ₆ H ₄ F ₂		333 K	24 h	37% (73:27:0)	
	CH ₂ Cl ₂		298 K	24 h	4% (100:0:0)	

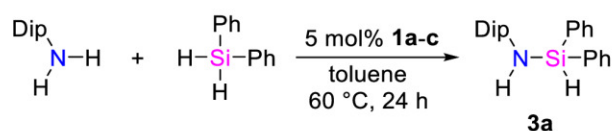
²⁹Si{¹H} NMR (79.49 MHz, C₆D₆): δ = -23.2 (**2c**),⁴ -27.0 (**2b**),⁴ -29.1 (**2a**).

2 eq. Diisopropylphenylamine + Phenylsilane



Conversion of Ph₂SiH₂: Catalyst **1c**: 64%

²⁹Si{¹H} NMR (79.49 MHz, C₆D₆): δ = -27.0 (**2b**),⁴ -28.7 (**2a**).

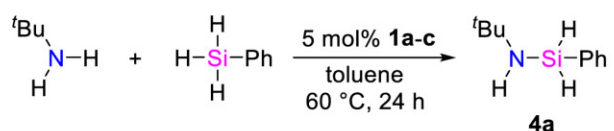
Diisopropylphenylamine + Diphenylsilane

Conversion of Ph ₂ SiH ₂ :	Catalyst 1a :	52%
	Catalyst 1b :	60%
	Catalyst 1c :	81%

¹H NMR (400.13 MHz, C₆D₆): δ = 1.13 (d, ³J_{HH} = 6.8 Hz, 12 H, CH₃), 3.07-3.11 (m, 1 H, NH), 3.51 (sept, ³J_{HH} = 6.8 Hz, 2 H, CH), 5.83 (d, ¹J_{SiH} = 212.2 Hz, ³J_{HH} = 3.4 Hz, 1 H, SiH), 7.03-7.07 (m, 3 H, Ph-H), 7.08-7.13 (m, 6 H, Ph-H), 7.61-7.66 (m, 4 H, Ph-H).⁴

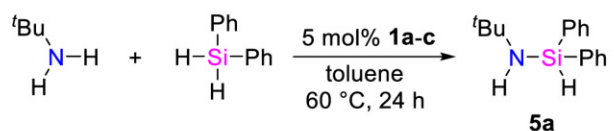
¹³C{¹H} NMR (100.62 MHz, C₆D₆): δ = 23.8 (CH₃), 28.9 (CH), 123.8, (Ph), 123.9 (Ph), 128.4 (Ph), 130.4 (Ph), 135.2 (Ph), 135.3 (Ph), 139.1 (Ph), 142.6.⁴

²⁹Si{¹H} NMR (79.49 MHz, C₆D₆): δ = -18.7.⁴

tert-Butylamine + Phenylsilane

Conversion of PhSiH ₃ :	Catalyst 1a :	28%
	Catalyst 1b :	17%
	Catalyst 1c :	19%

²⁹Si{¹H} NMR (79.49 MHz, C₆D₆): δ = -38.3.^{5,6}

t-Butylamine + Diphenylsilane

Conversion of Ph ₂ SiH ₂ :	Catalyst 1a :	57%
	Catalyst 1b :	27%
	Catalyst 1c :	94%

¹H NMR (400.13 MHz, C₆D₆): δ = 0.92 (bs, 1 H, NH), 1.08 (s, 9 H, CH₃), 5.68 (d, ¹J_{SiH} = 204.4 Hz, ³J_{HH} = 3.9 Hz, 1 H, SiH), 7.15-7.20 (m, 6 H, Ph-H), 7.63-7.68 (m, 4 H, Ph-H).

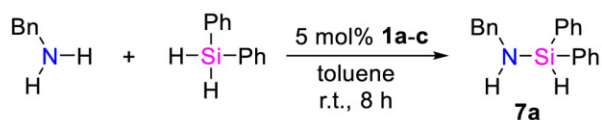
¹³C{¹H} NMR (100.62 MHz, C₆D₆): δ = 33.3 (C(CH₃)₃), 49.7 (C(CH₃)₃), 128.3 (Ph), 130.0 (Ph), 135.2 (Ph), 137.4 (Ph).

²⁹Si{¹H} NMR (79.49 MHz, C₆D₆): δ = -24.9.^{4,7,8}

Benzylamine + Phenylsilane

Conversion of PhSiH ₃ :	Catalyst 1a :	298 K	59%
		313 K	82%
	Catalyst 1b :	298 K	38%
		313 K	70%
	Catalyst 1c :	298 K	46%
		313 K	82%

²⁹Si{¹H} NMR (79.49 MHz, C₆D₆): δ = -19.2, -19.3 (**6c**),⁹ -20.5, -20.6, -22.3, -25.5 (**6a**),¹⁰ -32.3 (**6b**).¹⁰ (Note: This reaction has been reported before to give a complex mixture of multiple products.¹¹)

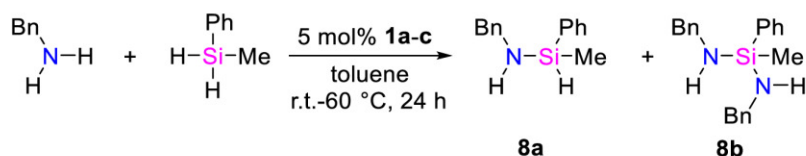
Benzylamine + Diphenylsilane

Conversion of Ph ₂ SiH ₂ :	Catalyst 1a :	298 K	90%
	Catalyst 1b :	298 K	82%
	Catalyst 1c :	298 K	84%

¹H NMR (400.13 MHz, C₆D₆): δ = 1.00 (bs, 1 H, NH), 3.85 (d, ³J_{HH} = 8.0 Hz, 2 H, CH₂), 5.62 (d, ¹J_{SiH} = 204.4 Hz, ³J_{HH} = 2.2 Hz, 1 H, SiH), 7.03-7.22 (m, 11 H, Ph-H), 7.62-7.68 (m, 4 H, Ph-H).^{10,12}

¹³C{¹H} NMR (100.62 MHz, C₆D₆): δ = 47.1 (CH₂), 126.9 (Ph), 127.4 (Ph), 128.3 (Ph), 128.6 (Ph), 130.3 (Ph), 135.3 (Ph), 135.6 (Ph), 143.6 (Ph).^{10,12}

²⁹Si{¹H} NMR (79.49 MHz, C₆D₆): δ = -17.0.¹⁰

Benzylamine + Methylphenylsilane

Conversion of PhMeSiH ₂ :	Catalyst 1a :	298 K	12%
		333 K	66%
	Catalyst 1b :	298 K	10%
		333 K	79%
	Catalyst 1c :	298 K	41%
		333 K	89%

8a (major product):

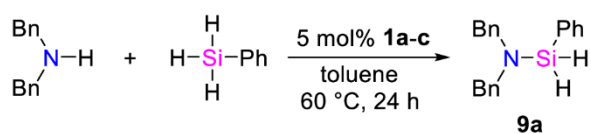
¹H NMR (400.13 MHz, C₆D₆): δ = 0.24 (s, 3 H, CH₃), 0.63 (bs, 1 H, NH), 3.73 (d, ³J_{HH} = 8.0 Hz, 2 H, CH₂), 5.07-5.11 (m, 1 H, SiH), 7.10-7.17 (m, 8 H, Ph-H), 7.51-7.56 (m, 2 H, Ph-H).¹⁰

¹³C{¹H} NMR (100.62 MHz, C₆D₆): δ = -2.8 (CH₃), 47.0 (CH₂), 126.7 (Ph), 126.8 (Ph), 127.4 (Ph), 128.2 (Ph), 130.0 (Ph), 134.5 (Ph), 137.7 (Ph), 143.9 (Ph).¹⁰

²⁹Si{¹H} NMR (79.49 MHz, C₆D₆): δ = -13.1.¹⁰

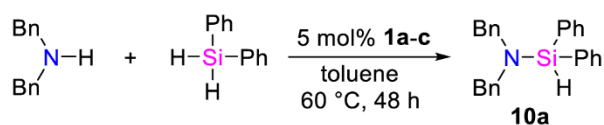
8b (minor product):

²⁹Si{¹H} NMR (79.49 MHz, C₆D₆): δ = -15.7.¹⁰

Dibenzylamine + Phenylsilane

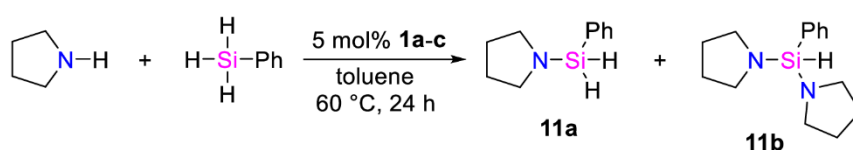
Conversion of PhSiH ₃ :	Catalyst 1a :	29%
	Catalyst 1b :	16%
	Catalyst 1c :	33%

²⁹Si{¹H} NMR (79.49 MHz, C₆D₆): δ = -19.9.⁵

Dibenzylamine + Diphenylsilane

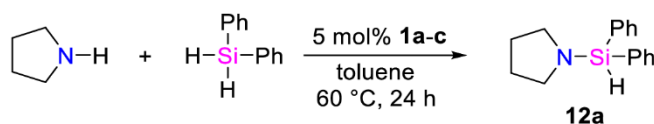
Conversion of Ph ₂ SiH ₂ :	Catalyst 1a :	10%
	Catalyst 1b :	20%
	Catalyst 1c :	32%

²⁹Si{¹H} NMR (79.49 MHz, C₆D₆): δ = -10.2.⁵

Pyrrolidine + Phenylsilane

Conversion of PhSiH ₃ :	Catalyst 1a :	26%
	Catalyst 1b :	17%
	Catalyst 1c :	13%

²⁹Si{¹H} NMR (59.63 MHz, C₆D₆): δ = -25.7 (**11b**),⁸ -29.2 (**11a**).⁸

Pyrrolidine + Diphenylsilane

Conversion of Ph ₂ SiH ₂ :	Catalyst 1a :	100%
	Catalyst 1b :	78%
	Catalyst 1c :	92%

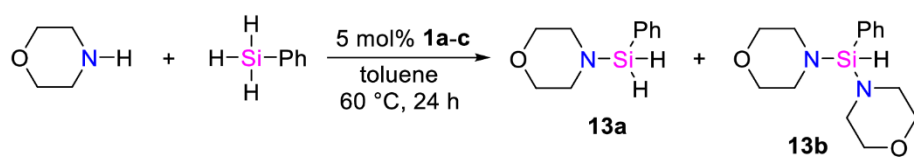
¹H NMR (400.13 MHz, C₆D₆): δ = 1.43-1.52 (m, 4 H, CH₂), 2.93-3.00 (m, 4 H, N-CH₂), 5.61 (s, ¹J_{SiH} = 203.0 Hz, 1 H, SiH), 7.03-7.21 (m, 6 H, Ph-H), 7.59-7.66 (m, 4 H, Ph-H).⁸

¹³C{¹H} NMR (100.62 MHz, C₆D₆): δ = 27.2 (CH₂), 48.4 (N-CH₂), 128.3 (Ph), 130.1 (Ph), 135.5 (Ph), 135.7 (Ph).⁸

²⁹Si{¹H} NMR (79.49 MHz, C₆D₆): δ = -18.0.⁸

6. Supporting Information

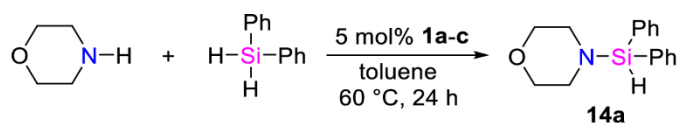
Morpholine + Phenylsilane



Conversion of PhSiH_3 :	Catalyst 1a :	38%
	Catalyst 1b :	50%
	Catalyst 1c :	37%

$^{29}\text{Si}\{^1\text{H}\}$ NMR (59.63 MHz, C_6D_6): $\delta = -19.6$ (**13b**),¹⁰ -23.0 (**13a**).¹⁰

Morpholine + Diphenylsilane



Conversion of Ph_2SiH_2 :	Catalyst 1a :	80%
	Catalyst 1b :	86%
	Catalyst 1c :	96%

^1H NMR (400.13 MHz, C_6D_6): $\delta = 2.75$ (t, $^3J_{\text{HH}} = 4.7$ Hz, 4 H, N- CH_2), 3.35 (t, $^3J_{\text{HH}} = 4.7$ Hz, 4 H, O- CH_2), 5.39 (s, $^1J_{\text{SiH}} = 205.6$ Hz, 1 H, SiH), 7.04-7.18 (m, 6 H, Ph- H), 7.53-7.59 (m, 4 H, Ph- H).¹⁰

$^{13}\text{C}\{^1\text{H}\}$ NMR (100.62 MHz, C_6D_6) $\delta = 46.8$ (N- CH_2), 68.4 (O- CH_2), 128.4 (Ph), 130.3 (Ph), 134.7 (Ph), 135.5 (Ph).¹⁰

$^{29}\text{Si}\{^1\text{H}\}$ NMR (79.49 MHz, C_6D_6): $\delta = -13.3$.¹⁰

General procedure for kinetic measurements

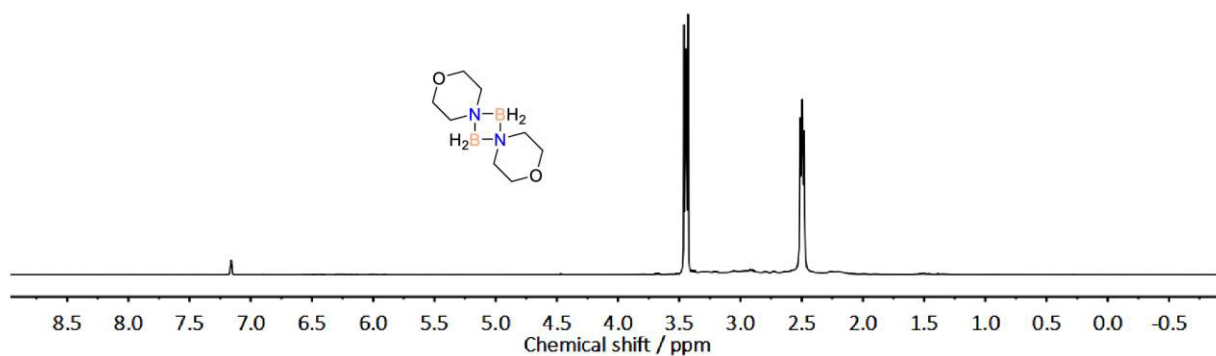
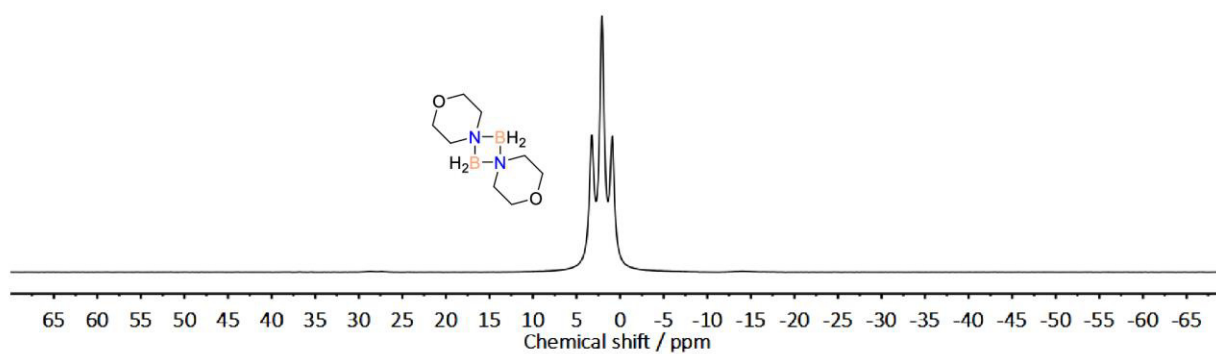
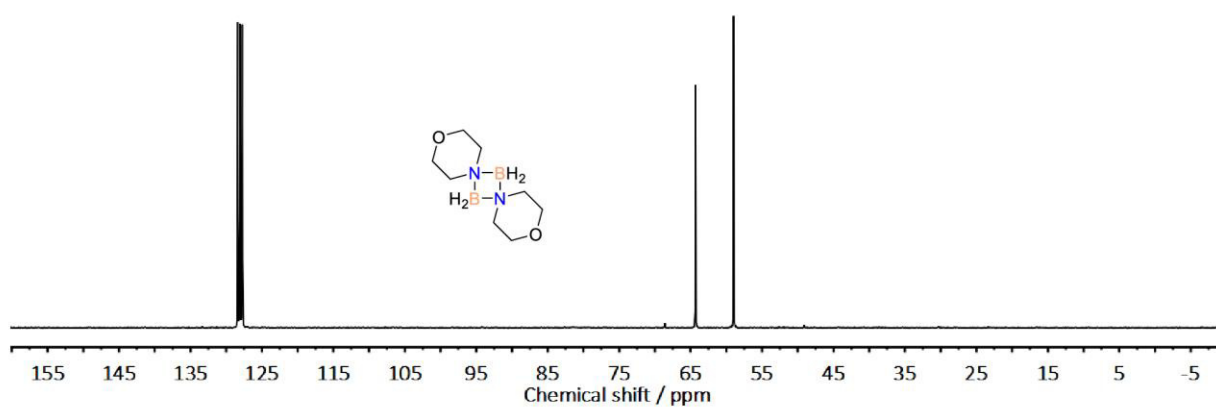
Gas evolution was measured with the *Man on the Moon X103*[®] kit supplied by Man on the Moon Tech, Universidad Zaragoza,¹³ equipped with a custom-made autoclave. All measurements were conducted under an inert gas atmosphere. In a typical run, the stock solutions of benzylamine and diphenylsilane were added to a stock solution of magnesocenophane in a 5 mL vial (2.5 mol%: benzylamine: 1.02 mmol, diphenylsilane: 1.00 mmol, magnesocenophane: 25.0 μ mol; 3.75 mol%: benzylamine: 1.12 mmol, diphenylsilane: 1.04 mmol, magnesocenophane: 39.0 μ mol; 5 mol%: benzylamine: 1.10 mmol, diphenylsilane: 1.02 mmol, magnesocenophane: 51.0 μ mol). The vial was placed in the autoclave and the autoclave sealed with the three-way valve closed to the sensor. The measurement was started approximately 10 min after the solutions had been combined, and the three-way valve was opened after data measurement had been engaged.

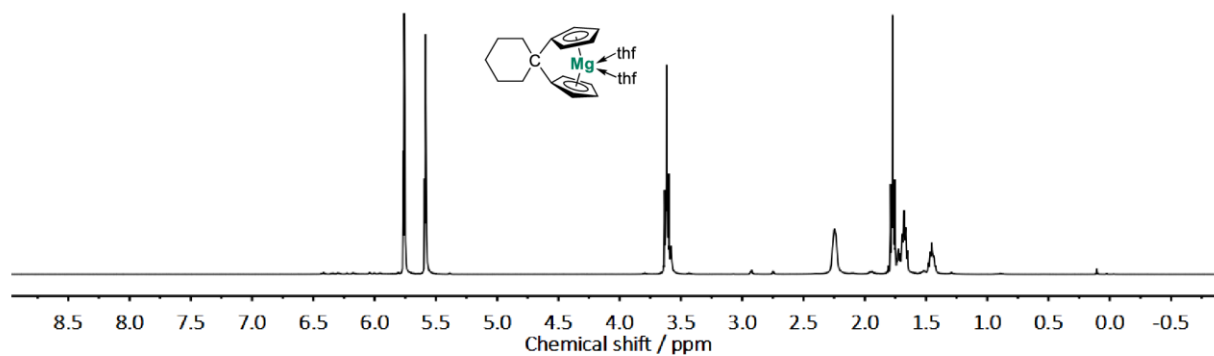
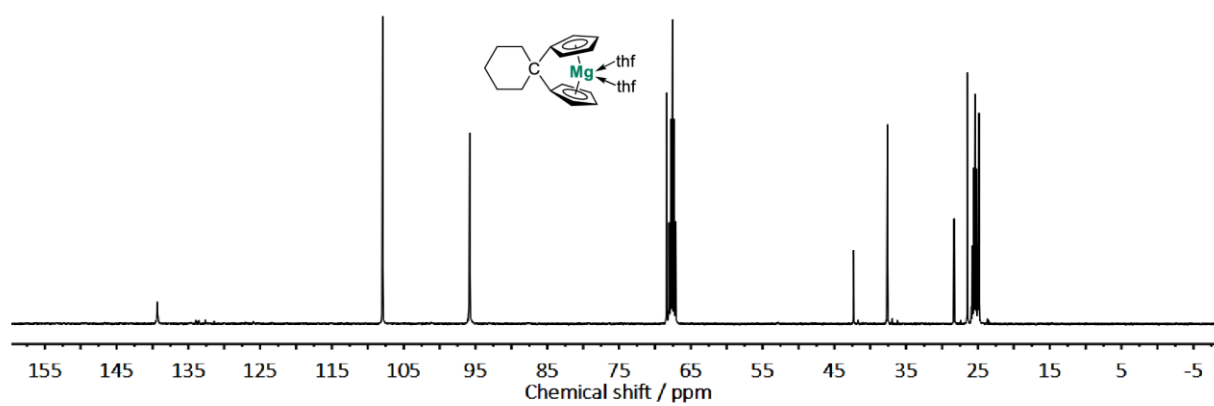
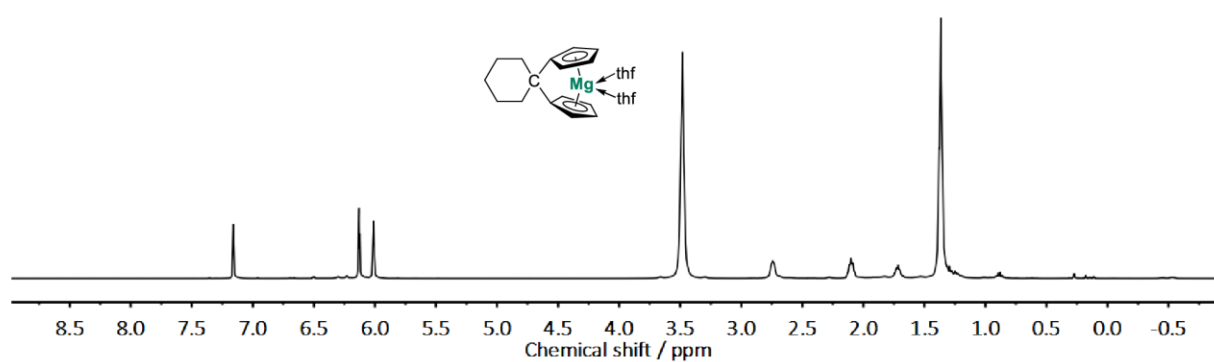
Concentrations were estimated by $p \cdot V = n \cdot R \cdot T$ from the measured hydrogen evolution (via pressure increase) and the volume of the reaction vessel.

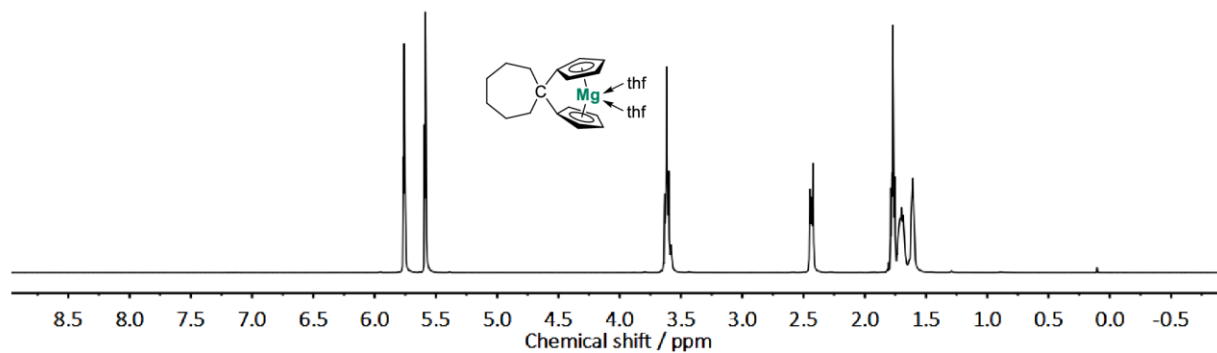
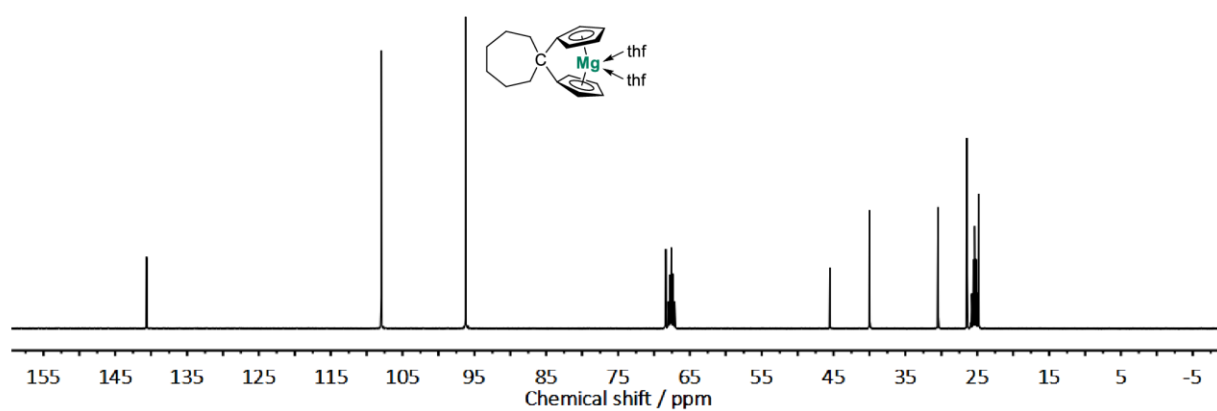
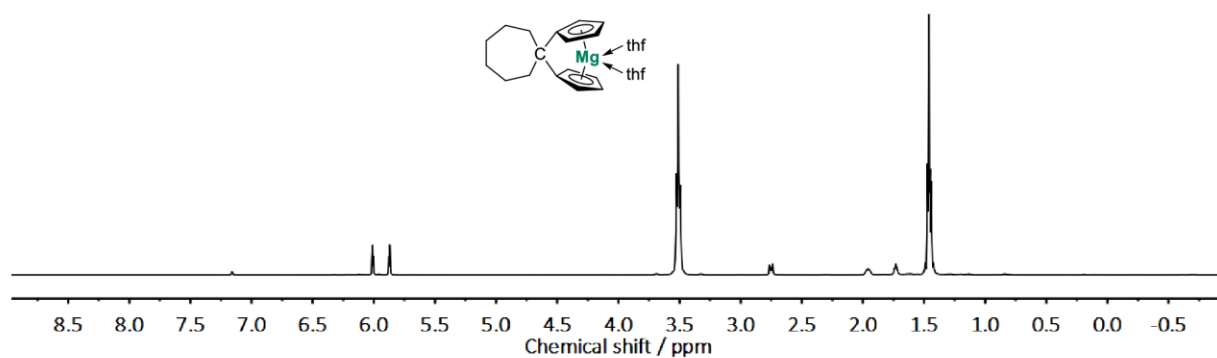


Figure S1. *Man on the Moon X103*[®] kit in a typical kinetic gas evolution measurement.

NMR Spectra

Figure S2. ¹H NMR (300.13 MHz, C₆D₆) spectrum of morpholinyldiborazane.Figure S3. ¹¹B NMR (96.29 MHz, C₆D₆) spectrum of morpholinyldiborazane.Figure S4. ¹³C NMR (75.48 MHz, C₆D₆) spectrum of morpholinyldiborazane.

Figure S5. ¹H NMR (400.13 MHz, thf-*d*₆) spectrum of **1b**·(thf)₂.Figure S6. ¹³C NMR (100.62 MHz, thf-*d*₆) spectrum of **1b**·(thf)₂.Figure S7. ¹H NMR (400.13 MHz, C₆D₆/thf) spectrum of **1b**·(thf)₂.

Figure S8. ^1H NMR (400.13 MHz, $\text{thf-}d_6$) spectrum of $1\text{c}\cdot(\text{thf})_2$.Figure S9. ^{13}C NMR (100.62 MHz, $\text{thf-}d_6$) spectrum of $1\text{c}\cdot(\text{thf})_2$.Figure S10. ^1H NMR (400.13 MHz, $\text{C}_6\text{D}_6/\text{thf}$) spectrum of $1\text{c}\cdot(\text{thf})_2$.

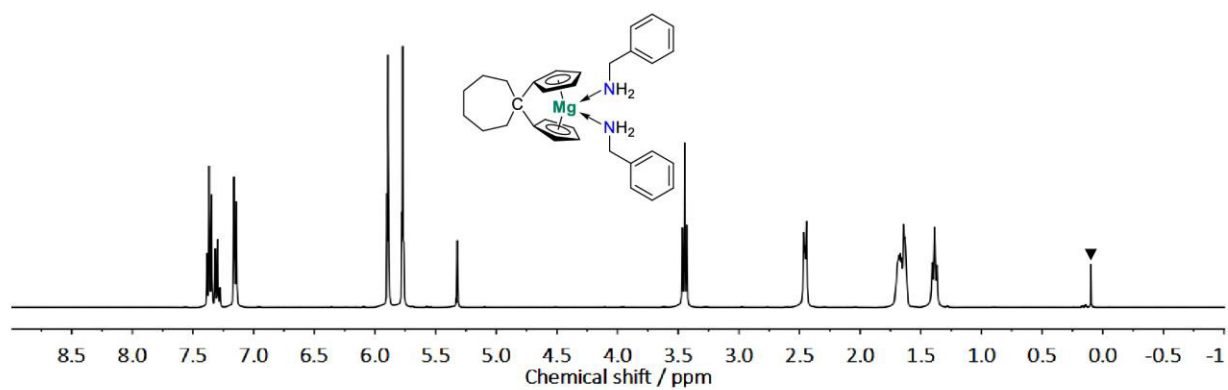


Figure S11. ¹H NMR (400.13 MHz, CD₂Cl₂) spectrum of **1c**·(BnNH₂)₂ (▼ silicon grease).

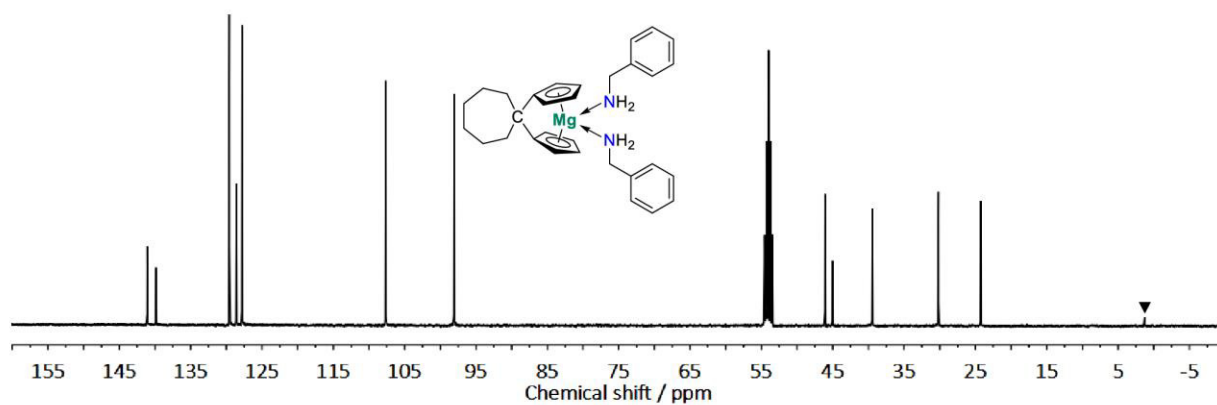
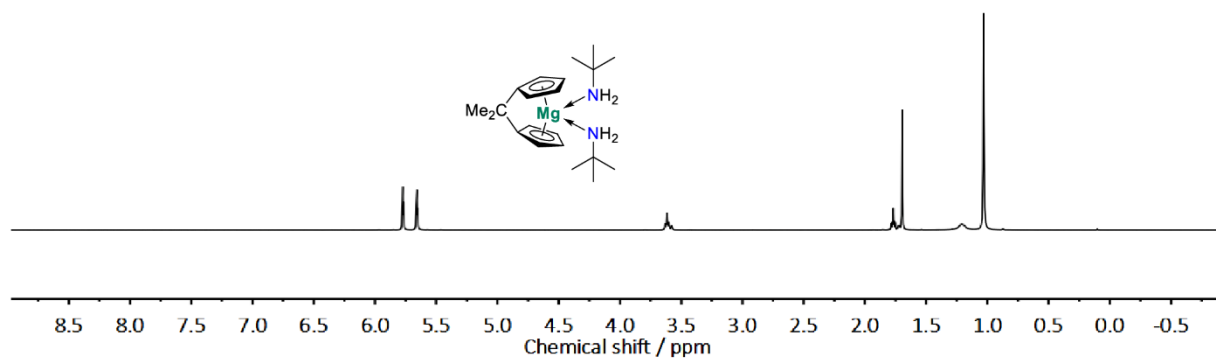
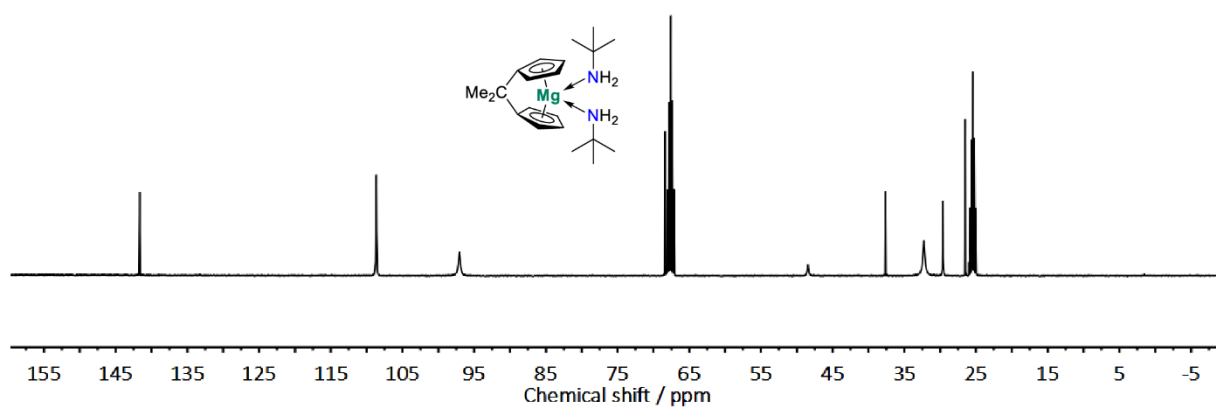


Figure S12. ¹³C NMR (100.62 MHz, CD₂Cl₂) spectrum of **1c**·(BnNH₂)₂ (▼ silicon grease).

Figure S13. ^1H NMR (400.13 MHz, $\text{thf-}d_6$) spectrum of $\mathbf{1a}\cdot(\text{tBuNH}_2)_2$.Figure S14. ^{13}C NMR (100.62 MHz, $\text{thf-}d_6$) spectrum of $\mathbf{1a}\cdot(\text{tBuNH}_2)_2$.

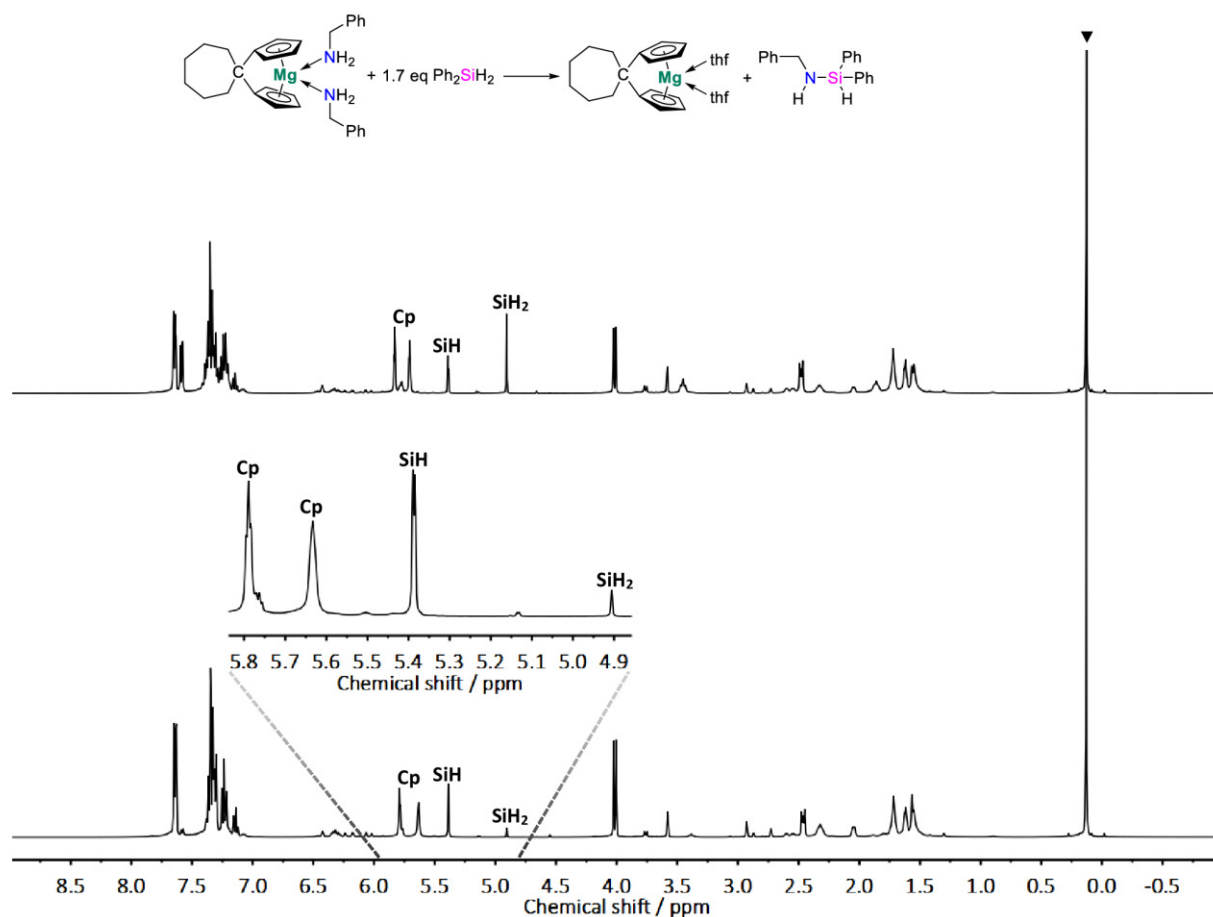


Figure S15. Top: ^1H NMR (400.13 MHz, thf-d_8) spectrum of the reaction of magnesocenophane bis(benzylamine) complex **1c**·(BnNH_2)₂ with phenylsilane after 24 h. Bottom: ^1H NMR (400.13 MHz, thf-d_8) spectrum of magnesocenophane bis(benzylamine) complex **1c**·(BnNH_2)₂ with phenylsilane after eleven days with expansion of the characteristic Cp/SiH-region (▼ silicon grease).

Kinetic Plots

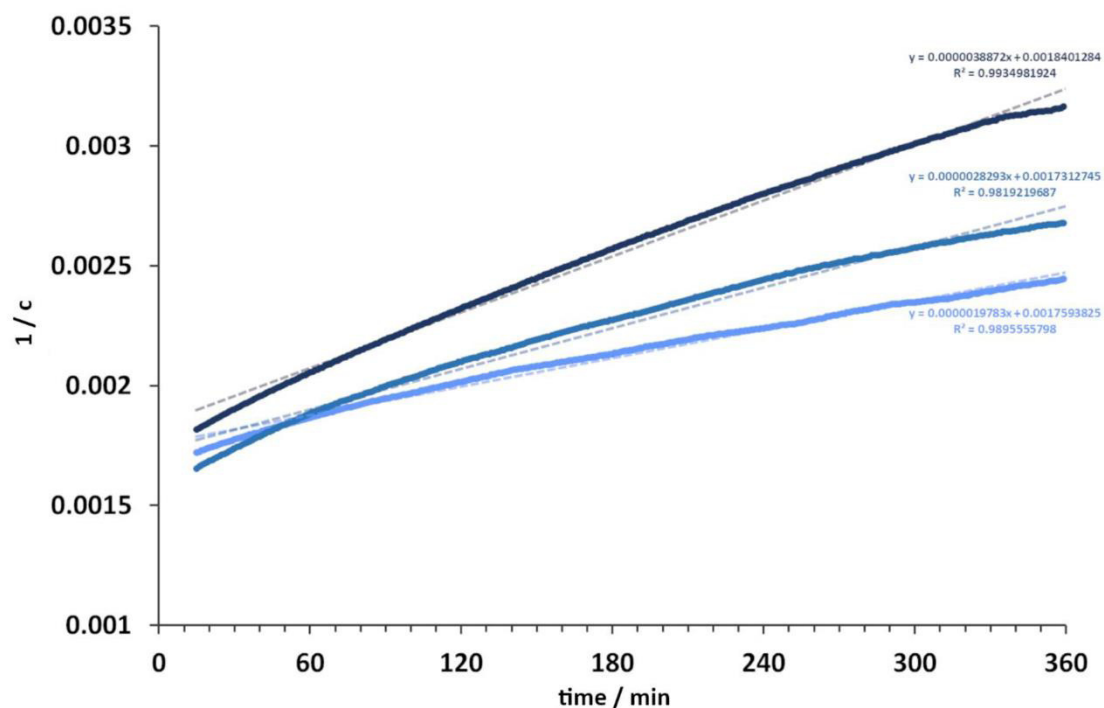


Figure S16. Plots of $1/c$ vs. t of the reaction of benzylamine and diphenylsilane catalyzed by 2.5 mol% (■), 3.75 mol% (■) and 5 mol% (■) of magnesocenophane **1c**.

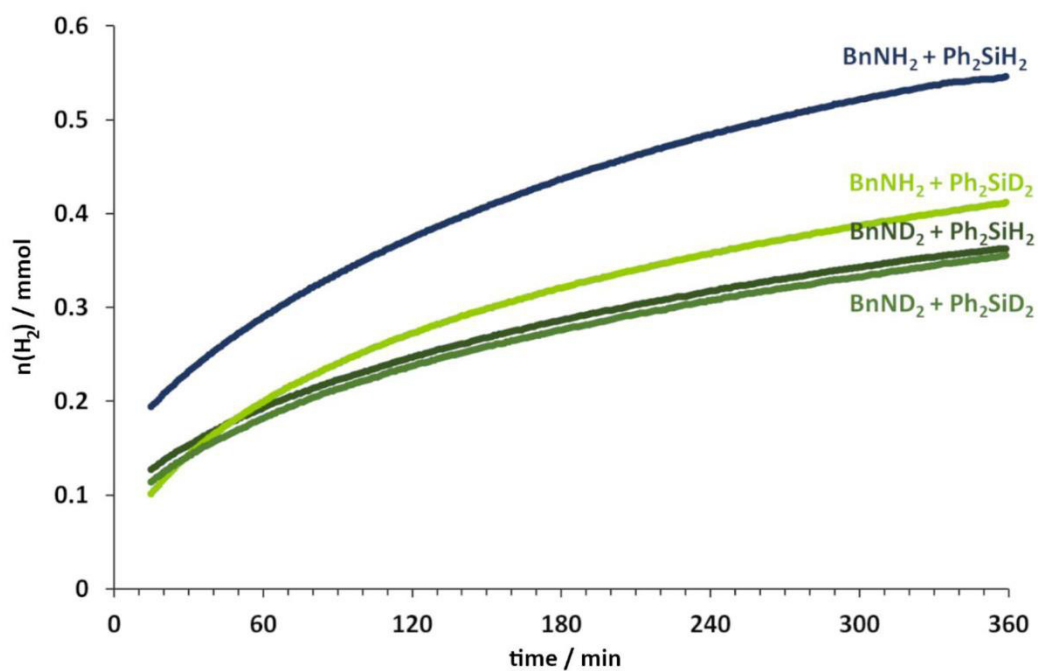


Figure S17. Plots of $n(\text{H}_2)$ vs. t of the reactions of non-deuterated and deuterated benzylamine and diphenylsilane catalyzed by 5 mol% of magnesocenophane **1c**.

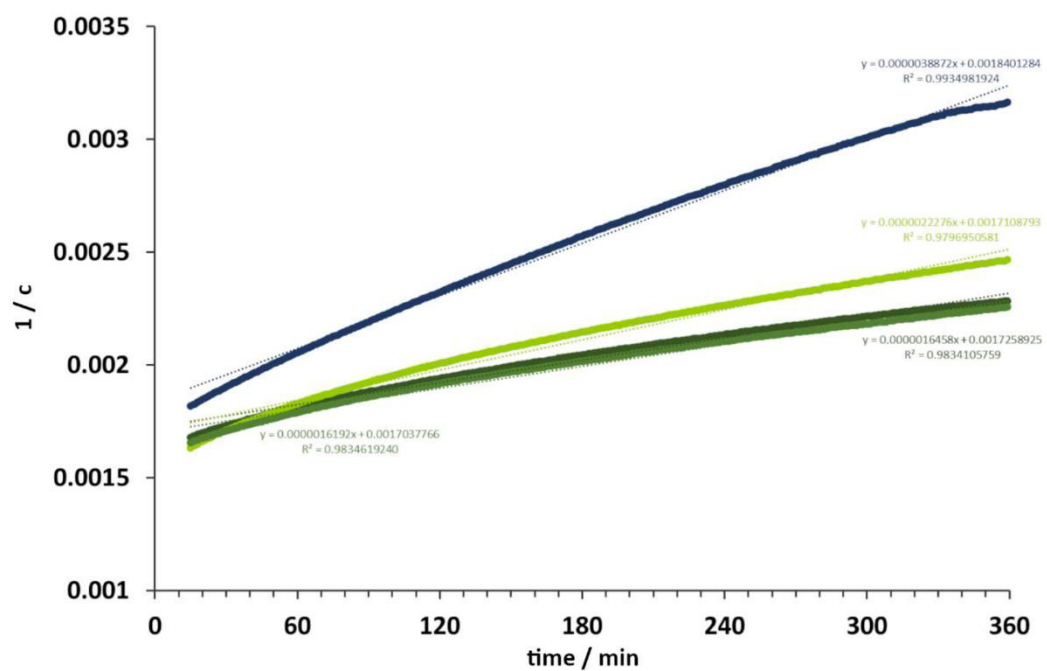


Figure S18. Plots of $1/c$ vs. t of the reactions of non-deuterated and deuterated benzylamine and diphenylsilane catalyzed by 5mol% of magnesocenophane **1c**.

XRD Data

Crystal structure data has been deposited with the Cambridge Crystallographic Data Centre (CCDC) and is available free of charge from the Cambridge Structural Database (see CCDC numbers).

crystal structure data of **1b**·(thf)₂

CCDC code	2059653	
Empirical formula	C ₂₄ H ₃₄ MgO ₂	
Formula weight	378.82	
Temperature	140(2) K	
Wavelength	0.71073 Å	
Crystal system	triclinic	
Space group	P-1	
Unit cell dimensions	a = 8.3371(11) Å	$\alpha = 88.825(5)^\circ$
	b = 14.2554(18) Å	$\beta = 85.592(4)^\circ$
	c = 18.114(2) Å	$\gamma = 78.525(4)^\circ$
Volume	2103.5(5) Å ³	
Z	4	
Density (calculated)	1.196 mg/m ³	
Absorption coefficient	0.100 mm ⁻¹	
F(000)	824	
Crystal size	0.567 x 0.181 x 0.124 mm ³	
Theta range for data collection	1.838 to 27.982°	
Index ranges	-10<=h<=10, -18<=k<=18, -3<=l<=23	
Reflections collected	33451	
Independent reflections	9985 [R(int) = 0.0680]	
Completeness to theta = 25.242°	99.5 %	
Absorption correction	semi-empirical from equivalents	
Max. and min. transmission	0.7456 and 0.6592	
Refinement method	full-matrix least-squares on F ²	
Data / restraints / parameters	9985 / 0 / 537	
Goodness-of-fit on F ²	1.069	
Final R indices [I>2σ(I)]	R1 = 0.0648, wR2 = 0.1468	
R indices (all data)	R1 = 0.0984, wR2 = 0.1623	
Extinction coefficient	n/a	
Largest diff. peak and hole	0.360 and -0.326 e.Å ⁻³	

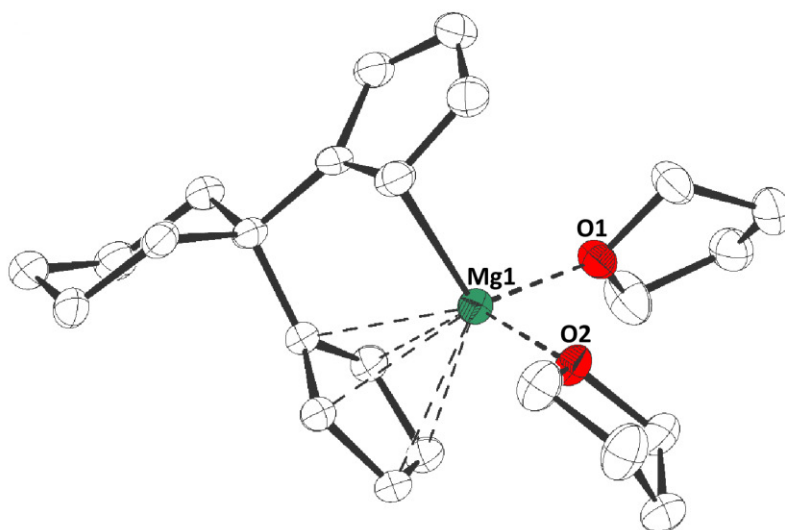


Figure S19. Molecular structure of **1b**·(thf)₂ in the crystal (displacement ellipsoids at 50% probability level; hydrogen atoms omitted for clarity).

crystal structure data of **1b**-dme

CCDC code	2059668	
Empirical formula	C ₂₀ H ₂₈ MgO ₂	
Formula weight	324.73	
Temperature	133(2) K	
Wavelength	0.71073 Å	
Crystal system	monoclinic	
Space group	P2 ₁ /n	
Unit cell dimensions	a = 13.5550(10) Å	$\alpha = 90^\circ$
	b = 20.1265(18) Å	$\beta = 117.303(3)^\circ$
	c = 14.5244(11) Å	$\gamma = 90^\circ$
Volume	3521.0(5) Å ³	
Z	8	
Density (calculated)	1.225 mg/m ³	
Absorption coefficient	0.108 mm ⁻¹	
F(000)	1408	
Crystal size	0.265 x 0.156 x 0.142 mm ³	
Theta range for data collection	1.874 to 27.158°	
Index ranges	-17<=h<=17, -25<=k<=25, -18<=l<=18	
Reflections collected	50156	
Independent reflections	7808 [R(int) = 0.0432]	
Completeness to theta = 25.242°	100.0 %	
Absorption correction	semi-empirical from equivalents	
Max. and min. transmission	0.7455 and 0.7126	
Refinement method	full-matrix least-squares on F ²	
Data / restraints / parameters	7808 / 40 / 486	
Goodness-of-fit on F ²	1.034	
Final R indices [$I > 2\sigma(I)$]	R1 = 0.0371, wR2 = 0.0900	
R indices (all data)	R1 = 0.0474, wR2 = 0.0975	
Extinction coefficient	n/a	
Largest diff. peak and hole	0.274 and -0.232 e.Å ⁻³	

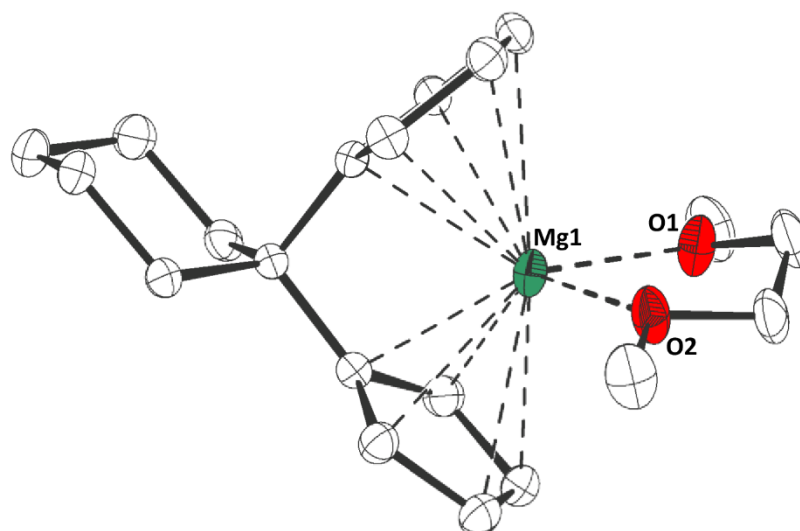


Figure S20. Molecular structure of **1b**-dme in the crystal (displacement ellipsoids at 50% probability level; hydrogen atoms omitted for clarity).

6. Supporting Information

crystal structure data of $1c \cdot (\text{thf})_2$

CCDC code:	2059664	
Empirical formula	$\text{C}_{25}\text{H}_{36}\text{MgO}_2$	
Formula weight	392.85	
Temperature	133(2) K	
Wavelength	0.71073 Å	
Crystal system	triclinic	
Space group	P-1	
Unit cell dimensions	$a = 8.2817(9)$ Å	$\alpha = 89.145(4)^\circ$
	$b = 14.9149(18)$ Å	$\beta = 88.130(4)^\circ$
	$c = 17.742(2)$ Å	$\gamma = 81.224(4)^\circ$
Volume	$2164.5(4)$ Å ³	
Z	4	
Density (calculated)	1.205 mg/m ³	
Absorption coefficient	0.100 mm ⁻¹	
F(000)	856	
Crystal size	0.412 x 0.120 x 0.082 mm ³	
Theta range for data collection	2.297 to 27.000°	
Index ranges	-10 <math>\leq h \leq 10, -19 <math>\leq k \leq 19, -1 <math>\leq l \leq 22	
Reflections collected	51579	
Independent reflections	9466 [R(int) = 0.1244]	
Completeness to theta = 25.242°	99.9 %	
Absorption correction	semi-empirical from equivalents	
Max. and min. transmission	0.7455 and 0.6862	
Refinement method	full-matrix least-squares on F ²	
Data / restraints / parameters	9466 / 112 / 589	
Goodness-of-fit on F ²	1.021	
Final R indices [I > 2σ(I)]	R1 = 0.0665, wR2 = 0.1281	
R indices (all data)	R1 = 0.1359, wR2 = 0.1622	
Extinction coefficient	n/a	
Largest diff. peak and hole	0.735 and -0.383 e.Å ⁻³	

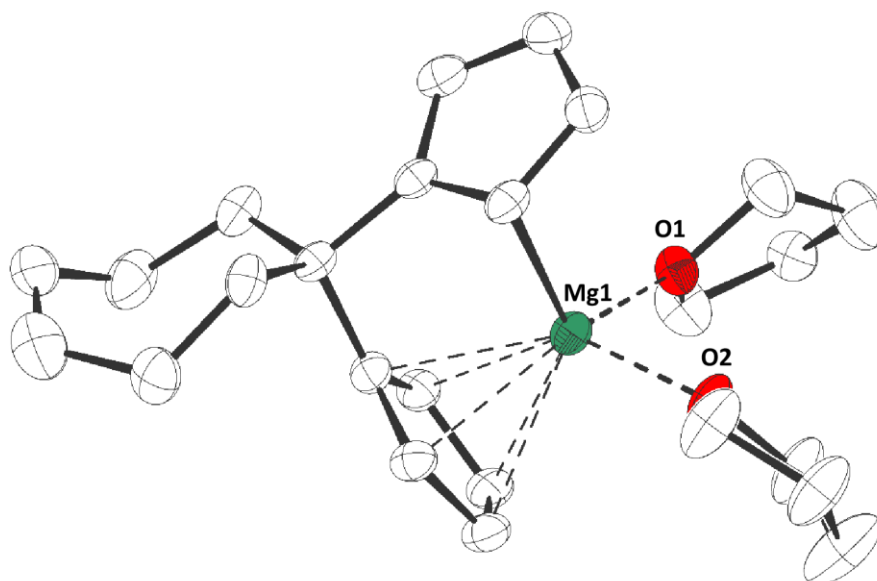


Figure S21. Molecular structure of $1c \cdot (\text{thf})_2$ in the crystal (displacement ellipsoids at 50% probability level; hydrogen atoms omitted for clarity).

crystal structure data of 1c·(thf)₂

CCDC code	2059665	
Empirical formula	C ₅₄ H ₈₀ Mg ₂ O ₅	
Formula weight	857.80	
Temperature	133(2) K	
Wavelength	0.71073 Å	
Crystal system	Monoclinic	
Space group	I2/a	
Unit cell dimensions	a = 14.3314(8) Å	α = 90°.
	b = 12.8761(8) Å	β = 98.378(4)°.
	c = 26.085(2) Å	γ = 90°.
Volume	4762.2(6) Å ³	
Z	4	
Density (calculated)	1.196 mg/m ³	
Absorption coefficient	0.098 mm ⁻¹	
F(000)	1872	
Crystal size	0.358 x 0.229 x 0.058 mm ³	
Theta range for data collection	2.137 to 26.998°.	
Index ranges	-18<=h<=18, -16<=k<=16, -33<=l<=33	
Reflections collected	49000	
Independent reflections	5203 [R(int) = 0.0861]	
Completeness to theta = 25.242°	100.0 %	
Absorption correction	Semi-empirical from equivalents	
Max. and min. transmission	0.7459 and 0.6950	
Refinement method	Full-matrix least-squares on F ²	
Data / restraints / parameters	5203 / 135 / 360	
Goodness-of-fit on F ²	1.024	
Final R indices [I>2sigma(I)]	R1 = 0.0540, wR2 = 0.1192	
R indices (all data)	R1 = 0.0891, wR2 = 0.1422	
Extinction coefficient	0.0018(2)	
Largest diff. peak and hole	0.344 and -0.382 e.Å ⁻³	

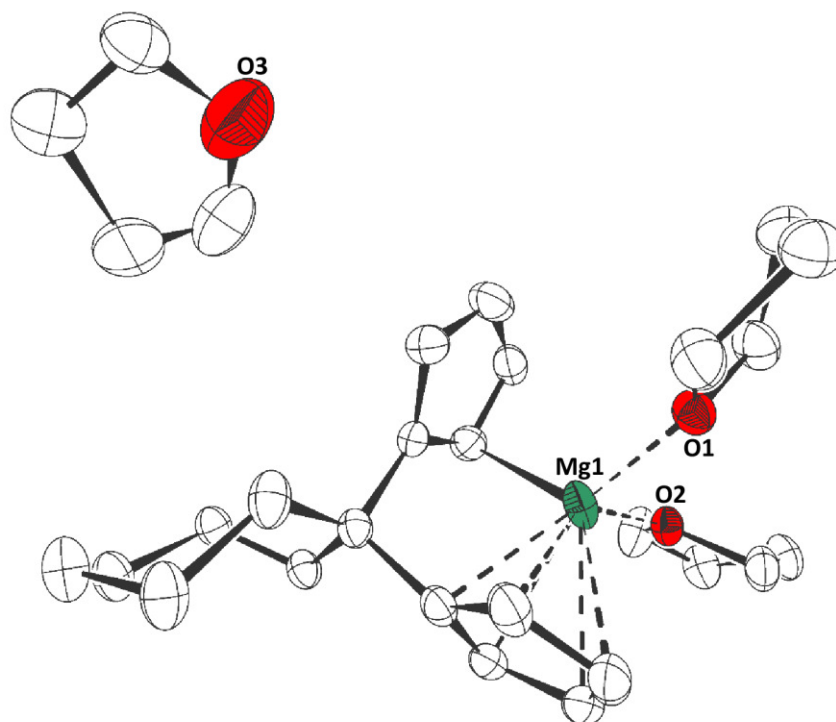


Figure S22. Molecular structure of **1c**·(thf)₂ + thf in the crystal (displacement ellipsoids at 50% probability level; hydrogen atoms omitted for clarity).

6. Supporting Information

crystal structure data of **1c**-dme

CCDC code	2059666	
Empirical formula	C ₂₃ H ₃₅ MgO ₃	
Formula weight	383.82	
Temperature	133(2) K	
Wavelength	0.71073 Å	
Crystal system	orthorhombic	
Space group	Pbcn	
Unit cell dimensions	a = 12.3033(3) Å	$\alpha = 90^\circ$
	b = 14.3052(3) Å	$\beta = 90^\circ$
	c = 24.2548(7) Å	$\gamma = 90^\circ$
Volume	4268.87(18) Å ³	
Z	8	
Density (calculated)	1.194 mg/m ³	
Absorption coefficient	0.103 mm ⁻¹	
F(000)	1672	
Crystal size	0.205 x 0.165 x 0.142 mm ³	
Theta range for data collection	2.183 to 27.922°	
Index ranges	-16<=h<=16, -18<=k<=16, -31<=l<=31	
Reflections collected	76582	
Independent reflections	5103 [R(int) = 0.0575]	
Completeness to theta = 25.242°	100.0 %	
Absorption correction	semi-empirical from equivalents	
Max. and min. transmission	0.7456 and 0.6894	
Refinement method	full-matrix least-squares on F ²	
Data / restraints / parameters	5103 / 0 / 271	
Goodness-of-fit on F ²	1.047	
Final R indices [I>2σ(I)]	R1 = 0.0400, wR2 = 0.0938	
R indices (all data)	R1 = 0.0533, wR2 = 0.1033	
Extinction coefficient	n/a	
Largest diff. peak and hole	0.242 and -0.288 e.Å ⁻³	

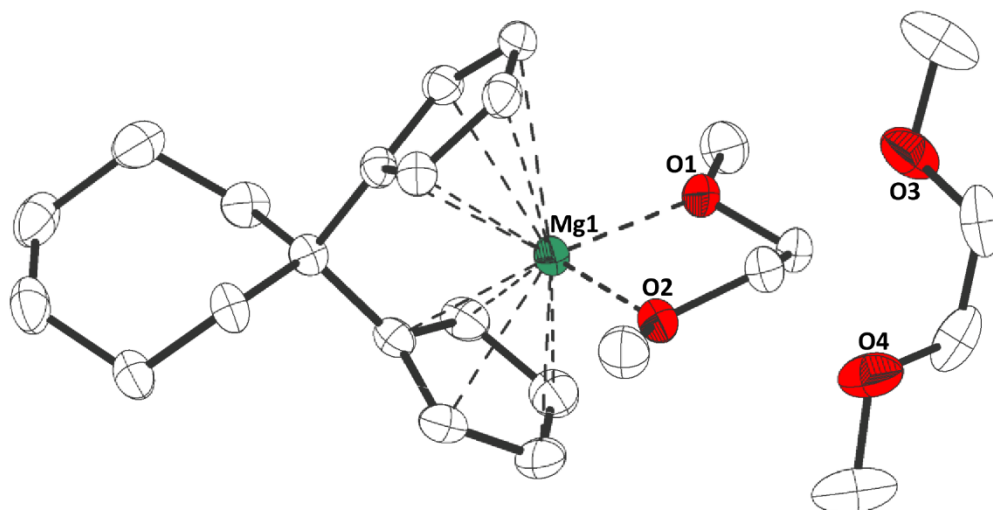


Figure S23. Molecular structure of **1c**-dme in the crystal (displacement ellipsoids at 50% probability level; hydrogen atoms omitted for clarity).

crystal structure data of 1c·(BnNH₂)₂

CCDC code	2059670	
Empirical formula	C ₃₁ H ₃₈ MgN ₂	
Formula weight	462.94	
Temperature	133(2) K	
Wavelength	0.71073 Å	
Crystal system	orthorhombic	
Space group	Pbca	
Unit cell dimensions	a = 16.7040(7) Å	α = 90°
	b = 11.4859(5) Å	β = 90°
	c = 27.1809(13) Å	γ = 90°
Volume	5214.9(4) Å ³	
Z	8	
Density (calculated)	1.179 mg/m ³	
Absorption coefficient	0.090 mm ⁻¹	
F(000)	2000	
Crystal size	0.360 x 0.116 x 0.061 mm ³	
Theta range for data collection	1.932 to 27.146°	
Index ranges	-21<=h<=21, -14<=k<=14, -34<=l<=34	
Reflections collected	61798	
Independent reflections	5774 [R(int) = 0.1247]	
Completeness to theta = 25.242°	100.0 %	
Absorption correction	semi-empirical from equivalents	
Max. and min. transmission	0.7455 and 0.5075	
Refinement method	full-matrix least-squares on F ²	
Data / restraints / parameters	5774 / 4 / 344	
Goodness-of-fit on F ²	1.025	
Final R indices [I>2σ(I)]	R1 = 0.0609, wR2 = 0.1387	
R indices (all data)	R1 = 0.1034, wR2 = 0.1707	
Extinction coefficient	0.0055(5)	
Largest diff. peak and hole	0.287 and -0.384 e.Å ⁻³	

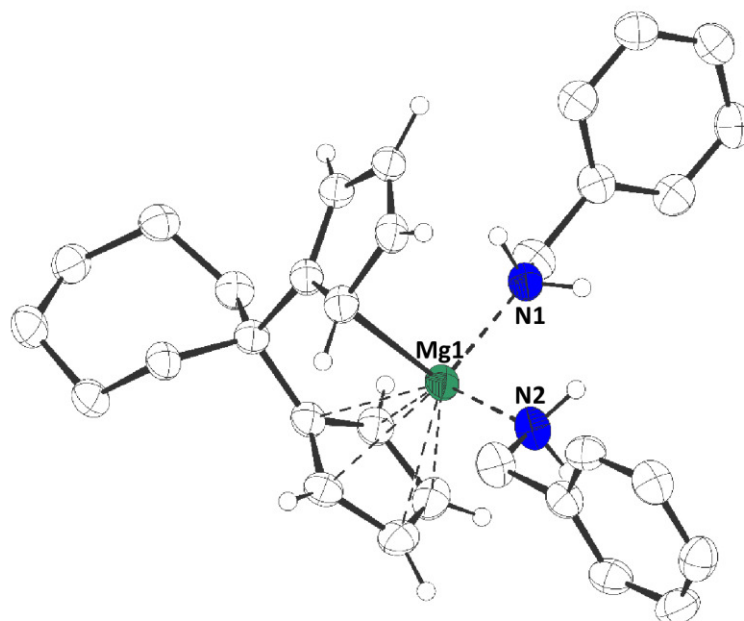


Figure S24. Molecular structure of **1c**·(BnNH₂)₂ in the crystal (displacement ellipsoids at 50% probability level; hydrogen atoms, except N-H and Cp-H, omitted for clarity).

6. Supporting Information

crystal structure data of **1a**·(*t*BuNH₂)₂

CCDC code	2059685	
Empirical formula	C ₂₅ H ₄₄ MgN ₂ O	
Formula weight	412.93	
Temperature	130(2) K	
Wavelength	0.71073 Å	
Crystal system	monoclinic	
Space group	P2 ₁ /n	
Unit cell dimensions	a = 8.1247(9) Å	α = 90°
	b = 18.9181(17) Å	β = 98.561(3)°
	c = 16.5530(18) Å	γ = 90°
Volume	2515.9(5) Å ³	
Z	4	
Density (calculated)	1.090 mg/m ³	
Absorption coefficient	0.088 mm ⁻¹	
F(000)	912	
Crystal size	0.376 x 0.204 x 0.184 mm ³	
Theta range for data collection	2.153 to 33.179°	
Index ranges	-12<=h<=12, -29<=k<=23, -25<=l<=25	
Reflections collected	47811	
Independent reflections	9622 [R(int) = 0.0279]	
Completeness to theta = 25.242°	99.9 %	
Absorption correction	semi-empirical from equivalents	
Max. and min. transmission	0.7465 and 0.7044	
Refinement method	full-matrix least-squares on F ²	
Data / restraints / parameters	9622 / 12 / 320	
Goodness-of-fit on F ²	1.032	
Final R indices [I>2σ(I)]	R1 = 0.0399, wR2 = 0.1037	
R indices (all data)	R1 = 0.0511, wR2 = 0.1115	
Extinction coefficient	n/a	
Largest diff. peak and hole	0.462 and -0.363 e.Å ⁻³	

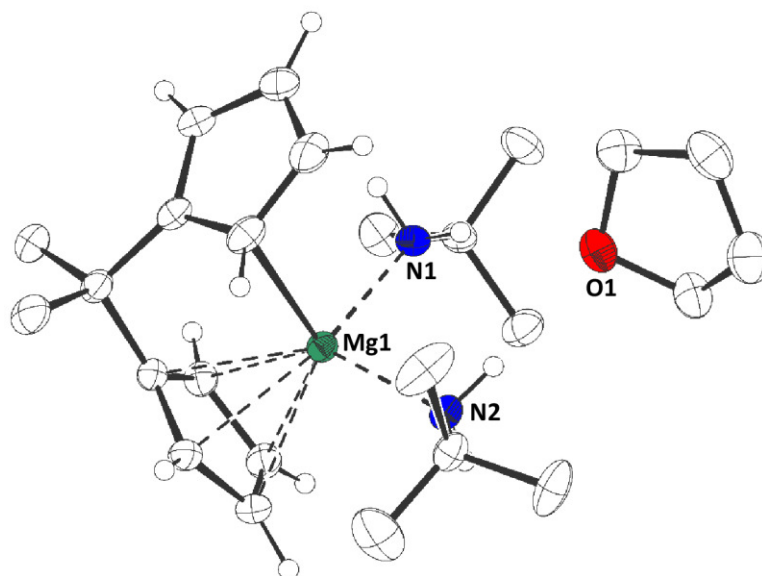


Figure S25. Molecular structure of **1a**·(*t*BuNH₂)₂ in the crystal (displacement ellipsoids at 50% probability level; hydrogen atoms, except N-H, omitted for clarity).

Computational Details

All calculations were performed using the Gaussian 16, Revision C.01 package of programs.¹⁴ All geometry optimizations have been carried out at the B3LYP-D3¹⁵/def2-TZVP¹⁶ level of theory. Every optimized structure was confirmed to be either a minimum or a maximum (transition state) on the potential energy surface by a subsequent frequency analysis (all positive eigenvalues for minima, one negative eigenvalues for maxima).

References

- [1] Cristian, L.; Nica, S.; Pavel, O. D.; Mihailciuc, C.; Almasan, V.; Coman, S. M.; Hardacre, C.; Parvulescu, V. I. Novel ruthenium-terpyridyl complex for direct oxidation of amines to nitriles. *Catal. Sci. Technol.* **2013**, *3*, 2646-2653.
- [2] Wirtz, L.; Haider, W.; Huch, V.; Zimmer, M.; Schäfer, A. Magnescenophane-Catalyzed Amine Borane Dehydrocoupling. *Chem. Eur. J.* **2020**, *26*, 6176-6184.
- [3] Fuller, A.-M.; Mountford, A. J.; Scott, M. L.; Coles, S. J.; Horton, P. N.; Hughes, D. L.; Hursthouse, M. B.; Lancaster, S. J. Synthesis, Structure, and Stability of Adducts between Phosphide and Amide Anions and the Lewis Acids Borane, Tris(pentafluorophenyl)borane, and Tris(pentafluorophenyl)alane. *Inorg. Chem.* **2009**, *48*, 11474-11482.
- [4] Xie, W.; Hu, H.; Cui, C. [(NHC)Yb{N(SiMe₃)₂}₂]-Catalyzed Cross-Dehydrogenative Coupling of Silanes with Amines. *Angew. Chem. Int. Ed.* **2012**, *51*, 11141-11144. / *Angew. Chem.* **2012**, *124*, 11303-11306.
- [5] Nako, A. E.; Chen, W.; White, A. J. P.; Crimmin, M. R. Yttrium-Catalyzed Amine-Silane Dehydrocoupling: Extended Reaction Scope with a Phosphorus-Based Ligand. *Organometallics* **2015**, *34*, 4369-4375.
- [6] Dunne, J. F.; Neal, S. R.; Engelkemier, J.; Ellern, A.; Sadow, A. D. Tris(oxazoninyl)boratomagnesium-Catalyzed Cross-Dehydrocoupling of Organosilanes with Amines, Hydrazine, and Ammonia. *J. Am. Chem. Soc.* **2011**, *133*, 16782-16785.
- [7] Baishya, A.; Peddara, T.; Nembenna, S. Organomagnesium amide catalyzed cross-dehydrocoupling of organosilanes with amines. *Dalton Trans.* **2017**, *46*, 5880-5887.
- [8] Ríos, P.; Roselló-Merino, M.; Rivada-Wheelaghan, O.; Borge, J.; López-Serrano, J.; Conejero, S. Selective catalytic synthesis of amino-silanes at part-per million catalyst loadings. *Chem. Commun.* **2018**, *54*, 619-622.
- [9] Mitzel, N. W.; Riede, J.; Schier, A.; Paul, M.; Schmidbaur, H. Preparative, Spectroscopic, and Structural Studies on Some New Silylamines. *Chem. Ber.* **1993**, *126*, 2027-2032.
- [10] Gasperini, D.; King, A. K.; Coles, N. T.; Mahon, M. F.; Webster, R. L. Seeking Heteroatom-Rich Compounds: Synthetic and Mechanistic Studies into Iron Catalyzed Dehydrocoupling of Silanes. *ACS Catal.* **2020**, *10*, 6102-6112.
- [11] Hill, M. S.; Liptrot, D. J.; MacDougall, D. J.; Mahon, M. F.; Robinson, T. P. Hetero-dehydrocoupling of silanes and amines by heavier alkaline earth catalysis. *Chem. Sci.* **2013**, *4*, 4212-4222.
- [12] Zhang, X.; Zhou, S.; Fang, X.; Zhang, L.; Tao, G.; Wei, Y.; Zhu, X.; Cui, P.; Wang, S. Syntheses of Dianionic α -Iminopyridine Rare-Earth Metal Complexes and Their Catalytic Activities toward Dehydrogenative Coupling of Amines with Hydrosilanes. *Inorg. Chem.* **2020**, *59*, 9683-9692. www.manonthemoontech.com
- [13] Gaussian 16, Revision C.01, Frisch, M. J.; Trucks, G. W.; Schlegel, H. B.; Scuseria, G. E.; Robb, M. A.; Cheeseman, J. R.; Scalmani, G.; Barone, V.; Petersson, G. A.; Nakatsuji, H.; Li, X.; Caricato, M.; Marenich, A. V.; Bloino, J.; Janesko, B. G.; Gomperts, R.; Mennucci, B.; Hratchian, H. P.; Ortiz, J. V.; Izmaylov, A. F.; Sonnenberg, J. L.; Williams-Young, D.; Ding, F.; Lipparini, F.; Egidi, F.; Goings, J.; Peng, B.; Petrone, A.; Henderson, T.; Ranasinghe, D.; Zakrzewski, V. G.; Gao, J.; Rega, N.; Zheng, G.; Liang, W.; Hada, M.; Ehara, M.; Toyota, K.; Fukuda, R.; Hasegawa, J.; Ishida, M.; Nakajima, T.; Honda, Y.; Kitao, O.; Nakai, H.; Vreven, T.; Throssell, K.; Montgomery, J. A.; Jr. Peralta, J. E.; Ogliaro, F.; Bearpark, M. J.; Heyd, J. J.; Brothers, E. N.; Kudin, K. N.; Staroverov, V. N.; Keith, T. A.; Kobayashi, R.; Normand, J.; Raghavachari, K.; Rendell, A. P.; Burant, J. C.; Iyengar, S. S.; Tomasi, J.; Cossi, M.; Millam, J. M.; Klene, M.; Adamo, C.; Cammi, R.; Ochterski, J. W.; Martin, R. L.; Morokuma, K.; Farkas, O.; Foresman, J. B.; Fox, D. J.; Gaussian, Inc., Wallingford CT, **2019**.
- [15] a) Becke, A. D. Density-functional thermochemistry. III. The role of exact exchange. *J. Chem. Phys.* **1993**, *98*, 5648-5652; b) Lee, C.; Yang, W.; Parr, R. G. Development of the Colle-Salvetti correlation-energy formula into a functional of the electron density. *Phys. Rev. B* **1988**, *37*, 785-789; c) Vosko, S. H.; Wilk, L.; Nusair, M. Accurate spin-dependent electron liquid correlation energies for local spin density calculations: a critical analysis. *Can. J. Phys.* **1980**, *58*, 1200-1211; d) Stephens, P. J.; Devlin, F. J.; Chabalowski, C. F.; Frisch, M. J. *Ab Initio* Calculation of Vibrational Absorption and Circular Dichroism Spectra Using Density Functional Force Fields. *J. Phys. Chem.* **1994**, *98*, 11623-11627; e) Grimme, S.; Antony, J.; Ehrlich, S.; Krieg, H. A consistent and accurate *ab initio* parametrization of density functional dispersion correction (DFT-D) for the 94 elements H-Pu. *J. Chem. Phys.* **2010**, *132*, 154104.
- [16] a) Weigend, F.; Ahlrichs, R. Balanced basis sets of split valence, zeta valence and quadruple zeta valence quality for H to Rn: Design and assessment of accuracy. *Phys. Chem. Chem. Phys.* **2005**, *7*, 3297-3305; b) Weigend, F. Accurate Coulomb-fitting basis sets for H to Rn. *Phys. Chem. Chem. Phys.* **2006**, *8*, 1057-1065.

6.3 Constrained Geometry *ansa*-Half-Sandwich Complexes of Magnesium – Versatile s-Block Catalysts

ChemCatChem

Supporting Information

Constrained Geometry *ansa*-Half-Sandwich Complexes of Magnesium – Versatile *s*-Block Catalysts

Lisa Wirtz, Kinza Yasmin Ghulam, Bernd Morgenstern, and André Schäfer*

Table of Contents

Experimental Details	2 – 11
NMR Spectra	12 – 29
XRD Data	30 – 35
Computational Details	36
References	37
Author Contributions	38

Experimental Details

All manipulations were carried out under an argon inert gas atmosphere (argon 5.0), using either Schlenk line techniques or a glovebox. *Ansa*-ligands (C₅H₅)SiMe₂NH*t*Bu¹, (C₅Me₄H)SiMe₂NH*t*Bu², (C₅Me₄H)SiPh₂NH*t*Bu³, and (C₅Me₄H)SiMe₂NHPh⁴ were synthesized according to literature known procedures. All other starting materials were obtained commercially. NMR spectra were recorded on Bruker Avance III 300 and Bruker Avance III 400 spectrometers. ¹H and ¹³C NMR spectra were referenced using the solvent signals ($\delta^1\text{H}$ (CHCl₃) = 7.26, $\delta^1\text{H}$ (C₆HD₅) = 7.16, $\delta^1\text{H}$ (thf-*d*7) = 3.58; $\delta^{13}\text{C}$ (C₆D₆) = 128.06, $\delta^{13}\text{C}$ (CDCl₃) = 77.16, $\delta^{13}\text{C}$ (thf-*d*8) = 67.57). ¹¹B, ¹⁹F and ²⁹Si NMR spectra were referenced using external standards ($\delta^{11}\text{B}$ (BF₃·OEt₂) = 0, $\delta^{19}\text{F}$ (CFCl₃) = 0, $\delta^{29}\text{Si}$ (SiMe₄) = 0). Single-crystal X-ray diffraction analyses were carried out at low temperatures on a Bruker AXS D8 Venture diffractometer with a microfocus sealed tube and a Photon II detector. Monochromated MoK α radiation (λ = 0.71073 Å) was used. The structures were solved by direct methods using SHELXT⁵ and were refined by full matrix least squares calculations on F2 (SHELXL2018⁶) in the graphical user interface ShelXle.⁷ Crystal structures have been deposited with the Cambridge Crystallographic Data Centre (CCDC) and are available free of charge from the Cambridge Structural Database (reference numbers: 2193652, 2193656, 2193657, 2193660, 2193661).

Synthesis of 1a-pyrrolidine:

ansa-Half-sandwich complex **1a** (40.0 mg, 0.18 mmol) and pyrrolidine (0.03 mL, 0.36 mmol) were dissolved in thf-*d*₈ and stirred for a few minutes. The reaction mixture was subsequently investigated by NMR spectroscopy.

¹H NMR (400.13 MHz, thf-*d*₈): δ = 6.17 (bs, 2 H; Cp-*H*), 5.97 (bs, 2 H; Cp-*H*), 2.76 (bs, 8 H, N-CH₂), 1.66 (bs, 8 H, CH₂), 1.05 (s, 9 H; C(CH₃)₃), 0.21 ppm (s, 6 H; Si-CH₃); ¹³C{¹H} NMR (100.62 MHz, thf-*d*₈): δ = 114.5 (Cp), 113.5 (Cp), 106.4 (Cp), 51.6 (C(CH₃)₃), 34.3 (C(CH₃)₃), 27.9 (CH₂), 26.6 (CH₂), 4.1 ppm (Si-CH₃); ²⁹Si{¹H} NMR (79.49 MHz, thf-*d*₈): δ = -14.6 ppm.

Synthesis of 1b-(*N,N'*-diisopropylcarbodiimide):

ansa-Half-sandwich complex **1b** (80.0 mg, 0.22 mmol) and *N,N'*-diisopropylcarbodiimide (28.0 mg, 0.22 mmol) were dissolved in C₆D₆ and stirred for a few minutes. The reaction mixture was subsequently investigated by NMR spectroscopy.

¹H NMR (400.13 MHz, C₆D₆): δ = 4.05 (bs, 2 H; CH), 2.47 (s, 6 H; Cp-CH₃), 2.19 (s, 6 H, Cp-CH₃), 1.18-1.03 (m), 0.68 ppm (s, 6 H; Si-CH₃); ¹³C{¹H} NMR (100.62 MHz, thf-*d*₈): δ = 169.9, 121.1, 117.1, 103.0, 72.3, 58.7, 53.3, 48.9, 44.1, 29.1, 26.8, 16.4, 12.1, 7.3, 1.3 ppm; ²⁹Si{¹H} NMR (79.49 MHz, thf-*d*₈): δ = -18.5 ppm.

General procedure for catalytic amine-borane dehydrocoupling with R₂NH·BH₃ substrates (BN1-BN4):

5 mol% catalyst and the corresponding amine-borane (**1a**: 41.3 μmol; ¹Pr₂NH·BH₃: 870 μmol; **1a**: 50.5 μmol; Me₂NH·BH₃: 1.02 mmol, (C₅H₁₀)NH·BH₃: 1.01 mmol, (C₄H₈O)NH·BH₃: 1.02 mmol; **1b**-dme: 44.0 μmol; ¹Pr₂NH·BH₃: 869 μmol; **1b**-dme: 52.2 μmol; Me₂NH·BH₃: 1.02 mmol; (C₅H₁₀)NH·BH₃: 1.01 mmol, (C₄H₈O)NH·BH₃: 1.02 mmol; **1c**-dme: 26.6 μmol; ¹Pr₂NH·BH₃: 522 μmol; **1c**-dme: 43.0 μmol; Me₂NH·BH₃: 849 μmol; **1c**-dme: 41.0 μmol; (C₅H₁₀)NH·BH₃: 810 μmol; **1c**-dme: 41.0 μmol; (C₄H₈O)NH·BH₃: 820 μmol; **1d**-dme: 44.3 μmol; ¹Pr₂NH·BH₃: 869 μmol; **1d**-dme: 52.1 μmol; Me₂NH·BH₃: 1.02 mmol; **1d**-dme: 49.5 μmol; (C₅H₁₀)NH·BH₃: 1.01 mmol; **1d**-dme: 52.1 μmol; (C₄H₈O)NH·BH₃: 1.02 mmol) were dissolved in 1 mL of dme in a 12 mL volume vial in a glovebox and stirred for 8 h at room temperature. Conversions were determined by integration of the ¹¹B NMR spectra. Signals for tetramethyldiborazane,^{8,9} diisopropylaminoborane,^{8,9} piperidinyldiborazane,^{9,10} and morpholinylidiborazane⁹ were assigned based on literature.

General procedure for catalytic amine-borane dehydrocoupling with R₂NH + HBpin substrates (BN5-BN7):

5 mol% catalyst, 1.65 mmol (1 eq) amine and 1.65 mmol (1 eq) pinacolborane were dissolved in 1 mL dme and were stirred for 1 h at room temperature in a close Schlenk tube. Conversions were determined by integration of the ¹¹B NMR spectra. Signals were assigned based on literature.¹¹⁻¹³

General procedure for catalytic amine silane cross-dehydrocoupling (SiN1-SiN8):

5 mol% catalyst, 1.60 mmol (1 eq) amine and 1.61 mmol (1 eq) diphenylsilane or 1.67 mmol (1 eq) methylphenylsilane were dissolved in 1 mL C₆D₆ and were stirred for 1 h (for **SiN1-SiN5, SiN7, SiN8**) or 16 h (for **SiN6**) at room temperature in a closed Schlenk tube. Conversions were determined by integration of the ¹H NMR spectra. Signals were assigned based on literature.^{9,14-20}

General procedure for catalytic hydroboration (HB1-HB6)

5 mol% catalyst, 1.86 mmol (1 eq) or 3.64 mmol (2 eq) of pinacolborane and 1.82 mmol (1 eq) of the corresponding alkyne, 1.87 mmol (1 eq) of the corresponding imine or 1.84 mmol (1 eq) of the corresponding nitrile were dissolved in 1 mL of C₆D₆ and stirred for 24 h at room temperature or 333 K in a closed Schlenk tube. Conversions were determined by integration of the ¹H NMR spectra. Signals were assigned based on literature.²¹⁻²⁵

SUPPORTING INFORMATION

WILEY-VCH

Intramolecular Hydroamination (HN1)

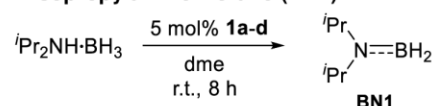
10 mol% catalyst and 2,2-diphenyl-4-penten-1-amine (196 mg, 0.83 mmol, 1 eq) were dissolved in 1 mL C₆D₆ and stirred for 24 h at 323 K in a closed Schlenk tube. Conversions were determined by integration of the ¹H NMR spectra. Signals were assigned based on literature.²⁶

Phenylacetylene + *N,N'*-Diisopropylcarbodiimide (CH1)

5 mol% catalyst, 1.82 mmol (1 eq) of phenylacetylene and 1.81 mmol (1 eq) of *N,N'*-diisopropylcarbodiimide were dissolved in 1 mL of C₆D₆ and stirred for 24 h at 333 K in a closed Schlenk tube. Conversions were determined by integration of the ¹H NMR spectra. Signals were assigned based on literature.^{27,28}

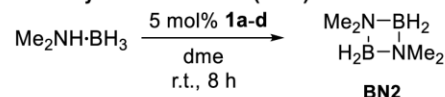
Phenylacetylene + *N,N'*-Dicyclohexylcarbodiimide (CH2)

5 mol% catalyst, 1.82 mmol (1 eq) of phenylacetylene and 1.84 mmol (1 eq) of *N,N'*-dicyclohexylcarbodiimide were dissolved in 1 mL of toluene and stirred for 24 h at 333 K in a closed Schlenk tube. The solvent was removed in vacuo and the residue dissolved in CDCl₃. Conversions were determined by integration of the ¹H NMR spectra and were estimated in relation to the carbodiimide conversion. Signals were assigned based on literature.^{27,28}

Diisopropylamine-Borane (BN1)

Catalyst	Borane conversion
1a	≥95%
1b-dme	≥95%
1c-dme	≥95%
1d-dme	≥95%

¹¹B NMR (128.38 MHz, dme): δ = 35.7 ppm (t, ¹J_{BH} = 130.8 Hz).^{8,9}

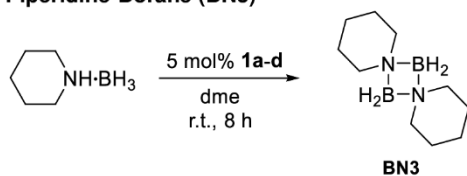
Dimethylamine-Borane (BN2)

Catalyst	Borane conversion
1a	82%
1b-dme	87%
1c-dme	80%
1d-dme	78%

¹¹B{¹H} NMR (96.29 MHz, dme): δ = 5.9 ppm.^{8,9}

SUPPORTING INFORMATION

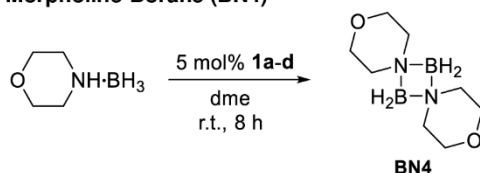
Piperidine-Borane (BN3)



Catalyst	Borane conversion
1a	≥95%
1b -dme	91%
1c -dme	87%
1d -dme	≥95%

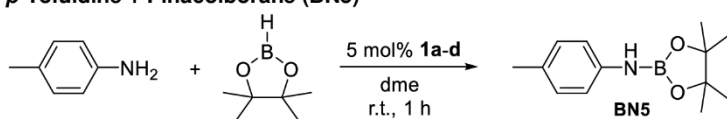
$^{11}\text{B}\{^1\text{H}\}$ NMR (96.29 MHz, dme): $\delta = 2.6$ ppm.^{9,10}

Morpholine-Borane (BN4)



Catalyst	Borane conversion
1a	≥95%
1b -dme	≥95%
1c -dme	91%
1d -dme	92%

$^{11}\text{B}\{^1\text{H}\}$ NMR (96.29 MHz, dme): $\delta = 2.6$ ppm.⁹

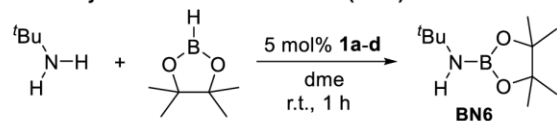
p-Toluidine + Pinacolborane (BN5)

Catalyst	Borane conversion
1a	≥99%
1b -dme	≥99%
1c -dme	≥99%
1d -dme	≥99%

^1H NMR (400.13 MHz, C_6D_6): $\delta = 6.97$ - 6.84 (m, 4 H, Ph-*H*), 4.66 (s, 1 H, *NH*), 2.09 (s, 3 H, CH_3), 1.09 ppm (s, 12 H, $\text{OC}(\text{CH}_3)_2$); ^{11}B NMR (96.29 MHz, C_6D_6): $\delta = 24.2$ ppm; ^{11}B NMR (96.29 MHz, dme): $\delta = 24.4$ ppm; $^{13}\text{C}\{^1\text{H}\}$ NMR (75.48 MHz, C_6D_6): $\delta = 141.5$, 129.8, 129.1, 118.1, 82.6, 24.7, 20.7 ppm.¹¹

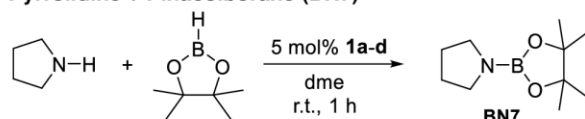
SUPPORTING INFORMATION

WILEY-VCH

tert-Butylamine + Pinacolborane (BN6)

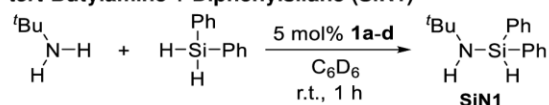
Catalyst	Borane conversion
1a	67%
1b-dme	70%
1c-dme	76%
1d-dme	48%

^1H NMR (300.13 MHz, C_6D_6): δ = 1.20-1.17 (m, 9 H, $\text{C}(\text{CH}_3)_3$), 1.12-1.08 ppm (m, 12 H, $\text{OC}(\text{CH}_3)_2$); ^{11}B NMR (96.29 MHz, C_6D_6): δ = 24.1 ppm; ^{11}B NMR (96.29 MHz, dme): δ = 24.4 ppm; $^{13}\text{C}\{^1\text{H}\}$ NMR (75.48 MHz, C_6D_6): δ = 81.4, 47.8, 32.3, 24.8 ppm.¹²

Pyrrolidine + Pinacolborane (BN7)

Catalyst	Borane conversion
1a	94%
1b-dme	95%
1c-dme	≥95%
1d-dme	72%

^1H NMR (300.13 MHz, C_6D_6): δ = 3.26-3.18 (m, 4 H, CH_2), 1.48-1.42 (m, 4 H, CH_2), 1.13 ppm (s, 12 H, $\text{OC}(\text{CH}_3)_2$); ^{11}B NMR (96.29 MHz, C_6D_6): δ = 23.7 ppm; ^{11}B NMR (96.29 MHz, dme): δ = 23.9 ppm; $^{13}\text{C}\{^1\text{H}\}$ NMR (75.48 MHz, C_6D_6): δ = 81.9, 46.1, 26.6, 25.0 ppm.¹³

tert-Butylamine + Diphenylsilane (SiN1)

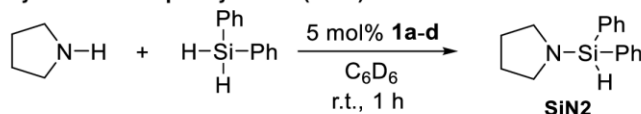
Catalyst	Amine conversion
1a	50%
1b-dme	65%
1c-dme	66%
1d-dme	31%

^1H NMR (400.13 MHz, C_6D_6): δ = 7.68-7.63 (m, 4 H, Ph-H), 7.20-7.16 (m, 6 H, Ph-H), 5.68 (d, $^1J_{\text{SiH}} = 204.4$ Hz, $^3J_{\text{HH}} = 3.4$ Hz, 1 H, SiH), 1.08 (s, 9 H, CH_3), 0.92 ppm (bs, 1 H, NH); $^{13}\text{C}\{^1\text{H}\}$ NMR (100.62 MHz, C_6D_6): δ = 137.4 (Ph), 135.2 (Ph), 130.0 (Ph), 128.3 (Ph), 49.6 ($\text{C}(\text{CH}_3)_3$), 33.3 ppm ($\text{C}(\text{CH}_3)_3$); $^{29}\text{Si}\{^1\text{H}\}$ NMR (79.49 MHz, C_6D_6): δ = -24.9 ppm.^{9,14-16}

SUPPORTING INFORMATION

WILEY-VCH

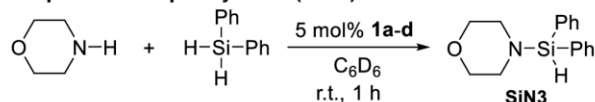
Pyrrolidine + Diphenylsilane (SiN2)



Catalyst	Amine conversion
1a	≥95%
1b -dme	≥95%
1c -dme	≥95%
1d -dme	≥95%

^1H NMR (400.13 MHz, C_6D_6): δ = 7.67-7.58 (m, 4 H, Ph-*H*), 7.21-7.13 (m, 6 H, Ph-*H*), 5.61 (s, $^1J_{\text{SiH}}$ = 203.6 Hz, 1 H, Si*H*), 3.00-2.93 (m, 4 H, N- CH_2), 1.52-1.43 ppm (m, 4 H, CH_2); $^{13}\text{C}\{^1\text{H}\}$ NMR (100.62 MHz, C_6D_6): δ = 135.7 (Ph), 135.5 (Ph), 130.1 (Ph), 128.3 (Ph), 48.4 (N- CH_2), 27.2 ppm (CH_2); $^{29}\text{Si}\{^1\text{H}\}$ NMR (79.49 MHz, C_6D_6): δ = -18.0 ppm.^{9,16}

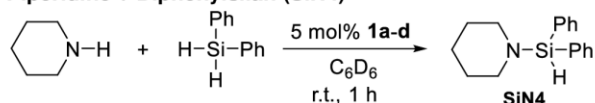
Morpholine + Diphenylsilane (SiN3)



Catalyst	Amine conversion
1a	≥95%
1b -dme	≥95%
1c -dme	≥95%
1d -dme	≥95%

^1H NMR (400.13 MHz, C_6D_6): δ = 7.61-7.54 (m, 4 H, Ph-*H*), 7.19-7.15 (m, 6 H, Ph-*H*), 5.41 (s, $^1J_{\text{SiH}}$ = 205.9 Hz, 1 H, Si*H*), 3.38 (t, $^3J_{\text{HH}}$ = 4.6 Hz, 4 H, O- CH_2), 2.77 ppm (t, $^3J_{\text{HH}}$ = 4.6 Hz, 4 H, N- CH_2); $^{13}\text{C}\{^1\text{H}\}$ NMR (100.62 MHz, C_6D_6): δ = 135.5 (Ph), 134.8 (Ph), 130.3 (Ph), 128.4 (Ph), 68.4 (O- CH_2), 46.9 ppm (N- CH_2); $^{29}\text{Si}\{^1\text{H}\}$ NMR (79.49 MHz, C_6D_6): δ = -13.3 ppm.^{9,17}

Piperidine + Diphenylsilane (SiN4)

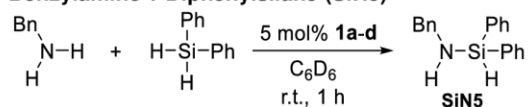


Catalyst	Amine conversion
1a	≥95%
1b -dme	≥95%
1c -dme	≥95%
1d -dme	≥95%

^1H NMR (400.13 MHz, C_6D_6): δ = 7.72-7.65 (m, 4 H, Ph-*H*), 7.26-7.18 (m, 6 H, Ph-*H*), 5.54 (s, $^1J_{\text{SiH}}$ = 205.1 Hz, 1 H, Si*H*), 2.93 (t, $^3J_{\text{HH}}$ = 5.3 Hz, 4 H, N- CH_2), 1.47-1.38 (m, 2 H, CH_2), 1.37-1.29 ppm (m, 4 H, CH_2); $^{13}\text{C}\{^1\text{H}\}$ NMR (100.62 MHz, C_6D_6): δ = 135.7 (Ph), 135.5 (Ph), 130.1 (Ph), 128.3 (Ph), 47.8 (N- CH_2), 27.9 (CH_2), 25.6 ppm (CH_2)¹⁸; $^{29}\text{Si}\{^1\text{H}\}$ NMR (79.49 MHz, C_6D_6): δ = -13.9 ppm.^{9,17}

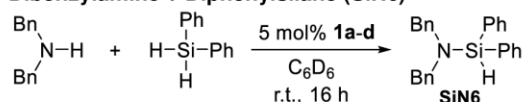
SUPPORTING INFORMATION

WILEY-VCH

Benzylamine + Diphenylsilane (SiN5)

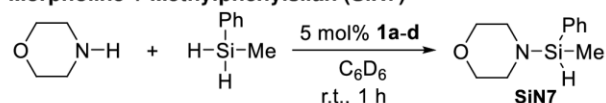
Catalyst	Amine conversion
1a	89%
1b-dme	92%
1c-dme	89%
1d-dme	≥95%

^1H NMR (400.13 MHz, C_6D_6): δ = 7.69-7.62 (m, 4 H, Ph-*H*), 7.22-7.10 (m, 11 H, Ph-*H*), 5.62 (d, $^1J_{\text{SiH}}$ = 204.6 Hz, $^3J_{\text{HH}}$ = 2.1 Hz, 1 H, SiH), 3.86 (d, $^3J_{\text{HH}}$ = 8.0 Hz, 2 H, CH_2), 1.00 ppm (bs, 1 H, NH); $^{13}\text{C}\{^1\text{H}\}$ NMR (100.62 MHz, C_6D_6): δ = 143.6 (Ph), 135.6 (Ph), 135.3 (Ph), 130.3 (Ph), 128.6 (Ph), 128.3 (Ph), 127.4 (Ph), 126.9 (Ph), 47.1 ppm (CH_2);^{9,17,18}; $^{29}\text{Si}\{^1\text{H}\}$ NMR (79.49 MHz, C_6D_6): δ = -17.0 ppm.^{9,17}

Dibenzylamine + Diphenylsilane (SiN6)

Catalyst	Amine conversion
1a	51%
1b-dme	87%
1c-dme	88%
1d-dme	0%

^1H NMR (400.13 MHz, C_6D_6): δ = 7.76-7.70 (m, 4 H, Ph-*H*), 7.22-7.16 (m, 16 H, Ph-*H*), 5.89 (s, $^1J_{\text{SiH}}$ = 205.9 Hz, 1 H, SiH), 4.01 ppm (s, 4 H, CH_2); $^{13}\text{C}\{^1\text{H}\}$ NMR (100.62 MHz, C_6D_6): δ = 140.2 (Ph), 135.8 (Ph), 135.4 (Ph), 130.3 (Ph), 128.8 (Ph), 128.6 (Ph), 128.5 (Ph), 127.2 (Ph), 50.6 ppm (CH_2);⁹; $^{29}\text{Si}\{^1\text{H}\}$ NMR (79.49 MHz, C_6D_6): δ = -10.3 ppm.¹⁹

Morpholine + Methylphenylsilane (SiN7)

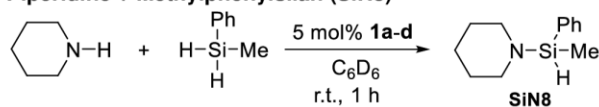
Catalyst	Amine conversion
1a	≥95%
1b-dme	≥95%
1c-dme	≥95%
1d-dme	≥95%

^1H NMR (400.13 MHz, C_6D_6): δ = 7.56-7.48 (m, 2 H, Ph-*H*), 7.26-7.20 (m, 3 H, Ph-*H*), 4.94 (q, $^1J_{\text{SiH}}$ = 200.8 Hz, $^3J_{\text{HH}}$ = 3.2 Hz, 1 H, SiH), 3.40 (t, $^3J_{\text{HH}}$ = 4.5 Hz, 4 H, O- CH_2), 2.71 (t, $^3J_{\text{HH}}$ = 4.8 Hz, 4 H, N- CH_2), 0.25 ppm (d, $^3J_{\text{HH}}$ = 3.2 Hz, 3 H, CH_3); $^{13}\text{C}\{^1\text{H}\}$ NMR (100.62 MHz, C_6D_6): δ = 137.0 (Ph), 134.6 (Ph), 130.0 (Ph), 128.3 (Ph), 68.4 (O- CH_2), 46.6 (N- CH_2), -3.9 ppm (CH_3); $^{29}\text{Si}\{^1\text{H}\}$ NMR (79.49 MHz, C_6D_6): δ = -9.7 ppm.¹⁹

SUPPORTING INFORMATION

WILEY-VCH

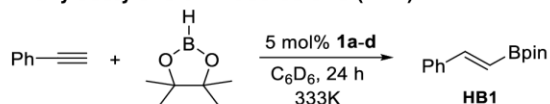
Piperidine + Methylphenylsilan (SiN8)



Catalyst	Amine conversion
1a	≥95%
1b -dme	≥95%
1c -dme	≥95%
1d -dme	≥95%

^1H NMR (400.13 MHz, C_6D_6): δ = 7.66-7.56 (m, 2 H, Ph-*H*), 7.27-7.20 (m, 3 H, Ph-*H*), 5.05 (q, $^1J_{\text{SiH}} = 199.6$ Hz, $^3J = 3.2$ Hz, 1 H, Si*H*), 2.48 (t, $^3J_{\text{HH}} = 4.9$ Hz, 4 H, N-*CH*₂), 1.48-1.40 (m, 2 H, *CH*₂), 1.35-1.27 (m, 4 H, *CH*₂), 0.33 ppm (d, $^3J_{\text{HH}} = 3.3$ Hz, 3 H, *CH*₃); $^{13}\text{C}\{^1\text{H}\}$ NMR (100.62 MHz, C_6D_6): δ = 138.1 (Ph), 134.5 (Ph), 129.8 (Ph), 128.2 (Ph), 47.6 (N-*CH*₂), 28.0 (*CH*₂), 25.7 (*CH*₂), -3.4 ppm (*CH*₃)^{18,20}; ^{29}Si NMR (79.49 MHz, C_6D_6): δ = -10.7 ppm.²⁰

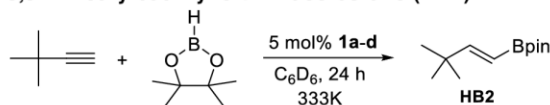
Phenylacetylene + Pinacolborane (HB1)



Catalyst	Phenylacetylene conversion
1a	81%
1b -dme	62%
1c -dme	64%
1d -dme	75%

^1H NMR (400.13 MHz, C_6D_6): δ = 7.65 (d, $^3J_{\text{HH}} = 18.4$ Hz, 1 H, C=*CH*), 7.33-7.29 (m, 2 H, Ph-*H*), 7.07-7.00 (m, 3 H, Ph-*H*), 6.36 (d, $^3J_{\text{HH}} = 18.4$ Hz, 1 H, C=*CH*), 1.12 ppm (s, 12 H, OC(*CH*₃)₂); ^{11}B NMR (96.29 MHz, C_6D_6): δ = 30.7 ppm; $^{13}\text{C}\{^1\text{H}\}$ NMR (100.62 MHz, C_6D_6): δ = 150.2, 138.0, 132.7, 129.1, 127.4, 83.2, 25.0 ppm.²¹

3,3-Dimethylbut-1-yne + Pinacolborane (HB2)



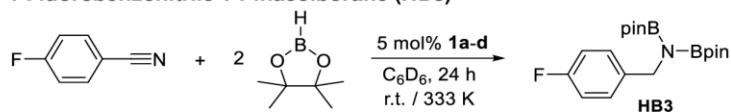
Catalyst	3,3-Dimethylbut-1-yne conversion
1a	81%
1b -dme	76%
1c -dme	88%
1d -dme	79%

^1H NMR (400.13 MHz, C_6D_6): δ = 6.86 (d, $^3J_{\text{HH}} = 17.9$ Hz, 1 H, C=*CH*), 5.56 (d, $^3J_{\text{HH}} = 19.7$ Hz, 1 H, C=*CH*), 1.09 (s, 12 H, OC(*CH*₃)₂), 0.91 ppm (s, 9 H, C(*CH*₃)₃); ^{11}B NMR (96.29 MHz, C_6D_6): δ = 30.5 ppm; $^{13}\text{C}\{^1\text{H}\}$ NMR (100.62 MHz, C_6D_6): δ = 164.3, 82.9, 35.0, 29.0, 25.1 ppm.²²

SUPPORTING INFORMATION

WILEY-VCH

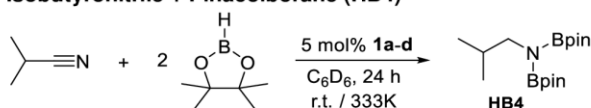
4-Fluorobenzonitrile + Pinacolborane (HB3)



Catalyst	Temperature	Nitrile conversion
1a	298 K	63%
1a	333 K	≥95%
1b dme	298 K	≥95%
1c dme	298 K	≥95%
1d dme	298 K	≥95%

1H NMR (400.13 MHz, C_6D_6): δ = 7.38-7.31 (m, 2 H, Ph-H), 6.89-6.82 (m, 2 H, Ph-H), 4.36 (s, 2 H, N-CH₂), 1.00 ppm (s, 24 H, OC(CH₃)₂); ^{11}B NMR (96.29 MHz, C_6D_6): δ = 26.4 ppm; $^{13}C\{^1H\}$ NMR (100.62 MHz, C_6D_6): δ = 163.3, 160.9, 139.5, 129.8, 115.1, 114.9, 82.5 (OC(CH₃)₂), 47.0 (N-CH₂), 24.7 ppm (OC(CH₃)₂); $^{19}F\{^1H\}$ NMR (282.38 MHz, C_6D_6): δ = -116.9 ppm.²³

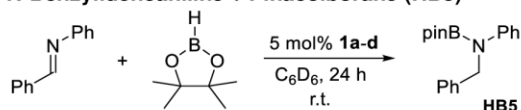
Isobutyronitrile + Pinacolborane (HB4)



Catalyst	Temperature	Amine conversion
1a	298 K	39%
1a	333 K	≥95%
1b dme	298 K	≥95%
1c dme	298 K	≥95%
1d dme	298 K	≥95%

1H NMR (400.13 MHz, C_6D_6): δ = 3.10 (d, $^3J_{HH}$ = 6.8 Hz, 2 H, N-CH₂), 1.89 (sept, $^3J_{HH}$ = 6.8 Hz, 1 H, CH(CH₃)₂), 1.02 (s, 24 H, OC(CH₃)₂), 0.89 ppm (d, $^3J_{HH}$ = 6.7 Hz, 6 H, CH(CH₃)₂); ^{11}B NMR (96.29 MHz, C_6D_6): δ = 26.3 ppm; $^{13}C\{^1H\}$ NMR (100.62 MHz, C_6D_6): δ = 82.1 (OC(CH₃)₂), 51.6 (N-CH₂), 31.1 (CH(CH₃)₂), 24.8 (OC(CH₃)₂), 20.3 ppm (CH(CH₃)₂).²³

N-Benzylideneaniline + Pinacolborane (HB5)

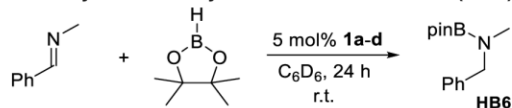


Catalyst	Imine conversion
1a	66%
1b dme	76%
1c dme	66%
1d dme	60%

SUPPORTING INFORMATION

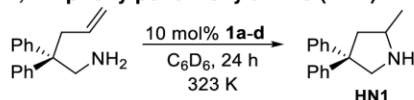
WILEY-VCH

^1H NMR (400.13 MHz, C_6D_6): δ = 7.43-7.38 (m, 2 H, Ph-*H*), 7.19-7.14 (m, 4 H, Ph-*H*), 7.13-7.02 (m, 6 H, Ph-*H*), 4.71 (s, 2 H, N- CH_2), 1.04 ppm (s, 12 H, $\text{OC}(\text{CH}_3)_2$); ^{11}B NMR (96.29 MHz, C_6D_6): δ = 25.2 ppm; $^{13}\text{C}\{^1\text{H}\}$ NMR (100.62 MHz, C_6D_6): δ = 146.7 (Ph), 140.9 (Ph), 128.7 (Ph), 126.8 (Ph), 126.6 (Ph), 120.9 (Ph), 83.0 ($\text{OC}(\text{CH}_3)_2$), 51.5 (N- CH_2), 24.7 ppm ($\text{OC}(\text{CH}_3)_2$).²⁴

N-Benzylidenemethylamine + Pinacolboran (HB6)

Catalyst	Imine conversion
1a	79%
1b-dme	70%
1c-dme	72%
1d-dme	54%

^1H NMR (400.13 MHz, C_6D_6): δ = 7.24-7.19 (m, 2 H, Ph-*H*), 7.18-7.13 (m, 2 H, Ph-*H*), 7.13-7.04 (m, 1 H, Ph-*H*), 4.09 (s, 2 H, N- CH_2), 2.53 (s, 3 H, N- CH_3), 1.12 ppm (s, 12 H, $\text{OC}(\text{CH}_3)_2$);²⁵ ^{11}B NMR (96.29 MHz, C_6D_6): δ = 24.6 ppm; $^{13}\text{C}\{^1\text{H}\}$ NMR (100.62 MHz, C_6D_6): δ = 140.7 (Ph), 128.6 (Ph), 128.1 (Ph), 127.0 (Ph), 82.4 ($\text{OC}(\text{CH}_3)_2$), 53.2 (N- CH_2), 33.3 (N- CH_3), 25.0 ppm ($\text{OC}(\text{CH}_3)_2$).

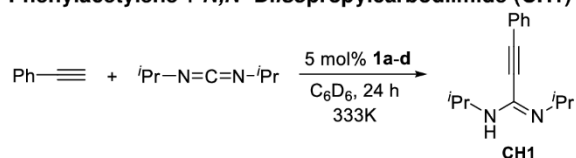
2,2-Diphenylpent-4-enylamine (HN1)

Catalyst	Amine conversion
1a	$\geq 95\%$
1b-dme	$\geq 95\%$
1c-dme	$\geq 95\%$
1d-dme	$\geq 95\%$

^1H NMR (400.13 MHz, C_6D_6): δ = 7.23-7.18 (m, 2 H, Ph-*H*), 7.15-7.07 (m, 6 H, Ph-*H*), 7.04-6.98 (m, 2 H, Ph-*H*), 3.53-3.44 (m, 1 H, CH_2N), 3.41-3.31 (m, 1 H, CH_2N), 3.21-3.09 (m, 1 H, CHN), 2.39 (dd, $^2J_{\text{HH}} = 12.4$ Hz, $^3J_{\text{HH}} = 6.4$ Hz, 1 H, CH_2), 1.82 (dd, $^2J_{\text{HH}} = 12.4$ Hz, $^3J_{\text{HH}} = 8.9$ Hz, 1 H, CH_2), 1.35 (bs, 1 H, NH), 1.01 ppm (d, $^3J_{\text{HH}} = 6.3$ Hz, 3 H, CH_3); $^{13}\text{C}\{^1\text{H}\}$ NMR (100.62 MHz, C_6D_6): δ = 148.6 (Ph), 148.0 (Ph), 128.5 (Ph), 127.6 (Ph), 127.5 (Ph), 126.2 (Ph), 126.1 (Ph), 58.7 (CH_2NH), 57.2 (CPh_2), 53.3 (CH-CH_3), 47.5 (CH_2), 22.5 ppm (CH_3).²⁶

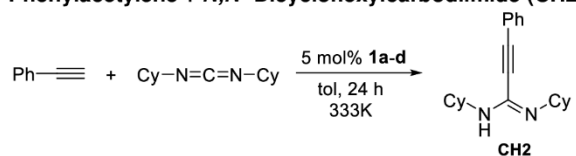
SUPPORTING INFORMATION

WILEY-VCH

Phenylacetylene + *N,N'*-Diisopropylcarbodiimide (CH1)

Catalyst	Carbodiimide conversion
1a	79%
1b-dme	73%
1c-dme	78%
1d-dme	63%

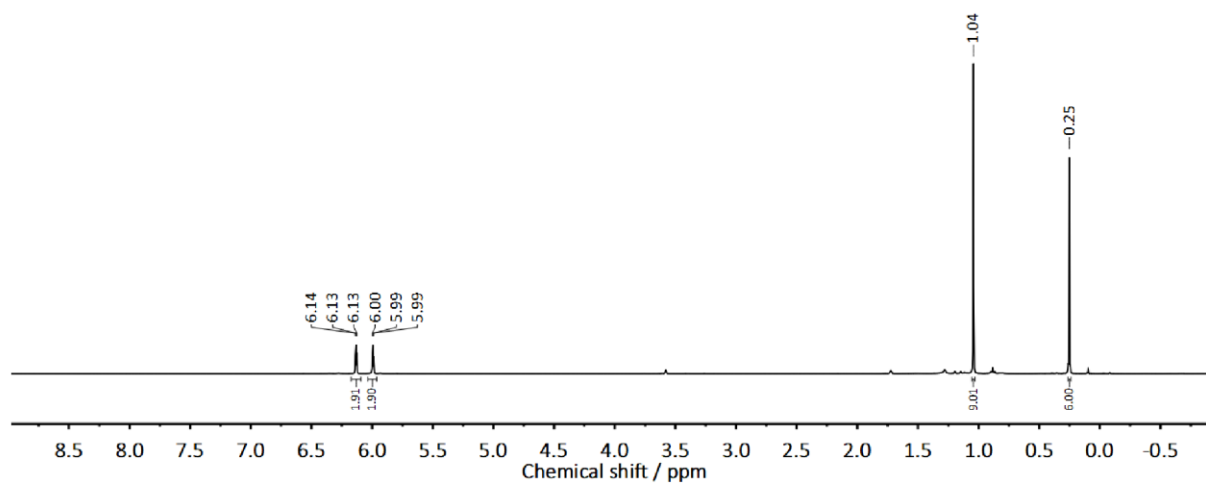
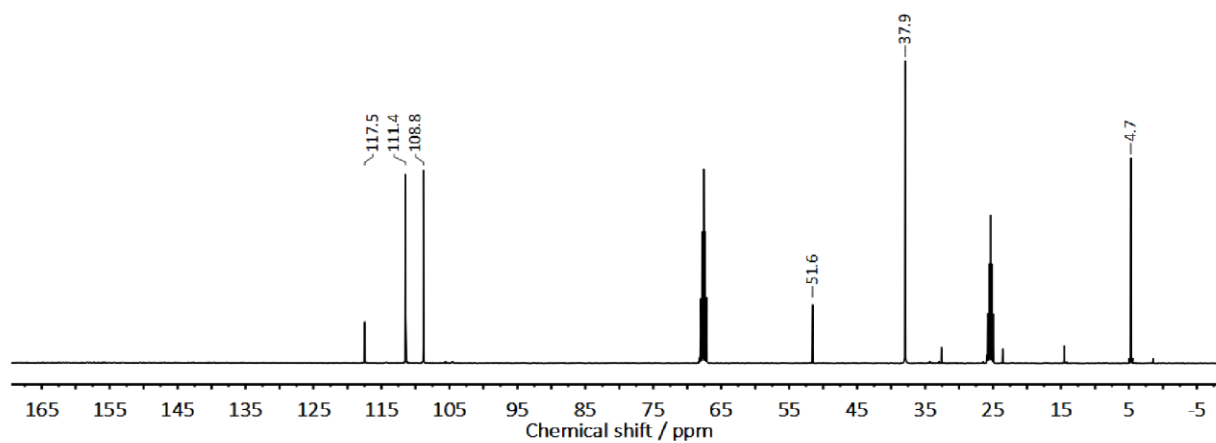
^1H NMR (300.13 MHz, CDCl_3): δ = 7.53-7.46 (m, 2 H, Ph-*H*), 7.38-7.30 (m, 3 H, Ph-*H*), 3.96 (s, 2 H, $\text{CH}(\text{CH}_3)_2$), 1.18 ppm (d, $^3J_{\text{HH}}$ = 6.7 Hz, 12 H, $\text{CH}(\text{CH}_3)_2$); $^{13}\text{C}\{^1\text{H}\}$ NMR (75.48 MHz, CDCl_3): δ = 141.3, 132.0, 129.3, 128.5, 121.6, 79.5, 24.7 ppm.^{27,28}

Phenylacetylene + *N,N'*-Dicyclohexylcarbodiimide (CH2)

Catalyst	Carbodiimide conversion
1a	62%
1b-dme	54%
1c-dme	61%
1d-dme	56%

^1H NMR (300.13 MHz, CDCl_3): δ = 7.48-7.27 (m, 5 H, Ph-*H*), 3.69-3.43 (m, 2 H, $\text{CH}(\text{CH}_3)_2$), 2.02-1.40 ppm (m, 20 H, $\text{CH}(\text{CH}_3)_2$); $^{13}\text{C}\{^1\text{H}\}$ NMR (75.48 MHz, CDCl_3): δ = 141.8, 132.0, 129.3, 126.7, 121.7, 79.5, 35.0, 25.9, 25.5 ppm.^{27,28}

NMR Spectra

Figure S1. ^1H NMR (400.13 MHz, thf-d_8) spectrum of 1a.Figure S2. ^{13}C NMR (100.62 MHz, thf-d_8) spectrum of 1a.

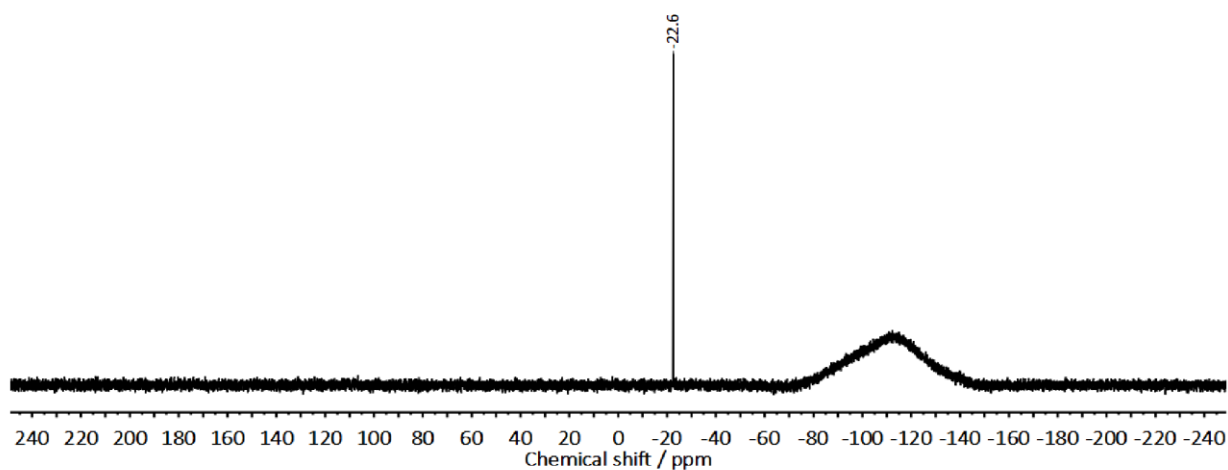


Figure S3. $^{29}\text{Si}\{^1\text{H}\}$ NMR (79.49 MHz, thf-d8) spectrum of **1a**.

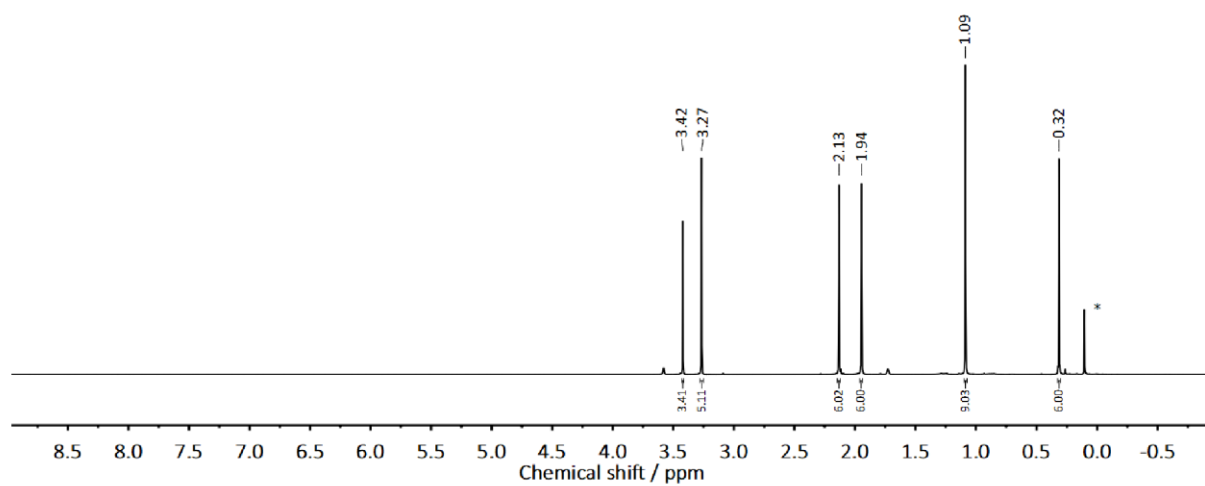


Figure S4. ^1H NMR (400.13 MHz, thf-d8) spectrum of **1b-dme** (* silicon grease).

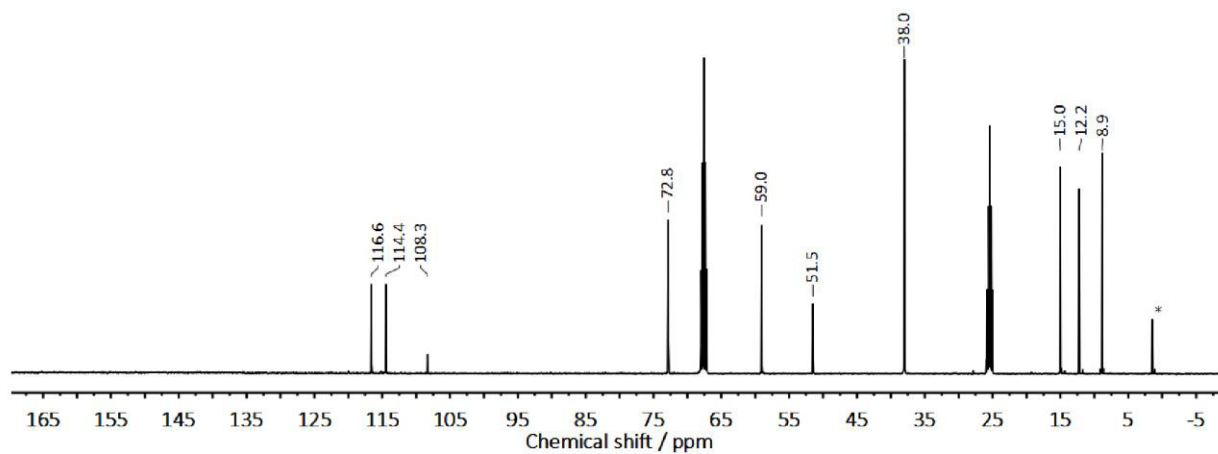


Figure S5. $^{13}\text{C}\{^1\text{H}\}$ NMR (100.62 MHz, thf-d8) spectrum of **1b**-dme (* silicon grease).

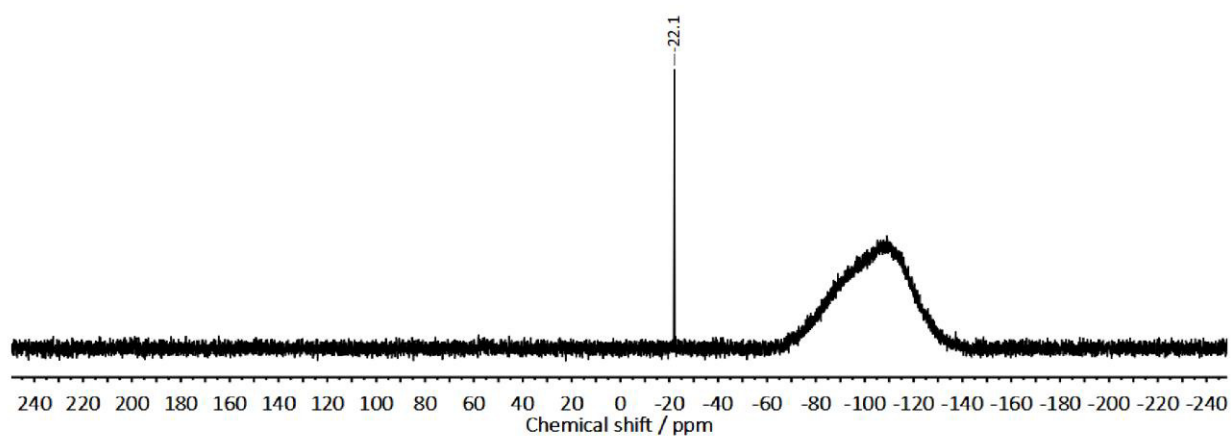


Figure S6. $^{29}\text{Si}\{^1\text{H}\}$ NMR (79.49 MHz, thf-d8) spectrum of **1b**-dme.

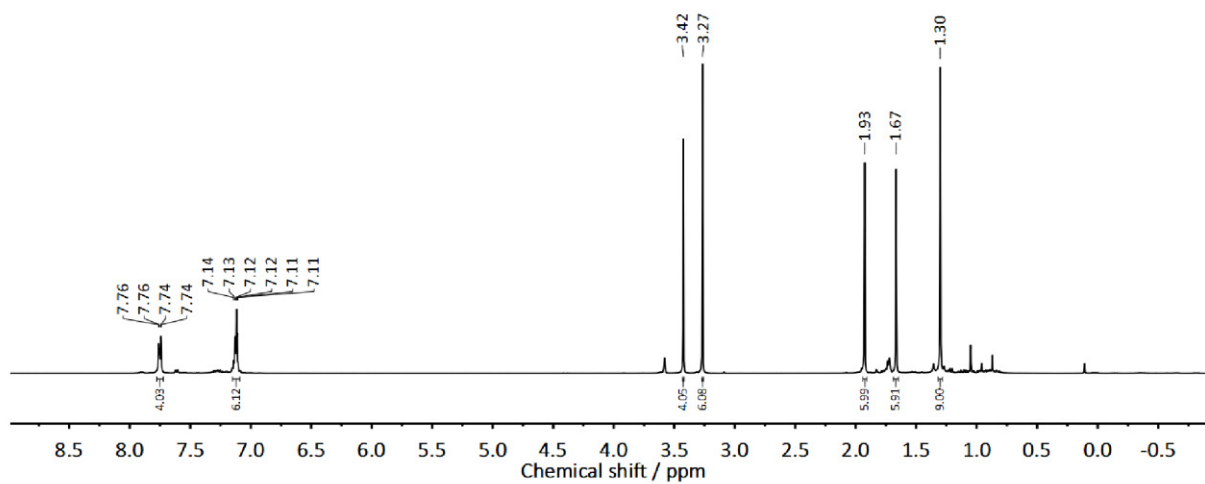


Figure S7. ^1H NMR (400.13 MHz, thf-d_8) spectrum of **1c-dme**.

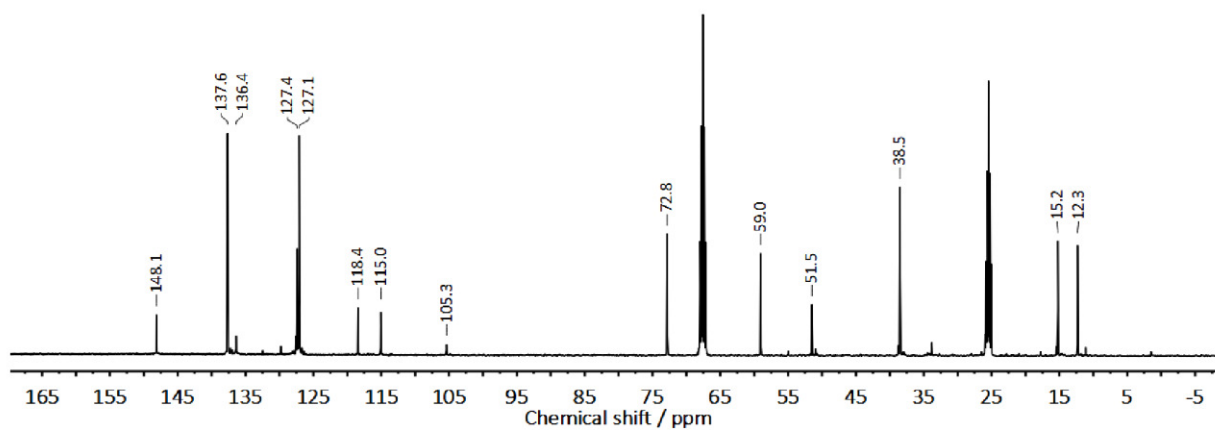


Figure S8. ^{13}C NMR (100.62 MHz, thf-d_8) spectrum of **1c-dme**.

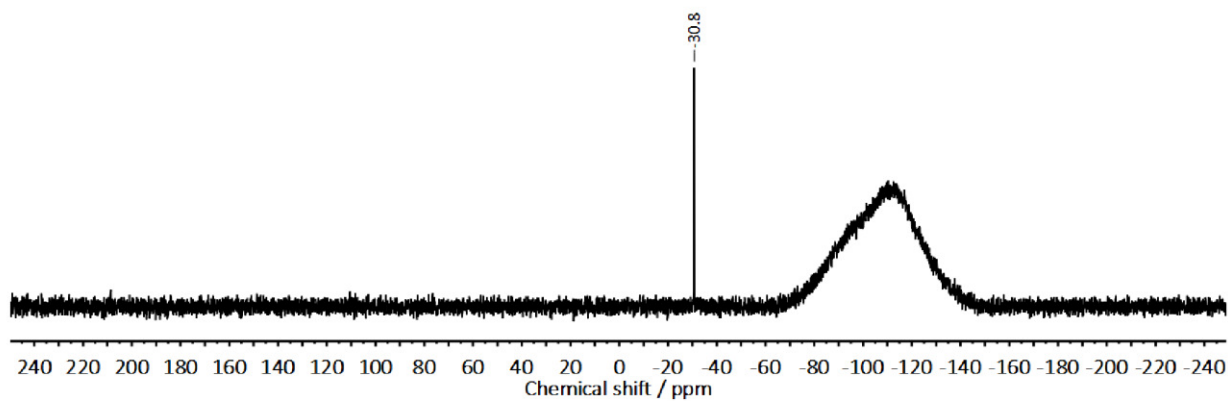


Figure S9. $^{29}\text{Si}\{^1\text{H}\}$ NMR (79.49 MHz, thf-d8) spectrum of **1c-dme**.

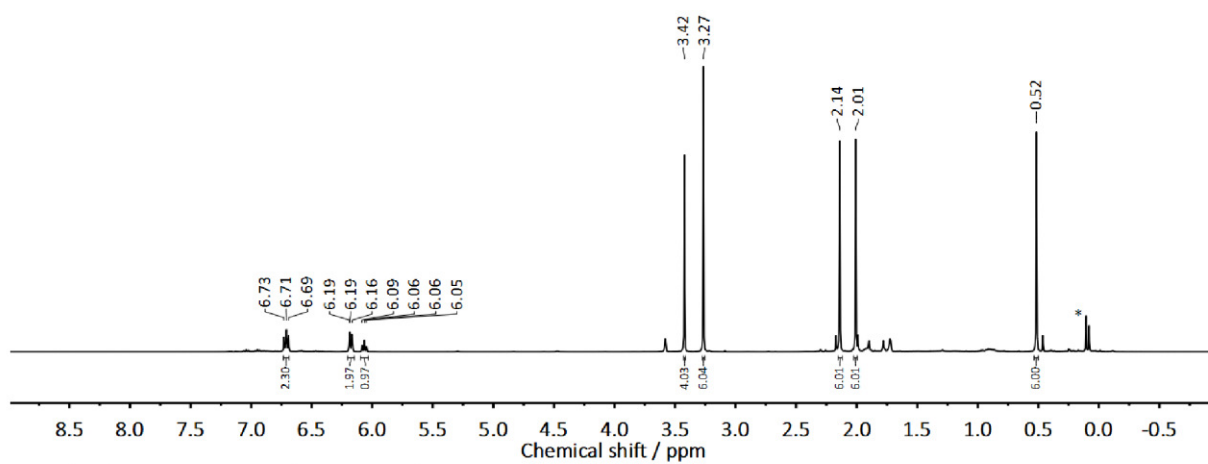


Figure S10. ^1H NMR (400.13 MHz, thf-d8) spectrum of **1d-dme** (* silicon grease).

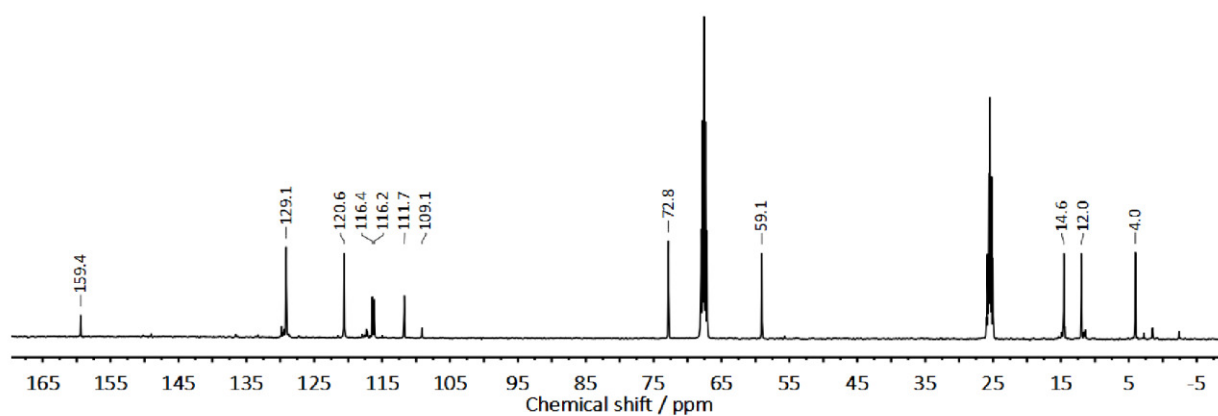


Figure S11. $^{13}\text{C}\{^1\text{H}\}$ NMR (100.62 MHz, thf-d8) spectrum of **1d-dme**.

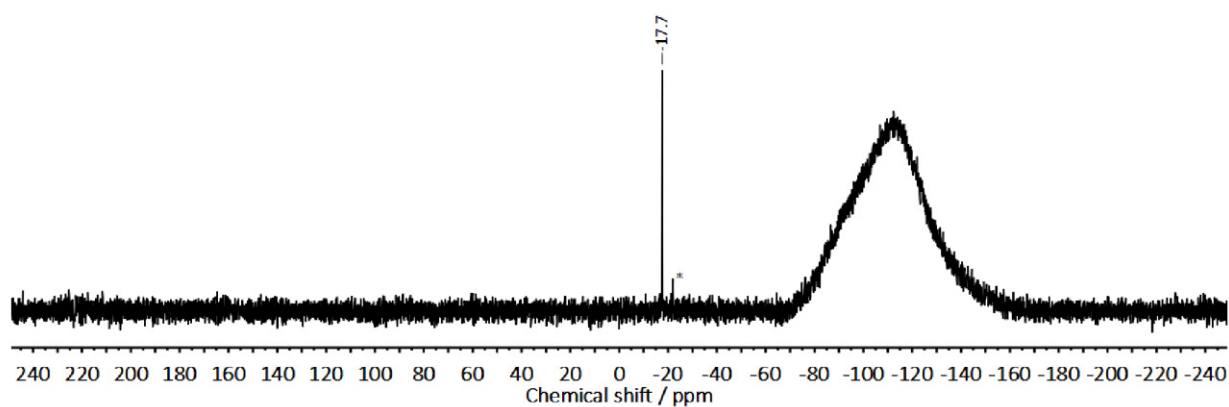


Figure S12. $^{29}\text{Si}\{^1\text{H}\}$ NMR (79.49 MHz, thf-d8) spectrum of **1d-dme** (* silicon grease).

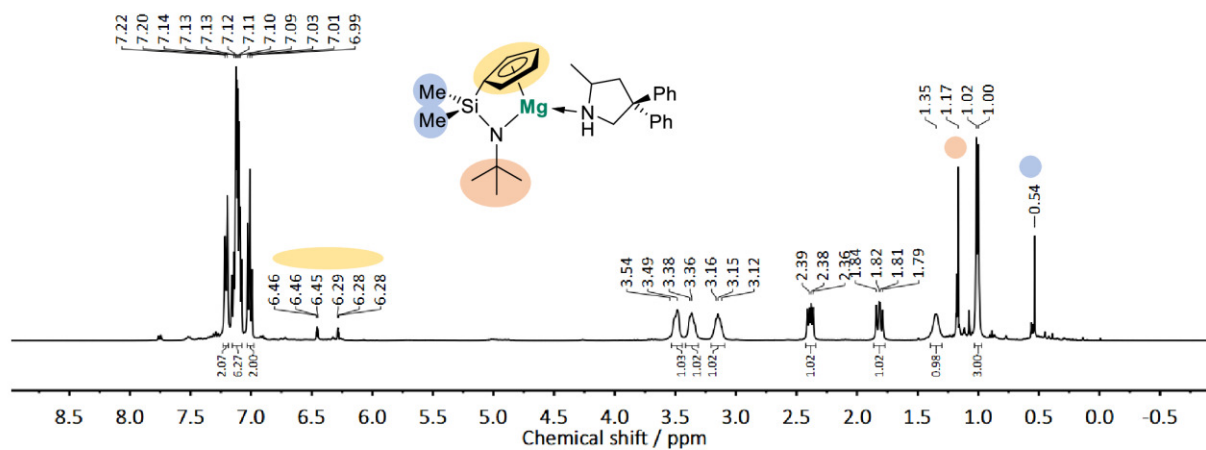


Figure S13. ¹H NMR (400.13 MHz, C₆D₆) spectrum of the intramolecular hydroamination reaction catalyzed by **1a**.

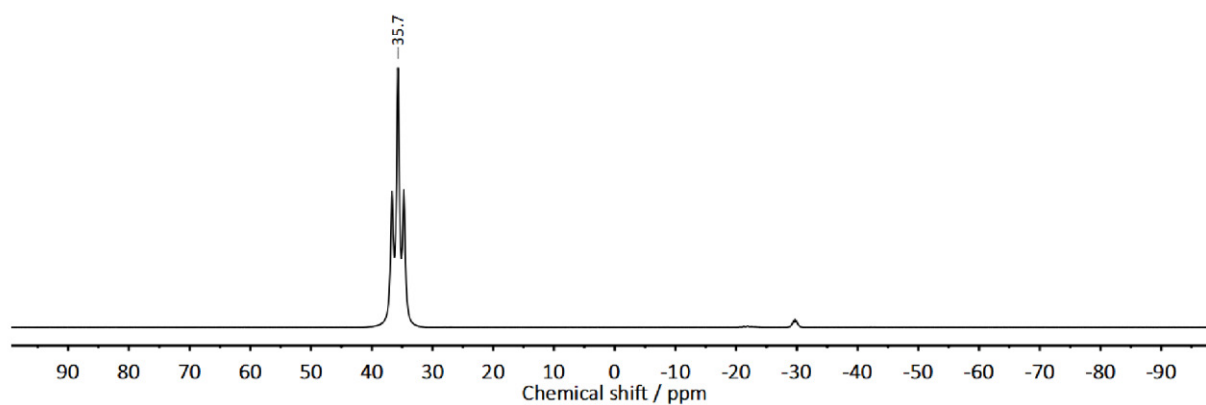


Figure S14. ¹¹B NMR (128.38 MHz, dme) spectrum of the coupling product **BN1** from a reaction catalyzed by **1b-dme**.

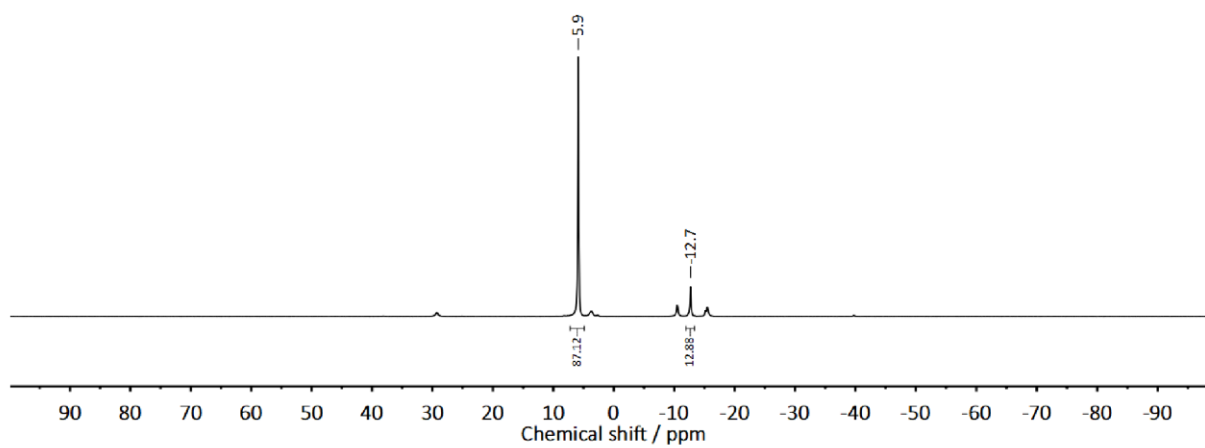


Figure S15. $^{11}\text{B}\{^1\text{H}\}$ NMR (96.29 MHz, dme) spectrum of the coupling product **BN2** from a reaction catalyzed by **1b**-dme.

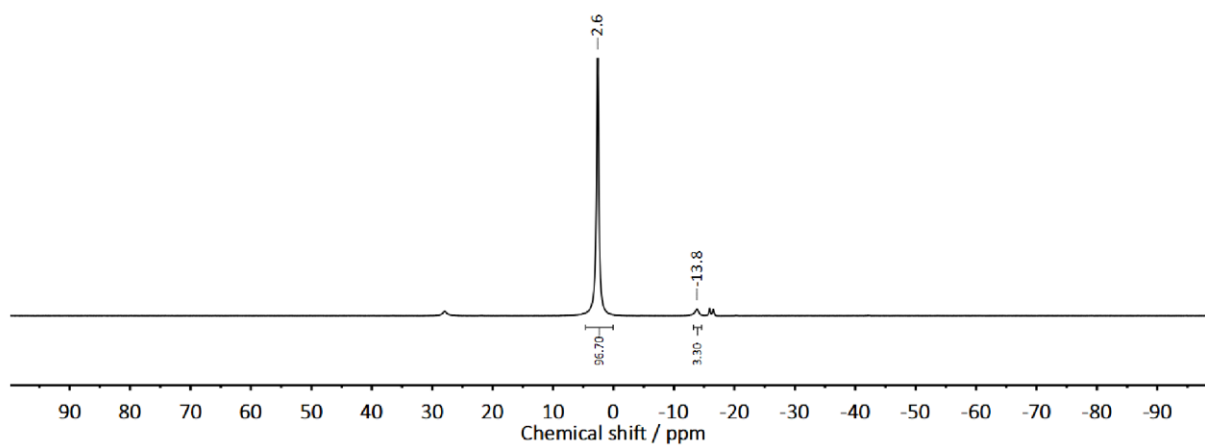


Figure S16. $^{11}\text{B}\{^1\text{H}\}$ NMR (96.29 MHz, dme) spectrum of the coupling product **BN3** from a reaction catalyzed by **1d**-dme.

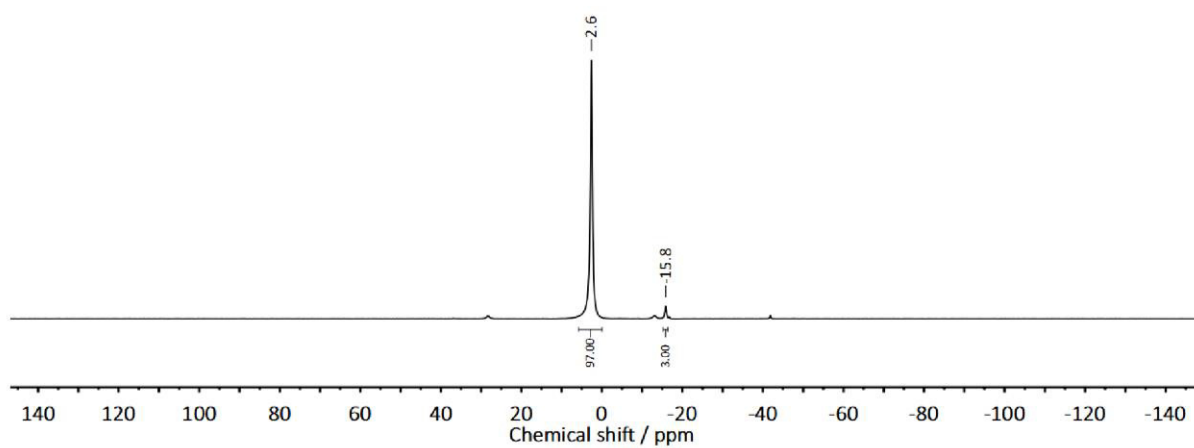


Figure S17. $^{11}\text{B}\{^1\text{H}\}$ NMR (96.29 MHz, dme) spectrum of the coupling product **BN4** from a reaction catalyzed by **1a**.

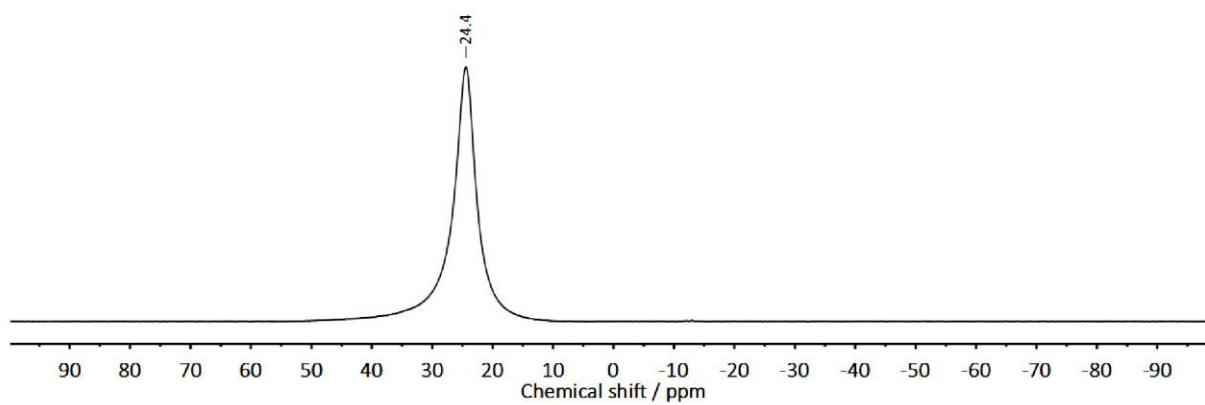


Figure S18. ^{11}B NMR (96.29 MHz, dme) spectrum of the coupling product **BN5** from a reaction catalyzed by **1c-dme**.

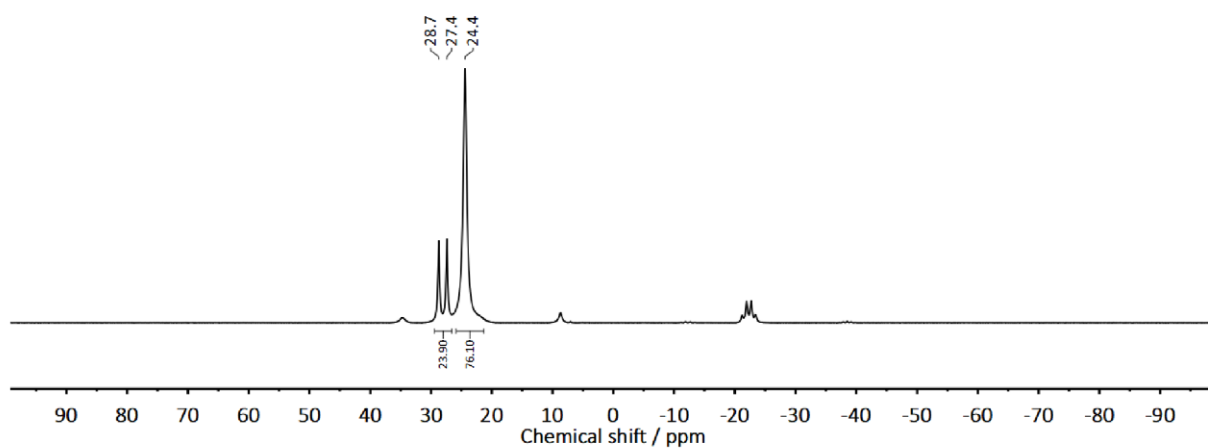


Figure S19. ^{11}B NMR (96.29 MHz, dme) spectrum of the coupling product **BN6** from a reaction catalyzed by **1a**.

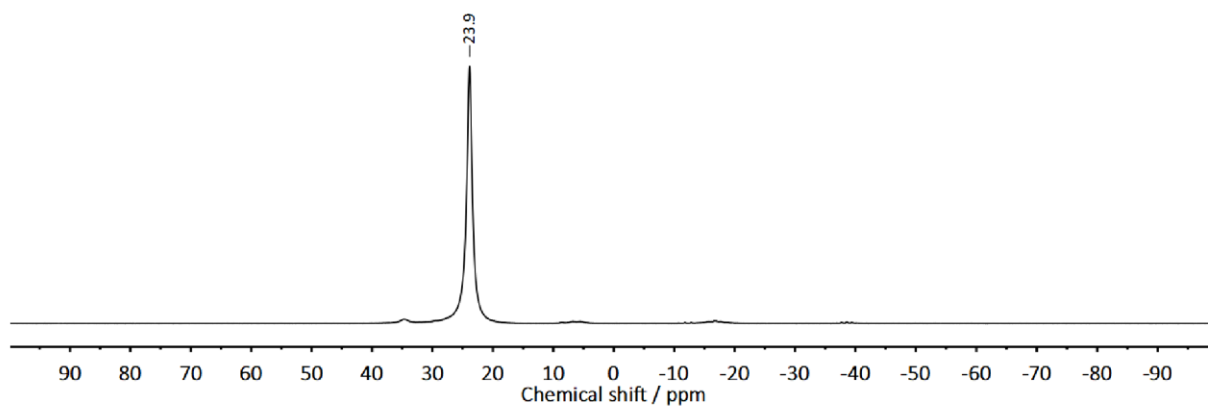


Figure S20. ^{11}B NMR (96.29 MHz, dme) spectrum of the coupling product **BN7** from a reaction catalyzed by **1c**-dme.

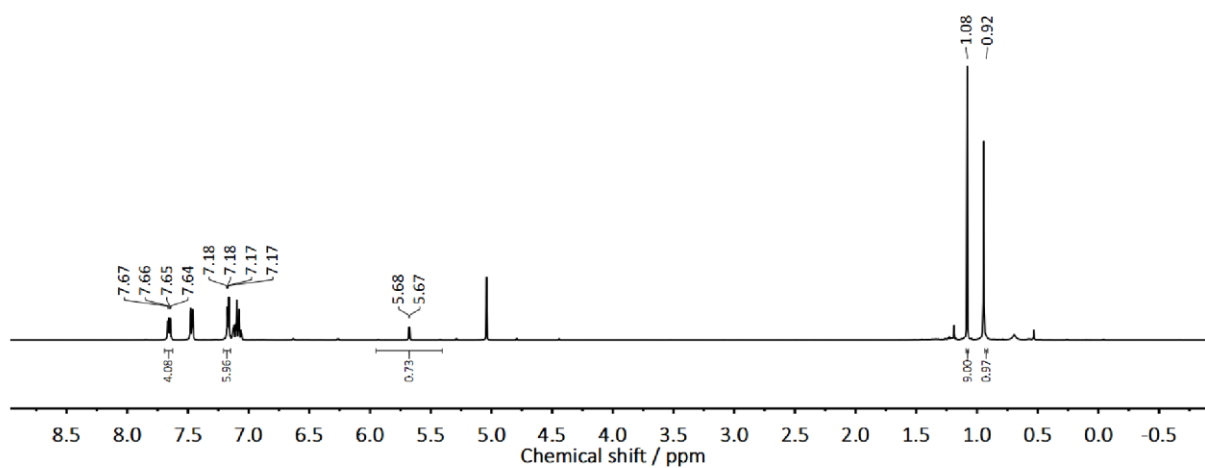


Figure S21. ¹H NMR (400.13 MHz, C₆D₆) spectrum of the coupling product SiN1 from a reaction catalyzed by **1a**.

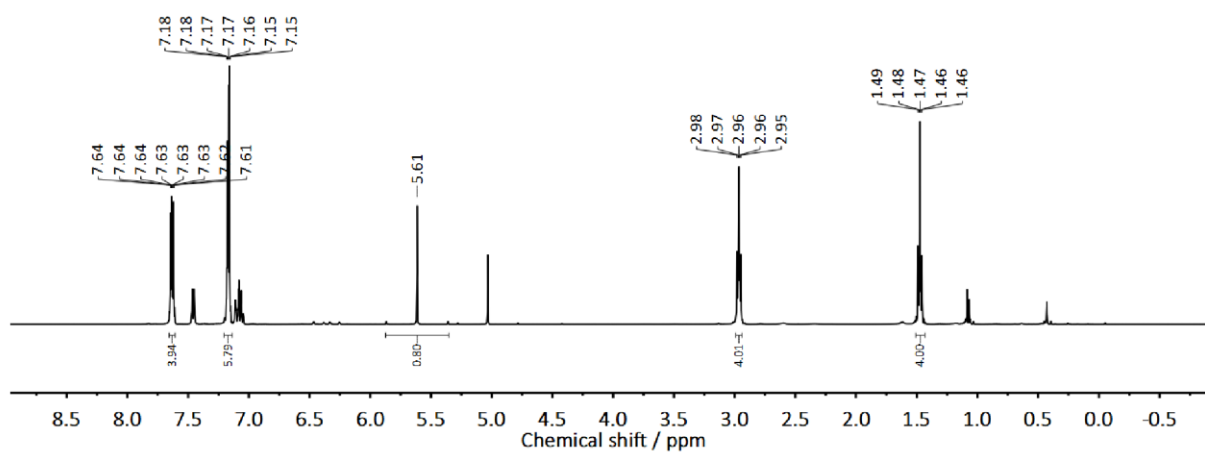


Figure S22. ¹H NMR (400.13 MHz, C₆D₆) spectrum of the coupling product SiN2 from a reaction catalyzed by **1a**.

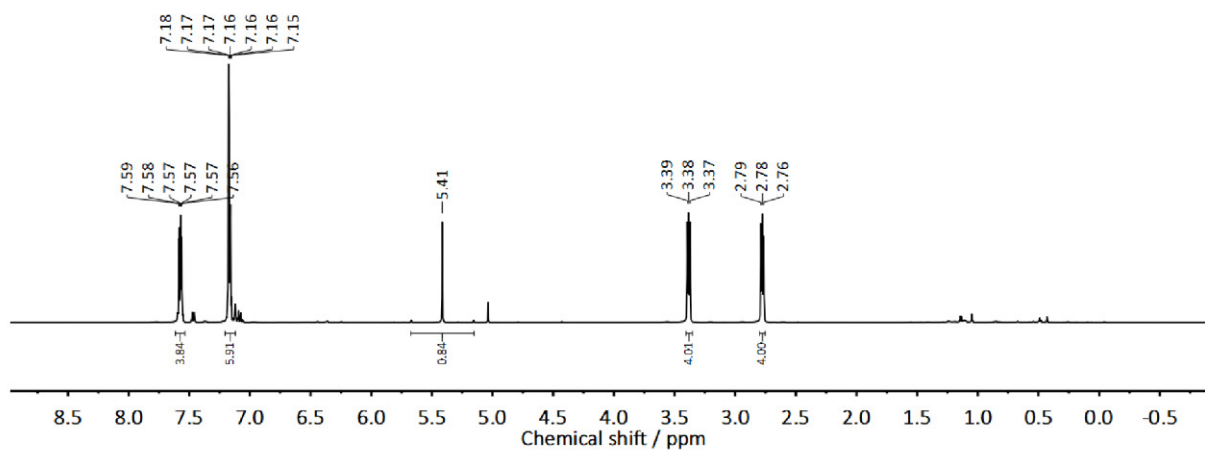


Figure S23. ¹H NMR (400.13 MHz, C₆D₆) spectrum of the coupling product SIN3 from a reaction catalyzed by **1a**.

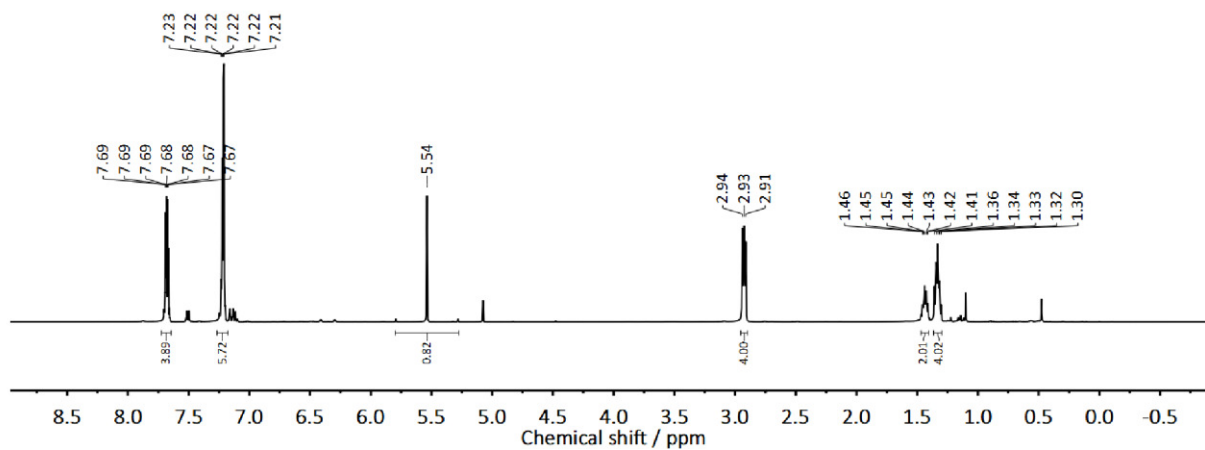


Figure S24. ¹H NMR (400.13 MHz, C₆D₆) spectrum of the coupling product SIN4 from a reaction catalyzed by **1a**.

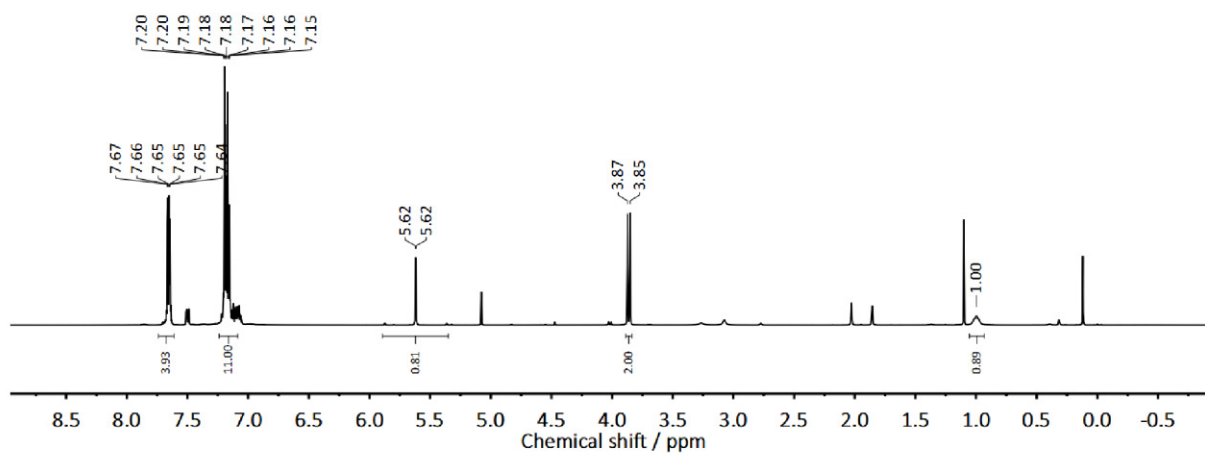


Figure S25. ¹H NMR (400.13 MHz, C₆D₆) spectrum of the coupling product SiN5 from a reaction catalyzed by **1b**-dme.

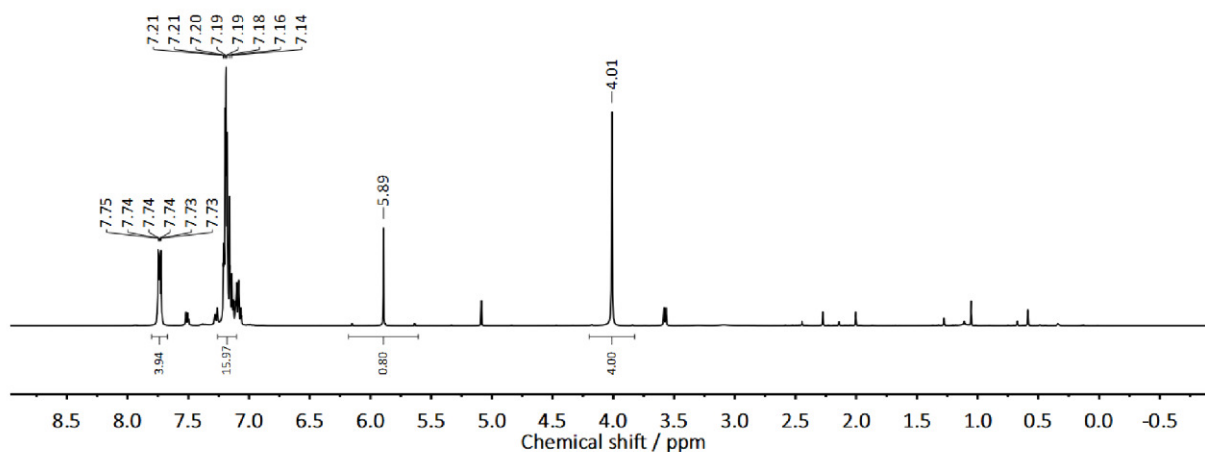


Figure S26. ¹H NMR (400.13 MHz, C₆D₆) spectrum of the coupling product SiN6 from a reaction catalyzed by **1b**-dme.

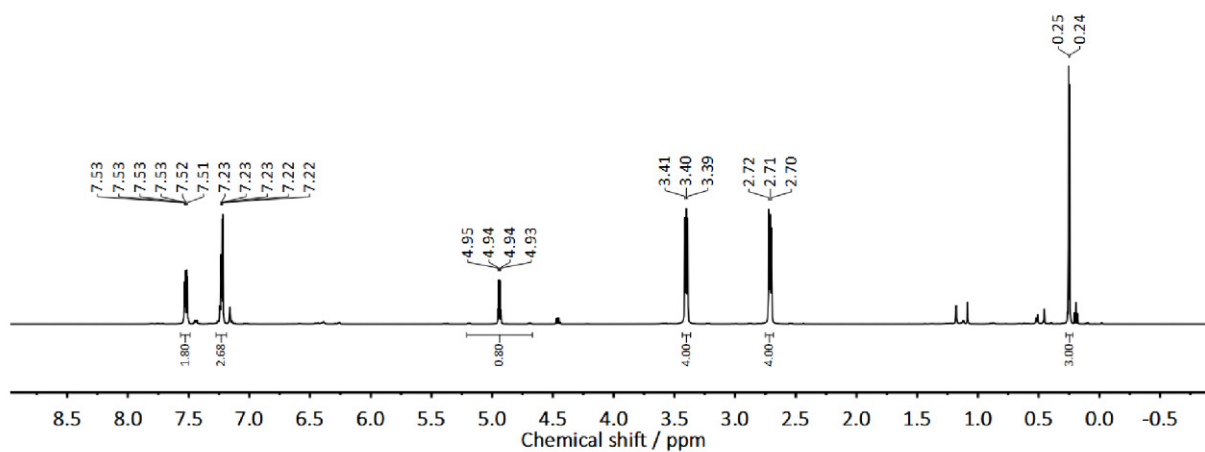


Figure S27. ¹H NMR (400.13 MHz, C₆D₆) spectrum of the coupling product SiN7 from a reaction catalyzed by **1a**.

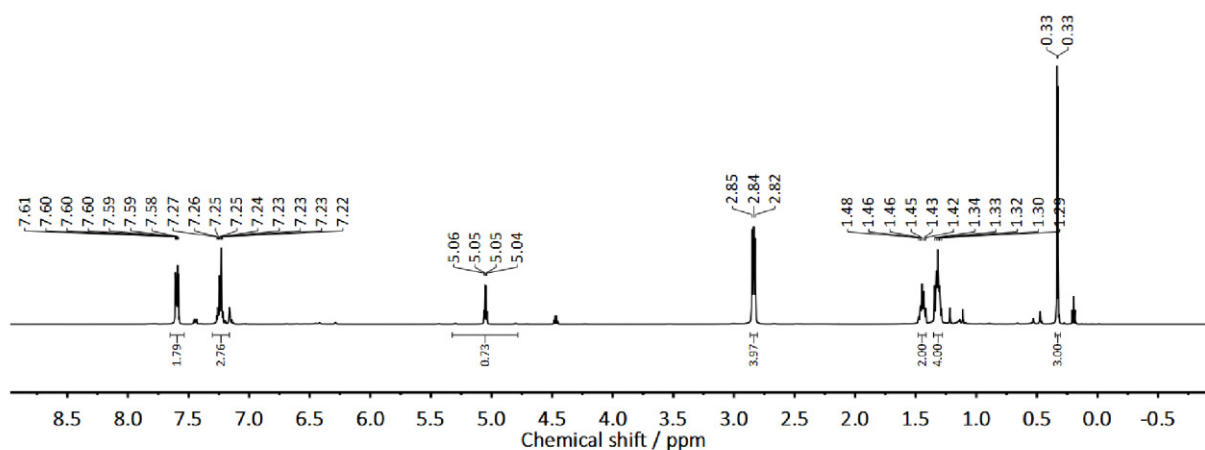


Figure S28. ¹H NMR (400.13 MHz, C₆D₆) spectrum of the coupling product SiN8 from a reaction catalyzed by **1a**.

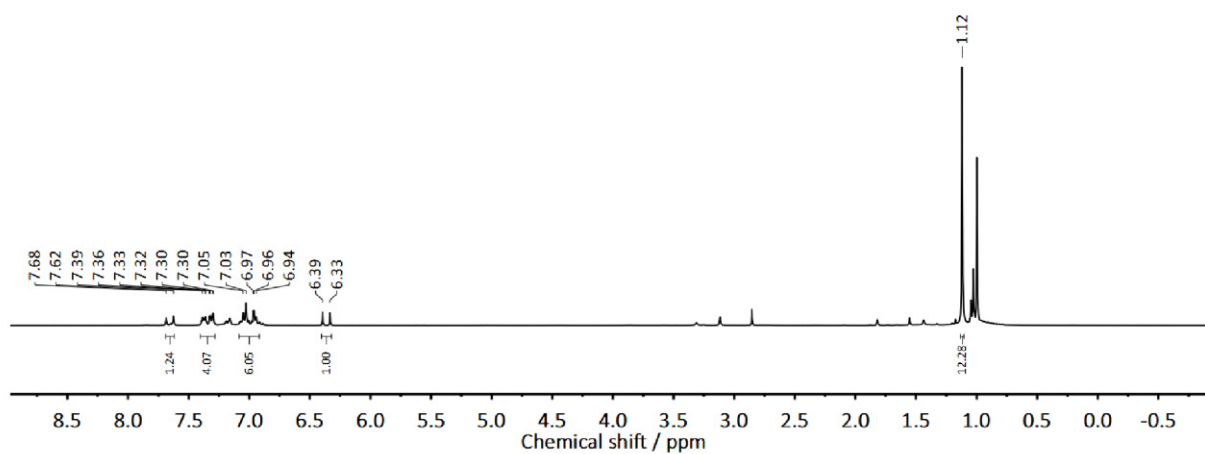


Figure S29. ¹H NMR (300.13 MHz, C₆D₆) spectrum of the coupling product **HB1** from a reaction catalyzed by **1c-dme**.

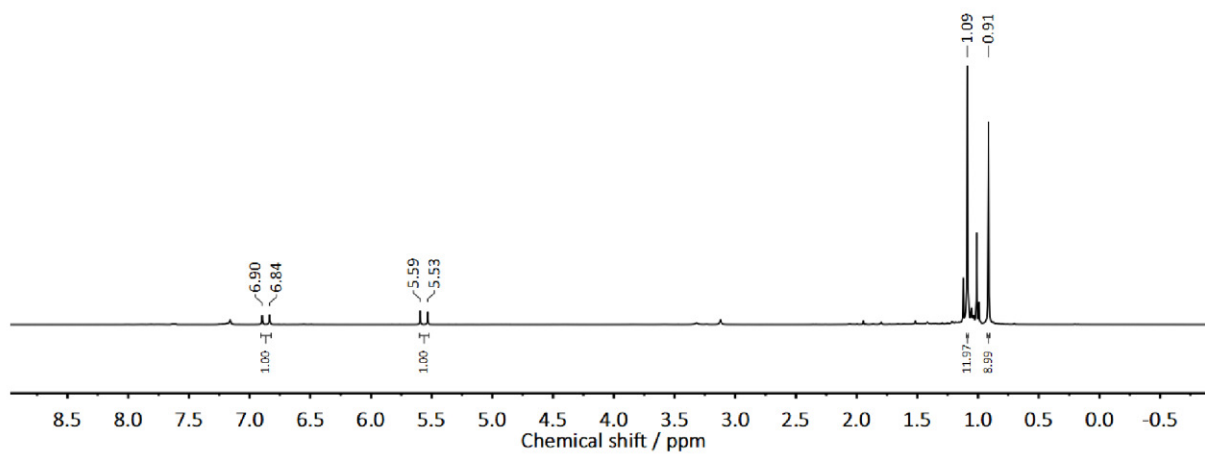


Figure S30. ¹H NMR (300.13 MHz, C₆D₆) spectrum of the coupling product **HB2** from a reaction catalyzed by **1c-dme**.

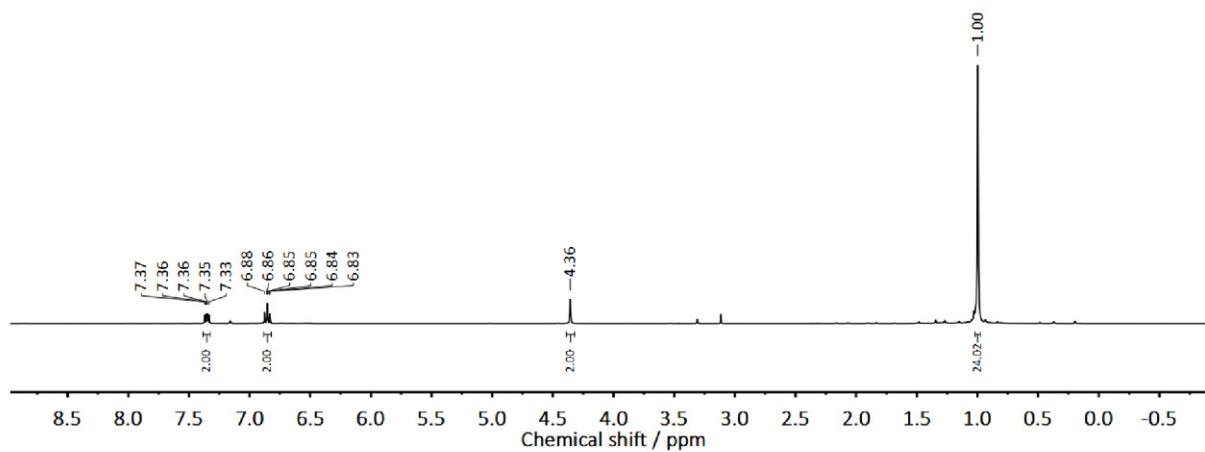


Figure S31. ¹H NMR (400.13 MHz, C₆D₆) spectrum of the coupling product **HB3** from a reaction catalyzed by **1b-dme**.

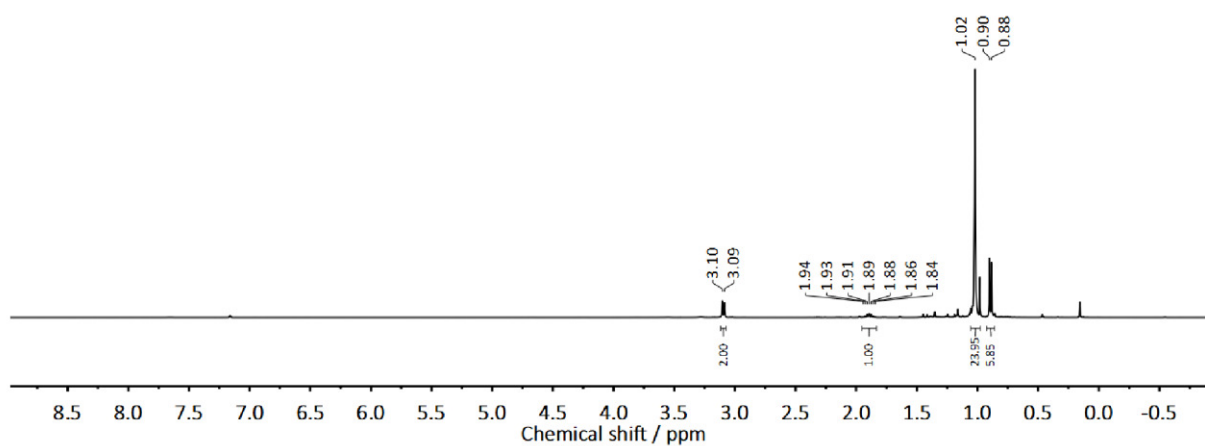


Figure S32. ¹H NMR (400.13 MHz, C₆D₆) spectrum of the coupling product **HB4** from a reaction catalyzed by **1b-dme**.

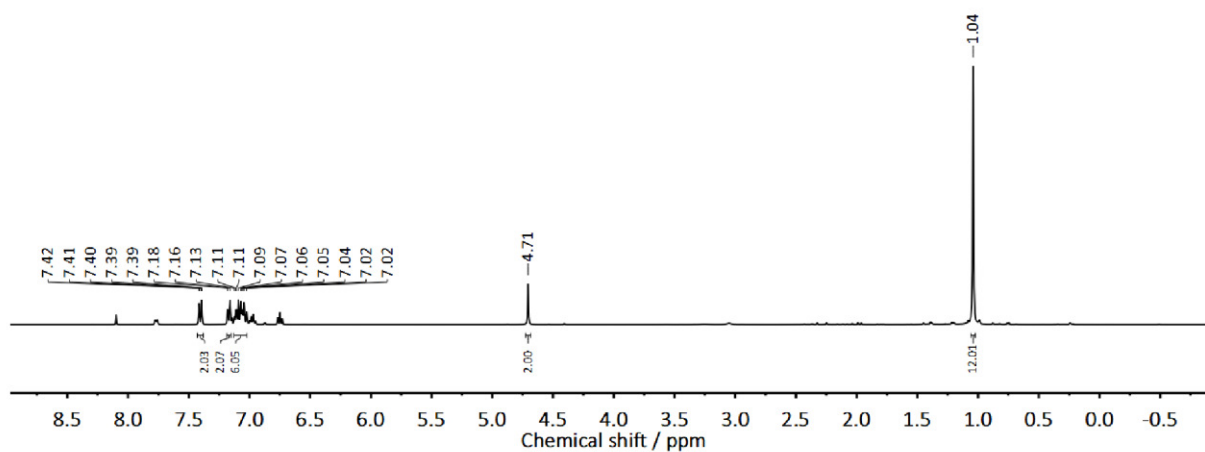


Figure S33. ¹H NMR (400.13 MHz, C₆D₆) spectrum of the coupling product **HB5** from a reaction catalyzed by **1b**-dme.

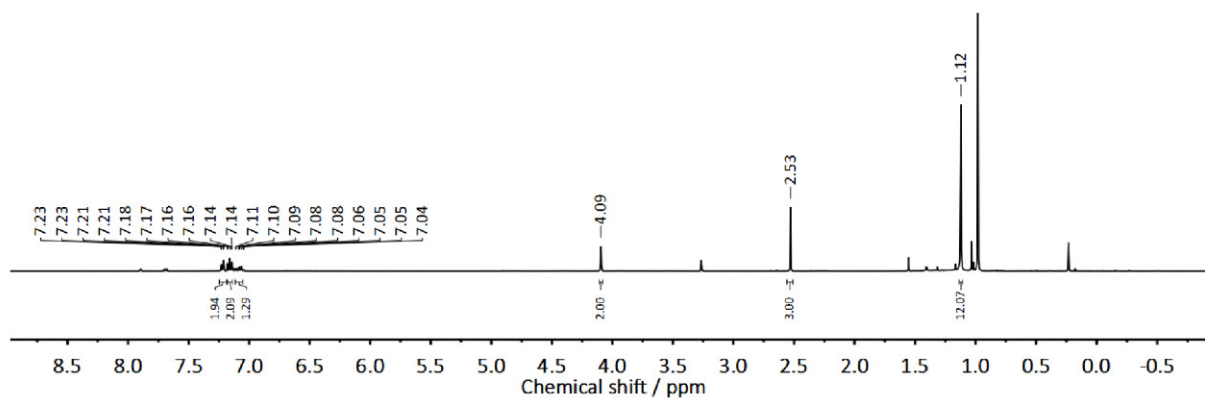


Figure S34. ¹H NMR (400.13 MHz, C₆D₆) spectrum of the coupling product **HB6** from a reaction catalyzed by **1a**.

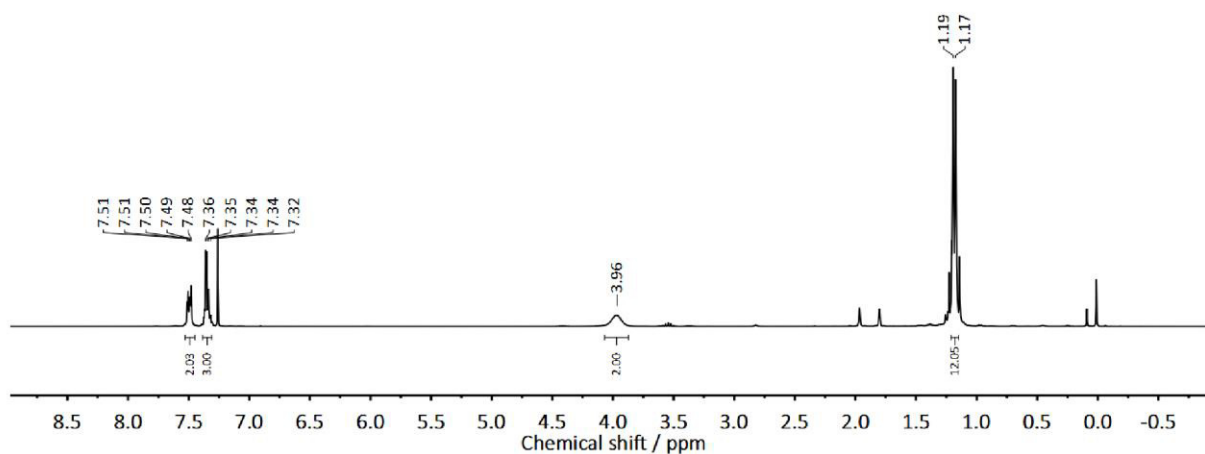


Figure S35. ¹H NMR (300.13 MHz, CDCl₃) spectrum of the coupling product CH1 from a reaction catalyzed by 1b-dme.

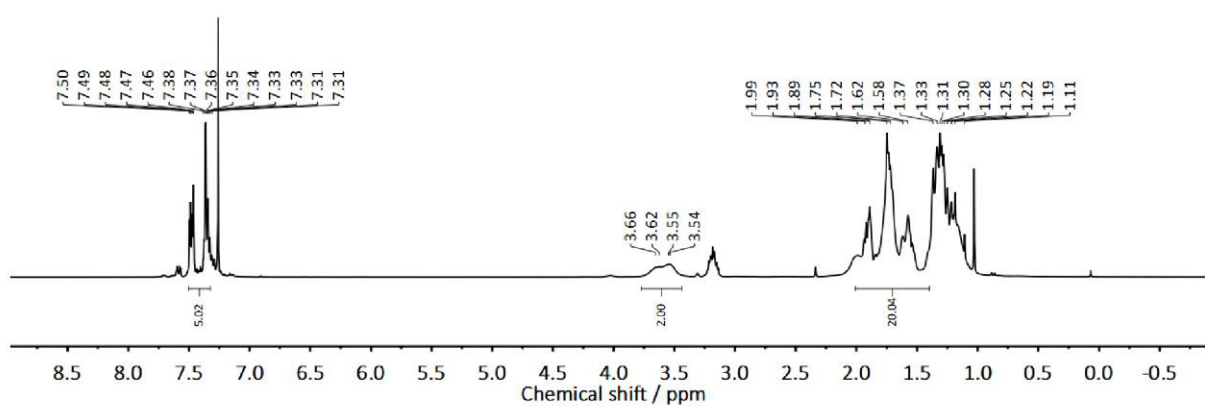


Figure S36. ¹H NMR (300.13 MHz, CDCl₃) spectrum of the coupling product CH2 from a reaction catalyzed by 1c-dme.

XRD Data

Crystal structure data has been deposited with the Cambridge Crystallographic Data Centre (CCDC) and is available free of charge from the Cambridge Structural Database (see CCDC number).

crystal structure data of **1a**·(thf)₂

CCDC code	2193660	
Empirical formula	C ₁₉ H ₃₅ MgNO ₂ Si	
Formula weight	361.88	
Temperature	133(2) K	
Wavelength	0.71073 Å	
Crystal system	orthorhombic	
Space group	<i>Pna</i> 2 ₁	
Unit cell dimensions	a = 13.8797(5) Å	α = 90°
	b = 10.3886(4) Å	β = 90°
	c = 44.2076(16) Å	γ = 90°
Volume	6374.3(4) Å ³	
Z	12	
Density (calculated)	1.131 mg m ⁻³	
Absorption coefficient	0.151 mm ⁻¹	
F(000)	2376	
Crystal size	0.302 x 0.222 x 0.095 mm ³	
Theta range for data collection	2.014 to 27.119°	
Index ranges	-17<=h<=17, -13<=k<=13, -56<=l<=56	
Reflections collected	83775	
Independent reflections	14061 [R(int) = 0.0616]	
Completeness to theta = 25.242°	100.0 %	
Absorption correction	semi-empirical from equivalents	
Max. and min. transmission	0.7455 and 0.6799	
Refinement method	full-matrix least-squares on F ²	
Data / restraints / parameters	14061 / 1 / 649	
Goodness-of-fit on F ²	1.057	
Final R indices [I>2sigma(I)]	R1 = 0.0492, wR2 = 0.1087	
R indices (all data)	R1 = 0.0712, wR2 = 0.1211	
Extinction coefficient	n/a	
Largest diff. peak and hole	0.510 and -0.321 e.Å ⁻³	

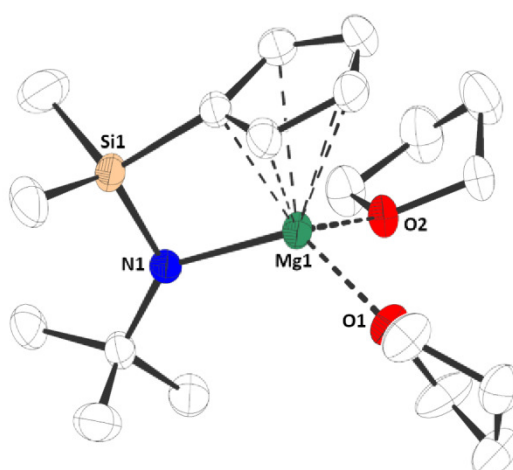


Figure S37. Molecular structure of **1a**·(thf)₂ in the crystal (displacement ellipsoids at 50% probability level; hydrogen atoms omitted for clarity).

crystal structure data of 1a-dme

CCDC code	2193656	
Empirical formula	C ₁₅ H ₂₉ MgNO ₂ Si	
Formula weight	307.79	
Temperature	203(2) K	
Wavelength	0.71073 Å	
Crystal system	monoclinic	
Space group	<i>P</i> 2 ₁ / <i>c</i>	
Unit cell dimensions	a = 9.6254(4) Å	α = 90°
	b = 12.6628(5) Å	β = 97.3700(10)°
	c = 15.4269(5) Å	γ = 90°
Volume	1864.77(12) Å ³	
Z	4	
Density (calculated)	1.096 g m ⁻³	
Absorption coefficient	0.161 mm ⁻¹	
F(000)	672	
Crystal size	0.381 x 0.317 x 0.096 mm ³	
Theta range for data collection	2.088 to 27.103°	
Index ranges	-12 ≤ h ≤ 12, -16 ≤ k ≤ 16, -18 ≤ l ≤ 19	
Reflections collected	34676	
Independent reflections	4121 [R(int) = 0.0382]	
Completeness to theta = 25.242°	100.0 %	
Absorption correction	semi-empirical from equivalents	
Max. and min. transmission	0.7456 and 0.7128	
Refinement method	full-matrix least-squares on F ²	
Data / restraints / parameters	4121 / 359 / 287	
Goodness-of-fit on F ²	1.057	
Final R indices [I > 2σ(I)]	R1 = 0.0471, wR2 = 0.1345	
R indices (all data)	R1 = 0.0575, wR2 = 0.1442	
Extinction coefficient	n/a	
Largest diff. peak and hole	0.361 and -0.341 e.Å ⁻³	

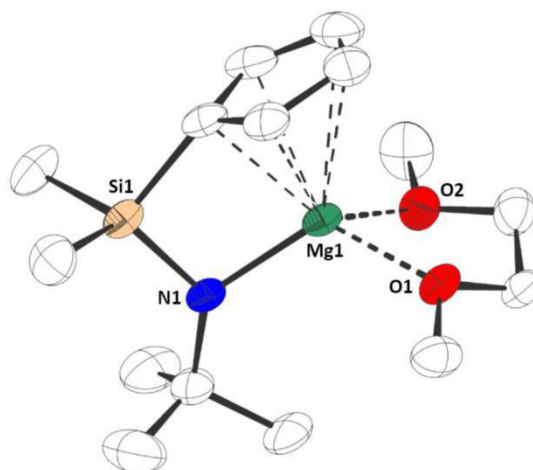


Figure S38. Molecular structure of 1a-dme in the crystal (displacement ellipsoids at 50% probability level; hydrogen atoms omitted for clarity).

crystal structure data of **1b-dme**

CCDC code	2193652	
Empirical formula	C ₁₉ H ₃₇ MgNO ₂ Si	
Formula weight	363.89	
Temperature	133(2) K	
Wavelength	0.71073 Å	
Crystal system	orthorhombic	
Space group	<i>P</i> 2 ₁ 2 ₁ 2	
Unit cell dimensions	a = 14.9068(4) Å	$\alpha = 90^\circ$
	b = 15.8982(5) Å	$\beta = 90^\circ$
	c = 9.3192(3) Å	$\gamma = 90^\circ$
Volume	2208.57(12) Å ³	
Z	4	
Density (calculated)	1.094 mg m ⁻³	
Absorption coefficient	0.145 mm ⁻¹	
F(000)	800	
Crystal size	0.200 x 0.151 x 0.109 mm ³	
Theta range for data collection	2.185 to 27.885°	
Index ranges	-17<=h<=19, -20<=k<=20, -12<=l<=12	
Reflections collected	45584	
Independent reflections	5277 [R(int) = 0.0484]	
Completeness to theta = 25.242°	99.9 %	
Absorption correction	semi-empirical from equivalents	
Max. and min. transmission	0.7456 and 0.7116	
Refinement method	full-matrix least-squares on F ²	
Data / restraints / parameters	5277 / 45 / 259	
Goodness-of-fit on F ²	1.067	
Final R indices [I>2sigma(I)]	R1 = 0.0317, wR2 = 0.0816	
R indices (all data)	R1 = 0.0363, wR2 = 0.0847	
Absolute structure parameter	-0.02(4)	
Extinction coefficient	n/a	
Largest diff. peak and hole	0.183 and -0.160 e.Å ⁻³	

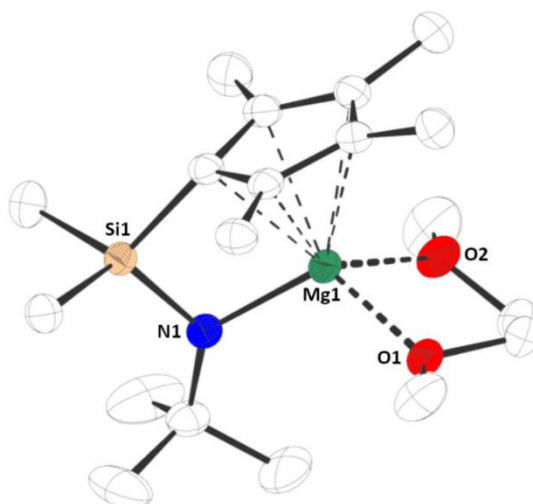


Figure S39. Molecular structure of **1b-dme** in the crystal (displacement ellipsoids at 50% probability level; hydrogen atoms omitted for clarity).

SUPPORTING INFORMATION

WILEY-VCH

crystal structure data of **1c-dme**

CCDC code	2193661	
Empirical formula	C ₂₉ H ₄₁ MgNO ₂ Si	
Formula weight	488.03	
Temperature	133(2) K	
Wavelength	0.71073 Å	
Crystal system	monoclinic	
Space group	<i>P2₁/c</i>	
Unit cell dimensions	a = 12.2408(4) Å	α = 90°
	b = 13.7047(5) Å	β = 103.8410(10)°
	c = 17.0712(4) Å	γ = 90°
Volume	2780.65(15) Å ³	
Z	4	
Density (calculated)	1.166 mg m ⁻³	
Absorption coefficient	0.132 mm ⁻¹	
F(000)	1056	
Crystal size	0.234 x 0.192 x 0.168 mm ³	
Theta range for data collection	1.928 to 27.903°	
Index ranges	-16 ≤ h ≤ 16, -17 ≤ k ≤ 18, -22 ≤ l ≤ 21	
Reflections collected	42882	
Independent reflections	6645 [R(int) = 0.0502]	
Completeness to theta = 25.242°	99.9 %	
Absorption correction	semi-empirical from equivalents	
Max. and min. transmission	0.7456 and 0.7199	
Refinement method	full-matrix least-squares on F ²	
Data / restraints / parameters	6645 / 63 / 355	
Goodness-of-fit on F ²	1.041	
Final R indices [I > 2σ(I)]	R1 = 0.0453, wR2 = 0.1259	
R indices (all data)	R1 = 0.0565, wR2 = 0.1356	
Extinction coefficient	n/a	
Largest diff. peak and hole	0.396 and -0.470 e.Å ⁻³	

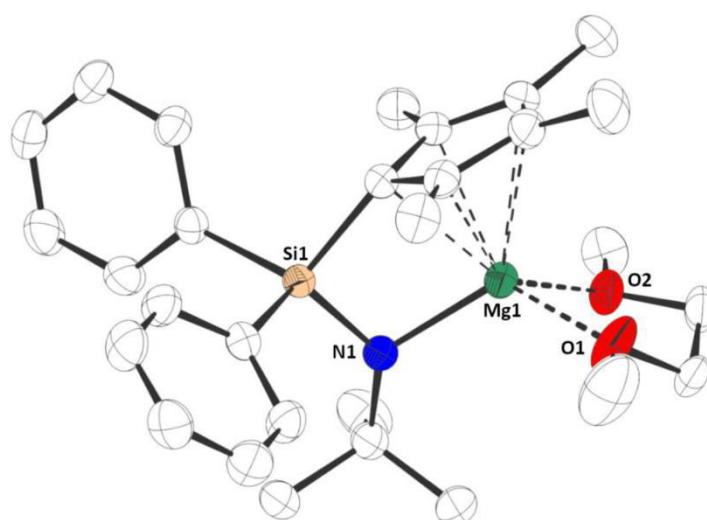


Figure S40. Molecular structure of **1c-dme** in the crystal (displacement ellipsoids at 50% probability level; hydrogen atoms omitted for clarity).

crystal structure data of **1d**·(dme)₂

Identification code	2193657	
Empirical formula	C ₂₅ H ₄₃ MgNO ₄ Si	
Formula weight	474.00	
Temperature	133(2) K	
Wavelength	0.71073 Å	
Crystal system	orthorhombic	
Space group	<i>Pbca</i>	
Unit cell dimensions	a = 13.6729(6) Å	$\alpha = 90^\circ$
	b = 17.1539(9) Å	$\beta = 90^\circ$
	c = 23.2814(11) Å	$\gamma = 90^\circ$
Volume	5460.5(5) Å ³	
Z	8	
Density (calculated)	1.153 mg m ⁻³	
Absorption coefficient	0.138 mm ⁻¹	
F(000)	2064	
Crystal size	0.232 x 0.174 x 0.106 mm ³	
Theta range for data collection	2.096 to 27.904°	
Index ranges	-17<=h<=17, -22<=k<=22, -30<=l<=30	
Reflections collected	74213	
Independent reflections	6528 [R(int) = 0.0729]	
Completeness to theta = 25.242°	100.0 %	
Absorption correction	semi-empirical from equivalents	
Max. and min. transmission	0.7456 and 0.7173	
Refinement method	full-matrix least-squares on F ²	
Data / restraints / parameters	6528 / 0 / 299	
Goodness-of-fit on F ²	1.059	
Final R indices [I>2sigma(I)]	R1 = 0.0379, wR2 = 0.0964	
R indices (all data)	R1 = 0.0528, wR2 = 0.1065	
Extinction coefficient	n/a	
Largest diff. peak and hole	0.285 and -0.257 e.Å ⁻³	

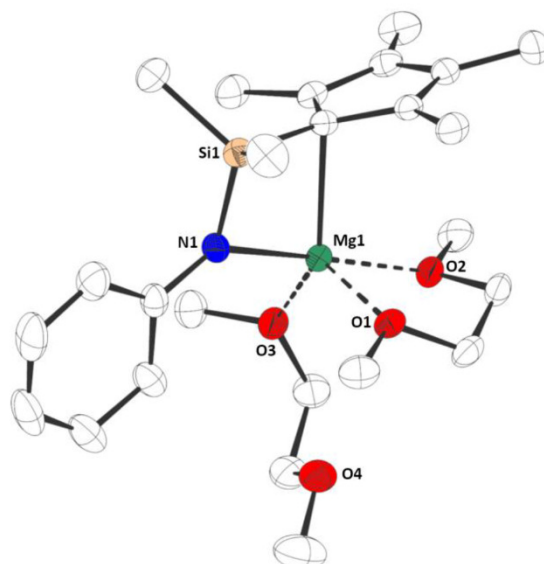


Figure S41. Molecular structure of **1d**·(dme)₂ in the crystal (displacement ellipsoids at 50% probability level; hydrogen atoms omitted for clarity).

SUPPORTING INFORMATION

WILEY-VCH

Table S1. Selected bond lengths in *ansa*-half-sandwich complexes **1a-d**-(dme/thf)_x.

Compound	Mg-C ^{Cp} [pm]	Mg-C ^{centroid} [pm]	Mg-N [pm]	Mg-O [pm]
1a -(thf) ₂	226.69(45); 228.40(44); 229.09(44); 245.81(47); 249.88(54); 252.25(44); 258.47(45); 263.27(53); 265.99(50); 286.42(45); 292.42(54); 299.24(55); 303.34(54); 308.18(54); 308.66(54)	234.59(14); 244.18(14); 244.97(14)	198.72(33); 199.14(33); 200.76(33)	202.67(31); 202.90(31); 203.24(33); 203.46(33); 203.78(32); 204.98(33)
1a -dme	228.92(18); 243.08(26); 243.94(22); 267.88(30); 268.05(27)	220.36(7)	199.20(17)	203.98(41); 210.11(44)
1b -dme	231.05(20); 238.54(21); 245.2(2); 257.23(23); 261.19(21)	215.05(6)	199.63(19)	205.86(17); 207.94(17)
1c -dme	229.58(16); 231.83(16); 253.73(16); 257.05(16); 269.52(17)	217.41(5)	202.46(15)	206.82(16); 207.10(16)
1d -(dme) ₂	231.70(14); 275.58(14); 303.32(15); 355.93(16); 369.00(15)	–	205.61(13)	207.14(11); 208.86(11); 210.66(11)

Computational Details

All calculations were performed using the Gaussian 16, Revision C.01 package of programs.²⁹ All geometry optimizations have been carried out at the B3LYP-D3³⁰/def2-TZVP³¹ level of theory. Every optimized structure was confirmed to be a minimum on the potential energy surface by a subsequent frequency analysis (all positive eigenvalues).

Table S2. Calculated bond dissociation energy (BDE), fluorid ion affinity (FIA) and global electrophilicity index (GEI) values.

Compound	BDE(thf) ₂ [kJ mol ⁻¹]	BDE(dme) [kJ mol ⁻¹]	FIA ³² [kJ mol ⁻¹]	GEI ²³ [eV]
1a	158.22	108.53	73.59	0.85
1b	157.60	112.86	62.67	0.84
1c	164.64	116.51	67.61	0.94
1d	160.99	116.57	66.14	0.87

References

- [1] H. G. Alt, K. Föttinger, W. Milius, *J. Organomet. Chem.* **1999**, *572*, 21-30.
- [2] D. W. Carpenetti, L. Kloppenburg, J. T. Kupec, J. L. Petersen, *Organometallics* **1996**, *15*, 1572-1581.
- [3] J. Pinkas, M. Horáček, V. Varga, K. Mach, K. Szarka, A. Vargová, R. Gyepes, *Polyhedron* **2020**, *188*, 114704.
- [4] Z. Hou, T. Koizumi, M. Nishiura, Y. Wakatsuki, *Organometallics* **2001**, *20*, 3323-3328.
- [5] G. M. Sheldrick, *Acta Cryst. A* **2015**, *71*, 3-8.
- [6] G. M. Sheldrick, *Acta Cryst. C* **2015**, *71*, 3-8.
- [7] C. B. Hübschle, G. M. Sheldrick, B. Dittrich, *J. Appl. Crystallogr.* **2011**, *44*, 1281-1284.
- [8] L. Wirtz, W. Haider, V. Huch, M. Zimmer, A. Schäfer, *Chem. Eur. J.* **2020**, *26*, 6176-6184.
- [9] L. Wirtz, J. Lambert, B. Morgenstern, A. Schäfer, *Organometallics* **2021**, *40*, 2108-2117.
- [10] A.-M. Fuller, A. J. Mountford, M. L. Scott, S. J. Coles, P. N. Horton, D. L. Hughes, M. B. Hursthouse, S. J. Lancaster, *Inorg. Chem.* **2009**, *48*, 11474-11482.
- [11] A. Harinath, S. Anga, T. K. Panda, *RSC Adv.* **2016**, *6*, 35648-35653.
- [12] D. J. Liptrot, M. S. Hill, M. F. Mahon, A. S. S. Wilson, *Angew. Chem. Int. Ed.* **2015**, *54*, 13362-13365; *Angew. Chem.* **2015**, *127*, 13560-13563.
- [13] T. Ohmura, K. Masuda, M. Sugimoto, *J. Am. Chem. Soc.* **2008**, *130*, 1526-1527.
- [14] W. Xie, H. Hu, C. Cui, *Angew. Chem. Int. Ed.* **2012**, *51*, 11141-11144; *Angew. Chem.* **2012**, *124*, 11303-11306.
- [15] A. Baishya, T. Peddaraio, S. Nembenna, *Dalton Trans.* **2017**, *46*, 5880-5887.
- [16] P. Rios, M. Roselló-Merino, O. Rivada-Wheelaghan, J. Borge, J. López-Serrano, S. Conejero, *Chem. Commun.* **2018**, *54*, 619-622.
- [17] D. Gasperini, A. K. King, N. T. Coles, M. F. Mahon, R. L. Webster, *ACS Catal.* **2020**, *10*, 6102-6112.
- [18] X. Zhang, S. Zhou, X. Fang, L. Zhang, G. Tao, Y. Wei, X. Zhu, P. Cui, S. Wang, *Inorg. Chem.* **2020**, *59*, 9683-9692.
- [19] A. E. Nako, W. Chen, A. J. P. White, M. R. Crimmin, *Organometallics* **2015**, *34*, 4369-4375.
- [20] N. Li, B.-T. Guan, *Adv. Synth. Catal.* **2017**, *359*, 3526-3531.
- [21] M. Magre, B. Maity, A. Falconnet, L. Cavallo, M. Rueping, *Angew. Chem. Int. Ed.* **2019**, *58*, 7025-7029; *Angew. Chem.* **2019**, *131*, 7099-7103.
- [22] D. Wei, B. Carboni, J.-B. Sortais, C. Darcel, *Adv. Synth. Catal.* **2018**, *360*, 3649-3654.
- [23] C. Weetman, M. D. Anker, M. Arrowsmith, M. S. Hill, G. Kociok-Köhn, D. J. Liptrot, M. F. Mahon, *Chem. Sci.* **2016**, *7*, 628-641.
- [24] Z. Zhang, S. Huang, L. Huang, X. Xu, H. Zhao, X. Yan, *J. Org. Chem.* **2020**, *85*, 12036-12043.
- [25] C. Yu, C. Guo, L. Jiang, M. Gong, Y. Luo, *Organometallics* **2021**, *40*, 1201-1206.
- [26] A. L. Reznichenko, K. C. Hultsch, *Organometallics* **2010**, *29*, 24-27.
- [27] F. M. Sroor, C. G. Hrib, L. Hilfert, S. Busse, F. T. Edelman, *New. J. Chem.* **2015**, *39*, 7595-7601.
- [28] Z. Feng, Z. Huang, S. Wang, Y. Wei, S. Zhou, X. Zhu, *Dalton Trans.* **2019**, *48*, 11094-11102.
- [29] Gaussian 16, Revision C.01, Frisch, M. J.; Trucks, G. W.; Schlegel, H. B.; Scuseria, G. E.; Robb, M. A.; Cheeseman, J. R.; Scalmani, G.; Barone, V.; Petersson, G. A.; Nakatsuji, H.; Li, X.; Caricato, M.; Marenich, A. V.; Bloino, J.; Janesko, B. G.; Gomperts, R.; Mennucci, B.; Hratchian, H. P.; Ortiz, J. V.; Izmaylov, A. F.; Sonnenberg, J. L.; Williams-Young, D.; Ding, F.; Lipparini, F.; Egidi, F.; Goings, J.; Peng, B.; Petrone, A.; Henderson, T.; Ranasinghe, D.; Zakrzewski, V. G.; Gao, J.; Rega, N.; Zheng, G.; Liang, W.; Hada, M.; Ehara, M.; Toyota, K.; Fukuda, R.; Hasegawa, J.; Ishida, M.; Nakajima, T.; Honda, Y.; Kitao, O.; Nakai, H.; Vreven, T.; Throssell, K.; Montgomery, J. A.; Jr. Peralta, J. E.; Ogliaro, F.; Bearpark, M. J.; Heyd, J. J.; Brothers, E. N.; Kudin, K. N.; Staroverov, V. N.; Keith, T. A.; Kobayashi, R.; Normand, J.; Raghavachari, K.; Rendell, A. P.; Burant, J. C.; Iyengar, S. S.; Tomasi, J.; Cossi, M.; Millam, J. M.; Klene, M.; Adamo, C.; Cammi, R.; Ochterski, J. W.; Martin, R. L.; Morokuma, K.; Farkas, O.; Foresman, J. B.; Fox, D. J.; Gaussian, Inc., Wallingford CT, **2019**.
- [30] a) Becke, A. D. Density-functional thermochemistry. III. The role of exact exchange. *J. Chem. Phys.* **1993**, *98*, 5648-5652; b) Lee, C.; Yang, W.; Parr, R. G. Development of the Colle-Salvetti correlation-energy formula into a functional of the electron density. *Phys. Rev. B* **1988**, *37*, 785-789; c) Vosko, S. H.; Wilk, L.; Nusair, M. Accurate spin-dependent electron liquid correlation energies for local spin density calculations: a critical analysis. *Can. J. Phys.* **1980**, *58*, 1200-1211; d) Stephens, P. J.; Devlin, F. J.; Chabalowski, C. F.; Frisch, M. J. *Ab Initio* Calculation of Vibrational Absorption and Circular Dichroism Spectra Using Density Functional Force Fields. *J. Phys. Chem.* **1994**, *98*, 11623-11627; e) Grimme, S.; Antony, J.; Ehrlich, S.; Krieg, H. A consistent and accurate *ab initio* parametrization of density functional dispersion correction (DFT-D) for the 94 elements H-Pu. *J. Chem. Phys.* **2010**, *132*, 154104.
- [31] a) Weigend, F.; Ahlrichs, R. Balanced basis sets of split valence, zeta valence and quadruple zeta valence quality for H to Rn: Design and assessment of accuracy. *Phys. Chem. Chem. Phys.* **2005**, *7*, 3297-3305; b) Weigend, F. Accurate Coulomb-fitting basis sets for H to Rn. *Phys. Chem. Chem. Phys.* **2006**, *8*, 1057-1065.
- [32] Fluoride ion affinities (FIA) were calculated according to a literature established method from the isodesmic reactions with Et₃B/Et₃BF₄. For more details see, for example: H. Großekappenberg, M. Reißmann, M. Schmidtman, T. Müller, *Organometallics* **2015**, *34*, 4952-4958.
- [33] Global electrophilicity indices ω were calculated following the method of Stephan and coworkers (Method C): A. R. Jupp, T. C. Johnstone, D. W. Stephan, *Inorg. Chem.* **2018**, *57*, 14764-14771.

Author Contributions

Lisa Wirtz:

Lead: Synthesis and characterization of **1a-d**, investigation of catalytic reactions, mechanistic investigations, DFT-calculations, writing, reviewing and editing of the manuscript and supporting information.

Kinza Yasmin Ghulam:

Supporting: Synthesis and characterization of **1b**.

Bernd Morgenstern:

Lead: X-ray analysis.

André Schäfer:

Lead: Project administration and supervision, funding acquisition;
Supporting: Writing, reviewing and editing of the manuscript and supporting information.